Dissertation zur Erlangung des Doktorgrades

der Fakultät für Chemie und Pharmazie

der Ludwig-Maximilians-Universität München

Cationic carrier supported peptide-based nanosystems for tumor targeting

Teoman Tillman Finn Berke Benli-Hoppe

aus Göttingen, Deutschland

2023

Erklärung

Diese Dissertation wurde im Sinne von § 7 der Promotionsordnung vom 28. November 2011 von Herrn Prof. Dr. Ernst Wagner betreut.

Eidesstattliche Versicherung

Diese Dissertation wurde eigenständig und ohne unerlaubte Hilfe erarbeitet.

München, den 03.02.23

.....

Teoman Benli-Hoppe

Dissertation eingereicht am: 03-Feb-2023

1. Gutachter: Prof. Dr. Ernst Wagner

2. Gutachter: Prof. Dr. Olivia Merkel

Mündliche Prüfung am: 28-Mrz-2023

I met a traveller from an antique land
Who said: "Two vast and trunkless legs of stone
Stand in the desart. Near them, on the sand,
Half sunk, a shattered visage lies, whose frown,
And wrinkled lip, and sneer of cold command,
Tell that its sculptor well those passions read
Which yet survive, stamped on these lifeless things,
The hand that mocked them and the heart that fed:
And on the pedestal these words appear:
"My name is Ozymandias, king of kings;
Look on my works, ye Mighty, and despair!"
No thing beside remains. Round the decay
Of that colossal wreck, boundless and bare
The lone and level sands stretch far away."

— Percy Shelley's "Ozymandias

Table of Contents

1 Introduction 8

1.1 Design and necessities of polymeric nanosystems for efficient tumor targeting and bioimaging in nanomedicine 8

1.2 Evolution of polyplex architecture 11

1.3 Cationic polymers: the shift from polydisperse polymers to sequence-defined platforms 12

1.4 Bypassing the blood-brain-barrier (BBB) via active transport mechanisms . 13

1.5 Tumor targeting mechanisms 15

1.6 Active targeting of tumor cells 16

1.7 Bioimaging and theranostic nanosystems 18

1.8 Carbon dot (CD) nanosystems 20

1.9 Aim of the thesis 22

2 Materials and Methods 24

2.1 Materials 24

2.1.1 Equipment for solid-phase synthesis 24

2.1.2 Nucleic acids 26

2.1.3 Carbon dots 26

2.1.4 Cell culture 27

2.2 Methods 28

2.2.1 Loading of a 2-chlorotrityl resin with Fmoc protected amino acid 28

2.2.2 Loading of a four-armed branching core Fmoc-Ala-Wang resin 28

2.2.3 OAA and DBCO agent synthesis 29

2.2.4 Kaiser test 40

2.2.5 Cleavage conditions 40

2.2.6 siRNA and pDNA polyplex formation 41

2.2.7 Carbon dot OAA formation 42
2.2.8 Post-modification/functionalization with DBCO agents 43
2.2.9 Particle size and zeta potential 44
2.2.10 Transmission electron microscopy (TEM) 44
2.2.11 Ellman's assay 44
2.2.12 Agarose gel shift assay 45
2.2.13 Ethidium bromide (EtBr) exclusion assay 45
2.2.14 Luciferase gene transfer 45
2.2.15 Cell viability assay (CellTiter-Glo® Assay) 46
2.2.16 Gene silencing mediated by GFP siRNA 46
2.2.17 Cell viability assay (MTT) 47
2.2.18 siRNA and pDNA Binding Assay 47
2.2.19 Cellular association assay 47
2.2.20 RP-HPLC analysis 48
2.2.21 Evaluation of the SPAAC reaction by HPLC and MALDI MS 48
2.2.22 Proton 1H NMR spectroscopy 49
2.2.23 MALDI mass spectrometry 49
2.2.24 Statistical analysis 49
2.2.25 Evaluation of the SPAAC reaction by HPLC and MALDI MS 50

3 Results 51

3.1 Transferrin receptor targeted polyplexes completely comprised of sequence-defined components 51
3.1.1 Introduction 51
3.1.2 Results 53
3.1.3 TfR targeting by siRNA polyplexes (This chapter was done by Mina Yazdi, Pharmaceutical Biology, LMU) 58
3.1.4 TfR targeting by pDNA polyplexes (This chapter was done by Şurhan Göl, Pharmaceutical Biology, LMU) 63

3.2 Ligand targeted carbon dots as organic vector-based system for cell transfection 68
3.2.1 Introduction 68
3.2.2 Results 69
3.2.3 DBCO-PEG-Ligand conjugates for click modification of rCD-OAA conjugates 78
3.2.4 Targeting effects of rCD-OAA conjugates 79
4 Discussion 82
4.1 Transferrin receptor targeted polyplexes completely comprised of sequence-defined components 82
4.2 Ligand coated photoluminescent carbon dots as organic carrier-based system for targeted enhanced intracellular delivery 83
5 Summary 85
6 Appendix 87
6.1 Abbreviations 87
6.2 Summary of SPSS derived OAAs 94
6.3 Summary of SPSS derived shielding and targeting agents 97
6.4 Analytical Data 99
6.4.1 ^{1}H NMR Spectra of OAAs 99
6.4.2 Mass spectra of shielding and targeting agents 117
6.4.3 Evaluation of the SPAAC reaction by HPLC and MALDI MS 128
6.4.4 HPLC chromatograms of DBCO agents 129
6.4.5 Particle size (Z-average), polydispersity index (PDI), and zeta potential of siRNA polyplexes. 133
6.4.6 Particle size (Z-average), polydispersity index (PDI), and zeta potential of pDNA polyplexes. 133
6.4.7 Agarose gel shift of siRNA polyplexes 135
6.4.8 Agarose gel shift of pDNA polyplexes 136

6.4.9 eGFPLuc gene silencing activity of siRNA polyplexes 137
6.4.10 Ethidium bromide (EtBr) exclusion assay of pDNA polyplexes 138
6.4.11 TEM data of pDNA polyplexes 139
6.4.12 MTT assay of pDNA polyplexes 140
6.4.13 Cellular association of pDNA polyplexes 141
6.4.14 Summary of SPSS derived 4-armed OAAs for rCD coating and entrapment and rCD 144
6.4.15 rCD-1696 (w/w) titration 146
6.4.16 Time dependency of incubation for the formulation of rCD-OAA conjugation 147
6.4.17 Cellular uptake of rCD-1696-Ligands in U87 cell line 148
7 References 149
8 Publications 161
9 Acknowledgements 163

1 Introduction

The sections **1.1** to **1.3** provide a brief introduction into the research field of polymer-based delivery systems for tumor targeting. It was adapted from:

Benli-Hoppe T., Wagner E. (2020) Polymer-Based Tumor-targeting Nanosystems. In: Huang R., Wang Y. (eds) New Nanomaterials and Techniques for Tumor-targeted Systems. Springer, Singapore

1.1 Design and necessities of polymeric nanosystems for efficient tumor targeting and bioimaging in nanomedicine

At present, numerous polymeric nanosystems are being developed as cancer therapeutics. A broad spectrum of possible chemical modifications facilitates dynamic designs, where tumor-specific pharmacology [1, 2] and microenvironment can modulate improved delivery and release at the tumor site [3, 4]. Applied polymeric systems span the full nanomaterial size scale, from single polymer chains and drug conjugates up to large nanoparticle assemblies [5-12]. They can be classified by their unique physicochemical structures and properties, including solid polymeric NPs, polymeric micelles, polymer conjugates, polymersomes, polyplexes, and polymer-lipid hybrid systems [10-15]. Polymer NPs can be defined by their composition and morphology in a central core and a homogeneously or heterogeneously monolayer or multilayer shell. The therapeutic agent may either be conjugated to the NP, encapsulated between core and shell, or incorporated within the polymeric core. For a schematic overview of polymer-based platforms see **Figure 1.1**.

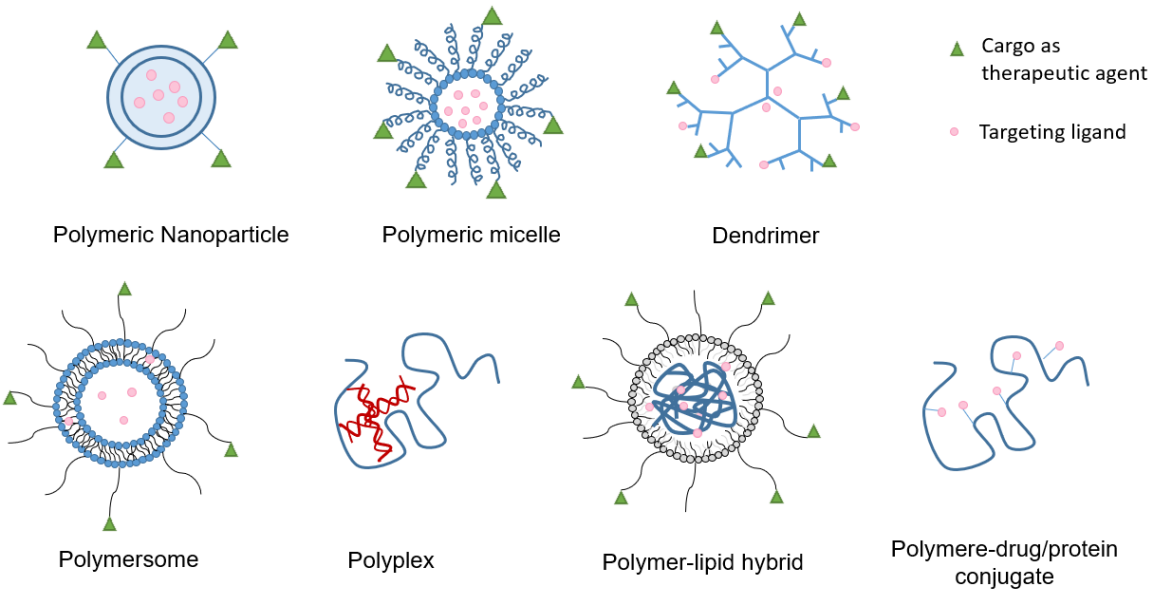

Figure 1.1. Schematic overview of polymeric nanosystems. The blue color represents the polymeric platform. Figure adapted from [14]; Copyright of the original © 2019; DOVE Medical Press.

Polymers employed for fabrication of these nanocarrier platforms may be either of natural origin, such as albumin [16], hyaluronic acid (HA) [17], chitosan (CS) [18] and sodium alginate, or of synthetic origin, such as polyacrylic acid (PAA), polyglycolic acid (PGA), poly(lactide-co-glycolide) (PLGA), polylactic acid (PLA), dendrimers, and hyperbranched polymers [19] (for chemical structures see **Figure 1.2**). The design of polymeric nanosystems can be tailored for transport of a variety of drugs, proteins, nucleic acids, and bioimaging agents.

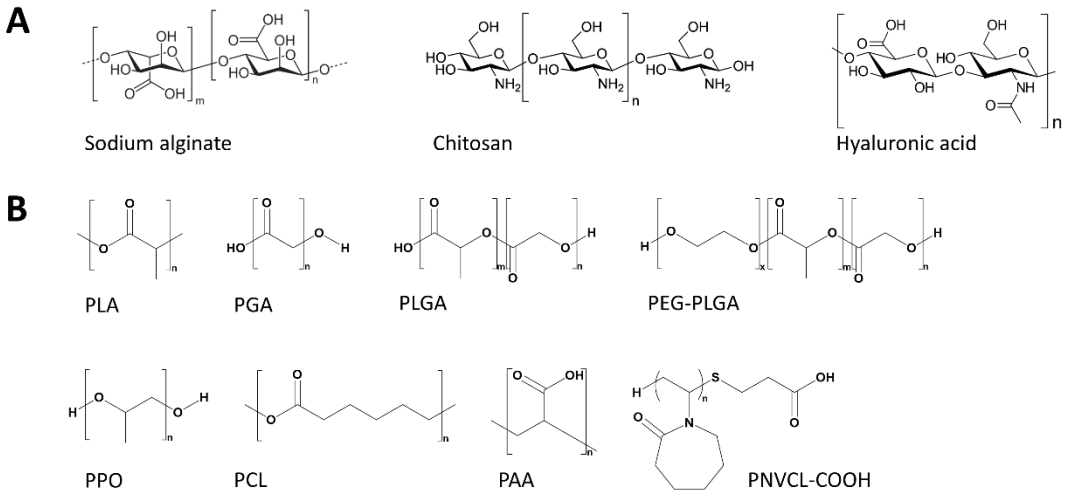

Figure 1.2. Carrier polymers. (A) Natural polymers: sodium alginate, chitosan (CS), hyaluronic acid

(HA). (B) Synthetic polymers: poly(lactic acid) (PLA); polyglycolic acid (PGA); poly(lactide-co-glycolide) (PLGA); poly(ethylene glycol)-poly(lactide-co-glycolide); (PEG-PLGA); poly(propylene oxide) (PPO); poly-ε-caprolactone (PCL); poly(acrylic acid) (PAA); poly(N-vinylcaprolactam) (PNVCL)

A prolonged blood circulation time is considered as a critical requirement for a preferred accumulation at the tumor site via the enhanced permeability and retention effect (EPR) [1, 2]. Therefore, nanosystems must be designed to protect drugs from clearance by kidney, liver, and reticuloendothelial system from unfavorably fast metabolism during systemic circulation. For this purpose, functionalization of the polymeric framework with shielding moieties like polyethylene glycol (PEG) [20-22], N-(2-hydroxypropyl) methacrylamide (pHPMA) [23, 24], hydroxyethyl starch (HES) [25], hyaluronic acid (HA) [26], poly(2-oxazoline) [27] or polysarcosine [28] can help to reduce nonspecific distribution [29], to achieve longer blood circulation times and to reach tumor target tissue. In addition to passive targeting processes, active drug-targeting by targeting ligands (peptide, aptamer, antibody, antibody fragment, small molecule) for specific tumor cell surface antigens [14, 30-36] and tumor microenvironment (TME)-triggered programmed drug release and activation mechanisms [3, 4] can be utilized. Polymer-based intracellular drug delivery may also overcome multi-drug resistance (MDR) processes. Altogether, such measures should result in an increased antitumor efficacy with minimal systemic side effects [37-40].

However, despite their numerous advantages, polymeric nanosystems also have disadvantages. Depending on the application and the type of drug, various complex synthetic procedures and nanosystem assemblies may have to be applied. Such methods include spontaneous self-assembly by electrostatic and other noncovalent interactions, solvent evaporation, nanoprecipitation, emulsion diffusion and salting out [41-43]. In some cases the acidity of their degradation products, the large scale production, the reproducibility of batch to batch in their synthesis is still a challenge for many polymer-based nanosystems [44]. In addition, there are still many unanswered questions about their toxicity profile and their long-term biological effects. Reviewing published work, Wilhelm et al highlighted the real efficacy of only 0.7% of the dose of nanoparticles accumulating at the target tumor site on average [45]. This suggests that there is room for further optimization.

The excellent therapeutic potential at both preclinical and clinical development stages led to diverse applications and perspectives of polymer-based nanosystems in bioimaging and nanomedicine. The fact that some formulations are already in clinical use further validates the efficiency of polymeric platforms for delivery of anticancer agents.

1.2 Evolution of polyplex architecture

Among synthetic nucleic acid carriers, cationic polymer-based nanosystems are widely investigated. An overview of the first five decades in developing nucleic acid – polycation polyelectrolyte complexes termed polyplexes [13] can be found in references [31, 46]. Polyplexes offer various benefits, such as lower immunogenicity compared to viral vectors, and, importantly, the capability of carrying either natural or chemically modified nucleic acid material. However, due to the presence of numerous positive charges on the surface of polyplexes, binding with serum complement proteins and activation of innate immune system, aggregation and non-specific interaction remains major issues in their application [29, 47-49]. Consequently, more stable packaging of polyplexes (e.g. by introducing hydrophobic elements or covalent cross-links within the particle core) and shielding the positive surface charges against undesired specific interactions with the bio-macromolecules, such as serum proteins, and avoiding an undesirable immune response are important measures to overcome these problems [50, 51]. These considerations resulted in the design of PEGylated polyplexes, which are polyelectrolyte complexes formulated by the self-assembly of oppositely charged anionic nucleic acids with PEG-polycation block copolymers. Alternatively, to the use of di-block polymers, polyplex cores were formed with polycations and subsequently modified with shielding PEG or other shielding polymers [20, 52, 53]. The outer hydrophilic PEG layer of the core-shell architecture provides a stealth effect, minimizing non-specific interactions and prolonging circulation time *in vivo* [31, 54]. The plasmid DNA (pDNA) or siRNA is complexed and condensed through electrostatic interactions, hydrogen bonding, coordinative interactions, and hydrophobic interactions [55]. However, entropy-driven electrostatic interactions between the cationic groups of the polymer and the negatively charged nucleic acids are the most prominent way of condensation [13, 31]. Condensation is necessary to prevent degradation and the release of cargo at off-target sites,

neutralize negative charges, and reduce the size of larger nucleic acids such as pDNA [56, 57] with the aim of liberating the cargo in the cytosol, in case of siRNA [58], or the nucleus, in case of DNA [59, 60]. In both cases, cell uptake by endocytosis into cellular vesicles and endosomal escape mechanisms are involved [61-65]. Therefore binding to the nucleic acid should be reversible, resulting in a well available therapeutic cargo once the specific target site is reached [66]. Another important factor of influencing the biological activity of polyplexes is the modulation of their shape (folded rod or collapsed sphere) and size, which can be precisely controlled by the length of the polycationic segments of the block copolymers [67-69] for additionally control the packaging of nucleic acid into an appropriate structure to achieve effective gene expression [70].

1.3 Cationic polymers: the shift from polydisperse polymers to sequence-defined platforms

The most studied cationic polymers for the preparation of polyplex systems have been linear (LPEI) or branched (BPEI) polyethylenimine (PEI) and poly(L-Lysine) (PLL) [31, 71, 72]. PEI displays a high concentration of positively charged amino groups (primary to tertiary), which enables effective electrostatic binding and condensation of negatively charged DNA [73]. Additionally, it possesses buffering capacity and polymer-swelling at the acidic pH of the endosomes [74]. Optimized versions of PEI have already been applied in human clinical trials for cancer therapy. Nevertheless, PEI has also drawbacks like cytotoxicity and non-degradability. PLL, on the other hand, consists of only primary amines in its side chain, which interact with the DNA for the condensation. However, PLL has no intrinsic buffer-based endosomal escape mechanism, making it inferior as a gene delivery system when compared to PEI [75, 76]. Functionalization with endosomolytic agents such as virus-derived peptides is required to overcome the drawback of polymers such as PLL [77-80]. Non-degradability of PEI is associated with medium- to long-term cytotoxicity [81]. Therefore, the development of biodegradable analogs has been one line of optimization [82-84]. Both PEI and PLL are suitable polymers for polyplexes [85-92] but also pose risks such as triggering the complement activation of the innate immune system, which can lead to anaphylactic shocks [93]. Moreover, their polydisperse chemical nature as well as

difficulties in precise modifications hampers their broader development. Therefore, the design of new more defined platforms, such as sequence-defined polymers [94, 95] as carrier systems to tackle these issues has been a major research focus in pDNA and siRNA delivery. Cationic (oligoethanamino)amide-based polymers synthesized by using Fmoc/Boc-protected oligo(ethane amino)acids as building blocks for solid-phase-supported assembly represents one novel promising approach towards fully controlled syntheses of effective gene carriers, as firstly described by [96-101]. In addition to natural amino acids, artificial oligoamino acids such as succinoyl tetraethylene pentamine (Stp) were introduced, providing a moderate positive charge density responsible for nucleic acid binding, intracellular endosomal release behaviour within tumor cells based on the PEI-like proton sponge effect and high biocompatibility due to decreased electro-positivity and medium-small molecular weights [102].

1.4 Bypassing the blood-brain-barrier (BBB) via active transport mechanisms

Biological barriers impede the efficient delivery of theragnostic substances to their intended destination and are thus one of the most important challenges in modern medicinal therapy. One of the most protected system in our body is the central nervous systems (CNS). It is strictly regulated by the blood-brain barrier (BBB). The BBB represents the metabolic and physiological barrier between blood circulation and neural tissues. It protects the brain from toxins and regulates its nutritional supply and homeostasis. The BBB is a membrane consisting of a complex interaction between mainly a single layer of brain capillary endothelial cells (BCECs) and several cell types, such as astrocytes and pericytes.[103-106] The protective characteristic of the BBB is mainly transmitted through restrictive cell-to-cell connections, so-called tight junctions. Therefore, targeting brain tumors can be a quite challenging endeavor, therefore requires special attention. The transport of compounds is hampered due to the tight junctions between the BCECs, low vesicular transport, high metabolic activity, and the presence of efflux pumps (e.g., multi-drug resistant protein (MDR) or P-glycoprotein (P-gp). It is only limited to small lipophilic molecules (<500 Da), which can pass through diffusion. To maintain homeostasis of the brain several active transport mechanisms are present in the BBB, namely endogenous

transport mostly through carrier-mediated transport, receptor-mediated transport, and absorptive-mediated transport. With these selective transport systems, essential nutrients including amino acids, glucose, hormones, and proteins can bypass the BBB and reach the brain. Besides the inward vacillating receptor-mediated transport mechanisms there is outwards directed transport through the efflux pumps, eliminating potentially harmful substances. However, only a healthy BBB can maintain its full function. If erupted by high-grade glioma or brain metastases the BBB becomes leaky.[107] But besides a damaged BBB, its restrictive nature is so strong and efficient that several invasive strategies have been developed to tackle the delivery of drugs to the CNS to be able to treat tumors, most importantly gliomas, which are the most common and aggressive form of brain cancer.[108] However, these approaches can be potentially harmful and, in some cases, inefficient. Receptor-mediated transcytosis is known to be harmless and well-suitable for the transport of large therapeutic agents across the BBB, which is why research has focused on describing, targeting, and exploiting these mechanisms. There are three endocytose-mediated pathways through the BBB for macromolecules: adsorptive-mediated transcytosis (AMT), receptor-mediated transcytosis (RMT), and carrier-mediated transcytosis (CMT).[105]

A well-described strategy for receptor-mediated transcytosis across the BBB is by using the LRP1 receptor (low-density lipoprotein receptor-related peptide), which is a member of the low-density lipoprotein receptor (LDLR) family.[109, 110] High interactive ligand counterparts for the LRP1 receptor are peptides derived from the angiopep series. They were detected by sequence alignment of aprotinin with other human proteins containing a Kunitz domain. The internalization pathway is based on clathrin- and caveolin-mediated endocytosis.[111] Angiopep-2 prove to be the best performer of this series. It resembles great LRP1 targeting, resulting in effective penetration of the BBB. Therefore, Angiopep-2 is a well-described peptide, which already reached clinical evaluation for glioma treatment.[112] It is widely used to transport small molecule drugs,[113-116] peptides,[117] and nucleic acid delivery systems[118-122] through the BBB, resulting in glioblastoma retention and growth inhibition. Furthermore, Angiopep-2 modified polyplex could show enhanced gene silencing and survival rates of treated glioblastoma-bearing mice.[123, 124] As a consequence of this success the peptide structure of Angiopep-2 was taken as a basis for investigating potential

enhancements, resulting in the identification of L57, as the first artificial LRP1 ligand that showed better performance in cellular uptake and BBB permeability and *in vivo* stability as Angiopep-2.[125, 126]

1.5 Tumor targeting mechanisms

When nano-sized transport systems accumulate in the tumor by extravasation through the leaky tumor capillary window, they reach their target tissue in a passive manner. In addition, due to the lack of a lymphatic system, the delivery systems are inefficiently removed and thus remain in the tumor tissue. This effect was first described by Matsumara et al and named it “enhanced permeability and retention (EPR) effect. It paves the way for passive tumor-selective delivery of nanoparticle-based platforms (see**: 1.1**).[127-129] Today the clinical relevance of the EPR effect is a controversial topic and is widely debated in the scientifical world. The extent of passive targeting is highly dependent on the specific tumor pathophysiology, which can be extremely variable. This variability dictates the eligibility of a specific tumor to receive nanoparticles-based therapy.[130] Tumor sites show higher accumulation rates compared to controls, but still, only a small fraction of around 5% of the administered dose, reaches the target site, whit a major portion accumulating in the liver and spleen.[131] For a nanoparticular formulation to reach its target site through the EPR effect, the circulation time has to be substantially longer, and circumvented recognition from the immune system is also crucial. In case of detection from the systemic immune system, the carriers would be opsonized and neutralized. To tackle this hurdle the biophysical properties of a delivery system must be optimized by integrating shielding agents like PEG, pHPMA, HES, HA, poly(2-oxazoline), or polysarcosine (see: **1.2**) into the formulation to minimize the risk of unspecific interactions with biological components.

Besides the exploitation of the EPR effect, research is focusing on active tumor-cell targeting. Upon reach of the nanoparticles-based systems into the tumor site, crossing of cell membranes is required for the enforcement of the therapeutical activity, i.e., delivery of cargo. The most common pathway to enter the cell is via active endocytosis pathways, triggered through receptor-mediated interaction on the

cell surface.[132] To achieve high affinity to tumor cell receptors a broad range of ligands for surface modification of delivery systems can be used. This range comprehends compounds such as vitamins, carbohydrate-based drugs, peptides, proteins, antibodies, and aptamers (see: **1.1**). The internalization uses clathrin- or caveolae-mediated endocytosis.[133-136] Decades of research have identified overexpressed receptors, located on tumor vasculature, many of which are involved in tumor angiogenesis, tumor progression, and metastasis. Frequently, receptors are expressed by both tumor cells and tumor endothelial cells, providing corresponding ligands with dual targeting abilities. Previously, the goal has been to identify suitable receptor candidates that efficiently initiate described cellular internalization. By now, the research in this field was able to identify a consortium of many different receptor-ligand types with optimized structures enabling high receptor affinity. Active targeting enhances the attraction to tumor vasculature and therefore reduces non-specific accumulation in non-tumor tissue, resulting in a lower risk of side effects and a reduction of required therapeutical doses. Another big benefit of active targeting is the shorter circulation time needed for this targeted nanoparticle formulation to passively accumulate into tumor sites through the EPR effect. Some tumors are also known to not support the EPR effect due to a lack of fenestration and leaky vasculature,[137] which makes active tumor targeting a by far better approach in cancer therapy.

1.6 Active targeting of tumor cells

To enhance therapy effects and push down disadvantageous side effects for various diseases like cancer or Alzheimer's and Parkinson, aimed receptor targeting is utilized. Especially in the field of antitumoral therapy the focus on active tumor targeting can lead to enhanced therapeucitc efficacy.[138] Once on the tumor side, a specific defined receptor-targeted carrier system can more efficiently cross the cell membrane through active endocytosis than an untargeted vector. Therefore, active targeting by surface modifying the carrier-cargo system (nanoparticular system) can strongly increase the internalization rate and specificity. Over the past years, many suitable receptors for promoting cellular uptake have been identified. Research in this field has led to highly advanced types of ligands with optimized structures in terms of

receptor affinity and *in vivo* stability. Therefore, another major focus of this thesis lies in the definition of highly affine receptor ligands with the addition of altering their structure to enhance their stability properties.

The transferrin receptor (TfR) appears as a suitable choice for tumor targeting, due to its low levels of expression in the majority of normal human cells and its overexpression in various types of tumor cells.[139, 140] The 80 kDa serum protein transferrin (Tf) transports iron into the cells via TfR-mediated endocytosis, and iron is needed for DNA synthesis, cell division, and cellular metabolism.[141] Research efforts have utilized the TfR-mediated cellular uptake for the delivery of peptides, proteins, drug formulations, and nucleic acids.[20, 78, 142-157] Transferrin-guided nucleic acid delivery has already reached the stage of clinical testing in humans in the case of ex vivo pDNA transfer into patient tumor cells[158, 159] and *in vivo* delivery of siRNA into tumors.[160, 161] The use of a large serum-derived protein in a pharmaceutical formulation presents a challenge concerning to precise incorporation chemistry as well as a suitable protein source and stability. Smaller synthetic ligands for the same receptor would be preferable. Lee et al. reported a 12-amino acid short TfR-targeting peptide (sequence: H-THRPPMWSPVWP-NH_2), which was identified by phage display. This peptide specifically binds the TfR at a region that differs from the binding site of the natural ligand Tf, and can promote efficient cellular uptake via receptor-mediated endocytosis.[162] To overcome the rapid degradability of this standard peptide sequence by serum proteases (with a half-life of ≈30 min only), Giralt and colleagues synthesized a protease-resistant retro-enantio peptide (reTfR), containing all amino acids in *(D)*-configuration and in a reversed N to C sequence order (H-pwvpswmpprht-NH_2).[163] This synthetic protease-resistant reTfR peptide could provide a high permeability potential for cargo delivery in a cellular blood-brain barrier model. Clinically important, the slow clearance of the reTfR from blood circulation facilitated a high accumulation in the mice brains with no toxicity effects compared to their parent peptide significantly at a late time point after intravenous injection. The main aim in this thesis was to incorporate this small synthetic reTfR ligand as a targeting module into nucleic acid polyplexes that are totally based on precise, sequence-defined components. Compacting siRNA or pDNA with previously developed T-shaped lipo-oligoaminoamides (lipo-OOAs)[164, 165] into nanoparticles

followed by modification with monodisperse PEG and the reTfR ligand resulted in enhanced gene silencing or gene transfer, respectively, in receptor-expressing cells.

An additional very interesting approach for TfR-mediated endocytosis was developed by Santi. et al. [166] They created a distinct affinity of intravenously injected nanoparticles to the TfR, which lead to an increase in transcytosis across the BBB by generating an artificial Tf protein corona. They named their approach “the trojan horse”. For this purpose, they designed a peptide named Tf2 (CGGGHKYLRW). It can bind Tf on suitable pockets not involved in binding to TfR or iron. With its low unspecific protein adsorption and high binding energy toward Tf it can be efficiently internalized in cells with a Tf-dependent pathway. The group of Huang applied this strategy to create doxorubicin-loaded COF (covalent organic frameworks) targeted with Tf2 to enhance transport across the BBB. They could show a significant increase in survival time for glioma-bearing mice.[167]

Another relevant receptor for targeting is Integrin αvβ3. This receptor type is most associated to cell metastasis, cell survival and cell proliferation and is therefore highly overexpressed in many cancers. It is one of the best known, and researched receptors overexpressed on tumor cells and tumor vasculature. And is therefore an ideal receptor for targeting cancer therapeutics to improve their delivery and therapeutic efficacy.[168-173] Integrins symbolize a well described ligand option for the active integrin-mediated endocytosis pathway. Research on integrin targeting has shown that RGD functionalization of nanoparticular systems affects not only tumor accumulation and cellular internalization but also intracellular transport mechanisms. The team of Kataoka et al. detected that RGD polyplexes preferred to accumulate in the perinuclear region of cells within three hours after incubation, which was not observed in their unmodified control group.[174, 175]

1.7 Bioimaging and theranostic nanosystems

Improved pharmacokinetics and tumor accumulation will be a prime task in optimization the mentioned polymeric drug delivery system. Far less standardization will be possible with regards to the individual patient. Here, the heterogeneity of tumors, tumor stroma and size-dependence of vascularization is an open question

with high variability within the same patient and between different patients [2, 176-178]. This uncertainty poses a formidable delivery challenge, which requires novel approaches such as performing tumor imaging before administration of the therapeutic nanoagent. In the ideal situation, functional bioimaging would detect and confirm the molecular target (such as a tumor-specific target receptor) and the accessibility of the tumor (across vasculature, stroma) with a diagnostic nanoagent which would be harmless and would generate no side effects in non-target organs. The functional results from such a bioimaging would indicate the suitability of nanoagents. In case of alternative options, the most suitable nanoagent (size, surface modification) might be selected.

Theranostic nanoagents present the special case where the same nanosystem can be used as nontoxic diagnostic and subsequently as antitumoral therapeutic tool. Spitzweg and collaborators applied tumor-targeted pDNA polyplexes encoding sodium iodide symporter (NIS) as a well-defined theranostic gene [179, 180]. Functional NIS expression can be detected using the diagnostic radioisotope iodide ^{123}I by scintigraphy or using ^{124}I- / ^{18}F tetrafluoroborate for positron emission tomography. Using three cycles of polyplex and therapeutic radioiodide ^{131}I application significantly reduced tumor growth and prolonged survival of mice in several models [181-183].

Numerous polymeric nanoagents have been designed for multifunctional imaging and theranostics of cancer; the current section provides only a snapshot of activities [184, 185]. For pre-selection of cancer patients, integration of imaging properties into nanotheranostics should facilitate clinical translation and personalized nanomedicine administration. Imaging modalities include magnetic resonance imaging, incorporating superparamagnetic iron oxide nanoparticles (SPION) as MRI contrast agent into drug formulations [186, 187]. Ultrasound irradiation has been applied, with low-power diagnostic or high-power therapeutic irradiation, for example using theranostic polymer microcapsules composed of hydrogen-bonded multilayers of tannic acid and poly(N-vinylpyrrolidone) that produce high imaging contrast and deliver the anticancer drug doxorubicin upon irradiation [188]. Optical imaging with Near-Infrared (NIR) light enables deep tissue penetration and the design of NIR-activatable polymeric nanoformulations for combined imaging and therapy of cancer [189]. NIR agents include standard small-molecule dyes, but also polymer-coated

quantum dots [190] or carbon nanodots for cancer-targeted photo-thermo-chemotherapy [191, 192].

1.8 Carbon dot (CD) nanosystems

In the development of material science, carbon-based materials play a significant role. The vast field of carbon-based technology includes traditional industrial carbon (e.g., activated carbon, black carbon), new industrial carbon (e.g., carbon fibers, graphite), new carbon nanomaterials e.g., graphene, carbon nanotubes (CNT) and carbon dots (CD). The applicational field for carbon-based material is vast. However, most important is the field of chemistry and materials, but also many other areas due to their attribute of being environmentally friendly.

The new rising star of this domain is the carbon dots (CDs), also called carbon nanodots. They have attracted appreciable attention because of their excellent and tuneable photoluminescence (PL), low toxicity, small size, high quantum yield (QY), low cost, and excellent biocompatibility. Due to their excellent attributes, they provide important applications in many fields, including counting catalysis, anticounterfeiting, optoelectronic devices, and biomedicine. [193-201] The consensus of the definition of CDs is the quasi-0D carbon-based material with a size of 20 nm and below and with fluorescence attributes.[202] The newer generation of CDs have excellent fluorescence, which lead to a broad field of usage and many significant breakthroughs, including room temperature phosphorescence (RTP)[203, 204], thermally activated delayed fluorescence (TADF)[205], multiphoton luminescence[206, 207],multicolour [208, 209]and near infrared emissions, as well as various more application options. CDs are classified into 3 different classes, according to their different formation mechanisms, nanostructures, and properties: carbon quantum dots (CQDs), graphene quantum dots (GQDs) and carbonized polymer dots (CPDs).[210]

One of the most promising and frequently reported applicational fields of CDs is biomedicine. Their quasi-nonexistent cytotoxicity proven in *in vitro* studies, together with their excellent biocompatibility even at higher doses, makes them suitable for multiple applications in biomedicine.[194, 211-215] *In vivo* experiments could show rapid excretion via hepatobiliary system and kidney. No symptoms of inflammation are

observed in the heart, lung, brain, bladder, spleen, liver, tentacles, and kidney in rats, based on haematological analysis and blood chemistry.[216] The addressed reports conclude a safe biomedical application for *in vitro* and *in vivo* experiments. In addition to their biological safety, CDs can be produced at low costs in big quantities, are nanosized, enabling modification of their surface, have high photosensitivity, multiphoton photoluminescence, unique down-conversion photoluminescence, high brightness of fluorescence, making them excellent alternatives for traditional used fluorescent markers in therapy, diagnostics, and healthcare supplements. Therefore, CDs are very advantageous for Biomedical applications like bioimaging, phototherapy, drug/gene delivery, and nanomedicine.

In comparison to traditional fluorescent dyes, CDs have become the next-generation fluorescent bioimaging agents, thanks to their strong fluorescence, paired with excellent biocompatibility and non-invasiveness. Therefore, CDs are the next generation of fluorescence probes for *in vitro* and *in vivo* bioimaging. A diverse variety of CDs have been reported for cell, microorganism, and plant tissue images.[217-224] CDs can quickly enter the cells through energy- and temperature dependent micropinocytosis-, caveolae-, clathrin-, and/or lipid raft-mediated endocytosis. There they are quickly distributed into lysosomes, endoplasmic reticulum, mitochondria, Golgi apparatus, and nucleus, all dependent of the different nanostructures/-conformations and types of cells.[225-231] Thus, CDs are exceptional to understand and studying organ related diseases such as Alzheimer's disease, Parkinson's disease, cardiac dysfunction, diabetes, and cancer.

CDs gained much attention as promising candidates in the field of phototherapeutic therapy due to their outstanding optical properties, high water solubility, and photostability. The issue of impeding the effect of CDs in photodynamic therapy, because of the hypoxic tumor microenvironment and rapid consumption of oxygen, resulting in an irreversible tumor metastasis or drug resistance was overcome by Zhang et al.[232]

Among their features, CDs can encapsulate drugs or genes, making them suitable delivery vectors. Therefore, CDs are of high theranostic use. CDs are advantageous in visualizing drug accumulation and activities at specific pathological sites, due to their fluorescent attributes, which are needed to estimate therapeutic efficacies of

medicines.[233-237] Especially in gene therapy CDs can address to be strategic vectors for efficient gene transfection. Notably, their small size contributes to adequate cellular uptake and gene transfection. Besides that, their potential of integrating surface modification can be utilized to create tailormade therapy of the respective destination with minimal side effects. In addition to that, their unique fluorescence can be used to track the internalization of genes, resulting in increase of their therapeutic potential greatly, which makes them very interesting new candidates in non-viral vector-based gene therapy. [238-241] That is why the Joint Sino-German Research Project focuses on CDs as a basis to bypass the BBB to enable therapy inside the brain e.g., against Alzheimer's disease, Parkinson's disease, and Glioblastoma (see **3.2.1**). Here the main goal is to target carbon dots with LRP1 for the potential delivery of small molecules, proteins, and drugs across the BBB. This thesis contributes to this collaboration by designing, characterization, and evaluating of a 4-armed OAA library, consisting of 21 carriers, tailormade to encapsulate red carbon dots (rCDs) as their cargo. The goal is to further enhance the particle properties of rCDs and to enable SPAAC lead surface modification of the rCD-OAA conjugates to introduce potential targeting strategies to bypass the BBB. More information on this is in section **3.2** ff.

In summary, this chapter demonstrated that CDs posse's unique optical features, excellent biocompatibility, low cost, easy modification, and functionalization, and display a vast potential for a huge spectrum of applications. However, the technology still stands in its beginning footsteps. More development of advanced technology and characterization, controllable and reproducible synthesis methods, large-scale production, and more understanding of structure-performance relationships, is on the way, which will further evolve and excel this technology, and one small step of this evolvement will be done by the Joint Sino-German Research Project (see **3.2** ff), which is one part of this thesis.

1.9 Aim of the thesis

In the field of polymeric carrier systems sequence-defined cationic oligoamidoamides (OAAs), tailor-made for nucleic acids or other polyanionic materials, like the highly

negative charged rCDs (see **1.8**) as cargo, are of major interest in this thesis. OAAs are precisely synthesized by sequence-defined solid-phase supported synthesis. Through well-established structure-activity relationships, OAAs can be synthesized, and highly optimized for their cargo and variety of use. Therefore, this thesis focuses on the synthesis, characterization, and biological testing of a broad variety of OAAs (see **6.2**) and their nanoparticular form, which is created by self-assembly (see **1.1**) of different cargo (siRNA; pDNA; rCD) conjugation. To further enhance the therapeutical effect of OAA based frameworks, and push down disadvantages, receptor targeting is utilized (see **1.6**). Thus, another major focus of this thesis lies in the definition and testing of highly affine receptor ligands (see **6.3**) with the addition of altering their structure to enhance their stability properties.

Hence, as a first aim of this thesis (see **1.4** to **1.6; 3.1** ff) a 12-amino acid small protease-resistant retro-enantio peptide known for binding the TfR,[163] had to be modified by introducing PEG_{24} as a shielding agent and a DBCO motif to enable SPAAC surface modifications. The so created reTfR1 peptide ligand and its sequence modifications had then to be conjugated as targeting agents to siRNA and pDNA containing polyplexes for gene delivery. The used carrier system is based on sequence-defined T-shaped lipo-OAAs, since they prove their value in former publications.[164, 165] The goal is to prove and ensure the efficacy of TfR targeting of the reTfR peptide ligand in its modified versions on a siRNA and pDNA based nanoparticular model with the far sight of facilitating TfR targeted *in vivo* experiments.

The second half of this thesis (see **1.4** ff; **3.2** ff) focuses on LRP1-targeted and TfR-targeted carbon nanodot based models to cross the BBB and target glioblastoma cells. For this, all 4-armed OAAs of the rCD-Library had to be screened on particle properties under many different conditions, to create an advanced protocol for how to handle rCD-OAA conjugations and to find a “best performer” or “lead structure” for further evaluation. In addition, many peptide-based ligands had to be designed, and tested in cell culture by Fengrong Zhang (Pharmaceutical Biotechnology; LMU), and collaboration partner (Prof. Dr. Rongqin Huang) to further screen them via the established rCD-1696 conjugation on a trans-well BBB model.

2 Materials and Methods

2.1 Materials

2.1.1 Equipment for solid-phase synthesis

The solvents, reagents and buffers used for the experiments are presented in three Tables listed below.

Table 2.1 Solvents used for experimental procedures

Solvent	CAS-No.	Supplier
Acetonitrile [1]	75-05-8	VWR Int. (Darmstadt, Germany)
Chloroform [2]	67-66-3	VWR Int. (Darmstadt, Germany)
Chloroform-d [3]	865-49-6	Euriso-Top (Saint-Aubin Cedex, France)
Deuterium oxide [3]	7789-20-0	Euriso-Top (Saint-Aubin Cedex, France)
Dichloromethane [4]	75-09-2	Bernd Kraft (Duisburg, Germany)
*N,N-D*imethylformamide [5]	68-12-2	Iris Biotech (Marktredewitz, Germany)
Dimethyl sulfoxide [6]	67-68-5	Sigma-Aldrich (Munich, Germany)
Ethanol absolute [4]	64-17-5	VWR Int. (Darmstadt, Germany)
Ethyl acetate [7]	141-78-6	Staub & Co. (Nürnberg, Germany)
n-Heptane [8]	142-82-5	Grüssing (Filsum, Germany)
n-Hexane [8]	110-54-3	Brenntag (Mülheim/Ruhr, Germany)
Methanol [4]	67-56-1	Fisher Scientific (Schwerte, Germany)
Methanol-d4 [3]	811-98-3	Euriso-Top (Saint-Aubin Cedex, France)
Methyl-*tert*-butyl ether [9]	1634-04-4	Brenntag (Mülheim/Ruhr, Germany)
N-Methyl-2-pyrrolidone [5]	872-50-4	Iris Biotech (Marktredewitz, Germany)
Tetrahydrofuran [4]	109-99-9	Fisher Scientific (Schwerte, Germany)
Water [10]	7732-18-5	In-house purification

[1] HPLC grade; [2] DAB grade; [3] NMR grade (> 99.9 %); [4] analytical grade; [5] peptide grade; [6] BioReagent grade (> 99.9 %); [7] purum, distilled before use; [8] purissimum; [9] synthesis grade; [10] purified, deionized.

Table 2.2 Reagents used for experimental procedures

Reagent	CAS-No.	Supplier
1-Hydroxybenzotriazole	123333-53-9	Sigma-Aldrich (Munich, Germany)
2-Chlorotritylchloride resin	42074-68-0	Iris Biotech (Marktredewitz, Germany)
Acetic acid	64-19-7	Sigma-Aldrich (Munich, Germany)
Acetic anhydride	108-24-7	Sigma-Aldrich (Munich, Germany)
Agarose NEEO Ultra	9012-36-6	Carl Roth (Karlsruhe, Germany)
Bromophenol blue	115-39-9	Sigma-Aldrich (Munich, Germany)
DBCO-dPEG®$_{24}$-TFP ester	11370	Quanta Biodesign (Powell, OH, USA)
DBCO-maleimide	760668	Sigma-Aldrich (Munich, Germany
DBCO-N-hydroxysuccinimidyl ester	761524	Sigma-Aldrich (Munich, Germany
DBU	6674-22-2	Sigma-Aldrich (Munich, Germany)
Dde-L-Lys(Fmoc)-OH	156648-40-7	Iris Biotech (Marktredewitz, Germany)
Dibenzocyclooctyne(DBCO)-acid	1353016-70-2	Sigma-Aldrich (Munich, Germany)
Diisopropylcarbodiimid (DIC)	693-13-0	Sigma-Aldrich (Munich, Germany)
EDTA disodium salt dihydrate	6381-92-6	Sigma-Aldrich (Munich, Germany)
Fmoc-8-aminooctanoic acid	126631-93-4	Iris Biotech (Marktredewitz, Germany)
Fmoc-Ala-Wang resin	856001	Sigma-Aldrich (Munich, Germany)

Fmoc-L-Ala-OH* H_2O	35661-39-3	Iris Biotech (Marktredewitz, Germany)
Fmoc-L-Arg(Pbf)-OH	154445-77-9	Iris Biotech (Marktredewitz, Germany)
Fmoc-D-Arg(Pbf)-OH	187618-60-6	Iris Biotech (Marktredewitz, Germany)
Fmoc-L-Asn(Trt)-OH	71989-14-5	Iris Biotech (Marktredewitz, Germany)
Fmoc-L-Asp(OtBu)-OH	71989-14-5	Iris Biotech (Marktredewitz, Germany)
Fmoc-D-Asp(OtBu)-OH	112883-39-3	Iris Biotech (Marktredewitz, Germany)
Fmoc-L-Cys(Trt)-OH	103213-32-7	Iris Biotech (Marktredewitz, Germany)
Fmoc-L-Glu-O*t*Bu	84793-07-7	Merck Millipore (Darmstadt, Germany)
Fmoc-L-Gln(Trt)-OH	132327-80-1	Iris Biotech (Marktredewitz, Germany)
Fmoc-L-Gly-OH	29022-11-5	Iris Biotech (Marktredewitz, Germany)
Fmoc-L-His(Trt)-OH	109425-51-6	Iris Biotech (Marktredewitz, Germany)
Fmoc-D-His(Trt)-OH	135610-90-1	Iris Biotech (Marktredewitz, Germany)
Fmoc-L-Ile-OH	71989-23-6	Iris Biotech (Marktredewitz, Germany)
Fmoc-D-Ile-OH	143688-83-9	Iris Biotech (Marktredewitz, Germany)
Fmoc-L-Leu-OH	35661-60-0	Iris Biotech (Marktredewitz, Germany)
Fmoc-D-Leu-OH	114360-54-2	Iris Biotech (Marktredewitz, Germany)
Fmoc-L-Lys(Boc)-OH	71989-26-9	Iris Biotech (Marktredewitz, Germany)
Fmoc-D-Lys(Boc)-OH	92122-45-7	Iris Biotech (Marktredewitz, Germany)
Fmoc-L-Lys(Fmoc)-OH	78081-87-5	Iris Biotech (Marktredewitz, Germany)
Fmoc-L-Lys(ivDde)-OH	204777-78-6	Iris Biotech (Marktredewitz, Germany)
Fmoc-L-Lys(N_3)-OH	159610-89-6	Iris Biotech (Marktredewitz, Germany)
Fmoc-L-Met-OH	71989-28-1	Iris Biotech (Marktredewitz, Germany)
Fmoc-D-Met-OH	112883-40-6	Iris Biotech (Marktredewitz, Germany)
Fmoc-L-Phe-OH	35661-40-6	Iris Biotech (Marktredewitz, Germany)
Fmoc-D-Phe-OH	86123-10-6	Iris Biotech (Marktredewitz, Germany)
Fmoc-L-Pro-OH* H_2O	71989-31-6	Iris Biotech (Marktredewitz, Germany)
Fmoc-L-Ser(tBu)-OH	71989-33-8	Iris Biotech (Marktredewitz, Germany)
Fmoc-D-Ser(tBu)-OH	128107-47-1	Iris Biotech (Marktredewitz, Germany)
Fmoc-L-Thr(tBu)-OH	71989-35-0	Iris Biotech (Marktredewitz, Germany)
Fmoc-D-Thr(tBu)-OH	138797-71-4	Iris Biotech (Marktredewitz, Germany)
Fmoc-L-Trp(Boc)-OH	43824-78-6	Iris Biotech (Marktredewitz, Germany)
Fmoc-D-Trp(Boc)-OH	163619-04-3	Iris Biotech (Marktredewitz, Germany)
Fmoc-L-Tyr(tBu)-OH	71989-38-3	Iris Biotech (Marktredewitz, Germany)
Fmoc-D-Tyr(tBu)-OH	118488-18-9	Iris Biotech (Marktredewitz, Germany)
Fmoc-L-Val-OH	68858-20-8	Iris Biotech (Marktredewitz, Germany)
Fmoc-D-Val-OH	84624-17-9	Iris Biotech (Marktredewitz, Germany)
Fmoc-*N*-amido-dPEG$_{24}$-acid	756526-01-9	Quanta Biodesign (Powell, OH, USA)
Fmoc-OSu	82911-69-1	Iris Biotech (Marktredewitz, Germany)
Fmoc-Stp(Boc_3)-OH	-	In-house synthesis [100]
GelRed	-	Biotium Inc. (Hayward, CA, USA)
HBTU	94790-37-1	Multisyntech (Witten, Germany)
HEPES	7365-45-9	Biomol (Hamburg, Germany)
H-Rink-Amide-ChemMatrix®	CM-7600	Iris Biotech (Marktredewitz, Germany)
Hydrazine monohydrate	7803-57-8	Sigma-Aldrich (Munich, Germany)
Hydrochloric acid solution	7647-01-0	Sigma-Aldrich (Munich, Germany)
MTT	298-93-1	Sigma-Aldrich (Munich, Germany)
Myristic acid	544-63-8	Sigma-Aldrich (Munich, Germany)
N,N-Diisopropylethylamine	7087-68-5	Iris Biotech (Marktredewitz, Germany)
N-Hydroxysuccinimide (NHS)	6066-82-6	Sigma-Aldrich (Munich, Germany)
Ninhydrin	485-47-2	Sigma-Aldrich (Munich, Germany)
Oleic acid	112-80-1	Sigma-Aldrich (Munich, Germany)
Phenol	108-95-2	Sigma-Aldrich (Munich, Germany)
Piperidine	110-89-4	Iris Biotech (Marktredewitz, Germany)
Potassium cyanide	151-50-8	Sigma-Aldrich (Munich, Germany)
Pybop®	128625-52-5	Multisyntech GmbH (Witten, Germany)
Sephadex® G-10	9050-68-4	GE Healthcare (Freiburg, Germany)
Sephadex® G-25	17-0033-01	Sigma-Aldrich (Munich, Germany)
Sodium hydroxide (anhydrous)	1310-73-2	Sigma-Aldrich (Munich, Germany)
Sodium hydroxide solution	1310-73-2	Sigma-Aldrich (Munich, Germany)

STOTDA	172089-14-4	Sigma-Aldrich (Munich, Germany)
Succinic anhydride	108-30-5	Sigma-Aldrich (Munich, Germany)
Super DHB	63542-76-7	Sigma-Aldrich (Munich, Germany)
TCEP	51805-45-9	Sigma-Aldrich (Munich, Germany)
Tetraethylene pentamine·5HCl	4961-41-5	Sigma-Aldrich (Munich, Germany)
Transferrin human	11096-38-0	Sigma-Aldrich (Munich, Germany)
Triethylamine	121-44-8	Sigma-Aldrich (Munich, Germany)
Trifluoroacetic acid	76-05-1	Iris Biotech (Marktredewitz, Germany)
Triisopropylsilane	6485-79-6	Sigma-Aldrich (Munich, Germany)
Triton™ X-100	9002-93-1	Sigma-Aldrich (Munich, Germany)

Table 2.3 Buffers used for experimental procedures

Buffer	Composition
10 mM HCl SEC solvent	693 mL water, 300 mL acetonitrile, 7 mL 1M HCl solution
Electrophoresis loading buffer	6 mL glycerine, 1.2 mL 0.5 M EDTA solution (pH 8.0), 2.8 mL H_2O, 20 mg bromophenol blue
Ellman buffer	0.1 M sodium phosphate buffer (pH 8.0), 1 mM EDTA
HBG	20 mM HEPES, 5 % glucose, pH 7.4
TBE buffer	89 mM Trizma® base, 89 mM boric acid, 2 mM EDTA-Na_2

2.1.2 Nucleic acids

Plasmid pCMVLuc (encoding *Photinus pyralis* firefly luciferase under control of cytomegalovirus promotor and enhancer)[242] was obtained from Plasmid Factory GmbH (Bielefeld, Germany). siRNA duplexes were obtained from Axolabs GmbH (Kulmbach, Germany): eGFP-targeting siRNA (siGFP), sense strand: 5'-AuAucAuGGccGAcAAGcAdTsdT-3'; antisense strand: 5'-UGCUUGUCGGCcAUGAuAUdTsdT-3') for silencing of eGFPLuc; control siRNA (siCtrl) (sense strand: 5'-AuGuAuuGGccuGuAuuAGdTsdT-3'; antisense strand: 5'-CuAAuAcAGGCcAAuAcAUdTsdT-3'); small letters: 2′methoxy; s: phosphorothioate linkage. Linear polyethylenimine (L-PEI) 22kDa was synthesized as described before.[243, 244]

2.1.3 Carbon dots

Carbon dots were provided by the collaboration partner Rongqin Huang, Fudan University, Shanghai, China, of the Joint Sino-German Research Project collaboration (LRP1-targeted carbon nanodots for crossing BBB and delivering small molecule or protein drugs into the brain).[167, 245]

2.1.4 Cell culture

Cell culture work was carried out by Şurhan Göl, Mina Yazdi, Anna-Lina Lessel, Fengrong Zhang, Simone Berger (Pharmaceutical Biotechnology, LMU), and Rebekka Spellerberg (Klinikum LMU). All cell culture media, antibiotics, and fetal bovine serum (FBS) were purchased from Invitrogen (Karlsruhe, Germany). The human erythroleukemic suspension cell line K-562 (ATCC CCL-243), the human adherent cervix carcinoma cell line KB (DSMZ ACC136, Hela subline), the human prostate carcinoma cell line DU-145 (DSMZ ACC 261) were cultured in RPMI-1640 medium and the murine adherent neuroblastoma cell line Neuro-2a (N2a, ATCC CCL-131) and Human brain glioblastoma cell line (U87) was cultured in Dulbecco's Modified Eagle Medium (DMEM)-low glucose (1 g/l glucose). KB/eGFPLuc and DU145/eGFPLuc cells stably transfected with the eGFPLuc (enhanced green fluorescent protein/luciferase) fusion gene,[58, 98, 99] were also grown in RPMI-1640 medium. The cell culture mediums were supplemented with 10% FBS, 4 mM L-glutamine, 100 U/ml penicillin and 100 µg/mL streptomycin. All cells were kept at 37°C and 5 % CO_2 in an incubator with a relative humidity of 95%.

2.2 Methods

2.2.1 Loading of a 2-chlorotrityl resin with Fmoc protected amino acid

First 1 g of 2-chlorotrityl chloride resin (1.17 mmol chloride) was swollen in water-free DCM for 20 to 30 min, the first Fmoc-protected α-*L*-amino acid (0.45 equiv Fmoc-*L*-Arg(Pbf)-OH, Fmoc-N-amido-dPEG$_{24}$-acid) dissolved in water-free DCM and DIPEA (1.35 equiv) were added to the resin, and it was incubated for 1 h. The reaction solvent was drained and a mixture of DCM/methanol/DIPEA (50:40:10) was added for an incubation of 30 – 60 min. After removal of the reaction mixture, the resin was washed three times with DMF, three times with DCM and two times with n-hexane in this order. Then the resin was dried *in vacuo*. Around 30 mg of the dry resin was collected to determine the loading efficacy of the resin. Therefore, three precisely measured resin samples were taken and were treated with 1 ml deprotection solution (20% (v/v) piperidine in DMF) for an incubation of 90 min under constant shaking. After centrifugation, 25 µl of supernatant was diluted with 975 µl DMF and absorption was measured at wavelength λ = 301 nm. For the blank 25 µl of protection solution was diluted with 975 µl DMF. The loading was then calculated with help of following equation: $\textit{resin load [mmol/g]} = \frac{A \times 1000}{m\,[mg] \times 7800 \times f}$ with *f* as dilution factor. Afterward, the whole resin was deprotected by a four-time treatment with 20% (v/v) piperidine in DMF for 10 min each. The deprotected resin was washed three times with DMF and three times with DCM. It was then dried *in vacuo* and stored at 4°C until usage. In case of peptide syntheses of reTfR and scr-reTfR conjugates, a H-Rink-Amide-ChemMatrix resin was used.

2.2.2 Loading of a four-armed branching core Fmoc-Ala-Wang resin

Due to the sterically demanding branched four-arm oligomers, a very low load of the four-arm branching core was used to avoid aggregation, as published by Lächel et al.[246] 600 mg of Fmoc-Ala-Wang resin (loading 0,3 mmol/g) was weighed into a 10 mL syringe reactor and pre-swelled with DCM (10 mL/g resin) for 20 min, using an overhead shaker Heidolph Reax 2 at 65 rpm. All solvents were mixed with 1 % of Triton™ X-100 (v/v). The resin was Fmoc deprotected. 0,25 equiv of Fmoc-L-Lys(Fmoc)-OH relative to free resin-bound amines was coupled on the Ala-Wang resin. In order to create a low loading resin, the rest of the free amino groups were

blocked by acetylating with a 10-fold excess of acetic anhydride (3,5 mmol/g resin; acetic anhydride and DIPEA in ratio of 8450/330/1220 µL/g resin). It was incubated 1 h. In the next step, resin was deprotected and coupled first with 8 equiv of Fmoc-L-His(Trt)-OH and second with 8 equiv Fmoc-L-Lys(Fmoc)-OH according to the first amount of Fmoc-L-Lys(Fmoc)-OH. 8 equiv of PyBOP, HOBt and 16 equiv of DIPEA was added. DMF and DCM were used as solvents. Before the last Fmoc deprotection, resin was dried under vacuum and loading was subsequently determined with exception that 20 % of piperidine, 2 % of DBU and 1 % of Triton™ X-100 in DMF (v/v) was used. Washed resin was dried under vacuum and stored in the fridge at 7 °C. To check if the coupling was successful, mini cleave was performed.

2.2.3 OAA and DBCO agent synthesis

Oligoaminoamids (OAAs) were synthesized using a 2-chlorotrityl resin preloaded with the first c-terminal amino acid of the respective topology as solid support. All sequences and topologies of OAAs can be found in **6.2**, all sequences of targeting and shielding agents based on DBCO motifs and azido-based motifs can be found in **6.3**. Unless otherwise stated, coupling steps were carried out using 4 equiv Fmoc-amino acid, 4 equiv HOBt, 4 equiv PyBOP or HBTU and 8 equiv DIPEA (10 mL g^{-1} resin) for 90 min. General steps of a manual and automated synthesis are shown in **Table 2.4** and **Table 2.5**.

Table 2.4 General steps of a manual synthesis cycle

Step	Description	Solvent	Volume	Time
1	Coupling	DCM/DMF 50/50	5 mL g^{-1} resin	90 min
2	Wash	DMF, DCM	10 mL g^{-1} resin	3 x 1 min DMF 3 x 1 min DCM
3	Kaiser test	-	-	-
4	Fmoc deprotection	20 % piperidine/DMF	10 mL g^{-1} resin	4 x 10 min
5	Wash	DMF, DCM	10 mL g^{-1} resin	3 x 1 min DMF 3 x 1 min DCM
6	Kaiser test	-	-	-

Table 2.5 General steps of an automatic synthesis cycle

Step	Description	Solvent	Volume	Time
1	Coupling	NMP/DMF	5 mL g^{-1} resin	90 min

2	Double-coupling	NMP/DMF	5 mL g^{-1} resin	90 min
3	Wash	DMF	8 mL g^{-1} resin	5 x 1 min
4	Fmoc deprotection	20 % piperidine/DMF	7 mL g^{-1} resin	4 x 10 min
5	Wash	DMF	8 mL g^{-1} resin	5 x 1 min

2.2.3.1 Synthesis of Lipo-OAAs

Lipo-OAAs were synthesized under normal Fmoc-based SPPS conditions with a 2-chlorotrityl chloride resin as solid support, which was preloaded with the first c-terminal amino acid. The backbone of each OAA was synthesized by using a Syro Wave synthesizer (Biotage, Uppsala, Sweden). The artificial amino acid building block Fmoc-Stp(Boc)$_3$-OH as well as the solid-phase compatible redox-sensitive disulfide building block (ssbb) were synthesized as analyzed before.[247, 248] Reagents were arranged in separate bottles as follows: four equiv of 1-hydroxybenzotriazole (HOBt) were dissolved in NMP, four equiv of 2-(1H-benzotriazol-1-yl)-1,1,3,3-tetramethyluronium-hexafluorophosphate (HBTU) in N,N-dimethylformamide (DMF), four equiv of Fmoc-α-*L*-amino acid were dissolved in DMF and eight equiv of N,N-diisopropylethylamine (DIPEA) in N-methyl-2-pyrrolidone (NMP). Each coupling was performed twice in 10 mL/g resin for 60 minutes at 50 °C temperature (RT) (double couplings), for the synthesizer. The couplings by hand were done as a single coupling with 120 minutes of incubation time. All cysteine couplings were done at room temperature to prevent initial cross linking of the thiol groups. Deprotection was done four times for 10 minutes each with 20% (v/v) piperidine in DMF (10 mL/g resin). After each coupling and deprotection step, a washing step of five cycles with DMF followed by a one-minute incubation step (10 mL/g resin) was done. Symmetrical branching points were introduced using Fmoc-*L*-Lys(Fmoc)-OH, and asymmetric branching points were introduced using Fmoc-*L*-Lys(Dde)-OH. Removal of the N-(1-(4,4-dimethyl-2,6-dioxocyclohexylidene)ethyl) (Dde) protection group was performed with 2% (v/v) hydrazine in DMF for 15 cycles, each with an incubation of two minutes. Then, the resin was cleaned with DMF for five cycles of one-minute incubation each, with 10% (v/v) DIPEA in DMF for five cycles of two minute-incubation each, and finally with DMF for six cycles of one minute-incubation each. With the whole lipo-OAA sequence completed, the resin was dried in vacuo prior to cleavage. The sequences with ssbb were cleaved off the resin by incubation with a mixture (10 mL/g resin) of 95% (v/v) TFA, 2.5% (v/v) H_2O and 2.5% (v/v) TIS for 90 minutes at RT. Cysteine-containing sequences were treated with a cleavage cocktail

(10 mL/g resin) consisting of 94% (v/v) TFA, 2.5% (v/v) H_2O, 2.5% (v/v) 1,2-ethanedithiol (EDT) and 1% (v/v) TIS. The lipo-OAAs were immediately precipitated in 40 mL – 20°C precipitation cocktail, consisting of 3 parts n-hexane to 1-part methyl *tert*-butyl ether (MTBE). After centrifugation (4000 g, 4°C, 15 minutes), the pellets were dried in vacuo or under a fume cupboard at room temperature with an N_2 gas flow. When fully dry the pellets were resolved in H_2O. Size exclusion chromatography was used to purify the OAA solution, using an Äkta system (GE Healthcare Bio-Sciences AB, Uppsala, Sweden) based on a P-900 solvent pump module, a UV-900 spectrophotometrical detector, a pH/C-900 conductivity module, a Frac-950 automated fractionator and a Sephadex G-10 column. 10 mM HCl / ACN 7:3 was used as solvent. The purified OAA solutions were lyophilized using a Christ Alpha 2-4 LDplus laboratory freeze-drier (Martin Christ Gefriertrocknungsanlagen, Osterode am Harz, Germany). OAA identities were validated by mass spectrometry and ^{1}H-NMR spectroscopy.

2.2.3.2 Synthesis of 4-armed OAAs

Four-armed OAA were synthesized under special Fmoc-based SPPS conditions with a preloaded Fmoc-Ala-Wang resin. The backbone of each OAA was synthesized by using a Syro Wave synthesizer (Biotage, Uppsala, Sweden). Reagents were arranged in separate bottles as follows: four equiv of 1-hydroxybenzotriazole (HOBt) were dissolved in DMF with 1 % Triton™ X-100 (v/v), four equiv of 2-(1H-benzotriazol-1-yl)-1,1,3,3-tetramethyluronium-hexafluorophosphate (HBTU) in N,N-dimethylformamide (DMF) with 1 % Triton™ X-100 (v/v), four equiv of Fmoc-amino acid were dissolved in the HOBt solution and eight equiv of N,N-diisopropylethylamine (DIPEA) in N-methyl-2-pyrrolidone (NMP) with 1 % Triton™ X-100 (v/v). Each coupling was performed twice in 10 mL/g resin for 12 minutes at 75 °C temperature (double couplings), for the synthesizer. The couplings by hand were done as a single coupling with 120 minutes of incubation. All cysteine couplings were done at room temperature (RT) to prevent initial cross linking of the thiol groups. Deprotection was done four times for 12 minutes each with 20 % (v/v) piperidine, 2 % DBU (v/v) and 1 % Triton™ X-100 (v/v) in DMF (10 mL/g resin). After each coupling and deprotection step, a washing step of five cycles with DMF followed by a one-minute incubation step (10 mL/g resin) was done. Symmetrical branching points were

introduced using Fmoc-*L*-Lys(Fmoc)-OH. With the whole four-armed OAA sequence completed, the resin was dried in vacuo prior to cleavage. The cysteine-containing sequences were treated with a cleavage cocktail (10 mL/g resin) consisting of 94 % (v/v) TFA, 2.5 % (v/v) H_2O, 2.5 % (v/v) 1,2-ethanedithiol (EDT) and 1 % (v/v) TIS. The four-armed OAAs were immediately precipitated in 40 mL – 20°C precipitation cocktail, consisting of 3 parts n-hexane to 1-part methyl *tert*-butyl ether (MTBE). After centrifugation (4000 g, 4°C, 15 minutes), the pellets were dried in vacuo or under a fume cupboard at room temperature with an N_2 gas flow. When fully dry the pellets were resolved in H_2O. Size exclusion chromatography was used to purify the OAA solution, using an Äkta system (GE Healthcare Bio-Sciences AB, Uppsala, Sweden) based on a P-900 solvent pump module, a UV-900 spectrophotometrical detector, a pH/C-900 conductivity module, a Frac-950 automated fractionator and a Sephadex G-10 column. 10 mM HCl / ACN 7:3 was used as solvent. The purified OAA solutions were lyophilized using a Christ Alpha 2-4 LDplus laboratory freeze-drier (Martin Christ Gefriertrocknungsanlagen, Osterode am Harz, Germany). OAA identities were validated by ^{1}H-NMR spectroscopy.

2.2.3.3 Synthesis of DBCO PEG shielding and targeting agents

After preparing the preloaded resin via swelling the structures were synthesized via solid-phase assisted peptide synthesis (SPPS) as described in previous report**.** [249, 250] The scheme of manual and automatic synthesis is described in **Table 2.4** and **Table 2.5**.

2.2.3.4 Synthesis of DBCO-PEG_{24} (PEG-1) and $DBCO_2$-STOTDA$_2$-K-PEG_{24} (PEG-2)

Manual couplings were performed as a single coupling with 2 h of incubation time using PyBOP as coupling reagent of choice. In the case of PEG-2, an additional symmetrical branching point was introduced after PEG_{24} coupling by Fmoc-*L*-Lys(Fmoc)-OH. N-Fmoc-N″-succinyl-4,7,10-trioxa-1,13-tridecanediamine (Fmoc-STOTDA-OH) was used as short hydrophilic spacer. Both for PEG-1 and PEG-2, the SPPS was completed by N-terminal coupling of DBCO-COOH. Cleavage from solid phase was performed under mild conditions with a mixture of 90% (v/v) DCM, 5% (v/v) TFA, 2.5% (v/v) H_2O and 2.5% (v/v) TIS.[35] Both DBCO agents were purified by

preparative HPLC (high performance liquid chromatography), lyophilized and mass was confirmed by mass spectrometry (MALDI-TOF).

2.2.3.5 Syntheses of R-PEG-1 and R-PEG-2

R-PEG-1 (DBCO-PEG_{24}-R) and R-PEG-2 ($DBCO_2$-$STOTDA_2$-K-PEG_{24}-R) were synthesized by loading a 2-chlorotrityl chloride resin with Fmoc-*L*-Arg(Pbf)-OH and, after Fmoc deprotection, coupling with a Fmoc-PEG_{24}-OH. Manual couplings were performed as a single coupling with 2 h of incubation time using PyBOP as coupling reagent of choice. In case of R-PEG-2, a branching lysine (Fmoc-(*L)*-Lys(Fmoc)-OH) was coupled followed by an additional PEG-spacer (Fmoc-STOTDA-OH). After structures were cleaved off the resin in the form of free N-terminal amines, they were dried and redissolved in HEPES buffer (20 mM, pH 7.4); the pH was adjusted using 1 M NaOH to 8.5 to ensure effective subsequent conjugation of the primary amines in solution with 1.2 equiv of DBCO-NHS ester per amine in DMF for 2 hours. Both DBCO agents were purified by preparative HPLC (high performance liquid chromatography), lyophilized and their mass was confirmed by mass spectrometry (MALDI-TOF). Introducing DBCO directly on solid phase is not possible due to the arginine Pbf protective group, which requires higher concentrations of TFA for deprotection than tolerated by DBCO.

2.2.3.6 Syntheses of targeting ligand conjugates reTfR-1 and reTfR-2 and their scrambled analogues

The syntheses of DBCO-PEG_{24}-TfRre (reTfR-1) and $DBCO_2$-$STOTDA_2$-K-PEG_{24}-TfRre (reTfR-2) were performed under normal Fmoc-based SPPS conditions. A H-Rink-Amide-ChemMatrix resin was used to create an amide group on the c-terminus of peptides. No initial coupling of the first amino acid or Fmoc deprotection was needed. The sequence of reTfR (H_2N-pwvpswmpprht-$CONH_2$) was synthesized by using (*D*)-amino acids and carried out by automated SPPS using a Syro Wave synthesizer (Biotage, Uppsala, Sweden). Reagents for the synthesizer were arranged in separate bottles as follows: four equiv of HOBt were dissolved in NMP together with four equiv of the respective Fmoc-α-(*D)*-amino acid, four equiv of HBTU in DMF, eight equiv of DIPEA in NMP. Each coupling on the synthesizer was performed twice

in 10 ml/g resin for 60 min at 50 °C temperature (RT) (double couplings). Fmoc-deprotection was done four times for 10 min each with 20% (v/v) piperidine in DMF (10 ml/g resin). After each coupling and deprotection step, a washing step of five cycles with DMF (10 ml/g resin) followed by a one-minute incubation step (10 ml/g resin) was done. Once the reTfR peptide was synthesized and the terminal Fmoc deprotected, Fmoc-dPEG$_{24}$-OH was coupled to the N-terminus. In case of reTfR-2, an additional Fmoc-Lys(Fmoc)-OH was coupled after Fmoc-dPEG$_{24}$-OH to introduce a symmetrical branching point, and after Fmoc deprotection, Fmoc-STOTDA-OH was conjugated to the two free amino groups of the deprotected lysine.[251] The reTfR-1 and reTfR-2 precursor structures containing free terminal amines were cleaved from the resin by incubation with TFA/H_2O/TIS (95:2.5:2.5, 10 ml/g resin) for 90 min, followed by immediate precipitation in 40 ml of precooled n-hexane / MTBE (3:1). The precipitation products were dried and redissolved in HEPES buffer (20 mM, pH 7.4); the pH was adjusted with a 1 M NaOH solution to 8.5 to ensure effective subsequent conjugation of the primary amines with 1.2 equiv DBCO-NHS ester, which is solved in DMF. The mix was incubated for 2 h and then purified by preparative HPLC (LaPrep system, VWR International GmbH, Darmstadt, Germany) and a Waters SymmetryPrep C18 column (7 µm, 19×150 mm) with an acetonitrile (ACN)/H_2O gradient with 0.1% TFA (5% ACN to 100% ACN over 20 min). The products were lyophilized and identified by mass spectrometry (MALDI-TOF). The scrambled DBCO-PEG peptide conjugates of reTfR (scr-reTfR: H_2N-vprhptsppmww-$CONH_2$) scr-reTfR-1 and scr-reTfR-2 were synthesized accordingly.

2.2.3.7 Syntheses of targeting ligand conjugates DBCO-PEG$_{12}$-Transferrin and DBCO-PEG$_{12}$-Albumin

Transferrin from human plasma was dissolved in HEPES buffer (20 mM, pH 7.4), DBCO-PEG$_{12}$-NHS ester was dissolved in DMSO. For the coupling reaction 2 equiv of DBCO-PEG$_{12}$-NHS was used. The reaction mixture was incubated for 3 h at room temperature under shaking and afterward purified by SEC using the Äkta purifier system (GE Healthcare Bio-Sciences AB, Uppsala, Sweden) based on a P-900 solvent pump module, a UV-900 spectrophotometrical detector, a pH/C-900 conductivity module, a Frac-950 automated fractionator and a Sephadex G-25 column. HEPES 20 mM, pH 7.4 was used as solvent. The purified DBCO-PEG$_{12}$-

Transferrin solutions was lyophilized. The protein concentration was determined by Bradford assay. The control DBCO-PEG protein conjugates of DBCO-PEG_{12}-Transferrin, DBCO-PEG_{12}-Human serum albumin (HAS) was synthesized accordingly.

2.2.3.8 Syntheses of targeting ligand conjugates DBCO-Tf2 and its scrambled analogon

For synthesizing DBCO-PEG_{24}-Tf2 (DBCO-CPEG_{24}-GGG-HKYLRW-COOH) a 2-chlorotrityl resin was preloaded with Fmoc-L-Trp(Boc)-OH, which is the first c-terminal amino acid of the Tf2 sequence. The structure up to the Fmoc-dPEG_{24}-OH was completed by automated SPSS (solid phase supported synthesis). Starting at Fmoc-dPEG_{24}-OH the remaining structure was manually coupled and Fmoc deprotected. After Fmoc deprotection of Fmoc-L-Cys(Trt)-OH, the structure was cleaved of the resin by incubation with TFA/EDT/H_2O/TIS (94:2.5:2.5:1, 10 mL/g resin) for 90 min, followed by immediate precipitation in 40 mL of precooled n-hexane - MTBE (3+1). The precipitated product was dried and resolved in HEPES buffer (20 mM, pH 7.4). The pH was adjusted using 1 M NaOH to 6,5 to ensure a sufficient maleimide reaction for chemical conjugation to the sulfhydryl of the sequence to create a stable thioether linkage. The DBCO-maleimide was solved in DMF. 2 equiv of DBCO-maleimide were used. The mixture was incubated for 16h at 4 °C in a shaking device and then purified by preparative HPLC (LaPrep system, VWR InternationalGmbH, Darmstadt, Germany) and a Waters SymmetryPrep C18column (7 µm, 19×150 mm) with an ACN/H_2O gradient with 0.1%TFA (5% ACN to 100% ACN over 20 min). The targeting ligand was lyophilized using a Christ Alpha 2-4 LDplus laboratory freeze-drier (Martin Christ Gefriertrocknungsanlagen, Osterode am Harz, Germany). The identity was validated by mass spectrometry. The scrambled DBCO-PEG peptide conjugates of Tf2 (scr-Tf2: DBCO-CPEG_{24}-GGG-WRKHLY-COOH) was synthesized accordingly.

2.2.3.9 Syntheses of targeting ligand conjugates DBCO-L57, its scrambled analogon, its retro-enantio version and its control Angiopep-2

For synthesizing DBCO-PEG$_{24}$-L57 (DBCO-CPEG$_{24}$-TWPKHFDKHTFYSILKLGKH-COOH) a 2-chlorotrityl resin was preloaded with Fmoc-L-His(Trt)-OH, which is the first c-terminal amino acid of the L57 sequence. The structure up to the Fmoc-dPEG$_{24}$-OH was completed by automated SPSS. Starting at Fmoc-dPEG$_{24}$-OH the remaining structure was manually coupled and Fmoc deprotected. After Fmoc deprotection of Fmoc-L-Cys(Trt)-OH, the structure was cleaved of the resin by incubation with TFA/EDT/H_2O /TIS (94:2.5:2.5:1, 10 mL/g resin) for 90 min, followed by immediate precipitation in 40 mL of precooled n-hexane - MTBE (3+1). The precipitated product was dried and resolved in HEPES buffer (20 mM, pH 7.4). The pH was adjusted using 1 M NaOH to 6,5 to ensure a sufficient maleimide reaction for chemical conjugation to the sulfhydryl of the sequence to create a stable thioether linkage. The DBCO-maleimide was solved in DMF. 2 equiv of DBCO-maleimide were used. The mixture was incubated for 16h at 4 °C in a shaking device and then purified by preparative HPLC (LaPrep system, VWR InternationalGmbH, Darmstadt, Germany) and a Waters SymmetryPrep C18column (7 µm, 19×150 mm) with an ACN/H_2O gradient with 0.1%TFA (5% ACN to 100% ACN over 20 min). The targeting ligand was lyophilized using a Christ Alpha 2-4 LDplus laboratory freeze-drier (Martin Christ Gefriertrocknungsanlagen, Osterode am Harz, Germany). The identity was validated by mass spectrometry. The scrambled DBCO-PEG peptide conjugates of L57 (scr-L57: DBCO-CPEG$_{24}$-KPFKHGTDLLKHFWYSHTKI-COOH) its retro-enantio version (DBCO-CPEG$_{24}$-hkGlklisyfthkdfhkpwt-COOH) and its control peptide on which it is originated, Angiopep-2 (DBCO-CPEG$_{24}$-TFFYGGSRGKRNNFKTEEY-COOH) were synthesized accordingly.

2.2.3.10 Syntheses of targeting ligand conjugates DBCO-cRGD

For synthesizing DBCO-cRGD (DBCO-PEG$_{24}$-c(RGDfK)) a 2-chlorotrityl resin was preloaded with Fmoc- Fmoc-L-Gly-OH, which is the first c-terminal amino acid of the non-cyclic RGD peptide. The structure up to the Fmoc-L-Asp(OtBu)-OH was completed by automated SPSS. After Fmoc deprotection of the aspartic acid residue, the structure was cleaved of the resin by incubation with TFA/DCM/TIS (5:92.5:2.5, 10 mL/g resin) for 30 min, followed by immediate precipitation in 40 mL of precooled

n-hexane - MTBE (3+1). The mild cleavage of 5 % TFA is used to cleave of the aliphatic peptide sequence from the 2-chlorotrityl resin, while letting the protection groups of the amino acids intact. The precipitated product was dried and resolved in DMF:DCM mixture (1:1). The cyclisation, created through reaction of the free amino group of the aspartic acid with the free carboxylic group of the glycine was done with using 16 h of incubation. The reaction mix was evaporated using reduced pressure till fully dry. The dry material was fully redissolved in a cleave cocktail of TFA/H_2O/TIS (95:2.5:2.5, 10 ml/g resin) and incubated for 90 min, followed by immediate precipitation in 40 ml of precooled n-hexane / MTBE (3:1). The precipitation products were dried and redissolved in HEPES buffer (20 mM, pH 7.4). The purification was done by preparative HPLC (LaPrep system, VWR InternationalGmbH, Darmstadt, Germany) and a Waters SymmetryPrep C18column (7 µm, 19×150 mm) with an ACN/H_2O gradient with 0.1%TFA (5% ACN to 100% ACN over 20 min). The targeting ligand was lyophilized using a Christ Alpha 2-4 LDplus laboratory freeze-drier (Martin Christ Gefriertrocknungsanlagen, Osterode am Harz, Germany). The identity was validated by mass spectrometry. The finished H_2N-c(RGDfK) was redissolved in HEPES buffer (20 mM, pH 7.4); the pH was adjusted with a 1 M NaOH solution to 8.5 to ensure effective subsequent conjugation of the primary amines with 1.2 equiv DBCO-dPEG$_{24}$-TFP, which is solved in DMF. The mix was incubated for 6 h and then purified by preparative HPLC (LaPrep system, VWR International GmbH, Darmstadt, Germany) and a Waters SymmetryPrep C18 column (7 µm, 19×150 mm) with an acetonitrile (ACN)/H_2O gradient with 0.1% TFA (5% ACN to 100% ACN over 20 min). The product was lyophilized and identified by mass spectrometry (MALDI-TOF).

2.2.3.11 Syntheses of targeting ligand conjugates DBCO-TGN

For synthesizing DBCO-PEG$_{24}$-TGN (DBCO-CPEG$_{24}$-TGNYKALHPHNG-COOH) a 2-chlorotrityl resin was preloaded with Fmoc-L-Gly-OH, which is the first c-terminal amino acid of the TGN sequence. The structure up to the Fmoc-dPEG$_{24}$-OH was completed by automated SPSS. Starting at Fmoc-dPEG$_{24}$-OH the remaining structure was manually coupled and Fmoc deprotected. After Fmoc deprotection of Fmoc-L-Cys(Trt)-OH, the structure was cleaved of the resin by incubation with TFA/EDT/H_2O/TIS (94:2.5:2.5:1, 10 mL/g resin) for 90 min, followed by immediate precipitation in 40 mL of precooled n-hexane - MTBE (3+1). The precipitated product

was dried and resolved in HEPES buffer (20 mM, pH 7.4). The pH was adjusted using 1 M NaOH to 6,5 to ensure a sufficient maleimide reaction for chemical conjugation to the sulfhydryl of the sequence to create a stable thioether linkage. The DBCO-maleimide was solved in DMF. 2 equiv of DBCO-maleimide were used. The mixture was incubated for 16h at 4°C in a shaking device and then purified by preparative HPLC (LaPrep system, VWR InternationalGmbH, Darmstadt, Germany) and a Waters SymmetryPrep C18column (7 µm, 19×150 mm) with an ACN/H_2O gradient with 0.1%TFA (5% ACN to 100% ACN over 20 min). The targeting ligand was lyophilized using a Christ Alpha 2-4 LDplus laboratory freeze-drier (Martin Christ Gefriertrocknungsanlagen, Osterode am Harz, Germany). The identity was validated by mass spectrometry.

2.2.3.12 Syntheses of targeting ligand conjugates DBCO-cdx

For synthesizing the D-peptide DBCO-PEG_{24}-cdx (DBCO-CPEG_{24}-GreirtGraerwsekf-COOH) a 2-chlorotrityl resin was preloaded with Fmoc-D-Phe-OH, which is the first c-terminal amino acid of the cdx sequence. The structure up to the Fmoc-dPEG_{24}-OH was completed by automated SPSS. Starting at Fmoc-dPEG_{24}-OH the remaining structure was manually coupled and Fmoc deprotected. After Fmoc deprotection of Fmoc-L-Cys(Trt)-OH, the structure was cleaved of the resin by incubation with TFA/EDT/H_2O/TIS (94:2.5:2.5:1, 10 mL/g resin) for 90 min, followed by immediate precipitation in 40 mL of precooled n-hexane - MTBE (3+1). The precipitated product was dried and resolved in HEPES buffer (20 mM, pH 7.4). The pH was adjusted using 1 M NaOH to 6,5 to ensure a sufficient maleimide reaction for chemical conjugation to the sulfhydryl of the sequence to create a stable thioether linkage. The DBCO-maleimide was solved in DMF. 2 equiv of DBCO-maleimide were used. The mixture was incubated for 16h at 4°C in a shaking device and then purified by preparative HPLC (LaPrep system, VWR InternationalGmbH, Darmstadt, Germany) and a Waters SymmetryPrep C18column (7 µm, 19×150 mm) with an ACN/H_2O gradient with 0.1%TFA (5% ACN to 100% ACN over 20 min). The targeting ligand was lyophilized using a Christ Alpha 2-4 LDplus laboratory freeze-drier (Martin Christ Gefriertrocknungsanlagen, Osterode am Harz, Germany). The identity was validated by mass spectrometry.

2.2.3.13 Syntheses of targeting ligand conjugates azido-reTfR1

For synthesizing the D-peptide Azido-PEG_{24}-TfR (N_3K-PEG_{24}-pwvpswmpprht-$CONH_2$) a H-Rink-Amide-ChemMatrix resin was used to create an amide group on the c-terminus of peptides. No initial coupling of the first amino acid or Fmoc deprotection was needed. The structure up to the Fmoc-dPEG_{24}-OH was completed by automated SPSS. Starting at Fmoc-dPEG_{24}-OH the remaining structure was manually coupled and Fmoc deprotected. After Fmoc deprotection of Fmoc-L-Lys(N3)-OH, the structure was cleaved of the resin by incubation with TFA/EDT/H_2O/TIS (94:2.5:2.5:1, 10 mL/g resin) for 90 min, followed by immediate precipitation in 40 mL of precooled n-hexane - MTBE (3+1). The precipitated product was dried and resolved in HEPES buffer (20 mM, pH 7.4). The Azido-PEG_{24}-TfR was purified by preparative HPLC (LaPrep system, VWR InternationalGmbH, Darmstadt, Germany) and a Waters SymmetryPrep C18column (7µm, 19×150 mm) with an ACN/H_2O gradient with 0.1%TFA (5% ACN to 100% ACN over 20 min). The targeting ligand was lyophilized using a Christ Alpha 2-4 LDplus laboratory freeze-drier (Martin Christ Gefriertrocknungsanlagen, Osterode am Harz, Germany). The identity was validated by mass spectrometry.

2.2.3.14 Syntheses of targeting ligand conjugates azido-cRGD

For synthesizing Azido-cRGD (N_2K-c(RGDfK(N_3))) a 2-chlorotrityl resin was preloaded with Fmoc- Fmoc-L-Gly-OH, which is the first c-terminal amino acid of the non-cyclic RGD peptide. To introduce a azido motif Fmoc-L-Lys(N3)-OH was used instead of Fmoc-L-Lys(Boc)-OH. The structure up to the Fmoc-L-Asp(OtBu)-OH was completed by automated SPSS. After Fmoc deprotection of the aspartic acid residue, the structure was cleaved of the resin by incubation with TFA/DCM/TIS (5:92.5:2.5, 10 mL/g resin) for 30 min, followed by immediate precipitation in 40 mL of precooled n-hexane - MTBE (3+1). The mild cleavage of 5 % TFA is used to cleave of the aliphatic peptide sequence from the 2-chlorotrityl resin, while letting the protection groups of the amino acids intact. The precipitated product was dried and resolved in DMF:DCM mixture (1:1). The cyclisation, created through reaction of the free amino group of the aspartic acid with the free carboxylic group of the glycine was done like stated in **2.2.3.10** with using 16 h of incubation time. The reaction mix was

evaporated using reduced pressure till fully dry. The dry material was fully redissolved in a cleave cocktail of TFA/H_2O/TIS (95:2.5:2.5, 10 ml/g resin) and incubated for 90 min, followed by immediate precipitation in 40 ml of precooled n-hexane / MTBE (3:1). The precipitation products were dried and redissolved in HEPES buffer (20 mM, pH 7.4). The purification was done by preparative HPLC (LaPrep system, VWR InternationalGmbH, Darmstadt, Germany) and a Waters SymmetryPrep C18column (7 µm, 19×150 mm) with an ACN/H_2O gradient with 0.1%TFA (5% ACN to 100% ACN over 20 min). The targeting ligand was lyophilized using a Christ Alpha 2-4 LDplus laboratory freeze-drier (Martin Christ Gefriertrocknungsanlagen, Osterode am Harz, Germany). The identity was validated by mass spectrometry.

2.2.4 Kaiser test

Free amines of deprotected amino acids on resin were determined qualitatively by Kaiser test[252]. To that extent, a small sample of DCM/DMF washed resin was transferred into an Eppendorf reaction tube. One drop each of following was used: 80 % phenol in EtOH (w/v), 5 % ninhydrin in EtOH (w/v) and 20 µM potassium cyanide (KCN) in pyridine (mixture of 1 mL aqueous 0.001 M KCN solution and 49 mL pyridine). The mixture was incubated at 99°C for 4 min under steady shaking. The presence of free amines was indicated by a deep blue color.

2.2.5 Cleavage conditions

2.2.5.1 General cleavage conditions

If not mentioned differently SPPS products were cleaved off the resin by incubation with TFA - EDT - H_2O - TIS (94:2.5:2.5:1.0; 10 mL g−1 resin) for 90 min. The cleavage solution was concentrated by flushing nitrogen. SPPS products were precipitated in 50 mL of pre-cooled MTBE–n-hexane (1:3). All OAAs were purified by size exclusion chromatography (SEC) using an Äkta purifier system (GE Healthcare Bio-Sciences AB, Uppsala, Sweden), a Sephadex G-10 column and 10 mM hydrochloric acid solution - acetonitrile (7:3) as solvent. The relevant fractions were lyophilized, obtaining HCl salts of all OAAs.

2.2.5.2 Cleavage of OAAs containing oleic acid

Due to reactive double bonds of oleic acid the cleavage of OAAs containing oleic acid was optimized by Reinhard et al.[253] The OAA still bound on resin was incubated with a mixture of TFA - EDT - H_2O - TIS (94 : 2.5 : 2.5 : 1.0; 10 mL g−1 resin, cooled to 4°C prior to addition) for 30 min, followed by immediate precipitation in 50 mL of pre-cooled MTBE - n-hexane (1:3). All OAAs were purified by size exclusion chromatography (SEC) using an Äkta purifier system (GE Healthcare Bio-Sciences AB, Uppsala, Sweden), a Sephadex G-10 column and 10 mM hydrochloric acid solution - acetonitrile (7:3) as solvent. The relevant fractions were lyophilized, obtaining HCl salts of all OAAs.

2.2.5.3 Cleavage of DBCO containing agents

If not mentioned differently SPPS products were cleaved off the resin by incubation with TFA - EDT - H_2O - TIS (94 : 2.5 : 2.5 : 1.0; 10 mL g−1 resin) for 90 min. The cleavage solution was concentrated by flushing nitrogen. SPPS products were precipitated in 50 mL of pre-cooled MTBE–n-hexane (1 : 3). All Targeting Ligand conjugates upon finishing were purified by preparative HPLC (LaPrep system, VWR InternationalGmbH, Darmstadt, Germany) and a Waters SymmetryPrep C18column (7 µm, 19×150 mm) with an ACN/H_2O gradient with 0.1%TFA (5% ACN to 100% ACN over 20 min).

2.2.6 siRNA and pDNA polyplex formation

siRNA or pDNA and lipo-OAAs at an indicated nitrogen/phosphate ratio (N/P) of 12 were separately diluted in equal volume of 20 mM HEPES buffer with 5% glucose (HBG buffer, pH 7.4). The N/P ratio was calculated under consideration of only protonatable nitrogens. Then nucleic acid and lipo-OAA solutions were rapidly mixed by pipetting (10 times) and incubated 45 min for siRNA and 30 min for pDNA formulations at room temperature (RT).

2.2.7 Carbon dot OAA formation

Red Carbon dots (rCDs) and oligoaminoamides (OAAs) were separately diluted in equal volume (50:50 (v%/v%) of HEPES buffer (20 mM; pH 7,4). The compaction and stability of this formed nano-complex is highly dependent of the ratio of OAA to rCD. For example, the ratio of rCD to 1696 (m/m) of 1 µg rCD to 4,56 µg of 1696 (m/m) were shown to work the best. rCD-OAA particle are prepared by flash mixing OAAs and rCDs by pipetting (10 times) followed by a 1 h incubation at room temperature (RT).

2.2.7.1 Preparation of stock solutions

To ensure minimal errors based on pipetting and scaling, it is beneficial to create stock solutions of 10 mg/mL (I) and furthermore dilute them to the end concentration of 1 mg/mL (II). As solvent for the carrier 1696, water can be used. For the peptide ligands, HEPES (20 mM; pH 7,4) is a more suiting solvent due to its more stable and inert characteristics towards DBCO agents, which are known for their acid-catalyzed 5-endodig cyclo-isomerization. For red CDs, a 0,1 mg/mL stock solution in H_2O was used. Before using the stock solution of rCD it was centrifuged for 10 min at 7000 g. For adjusting the end volume of the rCD-1696 particle solution the red CD solution is further diluted (see 2. rCD-1696). All stock solutions and working solutions can be stored in a freezer at -20 °C. The stock solutions 10 mg/mL of 1696 and all the ligands 1 to 11 can be created directly in the vials, in which they are sent to exclude loss of reagents and errors due to scaling. For example, dissolve the 22.3 mg lyophilized 1696 directly in 2.23 mL water.

2.2.7.2 rCD-1696 – coating and entrapment

All following quantities relate to the end volume of rCD-OAA of 100 µL. In case of adjusting the end volume, all following quantities must be changed accordingly! Studies have shown that the ratio of rCD solution to 1696 solution is most effective at a ratio of 50:50 (v%/v%). The formation of the rCD-1696 particles is spontaneous and accords due to electrostatic and hydrophobic interactions upon mixing negatively charged rCDs with positively charged 1696 oligoaminoamide (OAA). The compaction and stability of this formed nano-complex is highly dependent of the ratio of 1696 to rCD. The ratio of rCD to 1696 (m/m) of 1 µg rCD to 4,56 µg of 1696 (m/m) were

shown to work the best. For the incubation time of rCD-1696 to ensure efficient caging and entrapment of rCDs 1 h is chosen. After 1 h the benefit of additional entrapment is negligible. All incubation steps are done at room temperature.

2.2.7.3 rCD-1696 targeting via strain-promoted azide-alkyne cycloaddition (SPAAC) reaction

Further surface functionalization to enable the integration of following peptide ligands, bearing DBCO motifs (1 to 9 and 11), can be achieved with SPAAC, since 1696 has 4 N-terminal azidolysine groups. The amount of DBCO agents is calculated according to corresponding equivalents (equiv) of azido-oligomer (1696). The equivalents represent the molar ratio of DBCO agent to azido agent. Since 1696 as a 4-arm has 4 azidolysine moiety's a mol-to-mol ratio of hypothetically one clicked arm of the four arms would have an equivalent of 0,25. Two clicked arms would have an equivalent of 0,5 and so on. In our lab on our systems 0,5 equiv seems to be a good ratio of DBCO-ligand agent to azido-carrier, which is why in the following all the calculations are done with 0,5 equiv. However, it is important to underline, that all equiv from 0,25 to 1 or even higher should get tested! As volume of DBCO agent to the created rCD-1696 particles ¼ is used. Resulting in 20 µL of DBCO agent working solution for a total volume of 100 µL rCD-1696.

2.2.8 Post-modification/functionalization with DBCO agents

The amount of DBCO agents is calculated according to corresponding equivalents (equiv) of azido-oligomer (azido-OAA). The equivalents represent the molar ratio of DBCO agent to azido agent. For post-functionalization, a minimum of at least 0.25 equiv of DBCO agent (dissolved in HEPES buffer (20 mM; pH 7,4)) per azido-lipo-OAA or azido-4-armed-OAA were added to polyplex or carbon dot solution. This mixture was rapidly mixed at least 5x by pipetting and incubated for 4 h at RT. For comparison, the same procedures were also performed with nonmodified polyplexes, but HBG was added instead of modifying agents. As volume of DBCO agent to the created rCD-4-armed-OAA or the pDNA/siRNA-lipo-OAA particles ¼ was used.

2.2.9 Particle size and zeta potential

Particle size and zeta potential were measured in a folded capillary cell (DTS1070) by Zetasizer Nano ZS with backscatter detection (Malvern Instruments, Worcestershire, Germany). Nonmodified and modified (0.5 equiv of DBCO agents) pDNA polyplexes were prepared with final pDNA concentration of 1 µg pDNA in a total volume of 125 µl HBG. After size measurement, the pDNA samples were diluted to 800 µl with HBG and zeta potential measurement was done. In the case of siRNA, polyplexes were prepared with 4 µg siRNA in a total volume of 20 µl HBG, which was diluted with HEPES before measurement. For size (z-average) and PDI measurements, the equilibration time was 0 min, the temperature was 25 °C, refractive index was 1.330 and the viscosity was 0.8872 mPa·s. For the zeta potential measurements 15 sub runs at 25°C were chosen. The Smoluchowski equation was used for calculation of zeta-potential. All samples were measured in triplicate.

2.2.10 Transmission electron microscopy (TEM)

Polyplexes were prepared as described in 2.2.6, but in water instead of HBG. Carbon coated copper grids (Ted Pella, Inc. USA, 300 mesh, 3.0 mm O.D.) were hydrophilized by argon plasma (420 V, 1 min). They were placed on a 10 µl sample droplet for 3 min. Then the droplet was removed, and the grid was washed with 5 µl of staining solution (1.0% uranyl formate in purified water). Immediately afterward, it was stained for 5 sec with the same solution. The solution was removed, and the grid was allowed to be dried for 20 min. All grids were analyzed with a JEOL JEM-1100 (JEOL, Tokyo, Japan) electron microscope at 80 kV acceleration voltage. It was performed by Ö. Öztürk (Pharmaceutical Biotechnology, LMU).

2.2.11 Ellman's assay

30 µL rCD-OAA particle solution was mixed with 170 µL working solution (2.44 mL Ellman´s buffer (0.2 M Na_2HPO_4, 1 mM EDTA, pH 8.0) and 60 µL DTNB solution in methanol (c = 4 mg mL^{-1})). After 15 min incubation at 37°C absorption was measured at 412 nm using a GENESYS^{TM} UV-VIS spectrophotometer (Thermo Scientific). The

percentage of free mercapto groups is based on the theoretical amount (100 %) of thiols in case of full cleavage.

2.2.12 Agarose gel shift assay

An agarose gel of 1 % agarose was prepared by dissolving agarose in TBE buffer (10.8 g of trizma base, 5.5 g of boric acid, 0.75 g of disodium EDTA, and 1 L of water) followed by short boiling till everything was solved. After cooling down, GelRed™(Biotium, Inc., Hayward, CA, USA was added for nucleic acid detection. pDNA and siRNA polyplexes were prepared as described in **2.2.6**.

2.2.13 Ethidium bromide (EtBr) exclusion assay

pDNA polyplexes (2 µg pDNA, 200 µl polyplex volume) were formed at N/P 12 as described above and optionally modified with 0.5 equiv of PEG-1. Free pDNA (2 µg in 200 µl HBG) was used to determine the 100% value and HBG was used as blank. 700 µl of an EtBr solution (concentration: 0.5 µg/ml) was added to each sample of the modified and nonmodified polyplex solutions. After an incubation time of 3 min, the fluorescence intensity of EtBr was measured using a Cary Eclipse Fluorescence Spectrophotometer (Varian, which is now part of Agilent Technologies, Germany). The excitation wavelength was set to λ ex = 510 nm, and the emission wavelength to λ_{em} = 590 nm. The data is presented as fluorescence intensity of EtBr related to free pDNA.

2.2.14 Luciferase gene transfer

K562 suspension cells were seeded in 96-well plates with 3 × 104 cells per well at 2‑3 h before pDNA transfection. N2a cells were seeded in 96-well plates 1 × 104 per well at 24 h. Then the medium was replaced with 75µl of the fresh serum-containing medium right before the transfection. Polyplex solutions (N/P 12, 25 µl HBG containing 200 ng of pCMVLuc) were then added to each well. HBG and LPEI polyplexes (N/P 6) were used as negative and positive control, respectively. All samples and controls were performed in triplicate. K562 cells were incubated for 24 h at 37 °C. N2a cells were incubated for 4 h with polyplexes, then medium was

replaced, and the cells were incubated for further 20 h at 37 °C. Read-out (luciferase activity or metabolic activity measurement) was conducted 24 h after transfection. In the case of the luciferase assay, 100 µl of lysis buffer (12.5 mM tris(hydroxymethyl) aminomethane buffer (pH 7.8) with phosphoric acid, 1 mM dithiothreitol (DTT), 2 mM 1,2-diaminocyclohexane-N,N,N’,N’-tetraacetic acid (CDTA), 5% glycerol, 0.5% Triton® X-100; Promega, Mannheim, Germany) was added to each well and incubated for 45 min at RT. Luciferase activity was measured with a Centro LB 960 plate reader luminometer (Berthold Technologies, Bad Wildbad, Germany) in 35 µl cell lysate using a LAR buffer solution (20 mM glycylglycine, 1 mM $MgCl_2$, 0.1 mM EDTA, 3.29 mM DTT, 0.548 mM ATP (adenosine 5′ - triphosphate), 0.0013 mM Coenzyme A stock solution; pH 8-8.5) supplemented with 10% (v/v) of a mixture of 10 mM luciferin and 29.375 mM glycylglycine.

2.2.15 Cell viability assay (CellTiter-Glo® Assay)

For the cell viability assay, after 24 h incubation medium was removed and replaced with 25 µl of medium and 25 µl of CellTiter-Glo® Reagent (Promega, Mannheim, Germany) each well. Samples were incubated on an orbital shaker for 30 min at RT and measured with Centro LB 960 plate reader luminometer (Berthold Technologies, Bad Wildbad, Germany). The relative cell viability (in %) was calculated according to HBG- treated negative control cells by following formula: [A] test/[A] control × 100

2.2.16 Gene silencing mediated by GFP siRNA

The gene silencing activity was measured in KB/eGFPLuc or DU145/eGFP cells expressing eGFP (enhanced green fluorescent protein)-luciferase fusion reporter gene upon transfection with siRNA polyplexes. For this purpose, the cells were seeded in 96-well-plate (5 × 103 cells/well) 24 h prior to transfection followed by replacement with 80 µl of fresh medium. The corresponding polyplexes were prepared at N/P ratio of 12 with 500 ng of control siRNA (siCtrl) or GFP-siRNA (siGFP for targeting GFPLuc protein) in 20 µl HBG. The cells in triplicate were transfected with siRNA polyplexes for 1 or 4 h at 37°C. Then the medium containing polyplexes was replaced by fresh medium and incubated for further 47 or 44 h,

respectively. After a total incubation time of 48 h, the transfection efficiency was measured using a luminometer as aforementioned. The RLU are presented as percentage of the luciferase gene expression of the HBG buffer-treated cells.

2.2.17 Cell viability assay (MTT)

MTT assays were performed by using U87/eGFPLuc cells. 5000 cells per well were seeded onto 96-well plates, and medium was replaced with 80 µL fresh growth medium after 24 h. rCD-OAA (25 mg / mL of rCD) solutions were added to each well in 20 µL volume and incubated for 24 h at 37 °C. The medium was removed and 10 µL if MTT was added, followed by 4 h incubation. The mixture was removed and 100 µL DMSO was added, and 15 min incubated at 37 °C. MTT assay (Life Technologies, Darmstadt, Germany) was performed and measured using a SpectraFluor Plus microplate reader to evaluate the cytotoxicity. The experiments were performed in triplicates and the cell viability was calculated as percentage compared to untreated control cells.

2.2.18 siRNA and pDNA binding assay

A 2.5% (w/w) agarose gel for siRNA or a 1% (w/w) agarose gel for pDNA was prepared with TBE buffer (trizma base 10.8 g, boric acid 5.5 g, disodium EDTA 0.75 g, and 1 L of water). After boiling and cooling down to about 50 °C, GelRed (Biotium, Inc., Hayward, CA, USA) was added and the solution was casted in the electrophoresis unit. Polyplexes (containing 500 ng siRNA or 200 ng of pDNA in 20 µl HBG) were prepared and then mixed with 4 µL loading buffer (6 ml of glycerin, 1.2 ml of 0.5 M EDTA, 2.8 ml of H_2O, 0.02 g of bromophenol blue). All samples were transferred into the gel pockets and electrophoresis was performed at 120 V for 80 min in TBE buffer.

2.2.19 Cellular association assay

K562 suspension cells were seeded in 96-well plates with 3 × 104 cells per well at 2‑3 h before the experiment. N2a cells were seeded in 96-well plate with 2 × 104 cells per well, and KB and DU145 cells in 24-well plates at a density of 5 × 104 cells per

well at 24 h before the experiment. Prior to transfection, the medium was replaced by 75 µl of fresh medium per well for 96-wellplate and 450 µl for 24-well-plate. For treatment, polyplexes were prepared containing 200 ng pDNA (in 25 µl HBG including 20% Cy5 labeled pDNA) or 1.35 µg siRNA (in 50 µl HBG including 20% Cy5 labeled siRNA). HBG was used as negative control. All experiments were performed in triplicate. Seeded cells were incubated with corresponding polyplexes for 45 min at 37°C in 5% CO_2 and washed with phosphate-buffered saline (PBS) three times. Adherent cells were detached with trypsin/EDTA, centrifuged and cell pellets were resuspended in PBS buffer with 10% FBS for subsequent measurement. For the transferrin blockade experiment, same procedure was done, however, cells were incubated with free iron saturated human transferrin (hTf), 5 mg/ml, for 30 min on ice prior to transfection to block and deplete the cell surface transferrin receptors. Cellular association was measured by CytoFLEX S flow cytometer (Beckman Coulter, Brea, CA, USA) through excitation of Cy5 at 635 nm and detection of emission at 665 nm. Cells were gated based on the forward- and side-scatter profile. Dead cells were detected by 4′ ,6-diamidino-2-phenylindole fluorescence (DAPI) staining. FlowJo®7.6.5 flow cytometric analysis software (FlowJo, Ashland, OR, USA) was used for data analyses.

2.2.20 RP-HPLC analysis

Purity of the synthesized DBCO-PEG-reagents was analyzed by RP-HPLC using a VWR Hitachi Chromaster HPLC system (5160 pump module, 5260 auto sampler, 5310 column oven, 5430 diode array detector), a C18-column (YMC column, HS-302, HS12S05-1546WT, 150 x 4.6 mm I.D., S-5 µm, 12 nm, YMC Europe GmbH, Dinslaken, Germany) with aqueous 0.1 % TFA and an acetonitrile gradient of 5% (first 5 min), 5-40% (within 15 min), 40-95% (within 5 min).

2.2.21 Evaluation of the SPAAC reaction by HPLC and MALDI MS

The click-reaction of azido-lipo-OAA 1284 and DBCO agent R-PEG-1 at a molar ratio of 1:1 was monitored via HPLC (detection wavelength: 280 nm) at time points 0 h (mixing) and 4 h. The successfully clicked conjugate was also confirmed by MALDI mass (positive mode). HPLC analysis was performed using a VWR Hitachi

Chromaster HPLC system (5160 pump module, 5260 auto sampler, 5310 column oven, 5430 diode array detector), a C18-column (YMC column, HS-302, HS12S05-1546WT, 150 x 4.6 mm I.D., S-5 µm, 12 nm, YMC Europe GmbH, Dinslaken, Germany) and a gradient of 5 % to 50 % acetonitrile with 0.1 % TFA in 10 min, followed by 50 % to 100 % acetonitrile with 0.1 % TFA in 15 min.

2.2.22 Proton ^{1}H NMR spectroscopy

^{1}H-NMR spectra were recorded using an AVANCE III HD500 (500 MHz) by Bruker with a 5 mm CPPBBO probe. Spectra were recorded without TMS as internal standard and therefore all signals were calibrated to the residual proton signal of the deuterium oxide (D_2O) solvent. Chemical shifts are reported in ppm and refer to the solvent as internal standard (D_2O at 4.79 ppm). Integration was performed manually. The spectra were analyzed using MestreNova (Ver.12.0.3 by MestReLab Research). Integrals were normalized to the succinic acid peaks in terms of Stp containing OAAs. For four armed OAAs Imidazole peaks were taken for normalizing the peak.

2.2.23 MALDI mass spectrometry

1 µL matrix solution (10 mg/ml sDHB (super-DHB: 9:1 (w/w) mixture of 2,5-dihydroxybenzoic acid and 2-hydroxy-5-methoxybenzoic acid) in TA30 (AcN/H_2O (3:7) with 0.1% (v/v) TFA)) and 1.5 µL of sample solution (conc. 0.5 mg/ml) were spotted together on a MTP AnchorChip (Bruker Daltonics, Bremen, Germany) and were mixed before co-crystallization started. After co-crystallization, the spots were analyzed in positive or negative reflector mode using an Autoflex II mass spectrometer (Bruker Daltonics, Bremen, Germany).

2.2.24 Statistical analysis

Statistical analysis of the results (mean ± sd) was evaluated by two-tailed t-test (unpaired). Significance levels were set as ns, not significant; *$p \leq 0.05$, **$p \leq 0.01$, ***$p \leq 0.001$, ****$p \leq 0.0001$.

2.2.25 Evaluation of the SPAAC reaction by HPLC and MALDI MS

The click-reaction of azido-lipo-OAA 1284 and DBCO agent R-PEG-1 at a molar ratio of 1:1 was monitored via HPLC (detection wavelength: 280 nm) at time points 0 h (mixing) and 4 h. The successfully clicked conjugate was also confirmed by MALDI mass (positive mode). HPLC analysis was performed using a VWR Hitachi Chromaster HPLC system (5160 pump module, 5260 auto sampler, 5310 column oven, 5430 diode array detector), a C18-column (YMC column, HS-302, HS12S05-1546WT, 150 x 4.6 mm I.D., S-5 µm, 12 nm, YMC Europe GmbH, Dinslaken, Germany) and a gradient of 5 % to 50 % acetonitrile with 0.1 % TFA in 10 min, followed by 50 % to 100 % acetonitrile with 0.1 % TFA in 15 min.

3 Results

3.1 Transferrin receptor targeted polyplexes completely comprised of sequence-defined components

This chapter has been adapted from:

Benli-Hoppe, T., Göl, S., Öztürk, Ö., Berger, S., Wagner, E., Yazdi, M. (2022) Transferrin Receptor Targeted Polyplexes Completely Comprised of Sequence-Defined Components. Macromol. Rapid Commun. 2022, 43, e2100602.

(Benli-Hoppe and Göl are equal first authors and therefore equally contributed to this paper. Benli-Hoppe oversaw the synthesis part, Göl was in charge of the pDNA part, and the corresponding author Yazdi oversaw the siRNA part of this paper):

3.1.1 Introduction

Cancer gene therapy is a promising alternative for conventional cancer treatments.[254-259] Both viral vectors and synthetic nanocarriers have been explored for local or systemic administration of genetic materials in cancer patients. In this respect, the holy grail would present intravenously applied nanosystems with enhanced systemic circulation, protection against undesired interaction with cellular and other biological agents, and efficient accumulation in tumors of patients by passive and active targeting principles (see **1.5** and **1.6**). Building on good surface shielding against blood components by well-thought macromolecular designs [260-262] and the well-investigated EPR effect,[263] already impressive achievements have been made such as for tumor-targeted delivery of chemotherapeutic nanoagents.[2, 264, 265] For effective delivery of therapeutic nucleic acids, several additional requirements have to be fulfilled, such as protection of the nucleic acid cargo, and tumor-specific intracellular uptake, efficient endosomal escape, and transfer and release of the nucleic acid cargo (siRNA or pDNA) in an active form in the proper intracellular compartment.[266-268] Synthetic nucleic acid carriers were developed over several decades, including cationic peptides and polymers (forming ‘polyplexes’), liposomes (forming ‘lipoplexes’ or lipid nanoparticles ‘LNPs’), dendrimers, inorganic nanoparticles, and hybrid systems.[13, 31, 269-274] (see **1.1** to **1.3**).Ideally, these vehicles need to be biocompatible and non-toxic, and available in well-defined synthetic form and pharmaceutical grade.

For active tumor-targeted uptake of therapeutic nucleic acids, receptor-mediated endocytosis into tumor cells is an encouraging strategy. The transferrin receptor (TfR) appears as a suitable choice for tumor targeting, due to its low levels of expression in the majority of normal human cells and its overexpression in various types of tumor cells.[139, 140] The 80 kDa serum protein transferrin (Tf) transports iron into the cells via TfR-mediated endocytosis, and iron is needed for DNA synthesis, cell division, and cellular metabolism.[141] Research efforts have utilized the TfR-mediated cellular uptake for delivery of peptides, proteins, drug formulations, and nucleic acids.[20, 142-145, 147, 149, 151, 152, 156, 157, 275-284] Transferrin-guided nucleic acid delivery has already reached the stage of clinical testing in humans in the case of *ex vivo* pDNA transfer into patient tumor cells[159, 285] and *in vivo* delivery of siRNA into tumors.[286, 287]

The use of a large serum-derived protein in a pharmaceutical formulation presents a challenge with regard to precise incorporation chemistry as well as a suitable protein source and stability. Smaller synthetic ligands for the same receptor would be preferable. Lee et al. reported a 12-amino acid short TfR-targeting peptide (sequence: H-THRPPMWSPVWP-NH_2), which was identified by phage display. This peptide specifically binds the TfR at a region that differs from the binding site of the natural ligand Tf, and can promote efficient cellular uptake via receptor-mediated endocytosis.[162] To overcome the rapid degradability of this standard peptide sequence by serum proteases (with a half-life of ~30 min only), Ernest Giralt and colleagues synthesized a protease-resistant retro-enantio peptide (reTfR), containing all amino acids in *(D)*-configuration and in a reversed N to C sequence order (H-pwvpswmpprht-NH_2).[288]

The aim of the present study was to incorporate this small synthetic reTfR ligand as targeting module into nucleic acid polyplexes that are totally based on precise, sequence-defined components. Compacting siRNA or pDNA with previously developed T-shaped lipo-oligoaminoamides (lipo-OOAs)[164, 289] into nanoparticles followed by modification with monodisperse polyethylene glycol (PEG) and the reTfR ligand resulted in enhanced gene silencing or gene transfer, respectively, in receptor-expressing cells.

3.1.2 Results

3.1.2.1 Design and Synthesise of Sequence-Defined Polyplex Core Shell Components

In the first step, siRNA or pDNA were compacted into core nanoparticles (**Scheme 1, top**) using recently designed sequence-defined T-shaped lipo-OAAs.[164, 165] In the second step, the nanoparticles were modified with a shell of PEG-conjugated ligands. Lipo-OAAs (**Scheme 1, bottom**) contain an N-terminal azido-lysine, which can be utilized for dibenzocyclooctyne (DBCO)-PEG-ligand attachment by strain-promoting alkyneazide cycloaddition.[35, 164, 165, 249, 250] Ligands such as reTfR or controls are linked with a monodisperse PEG_{24} spacer as surface shielding agent via one or two N-terminally attached DBCO groups (**Scheme 3.2**). In literature, the click reaction between DBCO and azide units is stated to be selective, holds high yield and has good reaction kinetics.[290-292] We proved the successful DBCO coupling to our azido-bearing carriers via high-performance liquid chromatography (HPLC) and Matrix-Assisted Laser Desorption/ Ionization Time-Of-Flight (MALDI-TOF) mass spectrometry, exemplarily for the click reaction between azido-lipo-OAA 1284 (**Scheme 3.1**) and DBCO agent R-PEG-1 (**Scheme 3.2**). After a reaction time of 4 h (the used incubation time for polyplex post functionalization in this study), the main educts peaks on HPLC disappeared and a new peak is visible, indicating the successful click-reaction (**6.4.3**). The conjugate formation was confirmed by MALDI mass spectrometry (**6.4.3**). Notably, all nanocarrier subunits (core and shell) present sequence-defined materials that were synthesized in a precise manner by solid-phase supported peptide/polymer synthesis (SPPS). The design and selection of lipo-OAA core and reTfRPEG shell subunits are explained in Subsections **3.1.2.2** and **3.1.2.3**.

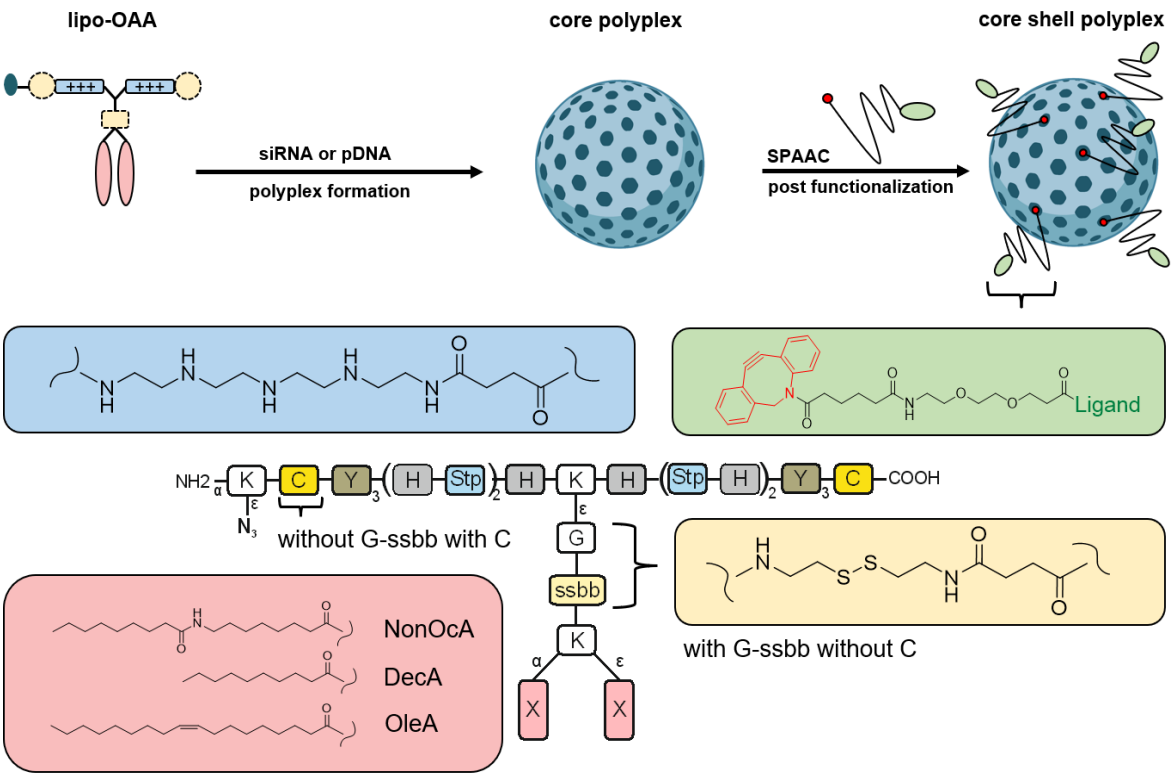

Lipo-OAA ID Number	Sequences (N → C)
1284	H_2N-K(N_3)-Y_3-(H-Stp)$_2$-H-K(G-ssbb-K(DecA)$_2$)-H-(Stp-H)$_2$-Y_3-COOH
1276	H_2N-K(N_3)-C-Y_3-(H-Stp)$_2$-H-K(K(DecA)$_2$)-H-(Stp-H)$_2$-Y_3-C-COOH
1285	H_2N-K(N_3)-Y_3-(H-Stp)$_2$-H-K(G-ssbb-K(NonOcA)$_2$)-H-(Stp-H)$_2$-Y_3-COOH
1258	H_2N-K(N_3)-C-Y_3-(H-Stp)$_2$-H-K(K(NonOcA)$_2$)-H-(Stp-H)$_2$-Y_3-C-COOH
1218	H_2N-K(N_3)-Y_3-(H-Stp)$_2$-H-K(G-ssbb-K(OleA)$_2$)-H-(Stp-H)$_2$-Y_3-COOH
1214	H_2N-K(N_3)-C-Y_3-(H-Stp)$_2$-H-K(K(OleA)$_2$)-H-(Stp-H)$_2$-Y_3-C-COOH

Scheme 3.1. Formation of pDNA or siRNA core–shell lipo-polyplexes in a two-step process. Upper part: pDNA or siRNA core lipo-polyplexes were prepared by flash mixing lipo-oligoaminoamides (lipo-OAAs) and nucleic acid and then incubated for 30 and 45 min, respectively. Postfunctionalization via strainpromoted alkyne-azide cycloaddition (SPAAC) for 4 h was performed with mono- or bivalent DBCO-PEG_{24}-ligand reagents containing a TfR-targeted peptide (reTfR) or controls as described in Scheme 3.2. Lower part: sequences of the investigated lipo-oligoaminoamides. The ID numbers are database identification numbers. K(N3): azido-lysine; C: cysteine; Y: tyrosine; H: histidine; G: glycine; Stp: succinoyl-tetraethylene-pentamine; ssbb: succinoylcystamine as disulfide building block; X: fatty acid residues of different chain lengths; NonOcA: 8-nonanamidooctanoic acid; DecA: decanoic acid; OleA: oleic acid.

3.1.2.2 Selection of Azido Lipo-OAAs

Different nucleic acid cargos such as siRNA or pDNA have different biophysical properties and intracellular target compartments and therefore require different nanocarriers for their delivery.[293] In optimization of carriers by 'chemical evolution' for different cargos,[294] clear and accurate structure-activity relations must be available. Natural evolution is based on optimizing sequences; therefore, our aim also has been to define nanocarriers as distinct clear sequences.[272, 295] For this purpose, we previously adapted SPPS of sequence-defined polymers[96, 296, 297] by designing succinoyl-tetraethylene-pentamine (Stp) as a new building block in Fmoc and $(Boc)_3$-protected form.[97, 98, 102, 298] This 'artificial amino acid' can be assembled into defined oligoaminoamides (OAAs). Based on the aminoethylene units of Stp, which are also contained in the gold standard transfection agent polyethylenimine (PEI),[81] nucleic acids can be complexed via electrostatic interactions with the nitrogens that in part are protonated at neutral pH; after cellular uptake, additional cationization of aminoethylene units at endosomal pH can promote endosomal escape into the cytosol. The incorporation of protonizable histidines for endosomal buffering was found to further enhance transfections.[65, 299] Cysteines enhance polyplex stability by intermolecular disulfide cross-links,[65, 98] and a redox-sensitive disulfide block (ssbb) supported intracellular release and improved cytocompatibility.[248] An initial screen of a broad range of OAA sequences and topologies had revealed that for the larger pDNA cargo a good condensation into compact nanoparticles is a key prerequisite,[299, 300] whereas for the far smaller siRNA a good polyplex stabilization is important. In the latter respect, the corporation of lipid domains as well as tyrosine tripeptides (Y3) into OAAs was found to favorably stabilize siRNA polyplexes.[98, 301] In the current study, six T-shaped lipo-OAAs were evaluated (**Scheme 3.1, bottom**), which differ in their lipidic diacyl side chains attached to the cationizable OAA backbone via a central branching lysine (K): decanoic acid (DecA), nonamido octanoic acid (NonOcA), or oleic acid (OleA). These lipo-OAAs have either a glycine-disulfide block (G-ssbb) at the branching point, [248] or terminal cysteines (C). All of them contain an N-terminal azidolysine, enabling post-functionalization with DBCO agents via click chemistry as previously reported.[35, 251, 289, 302]

The azido lipo-OAAs were included in two recent studies optimizing and evaluating lipo-OAAs for pDNA and siRNA delivery.[164, 289] In the chemical evolution for siRNA delivery, lipo-OAA *1214* (OleA, cysteines) was identified as the most effective siRNA carrier so far. The longer stabilizing OleA lipidic domain and stabilizing cysteines highlight the requirement for siRNA polyplex stabilization; as *1214* already proved as a successful carrier for *in vivo* delivery after click-shielding with hyaluronic acid,[289] this carrier was selected for reTfR targeting of siRNA polyplexes in the current study. For pDNA delivery by lipo-OAAs, the starting position was more sophisticated; the library screen revealed a balancing act in nanocarrier selection between favorable stability on the one hand, and good intracellular cargo release for transcription on the other hand.[164] Therefore, all six lipo-OAAs listed in **Scheme 3.1** were evaluated for TfR-mediated gene transfer.

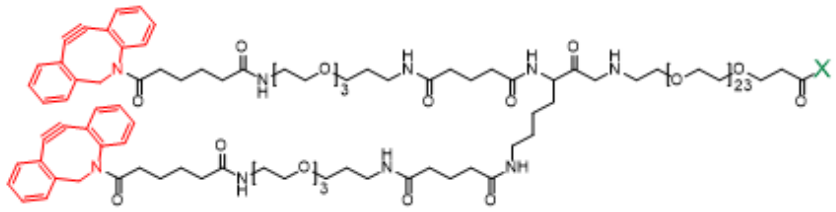

PEG-2-Ligand

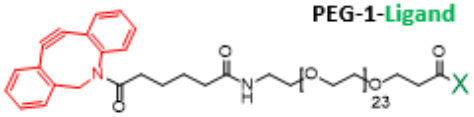

PEG-1-Ligand

PEG reagent	Sequence of Ligand X (N → C)	End group
PEG-1, PEG-2		-COOH
reTfR-1, reTfR-2	pwvpswmpprht-$CONH_2$	-$CONH_2$
R-PEG-1, R-PEG-2	R	-COOH
scr-reTfR-1, scr-reTfR-2	vprhptsppmww	-$CONH_2$

Scheme 3.2. Structures of the DBCO-PEG-ligand reagents synthesized via SPPS. Monovalent (PEG-1) and bivalent (PEG-2) DBCO linked with a monodisperse PEG_{24} chain to substituent X, which stands for: N–terminally attached retro-enantio peptide reTfR for targeting the transferrin receptor; its scrambled sequence (scr-reTfR) as control; or unmodified or arginine-modified PEG as further controls. Small letter codes: (D) amino acids; R: arginine.

3.1.2.3 DBCO-PEG-Ligand Conjugates for Click Modification of Polyplexes

The shielding and targeting conjugates of the current work are listed in **Scheme 3.2**. One or two incorporated dibenzocyclooctyne (DBCO) groups enable effective copper-free click conjugation with the azido-lysines of the investigated lipo-OAA

polyplexes. In our previous work,[35, 302] targeting conjugates containing two DBCO residues were found more effective for siRNA targeting to the EGF receptor or folate receptor. The current targeting ligand and control domains were synthesized by Fmoc-based SPPS, followed by coupling monodisperse Fmoc-amino-PEG_{24}-COOH (containing 24 ethylene oxide monomer units). Depending on whether one DBCO or two DBCO units (agents PEG-1/Ligand-1, PEG-2/Ligand-2) were to be incorporated, coupling of a branching lysine and a succinyl-trioxa-tridecandiamine (STOTDA) linker followed in the latter case. In case of the peptide-free PEG control agents (PEG-1 and PEG-2), the syntheses were completed by coupling with DBCO acid on resin and mild cleavage from the resin using a low concentration of TFA.[303] Since DBCO degrades via acid-mediated 5-endo-dig cyclo-isomerization [304] under standard higher TFA concentrations which are required for deprotection of peptide structures, syntheses of the peptide-containing conjugates continued with standard peptide deprotection and cleavage from solid support with free terminal amines, followed by coupling with DBCO-NHS ester in solution. Stock solutions of DBCO agents were prepared in HEPES buffer (pH 7.4) to prevent degradation of DBCO upon storage.

For TfR targeting, DBCO-PEG conjugates of the protease-resistant *retro-enantio* dodecapeptide reTfR[288] were generated (see **Scheme 3.2**). reTfR contains all amino acids in (*D)*-configuration and in the reversed N to C sequence order (pwvpswmpprht-NH_2) as compared to the original phage display-derived standard *(L)*-peptide.[162] Conjugates reTfR-1 (DBCO-PEG_{24}-reTfR) or reTfR-2 ($DBCO_2$-$STOTDA_2$-K-PEG_{24}-reTfR) were designed for single or dual click attachment to the azido-lysine containing polyplexes. Conjugates containing the scrambled peptide sequence vprhptsppmww-$CONH_2$, scr-reTfR-1 (DBCO-PEG_{24}-scr-reTfR) and scr-reTfR-2 ($DBCO_2$-$STOTDA_2$-K-PEG_{24}-scr-reTfR), served as control reagents. Mono- and bivalent DBCO-PEG (PEG-1; PEG-2) were used as negative controls. As arginine (R) provides the reTfR peptide and its scrambled version a positive charge, arginine modified PEG agents R-PEG-1 (DBCO-PEG_{24}-R) and R-PEG-2 ($DBCO_2$-$STOTDA_2$-K-PEG_{24}-R) were also synthesized. PEG-1/2 and R-PEG-1/2 might provide information on hydrophilic effects or electrostatic effects of these agents on the polyplexes. It is important to note that in the case of the peptide ligands (reTfR-1/2; scr-reTfR-1/2), the amide unit was used as end group to further increase stability against peptidases, also in the perspective of future *in vivo* experiments. Thus, the

synthesized DBCO agents feature different end groups, i.e., a carboxy group in the case of PEG-1/2 and R-PEG-1/2, and an amide in the case of reTfR-1/2 and scr-reTfR-1/2 (**Scheme 3.2**). This may affect the charge and stabilization of the polyplexes as well as their biological activity. Literature could show that different polymer end groups can have a decent impact on cellular uptake[305, 306] and *in vivo* performance[307] Jordan Green and co-workers could show that small molecule end group modifications of linear polymers can influence cellular uptake behavior largely independent of polymer/DNA binding, particle size, and particle surface charge[305, 306] Bekale et al. investigated PEG end group effects on the interaction withmodel proteins (human and bovine serum albumin) to comprehend the relationship between structural properties of PEG and polymer affinity toward proteins[308] Identity of all DBCO-PEG-peptide conjugates was confirmed by MALDI-TOF mass spectrometry (see **6.3** and **6.4.2**) and HPLC **(6.4.4**).

3.1.3 TfR targeting by siRNA polyplexes (This chapter was done by Mina Yazdi, Pharmaceutical Biology, LMU)

3.1.3.1 Physicochemical characterization of functionalized siRNA polyplexes

The T-shaped azido lipo-OAA 1214 (**Scheme 3.1**) with favorable efficacy[164] was selected for our TfR-mediated siRNA delivery system. The complexation of siRNA with the cationic 1214 was carried out in HEPES buffered 5% glucose (HBG; 20 x 10−3 m HEPES, pH 7.4) at an optimal protonatable nitrogen/phosphate (N/P) ratio of 12 as determined in the previous study.[165] Sizes, polydispersity index (PDI), and zeta potential of siRNA polyplexes were characterized by dynamic and electrophoretic light scattering (DLS, ELS). The nonmodified 1214/siRNA polyplexes showed a hydrodynamic diameter of around 150 nm with a low PDI of 0.18 and a relatively high positive zeta potential of around +32 mV (**Figure 3.1**). Post modification was applied to optimize nanoparticle functionality for delivery. Hence, the various PEG-shielding, TfR-targeting, and control agents as described in the previous section (**Scheme 3.2**) were assembled onto the 1214/siRNA polyplexes via a cooper-free click-reaction between the DBCO groups and the azidolysines on surface of the polyplexes analogously as previously reported.[35, 249] The post modification of the siRNA polyplexes with different molar equivalents (0.25–1.0 equiv) of reTfR and PEG conjugates resulted in well-formed nanoparticles with narrow size

distribution (**6.4.5**). However, for a better comparative efficiency study between all the different click reagents, 0.5 equiv was selected for post modification of siRNA and pDNA polyplexes in the subsequent experiments. The dimensionality of all 1214/siRNA formulations (N/P 12) after post modification with 0.5 equiv of shielding and targeting agents remained almost identical with nonmodified polyplexes (between 140 and 170 nm). The uniformity of particle population could be confirmed by the PDI around 0.2 in all cases. Compared to the nonmodified polyplexes, the reTfR-1 and reTfR-2 modified polyplexes showed slightly lower zeta potential of ≈+27 and ≈+22 mV, respectively. Polyplexes modified with scrambled reTfR were less positive than with the reTfR ligands. However, the PEG agents without ligand strongly decreased the surface charge of particles indicating an efficient shielding effect, which agrees with our previous studies.[35, 309] Moreover, the shielding effect upon modification with PEG-2 was higher than with PEG-1, which might be due to better polyplex incorporation in the case of two clickable DBCO units. The almost similar physiochemical properties attributed to the shielding effect were also observed for the R-PEGylated polyplexes (**Figure 3.1A**). With the increase of PEG equiv (including mono- or bivalent DBCO), the zeta potential of post functionalized polyplexes shifted toward almost neutral (**6.4.5**). In contrast, no or minor changes in the size and zeta potential were observed for targeted polyplexes with increased equiv of reTfR-1 and reTfR-2 (**6.4.5**). In further characterization of shielded and targeted polyplexes, the siRNA binding activity in HBG buffer (pH 7.4) was determined by 2.5% agarose gel shift assay. The intense siRNA binding in the 1214 complex core resulted in stable polyplexes over modification with 0.5 equiv of all click agents, and no mobility of complexed siRNA was observed (**6.4.7**). Consistently with DLS results, post modification with different ratios of reTfR and PEG agents led to almost complete siRNA binding in the polyplexes (**6.4.7**). It has been proved that the lipo-OAA 1214 design mediates high stability, successful delivery, and desired gene silencing activity of polyplexes upon sufficient endosomal release. Disulfide-crosslinks by terminal cysteines, together with tyrosine tripeptides and the hydrophobic interaction of the central dioleoyl-domain play stabilizing roles in the polyplex formation, and histidine-enrichment of OAAs can promote the endosomal escape of nano vectorized siRNA into the cytosol resulting in respective higher gene silencing outcomes.[98, 164, 301, 310]

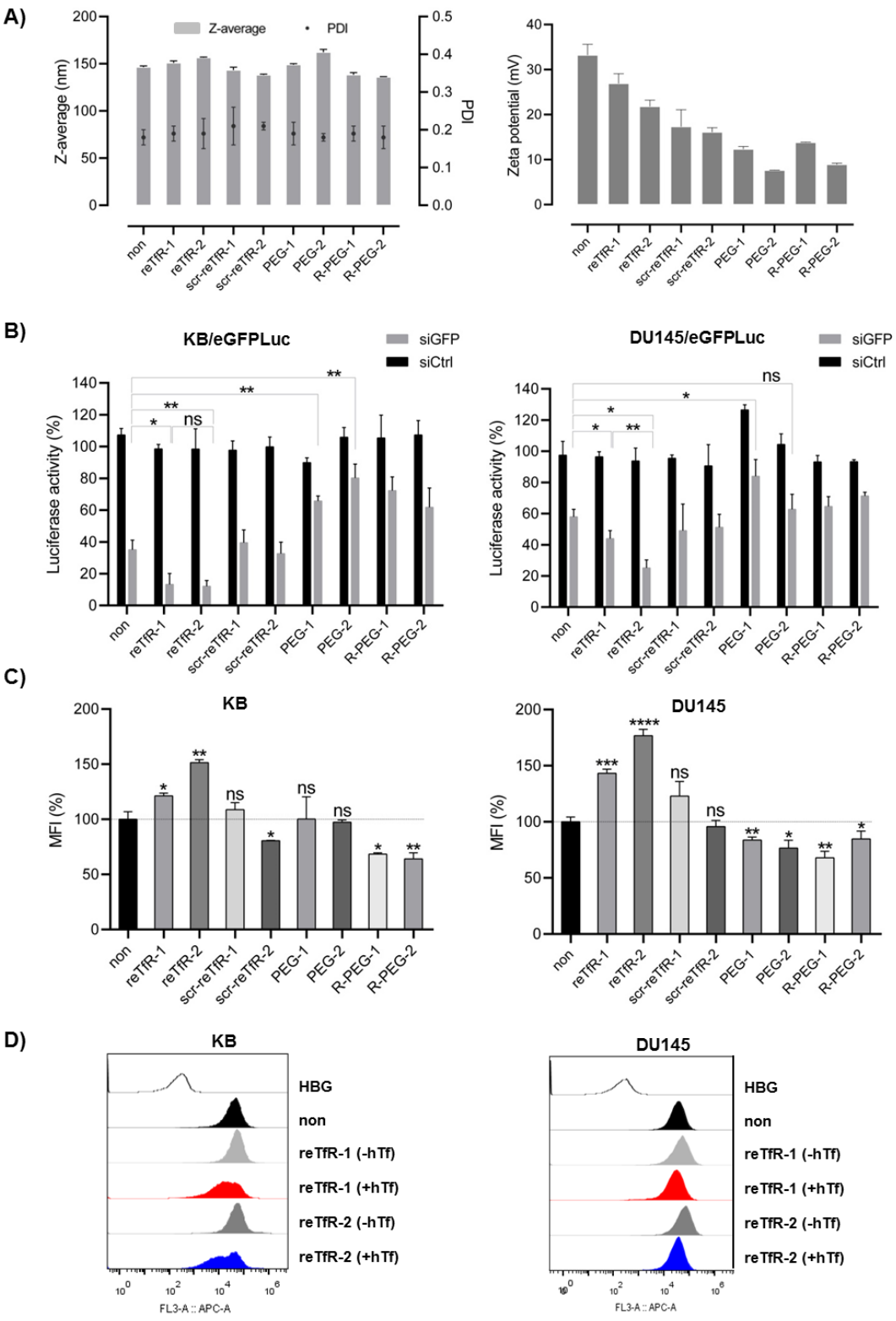

Figure 3.1. Transferrin receptor targeted siRNA polyplexes done by Mina Yazdi, Pharmaceutical Biology, LMU. A) Particle size (Z-average), polydispersity index (PDI) (left), and zeta potential (right) of siCtrl polyplexes determined by DLS & ELS. B) eGFPLuc gene silencing activity of 1214/siRNA polyplexes (500 ng siRNA/well, N/P 12) evaluated by luciferase assay in KB/eGFPLuc (left) and DU145/eGFPLuc (right) reporter cell lines after 1 h incubation followed by medium replacement and further incubation for 47 h at 37°C. C) Cellular association of siRNA polyplexes (containing 20% of Cy5-labeled siRNA) with KB and DU145 cells after 45 min incubation at 37°C acquired by flow

cytometry and presented as relative Mean Fluorescence Intensity (MFI, % of non-modified polyplexes). D) Receptor blockade assay in KB and DU145 cell lines acquired by flow cytometry after 30 min pre-incubation with (+) or without (-) iron saturated hTf (5 mg/ml) at 4°C, followed by 45 min incubation with polyplexes at 37°C. Data are presented as histogram (the Cy5 fluorescence intensity versus the number of events). All experiments were performed with 1214/siRNA polyplexes (N/P 12), and then either used non-modified or modified with 0.5 equiv of shielding and targeting agents (mean ± sd; n = 3). Equivalents (equiv) were defined as molar ratio of shielding/targeting agent to lipo-OAA. The statistical significance was determined by unpaired t-test (two-tailed analysis); ns, not significant; *p ≤ 0.05, **p ≤ 0.01, ***p ≤ 0.001, ****p ≤ 0.0001

3.1.3.2 Gene Silencing Activation of TfR-targeted siRNA Polyplexes

Transferrin receptor is overexpressed in many cancer types presenting a promising target for smart siRNA delivery.[149, 311] In our study, gene silencing efficiency of post-functionalized polyplexes was examined in TfR-positive KB/eGFPLuc squamous cell carcinoma [99] and DU145/eGFPLuc prostate carcinoma [253] cell lines stably expressing eGFP (enhanced green fluorescent protein)-luciferase fusion reporter gene [98] (**Figure 3.1B**). For this purpose, the cells were transfected for 1 h at 37°C with corresponding polyplexes encapsulating siRNA against GFP (siGFP) or control siRNA (siCtrl).[98] Then, gene silencing was measured after 48 h by luciferase reporter assay. Although the gene silencing efficiency upon post-modification with different equiv ratios (0.25-1) of reTfRs and PEGs were promising, 0.5 equiv was applied as a selected ratio for surface decoration of the polyplexes in line with the other experiment conditions (**6.4.9**). The data revealed comparable luciferase activity of the GFP-Luc protein in both cell lines, KB/ eGFPLUC and DU145/eGFPLUC (**Figure 3.1B**). A treatment with non-modified 1214/siRNA polyplexes for only 1 hour resulted in a GFP-Luc knock-down of around 60% in KB/eGFPLuc, whereas reTfR-modified polyplexes led to an increased gene silencing up to 80%. Similarly, reTfR-1 and reTfR-2 enhanced the gene knock-down in DU145/eGFPLuc from 40% obtained by non-coated polyplexes to 60% and 80%, respectively. The siCtrl control formulations exhibited no intrinsic cytotoxicity or alteration in the target gene expression. Interestingly, the GFP-Luc gene silencing efficiency could be enhanced by a longer co-incubation time (4 h) of cells with the targeted siGFP polyplexes (**6.4.9**). In contrast, no efficient targeting effect was found for the scrambled ligand controls. The surface modification with scrambled ligands, scr-reTfR-1, and scr-reTfR-2, did not improve the gene knock-down beyond the non-modified control, as opposed to reTfR-1 and reTfR-2 conjugates, displaying the specificity and high potency of these reTfR ligands. Moreover, the PEGylated and R-PEGylated

polyplexes had minor silencing activity compared to non-modified groups, presumably resulting from their shielded structures. Despite the potential advantages of PEGylation for shielding *in vivo*, it has been reported that PEG-shielded surface of siRNA nanoparticles can negatively affect their gene-silencing efficiency in cell culture.[312]

According to the obtained results, a pronounced TfR targeting could be successfully demonstrated in cervix (KB) and prostate (DU145) carcinoma cell lines. The reTfR-2 modification mediated higher gene silencing activity than reTfR-1, which can be attributed to its double amount of clickable DBCO units.[302]

3.1.3.3 Cellular Association of Functionalized siRNA Polyplexes

To correlate our findings of gene silencing activity with the cellular association, 1214/siRNA formulations (containing 20% of Cy5-labeled siRNA) with or without functionalization were incubated with KB and DU145 cells for 45 min and then cell association was examined by flow cytometry (**Figure 3.1C**). The 0.5 equiv of shielding and targeting agents were applied for polyplex modification in accordance with previous experiments. In agreement with transfection efficiency results, reTfR-modified polyplexes displayed higher cell association than the non-modified, PEGylated and R-PEGylated polyplexes in both cell lines. The delivery potential of the reTfR-modified polyplexes in DU145 was greater than KB cells. This translated into a higher gene silencing efficiency in DU145/eGFPLuc cells than in KB/eGFPLuc cells. The highest receptor-mediated binding/uptake was observed in the case of reTfR-2, which is consistent with the results of gene silencing measured by the luciferase assay. In contrast, polyplexes decorated with scr-TfR displayed the same moderate cell association as non-modified polyplexes, confirming the TfR-dependent cellular uptake mediated by reTfR-1 and TfR-2. The scr-reTfR-1 polyplexes showed slightly higher uptake than non-modified polyplexes in DU145, but still not as significant as for reTfR-1. The receptor-specific uptake mediated by the reTfR ligands was confirmed through a receptor blockade assay with iron saturated human transferrin (hTf) (**Figure 3.1D**). Pre-incubation with hTf could block and deplete the cell surface TfR and thus inhibit the reTfR-mediated binding/uptake of polyplexes with KB and DU145 cells. Because of the shielding effect, PEG-1 and PEG-2 decreased

the binding/internalization potential of polyplexes in the case of DU145 cells compared to non-modified polyplexes. A correlation could be found between lower zeta potential of shielded particles and subsequent decreased cellular association and gene silencing.[28, 312, 313] The results showed slightly better surface shielding effect followed by modification with arginine-PEG compared to PEG in KB cells. However, there is no significant difference between the cellular association potential of two types of PEGylating agents in DU145 cells.

In summary, this study on siRNA polyplexes proved the enhancing role of reTfR-decorated polyplexes for siRNA entry through a ligand-dependent manner in different cancerous cell lines. This promising approach of TfR targeting was next tested for delivery of pDNA.

3.1.4 TfR targeting by pDNA polyplexes (This chapter was done by Şurhan Göl, Pharmaceutical Biology, LMU)

3.1.4.1 Physicochemical characterization of functionalized pDNA polyplexes

For all following studies, plasmid pCMVLuc (encoding *Photinus pyralis* firefly luciferase under control of cytomegalovirus promotor and enhancer) [242] was used as nucleic acid cargo. pDNA core polyplexes were formed in HBG at a previously optimized N/P ratio of 12 using six T-shaped azido lipo-OAAs that were recently designed as part of a larger library screen.[164] These core polyplexes (**Scheme 3.1**) were post functionalized with 0.5 equiv of the different DBCO agents described in **Scheme 3.2**. pDNA polyplexes were characterized by DLS and ELS regarding nanoparticle size and zeta potential (**6.4.6**). Consistent with the previous study,[164] nonmodified pDNA core polyplexes were sized between 70 and 120 nm with positive zeta potentials between +14 and +32 mV. Their PDIs (**6.4.6**) were low (< 0.2), indicating well-formed nanoparticles. reTfR-1 and reTfR-2modified pDNA polyplexes also displayed low PDIs, sizes between 75 and 95 nm, and an only slightly reduced positive surface charge between +12 and +20 mV. The number of DBCO units (mono- vs bivalent) in the conjugate did not significantly affect their characteristics. Regarding the control reagents, PEG-1/2 or R-PEG-1/2 modification resulted in polyplexes of similar sizes around 100 nm diameter for most lipo-OAAs. These PEG reagents mediated a clear reduction in zeta potential, ranging for PEG-2 between +2

and +10mVand for R-PEG-2 between +5 and+8mV. Polyplexes with scrambled peptide conjugates scr-reTfR-1 and scr-reTfR-2 were in the expected range, with slightly larger sizes (95–266 nm) and a lower zeta potential (+10 to +16 mV) than the reTfR polyplexes. Notably, lipo-OAA 1285 showed comparable polyplex formation without or with reTfR targeting conjugates, but in contrast to the other lipo-OAAs a micrometer-sized aggregate formation with all six control conjugates (scr-reTfR-1/2, PEG-1/2, and RPEG- 1/2). This aggregate formation could not be confirmed via transmission electron microscopy (TEM, see further) and the reasons remain unclear. Lipo-OAA 1285 (like 1258) contains the detergent-like nonamido-octanoic acid (NonOcA) as lipidic domain, which might provide less lipophilic polyplex stabilization. Lipo-OAA 1258 displayed slightly larger polyplex sizes (130– 266 nm) upon scr-reTfR or R-PEG modification. TEM measurements showed homogenous and spherical shaped nanoparticles for all selected pDNA polyplexes in the range of 35–50 nm (**6.4.11**). This apparent discrepancy with DLS results was already previously observed and can be explained by fixation/dehydration for TEM and the high sensitivity of DLS for a minor fraction of aggregates. An agarose gel shift confirmed excellent pDNA binding ability without any pDNA release for all lipo-OAAs polyplexes without or with surface modification (**6.4.8**), indicating that the chosen OAAs were efficient for successful pDNA binding. To investigate the influence of PEGylation on pDNA compaction (**6.4.10**), an EtBr exclusion assay was performed. The change of EtBr fluorescent signal from 20% (related to uncompacted control pDNA) in case of nonmodified lipo-OAA polyplexes to 40% in case ofall six PEG-1 modified polyplexes indicates a change toward less condensed pDNA polyplexes. This influence of PEG is consistent with previous observations.[299, 314]

3.1.4.2 Gene Transfer Activation of TfR targeted pDNA Polyplexes

Two TfR overexpressing cell lines, the hard-to-transfect human erythroleukemic suspension cell line K562 (**Figure 3.2 A**) and the adherent murine neuroblastoma cell line Neuro2a (N2a) (**Figure 3.2 B**) were transfected with the various surface-modified pCMVLuc polyplexes and the resulting luciferase gene expression was measured after 24 h. In parallel, the metabolic cell activities were evaluated (**6.4.13**). None of the tested formulations showed significant cytotoxicity; only polyplexes of lipo-OAAs 1276 and 1258 (both lacking the bioreducible ssbb linkage, containing the less

lipophilic, more lytic DecA or NonOcA domains, respectively) had a slightly reduced metabolic activity in K562 cells, but still greater than 70%. This is consistent with previous findings.[248] Luciferase activity in K562 cells (**Figure 3.2 A**) was increased by the reTfR ligand modification in all six lipo-OAA polyplexes to various extent (3-fold to 140-fold). In most cases, reTfR-1 and reTfR-2 ligands mediated higher gene transfer efficiency than the scrambled control ligands scr-reTfR-1 and scr-reTfR-2, except for 1276. reTfR-2 modified polyplexes formed with the lipo-OAAs containing NonOcA, 1285 (ssbb), and 1258 (cys), displayed the highest transfection levels. PEG-1/2, as well as R-PEG-1/2 were initially designed as expected negative controls. Interestingly, for some carriers these shielding agents enhanced gene transfer by a mechanism obviously different from TfR mediated uptake; PEG-1/2 strongly promoted transfection of 1284 polyplexes and 1258 and 1218 polyplexes to a lesser extent. R-PEG conjugates promoted transfection of 1284, 1285, 1258, or 1218 polyplexes, but to a lower extent. In the case of N2a cells, the transfection medium was replaced after 4 h, to emphasize any short-term effects of surface modification on cell attachment and delivery before evaluating the transfection activity after 24 h (**Figure 3.2 B**). Apart from 1214 polyplexes, which generally were transfected poorly, transfections were increased by incorporation of reTfR-1/2 again. In N2a cells, reTfR-2 modified polyplexes performed best with the ssbb-containing lipo-OAAs in the sequence 1284 (DecA) > 1285 (NonOcA) > 1218 (OleA). The scrambled control ligands scr-reTfR-1 and scr-reTfR- 2 again mediated lower transfection, with one very notable exception: the best transfections for 1285 polyplexes were obtained with scr-reTfR control modification. However, as described in Section **3.1.4.1**, these control polyplexes present microsized aggregates, which might explain their special properties. Similar as observed for K562 cell transfections, control PEGylation resulted in TfR-independent enhancement of transfection. This was especially pronounced for modification of 1284, 1285, 1258, and 1218 polyplexes with R-PEG-1 and/or R-PEG-2 (**Figure 3.2 B**). To summarize the pDNA transfections, the reTfR ligands favorably promoted gene transfer efficiency both in K562 and N2a cells, with

a small advantage when using the bivalent DBCO containing conjugate reTfR-2.

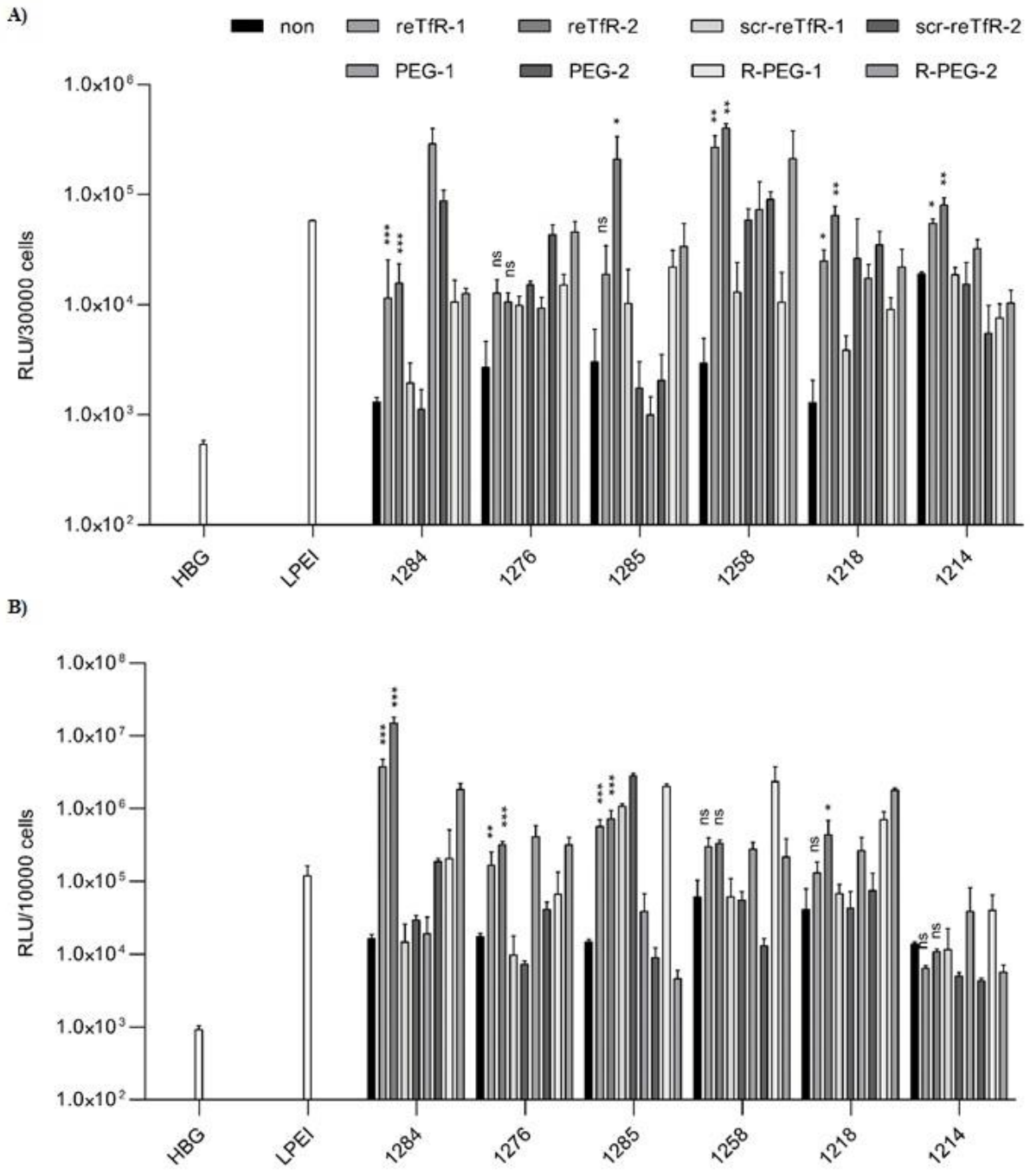

Figure 3.2. Luciferase gene transfer in K562 cells (**A**) and N2a cells (**B**). pDNA polyplexes (200 ng/well, N/P 12) modified with 0.5 equiv of shielding and targeting agents. Cells were incubated with polyplexes for 24 h in serum supplemented medium at 37°C and harvested for the luciferase assay. In case of (**B**), the transfection medium was replaced after 4 h by fresh medium. Linear PEI (LPEI, N/P 6) and HBG buffer served as positive and negative control, respectively (mean ± sd; n = 3). For the comparison of non-modified with reTfR-1 and reTfR-2 functionalized polyplexes, the statistical significance was determined by unpaired t-test (two-tailed analysis); ns, not significant; *p ≤ 0.05, **p ≤ 0.01, ***p ≤ 0.001. Done by Şurhan Göl, Pharmaceutical Biology, LMU.

Cell association studies of reTfR-1 and reTfR-2 modified polyplexes were performed in K562 cells (**6.4.13**) and N2a cells (**6.4.13**). It is not surprising that cell associations

(which also may include unspecific cell binding only) and gene transfer efficiencies only correlate in part; gene transfer also depends on efficient intracellular uptake, endosomal escape, and/or delivery into the cell nucleus as well as transcription. However, in both cases of 1285 reTfR and 1284 reTfR polyplexes, which are potent reTfR-enhanced transfection agents in K562 cells or N2a cells, respectively, a blockade of TfR by preincubation with iron saturated hTf reduced the cellular association of polyplexes (**6.4.13**). These results support the hypothesis of a Tf receptor-mediated gene transfer process of these reTfR polyplexes. The evaluation of six lipo-OAAs differing in their lipidic domains and redox-sensitive attachment, and different control PEGylation reagents PEG-1/2 and R-PEG-1/2 shed also light on other important receptor-unrelated effects of the gene transfer process. While a proper receptor ligand may mediate specific attachment and uptake into target cells, other parameters, such as the choice of lipo-OAA and PEGylation conjugates can affect extracellular and intracellular biophysical stability of core pDNA polyplexes, influencing also endosomal escape of internalized pDNA nanoparticles and, after delivery into the nucleus, unpackaging of pDNA for subsequent transcription into mRNA. Our previous work on the tested lipo-OAAs had revealed a balancing act between favorable stability of pDNA polyplexes on the one hand, efficient endosomal escape and good intracellular pDNA release for transcription on the other hand. Lipo-OAAs containing fatty acids with chain lengths around C6 to C10 displayed maximum gene transfer with around 500-fold higher gene expression than that of C18 lipo-OAA analogues.[164] The shorter fatty acids trigger increased endosomolytic activity, at the cost of reduced polyplex stability. Incorporation of hydrophilic PEG molecules is an additional measure to tune the polyplex stability. Consistent with previous observations,[299, 314] PEGylation mediated slight polyplex decondensation detectable with an EtBr assay (**6.4.10**). Such a polyplex destabilization by PEG or R-PEG conjugates, shifting the amphiphilic properties of the carrier subunits towards higher hydrophilicity and aqueous solubility might be the cause of the unexpected high transfection efficiency of R-PEG conjugated 1284, 1285, 1258, or 1218 polyplexes. Noteworthy, our studies also revealed that for TfR-specific delivery to a given target cell line, an optimized combination of lipo-OAA and ligand is required for the best transfection; reTfR-2/1258 or 1285 (both NonOcA-based) for K562 cells, and reTfR-2/1284 or 1285 (both ssbb-based, DecA, or NonOcA-based) for N2a cells.

3.2 Ligand targeted carbon dots as organic vector-based system for cell transfection

3.2.1 Introduction

This work is part of the Deutsche Forschungsgemeinschaft (DFG) based collaboration “Joint Sino-German Research Project” by Ernst Wagner, Ludwig-Maximilians-Universität, Munich, Germany; Rongqin Huang, Fudan University, Shanghai, China; Yi Wang, Donghua University, Shanghai, China with the title: “LRP1-targeted carbon nanodots for crossing BBB and delivering small molecule or protein drugs into the brain.” The goal of this collaboration is to create CD-based models for efficient BBB bypassing, to enable therapy inside the brain e.g., against Alzheimer’s disease, Parkinson’s disease, and Glioblastoma, in addition to utilizing the photoluminescence of the CDs for tracking the penetration through the BBB.[191, 315] For this, the group of Prof. Rongqin Huang developed new CD platforms for evaluation as vehicles for the current ongoing project, with the idea of providing practical clinical applications in the long run. For more information about CDs see chapters **1.7** and **1.8**.

Receptor-mediated transcytosis and adsorption-mediated pathways can be utilized to enhance permeability into the brain for drugs (see **1.4** to **1.6**). Due to its high specificity, receptor-mediated transcytosis across the BBB stands more in the focus of science. Here vesicles are formed and translocated across the brain endothelial through endocytosis mechanisms.[316] The classical receptor for BBB targeting is the overexpressed Transferrin receptor (TfR). However, TfR is physiological ubiquitous occurring in many organs, like the liver, therefore to a certain degree unspecific, which might limit its applicational range. Low-density lipoprotein receptor-related protein 1 (LRP1) on the other hand is a large single-pass transmembrane receptor, which is highly expressed in the brain endothelial cells and upregulated in some effector cells, like melanized neurons in the substantia nigra (SN) in Parkinson’s disease and glioma cells to name a few.[317, 318] Popular exploited ligands out of this family are Angiopep-2, aprotinin, apolipoprotein E, and lactoferrin.[319, 320] Here, especially Angiopep-2, a 19-amino-acid long ligand peptide is of interest, since it was reported to pass through the BBB and deliver covalently bound drug conjugates into the brain. In addition it is stated, that it also successfully mediated *in vivo* with targeted siRNA lipoplexes into glioma cells.[123] Furthermore, a new promising

Angiopep-2 orientated peptide ligand L57 was recently via phage display discovered.[125] The benefit from L57 to its old version Angiopep-2 was a significant increase in BBB permeability, indicating the potential of L57 to overthrow Angiopep-2 as an effective carrier for CNS delivery, which is why the Joint Sino-German Research Project focus is on the proposal of new modeled LRP1-targeted CDs for crossing BBB and delivering small molecule or protein drugs into the brain.

To enable LRP1-targeting for CDs the group of Prof. Wagner focuses on a novel coating strategy for CDs to introduce shielding and target domains. This comprises coating and caging of CDs with sequence-defined oligoaminoamides (OAAs) containing azidolysines to enable strain-promoted azide-alkyne cycloaddition (SPAAC) of shielding and targeting domains, which is the subject of this chapter.

3.2.2 Results

3.2.2.1 Design and Synthesise of Sequence-Defined 4-armed OAAs as Core Shell Components for CD entrapment and encapsulation

The first coating strategy uses a layer-by-layer coating and entrapment approach to entangle negatively charged red CDs (rCDs). rCDs were provided by Rongqin Huangs working group, namely Wei Guo. They are fabricated via a one-step hydrothermal method. As a precursor 1,5-dihydroxynaphthalin was used. Due to their pyrolytic creation, the 1,5-dihydroxynaphthalin units are polymerized and create a surface enriched with carboxyl, hydroxyl, phenolic hydroxyl, and carbonyl groups. Subsequently, the zeta potential of the rCDs is highly negative with abound -30 mV. Their particle size is rather big for CD systems with roughly 60 nm.

To encapsulate the rCDs to enable LNP1 targeting a library of 21 different sequence-defined, positive charged, 4-armed oligoaminoamides (OAAs) were synthesized (see **6.2** and **6.4.14**). In each arm of the OAAs at least six lysines are used. Close to the end of each arm, cysteines were incorporated; the thiol groups may crosslink the 4-armed OAAs to form a bio-reversible disulfide-based cage around the nanoparticle. Besides the cysteine and amino lysine motifs, three or four alternating lipophilic spacer units were introduced. For that purpose, tyrosines, as aromatic, lipophilic spacer and leucines, as aliphatic, lipophilic spacer were selected. These blocks vary from one to four. N-terminal azido-lysine groups are introduced to enable the SPAAC

controlled click chemistry for post shielding and targeting the rCD-OAA nanoparticles (see **Scheme 3.2**) with ligands such as L57 or controls, which are linked with monodisperse polyethylene glycol (PEG_{24}) spacer as surface shielding agent via one N-terminal attached DBCO group. Notably, all nanocarrier subunits (OAAs: **6.2** and ligand agents: **6.3**) present sequence-defined materials that were synthesized in a precise manner by solid-phase supported peptide/polymer synthesis (SPPS). Summing it up there are three major techniques utilized for efficient rCD-OAA conjugate formulation. First, the layer-by-layer coating, which is based on electrostatic, hydrophile interactions of the positive OAAs with the negative charged rCDs.[321] Secondly, a covalent bound cage of disulfide crosslinking in a 3D manner is layered around the rCD like a net[321], and thirdly the integration of azido units on the OAAs enables SPAAC controlled modifications. However, for an efficient wrapping of the rCD the polymeric carriers must have a particular length, otherwise, the network can be lost which leads to poor formulation attributes, like disability of the conjugated complex. To circumvent that particle destabilization and further enhance the layering effect, by coupling ε-Fmoc-amino lysines instead of normal α-Fmoc-amino lysines were also integrated into this OAA library. ε-connected lysines increase the length of the four arms to provide a more efficient wrapping around the rCD.

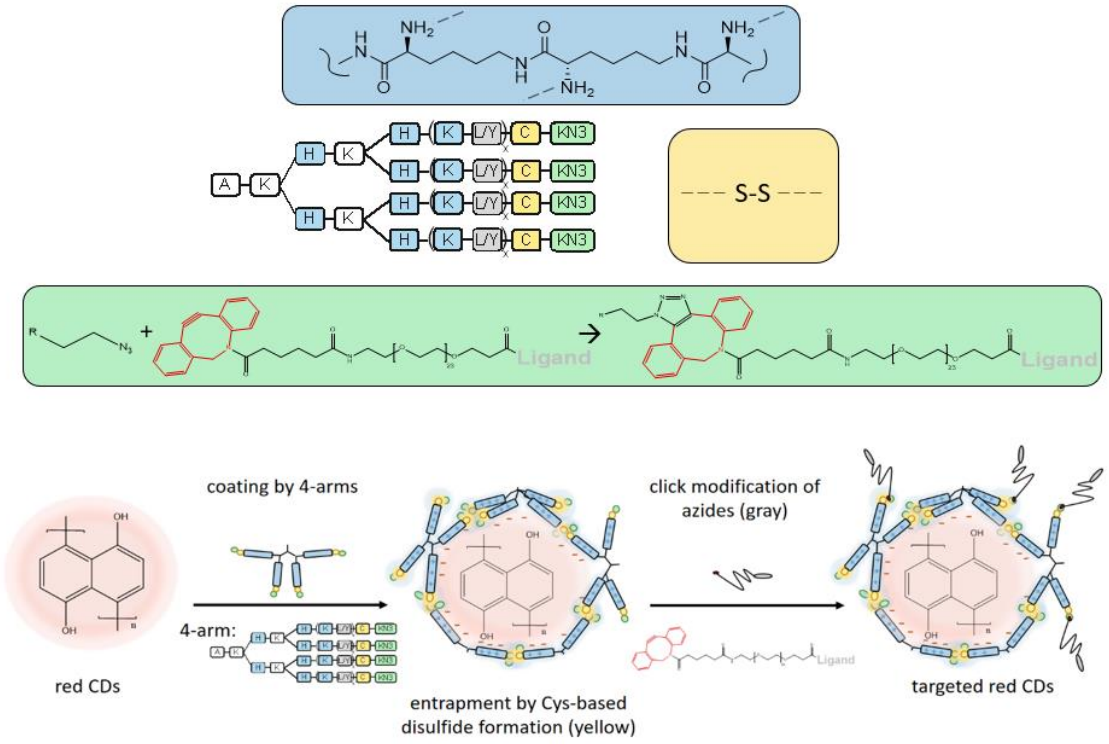

Scheme 3.2. Coating and entrapment of negatively charged red CDs (rCDs) by positively charged OAAs in a two-step process. rCD-OAA particle are prepared by flash mixing OAAs and rCDs followed

by a 1 h incubation. Post-functionalization via strain-promoted alkyne-azide cycloaddition (SPAAC) for 4 h is performed with monovalent DBCO-PEG_{24}-ligand reagent containing a TfR-targeted peptide (reTfR) to display targeting and for shielding effects monovalent DBCO-PEG5K without ligand domain. In the first step rCDs are coated and entrapped into core nanoparticles (Scheme 3.2, left, down) using a newly designed library of sequence-defined 4-armed OAAs (rCD-OAA). In the second step, the nanoparticles are modified with a shell of PEG-conjugated ligands for shielding and targeting (Scheme 3.2, right, down). Noncovalent (electrostatic, hydrophobic) reversible coating of CDs = blue; Forming a cage by disulfide-based crosslinking of coat azido-OAA = yellow; Coupling targeting/shielding by click chemistry = green

3.2.2.2 Selection of 4-armed OAAs based on physicochemical characterization of their according rCD-OAA formulations

Different cargos need different carrier based on their biophysical properties. Due to their negative surface charge rCDs need a polycationic carrier system to be able to get decent formulation conjugates. Therefore, the nanocarrier system, the OAA library constipated for the purpose of rCD caging and entrapment needed 100 % positively charged Ions at physiological pH, which is why lysines were chosen instead of the Stp building block (see **3.1.2.2**). As stated in **3.2.2.1** not just the normal α-Fmoc-amino lysines but also ε-Fmoc-amino lysines were used as an elegant way of increasing the size (pm) of each arm without changing the sequence. Since rCDs have not just a polyanionic outer surface but also a rather lipophilic core tyrosine and leucine were chosen to enable lipophilic interactions of carrier to CD. The purpose of choosing an aromatic and an aliphatic lipophilic amino acid was to address the beneficial effect of potential aromatic stacking. Finally, the rCD 4-armed OAA library was synthesized to address structure-activity relations between rCDs and OAAs in the sense of chemical evolution of carrier systems for perfect optimization to its cargo, rCDs, which is why all OAAs are sequence-defined synthesized via SPSS.

All structures of the synthesized 4-armed OAA library, tailormade for rCDs can coat and entrap the rCDs. However, some in a more effective manner than others (**6.4.14**). Centrifuged rCDs in this setting have a size of 235 nm (z-average) or 79 nm (normal), a negative zeta potential of around -20 mV, and a PDI of 0,406. All rCD-OAA conjugates have a positive zeta potential in a range of roughly +15 to +25 mV. The particle sizes (z-average/normal) and polydispersity index (PDI) however vary a lot, which leads to the conclusion, that some OAAs perform in their attributes to cage and entrap the rCDs superior to others. To have a proper comparison in the structure-activity relations between rCDs and OAAs it is important to compare one attribute at a time. To see what impact the length of the arms of the 4-armed OAAs

has, it makes sense to compare 1768, 1769, 1664 and 1696 with each other, as seen in **Figure 3.2.2.2.1** and **3.2.2.2.2**. 1768 has a length of ~2750 pm and is therefore the shortest of the four. Its particle formation of 232 nm (z-average) and PDI of 0,651 addresses its poor properties of caging and entrapment of rCDs. 1769 on the other hand has a length of ~5500 pm, due to its ε-lysine configuration instead of the α-lysine configuration of 1768. The rest of the structure is identical. Its property of rCD conjugation with 253 nm size (z-average) and 0,421 PDI however, is more efficient than its counterpart 1768, only due to its increased length. The same effect is seen between 1664 and its counterpart 1696, were 1664 has a α-Fmoc-amino lysines, and 1696 a ε-Fmoc-amino lysines configuration. rCD-1664 has a size of 264 nm (z-average) and a PDI of 0,310 while its counterpart rCD-1696 is 128 nm in size z-average) and 0,188 in PDI. 1664 length is ~3500 pm and 1696 length ~5500 pm. The difference in PDI, which is a very important measure of quality of particle formulation, is very different depending on the length of the arms, respectively. For this model, the length of the arms of the 4-armed OAAs has clear benefits in the formulation of the conjugate rCD-OAA with a length of ~5000 pm in comparison to ~3000 pm. However, the length alone does not guarantee an effective and efficient caging and entrapment of the rCDs. The impact of aromatic groups, leucine as aliphatic amino acid blocks, or tyrosine as aromatic amino acid blocks indicates another huge impact on rCD-OAA formulation quality. 1658 for example, with a length of ~3500 pm is built with leucine units (for structure see **6.2**) has the z-average of 219 nm with a PDI of 0,728 and its tyrosine counterpart 1664 (for structure see **6.2**), with same length of ~3500 pm, has a size of 264 nm (z-average) and 0,310 as PDI. The lengthy is identical, the sequences are identical with the difference of lipophilic aromatic acid composition and their properties of encapsulating rCD are very different when it comes to the PDI. The formulation efficacy of the tyrosine containing structure 1664 is above its counterpart 1658 with the only difference in having tyrosine block units instead of leucines, concluding, that the tyrosine stacking attribute can have a major effect on the quality of rCD conjugation. The importance of integrating tyrosine units in the OAA sequence is also indicated in the comparison of 1769 and 1696 (for structure see **6.2**). The arms of 1769 only contain lysine units ending in cysteine azidolysine whereas 1696 contains in addition to that also tyrosine triblocks. The length with ~5500 pm is the same but the difference in size and PDI is immense, as 1769 has a

size of 253 nm (z-average) and a PDI of 0,421, and 1696 the size of 128 nm (z-average) and the PDI of 0,188.

On the given data we can conclude that the length plays an elementary role in caging and 3D entrapment of rCDs by 4-armed OAAs. Just as important is the integration of tyrosine units in the 4-armed OAA sequence for additional tyrosine π-electron stacking for additional stability shown in the benefit to the PDI. Comparing the whole library of 21 4-armed OAAs in relation to size, zeta potential and most importantly the PDI the best performer of all these structures is 1696. It performs superior in comparison to its concurrence with a respectable size of the rCD-1696 of 128 nm (z-average) or 74 nm (normal), a zeta potential of 19 mV, and a PDI of 0,128. The clear benefit in particle property of the rCD-1696 conjugation is also beneficial in comparison to rCD on its own with a size of 235 (z-average) and a PDI of 0,406. Resulting, rCD-1696 is not just able to surface modify DBCO-ligands via SPAAC on its outer layer but also creates better attributed nanoparticles as rCD alone, measured on its size and PDI properties.

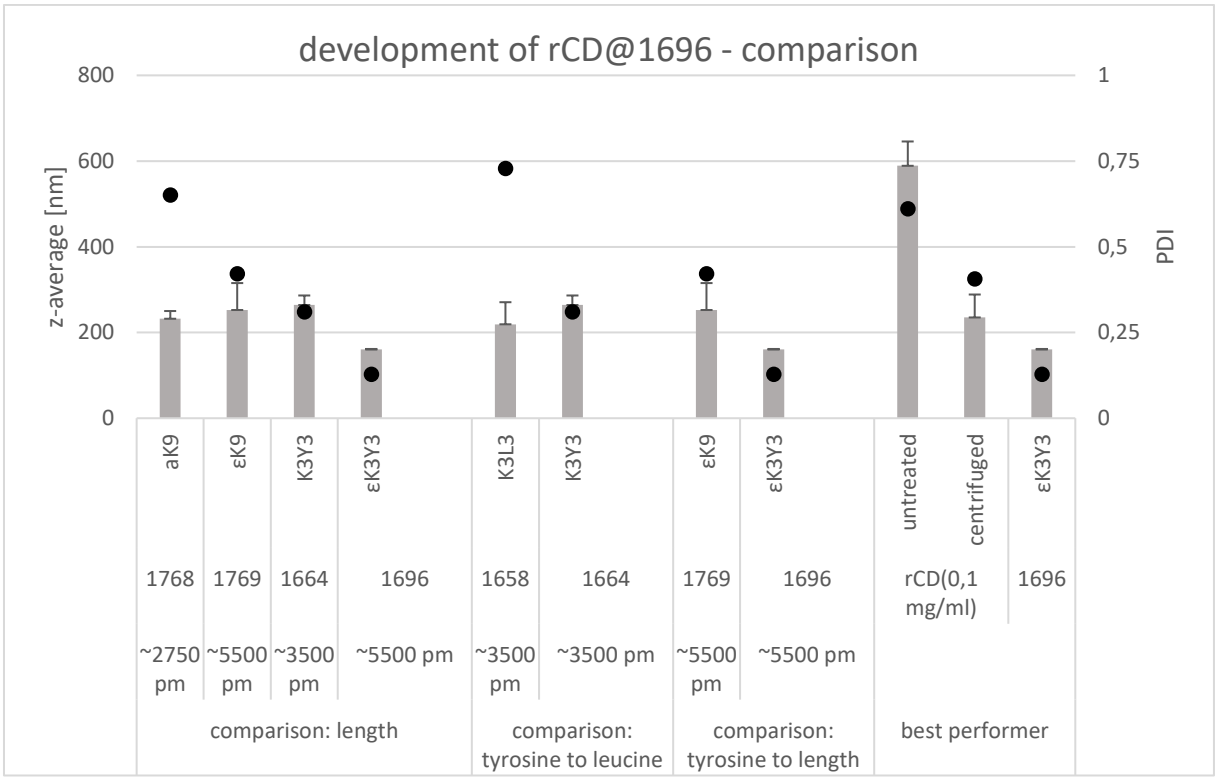

Figure 3.2.2.2.1. Development of rCD-OAA. From the library containing 21 different 4-armed OAAs to the best performer 1696. Particle diameter (z-average), polydispersity index (PDI), and length in pm of the arms of the OAAs, of rCD-OAA particles. Particle were formed of a w/w ratio of 2,7 (rCD 1 : OAA 2,7). DLS measurements using a Zetasizer Nano ZS (mean ± sd; n = 3). For more information see section: **6.4.15.**

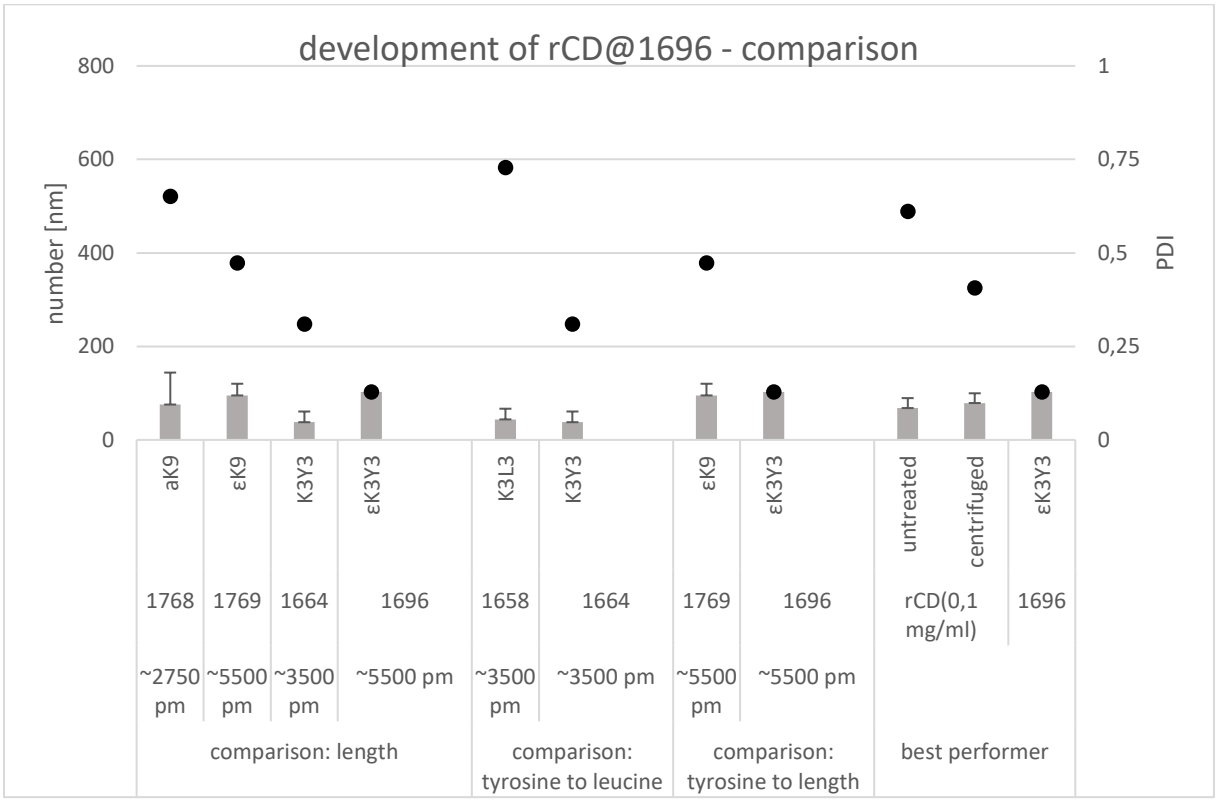

Figure 3.2.2.2.2. Development of rCD-OAA. From the library containing 21 different 4-armed OAAs to the best performer 1696. Particle diameter (number), polydispersity index (PDI), and length in pm of the arms of the OAAs, of rCD-OAA particles. Particle were formed of a w/w ratio of 2,7 (rCD 1 : OAA 2,7). DLS measurements using a Zetasizer Nano ZS (mean ± sd; n = 3). For more information see section: **6.4.15.**

3.2.2.3 Optimized formulation of rCD-1696

The method protocol of how to handle rCDs and how to conjugate them to the 4-armed OAA library carriers (see **2.2.7**) had to be evaluated and reevaluated to ensure the most efficient handling of these chemicals and the best formulation outcome of the rCD-OAA conjugates. The first preliminary data of rCD-OAA was done with a polymeric carrier from another 4-armed-library with the focus of encapsulating nucleic acid as cargo instead of carbon dots. Therefore, this preliminary carrier, namely 1463 (see hole library with structures **6.2**) was suboptimal for the rCDs, however, was used as a starting point in this work. The method protocol was respectively done with a rCD-1463 conjugation first and later reevaluated with the best performer 4-armed OAA from the rCD 4-armed OAA library (see **6.2**; **6.4.14**; **3.2.2.2**) 1696. All the data shown in **6.4.15** and chapter **3.2.2.2** with its figures **3.2.2.2.1** and **3.2.2.2.2** were executed with the reevaluated method protocol based on 1696.

Since the coating of the particles is done by noncovalent ionic interactions of the negatively charged rCDs (mainly carboxyl, hydroxyl, and phenolic hydroxyl functionals groups) with the positively charged OAAs (amino group of polylysines) the pH of incubation medium has a major effect in conjugation efficacy. The pH must be perfectly outbalanced to ensure, that most functional groups are charged. Different buffers with different pH were tested, HEPES buffer (20 mM; pH 7,4) showed the most beneficial outcome. As a Good buffer (also known as Good's buffer) it has the perfect pH to ensure encaging and entrapment and on the other hand is physiological, so it can be used *in vitro* and *in vivo*. It is nontoxic, membrane impermeable and therefore is a well-established and used buffer with excellent biological compatibility. It has minimal salt effects, allows well-behaved cationic interactions and is biochemical inert. As mentioned in **3.2.2.1** the reaction of the thiol groups of the cysteines, which leads to a covalent thiol-thiol bound, respectively to a cysteine-based crosslinking network, as the mechanism to introduce the entrapment of the rCD, is also highly pH dependent. To let the thiol groups, react, resulting in crosslinking, a not to acidic pH is needed. Again, the physiological pH, which HEPES perfectly provides comes in handy here. Summing up, for caging and entrapment of the rCDs by the 4-armed OAAs HEPES was used, due to its excellent properties of providing physiological pH and for being biological good compatible. The pH dependency of the encapsulation reaction to formulate the rCD-OAA conjugates is shown in **Figure 3.2.2.3.1**. The best pH for size and PDI of the rCD-1696 formulation is pH of 7,4, which as well as counting for the preliminary used 4-armed OAA 1463, due to its similarity of sequence and therefore same strategy for rCD coating and caging.

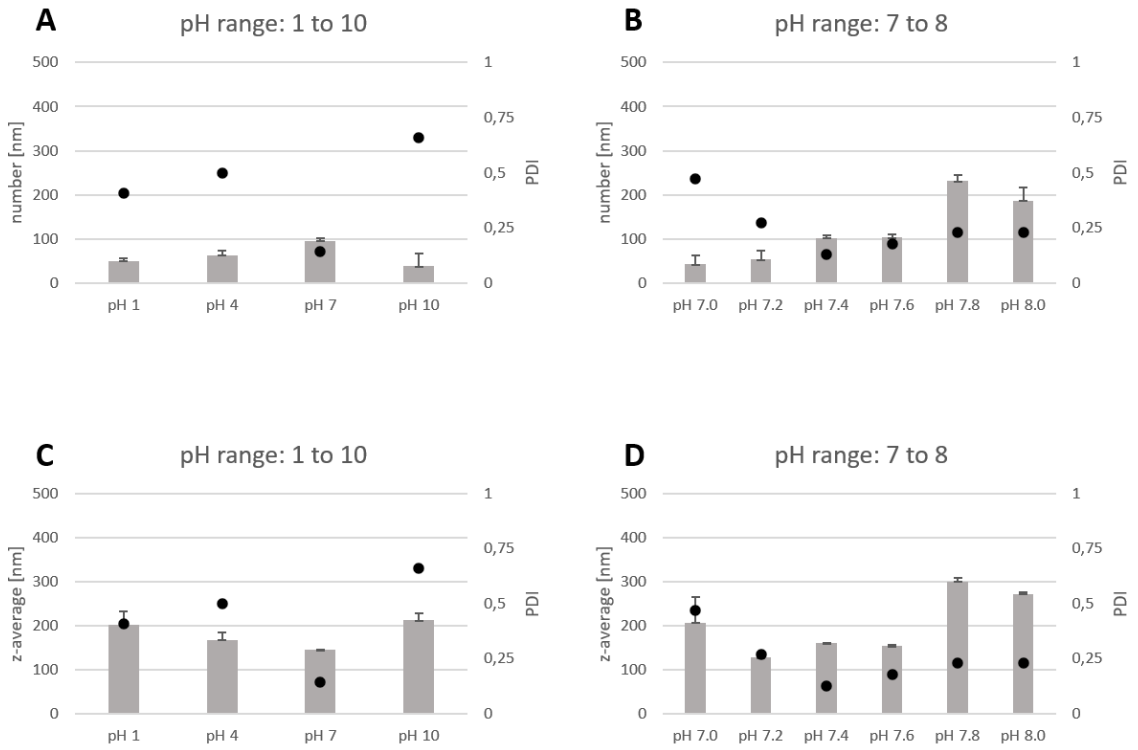

Figure 3.2.2.3.1. pH dependency of the conjugation of rCD-OAA exemplary for rCD-1696 with a pH range of 1 to 10 (**A**, **C**) and a more defined pH range of 7 to 8 (**B**, **D**) in dependency to particle diameter (z-average & number) and polydispersity index (PDI). Particle were formed of a w/w ratio of 2,7 (rCD 1 : OAA 2,7). DLS measurements using a Zetasizer Nano ZS (mean ± sd; n = 3). For the detailed protocol see **2.2.7**.

For reaction material and its equivalents, a titration of rCD to OAA (w/w) was done. As the starting point 1000 ng of rCD was taken and titrated with different amounts of OAA composed from 180 ng up to 9000 ng. As seen in **6.4.15** there are no benefits in using more than 2,7 of the amounts of 1969 to rCD, meaning 2700 ng of 1696 to 1000 ng of rCDs for its conjugation formulation, in size and PDI. Interestingly the turning point of the zeta potential of the rCD-1696 conjugation lies between 900 – 1800 ng of 1696 for 1000 nm rCD, showing, that this amount of 1696 is needed to fully encapsulate rCD, which results in a change from negative to positive zeta potential. After the equivalents of 5,4 1696 to rCD (5400 ng 1696 – 1000 ng rCD) the zeta does not change anymore by increasing in mV, which indicates the saturation of carrier in the formulation. The amount of 2700 nm OAA to 1000 ng rCD was chosen since it showed the best size and PDI of the conjugation. When adding higher equivalents of OAA no more benefits were detected. The same was seen for the

rCD-1463 (PDI: 0,600) formulation with the difference being by far not as good as the rCD-1696 (PDI: 0,188).

To ensure the best incubation time for the coating and caging reaction in **6.4.16** a time dependency to particle properties was done. The coating mechanism of the conjugation happens instant, comparable with the polyplex formulation of nucleic acid to polymeric cationic carrier nanoplatforms. Therefore, the time point of measuring (0 min to up to 24 h) does not have significant change in particle characterization. Size and PDI are in all time points similar. Interestingly, even at 24 h the rCD-1696 conjugation is still stable, visible in no change in size and PDI. The crosslinking reaction however takes more time. Here a Ellman's assay was done to quantify the free thiol groups in the formulation. As control water instead of HEPES was chosen, to also address the pH dependency of this reaction. Due to the nature of Fmoc-based SPPS and its TFA cleave protocol synthesis products like OAAs generate an acidic milieu upon dissolving them in water, since the buffer capacity of water is not as strong as in buffers like HEPES. Upon dissolving OAAs in HEPES the pH of the milieu stays 7,4 due to the buffering capacity of HEPES. The amount of cysteine existing in the solution at time point 0 min was chosen as 100 % (see **2.7.7**). After 1 h of incubation of the rCD-1696 in water no significant changes are seen, concluding, that no significant amount of thiol-thiol crosslinking happens. After 24 h of incubating rCD-1696 in water the free thiol is around 90 %, therefore roughly 10 % of potential thiol-thiol crosslinking occurs, which can be interpreted as no significant changes in thiol concentration, due to acidic water milieu, showing the importance of a well-controlled fine-tuned, stable pH. For the rCD-1696 HEPES solution after 1 h incubation the free thiol concentration is 58 %, concluding that 42 % potentially reacted. Up to 24 h 45 % free thiols are in solution for the rCD-1696 in HEPES, concluding 55 % of potential thiol-thiol crosslinking. The benefit of increased incubation time is therefore insignificant, which is why a time range of 1 h was chosen as a perfect incubation time for the rCD-OAA reaction in HEPES. The preliminary 4-armed OAA 1463 behaved very similar to 1696 in this regard as seen in **6.4.16**. The control experiment in water instead of well-tuned HEPES did not potentially crosslink more than roughly 12 % in 24 h, exhibiting again the importance of the pH for the entrapment reaction, as addressed in the fundamental work for this by Röder et al.[321]

In summary, experiments could show that the best buffer is HEPES with a physiological pH. The best ratio is 1-part rCD to 2,7 parts 1696 and the incubation time is 1 h. The preliminary protocol of model structure 1463 behaves very similar to the 4-armed library tailormade for rCDs, which is because of similar build of carrier. 1463 cysteines and azidolysines as all 4-armed OAAs of the library. The habitus of structures are all the same. The only major difference of 1463 is the existence of the building block Stp instead of polylysines in its structure, and no lipophilic amino acid blocks. Therefore, it was just a model structure, tailormade for nucleic acid but not carbon dots, since the Stp is not fully positively charged in physiological pH. 1463 however was the basis on which the 4-armed rCD library was created. 1696 was performing outstandingly well (**3.2.2.2**) in comparison to the rest of potential candidates from the library, making it the best performer, on which behalf all the experiments in **3.2.3** and **3.2.4** were executed.

3.2.3 DBCO-PEG-Ligand conjugates for click modification of rCD-OAA conjugates

Based on the data **3.2.2.2** 1696 is the leading 4-armed OAA and therefore is chosen for the subsequent experiments of shielding and targeting (see **3.2.3.1**). rCD-1696 particles with zero to four equivalents (equiv) of PEG_{5K}-DBCO (mol OAA/ mol shielding agent) do not display issues in post-modified particle formation. Even with 4 equiv of PEG_{5K} no agglomeration is observed. The zeta potential efficiently decreases to up to ~3 mV for 4 equiv, showing a successful shielding of the rCD-1696-PEG_{5K} particles as seen in **3.2.3.1**. When it comes to the targeting of rCD-1696 particle with reTfR-PEG_{24}-DBCO (**3.2.3.1**) the conjugation, seen in particle size, PDI and zeta is likewise beneficial. Size and PDI are not highly influenced by the increase of equiv of targeting ligand (mol OAA / mol ligand agent) except for an equiv of 4. Here size is doubled, however, PDI stays stable at around 0,2, indicating a still very homogeneous particle formation. The zeta is similar shielded as in the shielding experiment with PEG_{5K}. Tf2, L57, reL57 and Angiopep-2 were also tested with the rCD-1696 conjugation, each with an equiv of 0,5 equivalents (mol OAA/ mol targeting agent). The size and PDI are only slightly influenced by integrating 0,5 equiv of targeting agents into the rCD-1696 conjugation. In case of rCD-1696-L57 the PDI even becomes better with 0,16 to the untargeted rCD-1696 formulation.

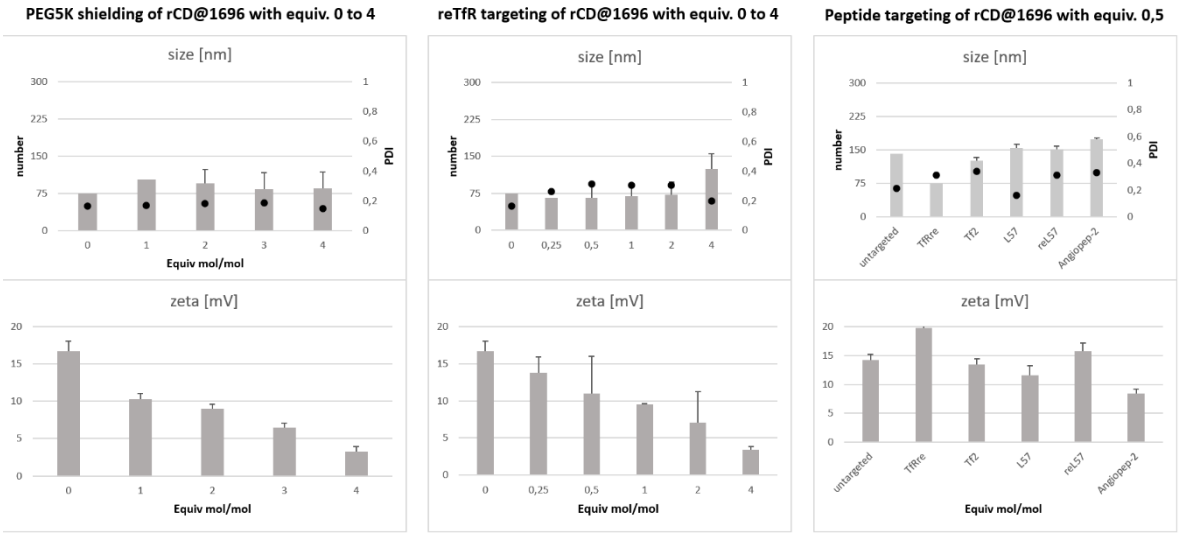

Figure 3.2.3.1. Particle diameter (number), polydispersity index (PDI), and zeta potential of rCD-1696 particles. Particle were formed of a w/w ratio of 2,7 (rCD 1 : 1696 2,7) and a molar ratio of 1696 0 to 4 equivalents for PEG_{5K}-DBCO (left) and reTfR1 (middle). The right side of the Figure shows particle diamterer (number) and polydispersity index (PDI) and zeta potential for untargeted rCDs, reTfR1, Tf2, L57, reL57 and Angiopep-2 with 0,5 equivalents. DLS measurements using a Zetasizer Nano ZS (mean ± sd; n = 3).

In summary, all targeting and shielding agents manage to build good particles with the rCD-1696 formulation related to its size and PDI. Even with relatively high equivalents of 4 (mol OAA/ mol targeting/shielding agent) the conjugations do not tend to agglomerate.

3.2.4 Targeting effects of rCD-OAA conjugates

As seen in 3.2.4.1 (done by Fengrong Zhang, Pharmaceutical Biotechnology; LMU) the cell viability (metabolic activity) of unmodified rCD, unmodified 1696, rCD-1696, as well as rCD-1696-L57 (molar ratio of 0,5: mol OAA/ mol shielding and/or targeting agent) is at 100 %, concluding no cell toxicity of the conjugation. When it comes to cellular uptake the ECD (Ex:561 nm, Em 590-630 nm) creates the highest mean fluorescence intensity. Here rCD alone, rCD-1696, rCD-1696-PEG5K (molar ratio of 0,5: mol 1696/ PEG5K-DBCO), rCD-1696-L57 (molar ratio of 0,5: mol 1696/ L57), rCD-1696-L57 (molar ratio of 2: mol 1696/ L57), and rCD-1696-L57 (molar ratio of 4: mol 1696/ L57), was screened. rCDs on their own create a signal intensity of roughly 100K, whereas the conjugation rCD-1696 is around 24K, effectively increasing signal intensity by a ~2,4-fold. The shielding of rCD-1696 with PEG5K-DBCO, rCD-1696-PEG5K, leads to a decrease in intensity to 18K. Integrating the targeting agent L57 to

the rCD-1696 formulation can manage to increase intensity by a high rate, dependent on the used equivalents. Were rCD-1696-L57 with 0,5 equiv has an intensity of 30K, the increase by 4 times to an equiv of 2 increases fluorescence intensity up to 54K. An even further increase in equivalents to 4 even manages to higher fluorescence intensity to around 60K which is a ~2,5-fold increase of fluorescence intensity compared to the untargeted rCD-1696, concluding clear targeting effect of L57 on U87 cells.

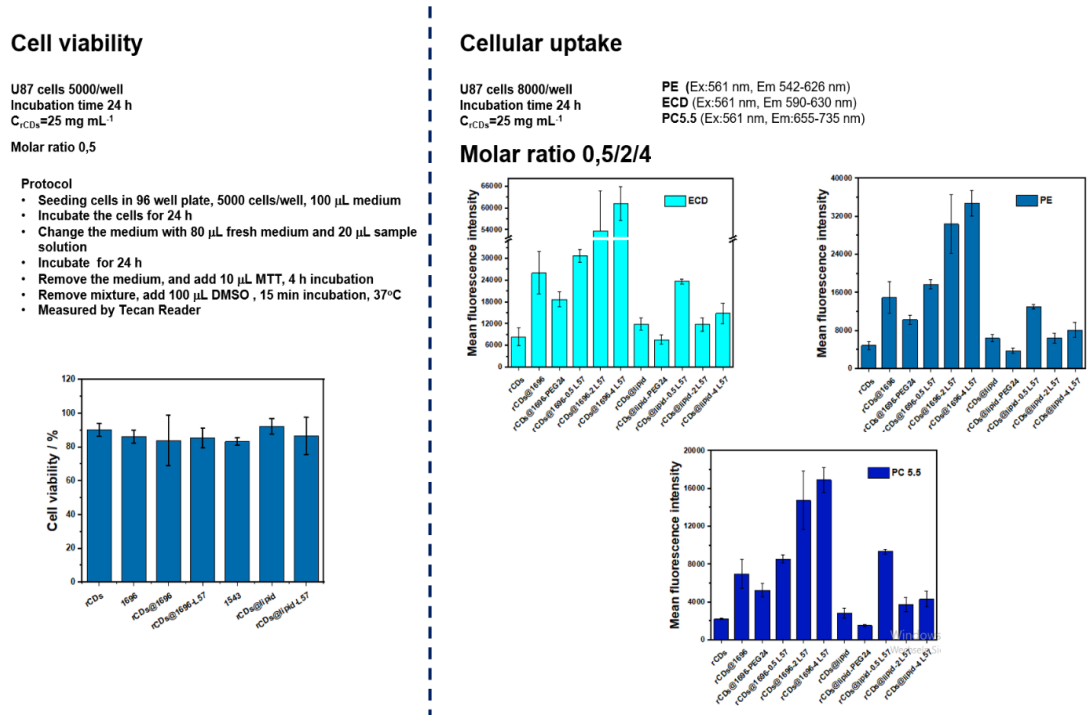

Figure 3.2.4.1. Cellular viability and cellular uptake of rCD-1696 conjugates, surface modified with targeting and shielding agents done by Fengrong Zhang, Pharmaceutical Biology, LMU. For the cellular viability (metabolic activity) U87 cells with 5000/well were chosen. The incubation time was 24 h with a C_{rCDs}=25 mg mL^{-1} and a molar ratio of 0,5 (mol OAA/ mol shielding & targeting agent). Cells determined by the CellTiter-Glo® assay after incubation. Metabolic activities are presented as percentage relative to HBG buffer-treated control cells (mean ± sd; n = 3). The cellular uptake was done with U87 cells with 8000/well, an incubation time of 24 h and a concentration C_{rCDs}=25 mg mL^{-1} (mean ± sd; n = 3). As channels for the mean fluorescence intensity PE (Ex:561 nm, Em 542-626 nm), ECD (Ex:561 nm, Em 590-630 nm), and PC5.5 (Ex:561 nm, Em:655-735 nm) were chosen.

In summary, Fengrong Zhang could show nontoxicity on U87 cells with rCD, 1696, rCD-1696, and rCD-1696-L57. In addition, the data of **3.2.4.1** displays a clear targeting effect of rCD-1696-L57 for U87 cells, concluding a promising candidate for the “Joint Sino-German Research Project”, as further displayed in **6.4.17**. rCD-1696-L57 seems to be a very interesting candidate for efficient BBB bypassing. However, more studies must be done to further evaluate the worth of rCD-1696-L57 by the

collaboration of Ernst Wagner, Ludwig-Maximilians-Universität, Munich, Germany; Rongqin Huang, Fudan University, Shanghai, China, and Yi Wang, Donghua University, Shanghai.

4 Discussion

4.1 Transferrin receptor targeted polyplexes completely comprised of sequence-defined components

The 80 kDa serum iron transport protein transferrin (Tf) has been previously used for targeted pDNA and siRNA delivery.[20, 143-150, 277] In the current study, an only 12-amino acid small protease-resistant retro-enantio peptide binding the TfR, which was recently reported by Giralt and colleagues,[163] has been successfully applied as targeting agent for siRNA and pDNA delivery in combination with sequence-defined T-shaped lipo- OAAs. As outlined in our previous studies and highlighted in the current work, the precise definition of nanocarrier subunits as synthetic sequences combined with screening in gene transfer or gene silencing studies enables a “chemical evolution” of nanocarriers that are tailor-made for specific targets. In the current studies, well stabilizing 1214 / reTfR-2 polyplexes were far better suitable for siRNA delivery than for pDNA delivery. The less stabilized NonOcA-OAA 1258 or 1285 / reTfR-2 was suitable for pDNA delivery into erythroleukemic K562 cells, and the ssbb-based bioreducible DecA- or NonOcA-OAAs 1284 or 1285 / reTfR-2 best suited for neuroblastoma cells. The use of a protease-resistant retro-enantio peptide is an encouraging transition from a protein-based ligand toward an optimized synthetic ligand.[87, 163, 322, 323] Conformational flexibility of a linear peptide ligand (due to the rotational flexibility) is expected to affect its affinity and provides room for future improvements. By computational simulation of the synthetic peptide-receptor interactions (i.e., molecular docking analysis), information about the conformational flexibility of binding sites can be obtained. By this, the ligand sequence might be tuned to fit best to the receptor and its bioactivity can be improved for *in vivo* application. Similar strategies were applied for optimizing cyclic RGD peptides for binding to the integrin receptor.[324-326] Such optimization approaches can speed the development of targeted polyplexes for nucleic acid-based therapy.

4.2 Ligand coated photoluminescent carbon dots as organic carrier-based system for targeted enhanced intracellular delivery

The main strategies in current times for non-viral delivering vehicles for therapy against neurodegenerative diseases and tumors are a vast platform of organic (see **1.1**), and inorganic nanoparticles, as well as biomolecules, and their derivations. They often lack decent *in vivo* stability, poor tumor specificity, toxicity, compromised therapeutic effect, and lack of theranostic effects,[327, 328] indicating the importance of new scientific development of modern, innovative *in vivo* strategies. One of the most promising new candidates in this field of organic nanoparticles are CDs, due to their low to non-cytotoxicity with excellent biocompatibility, water-solubility, and rather inexpensive production, on top of their excellent attributes of photoluminescence, which also enables them for not just therapeutic but theranostic use.[194, 211-215]

It is reported that CDs have been previously used for therapeutic and theranostic use against glioma, Parkinson's disease, and Alzheimer's disease.[241, 329-332] The current report is a part of the Joint Sino-German Research Project, which aims for a LRP1-targeted carbon nanodot-based model to cross the BBB and deliver small molecule or protein drugs into the brain (see **3.2.1**). The focus of this work was the design, characterization, and evaluation of a newly designed CD, namely red CDs (rCDs), with the premise to enable BBB targeting. For that, the rCDs were used as a basis to synthesize a 4-armed OAA library, consisting of 21 carriers, tailormade to encapsulate, or more precise to coat and entrap, the rCDs to enhance nanoparticle properties and to enable a SPAAC lead surface modification of the rCD-OAA conjugates to introduce potential targeting strategies to bypass the BBB (**3.2.2**). The best performer of the library screen is the 4-armed OAA 1696, resulting in the rCD-1696 formulation. As shown in the result part **3.2.4** rCD-1969 can successfully incorporate targeting ligands like reTfR1 and L57 to its surface, creating a CD-based model for BBB targeting and glioblastoma tumor cell lines like U87. Additionally, Zhang could show the dependency of increasing L57 targeting ligand (molar ratio OAA/ molar ratio targeting ligand) highly influences transfection efficacy of the formulation. The increase of L57 from 0,5 equiv to 4 equiv led to a twice as high fluorescence signal, which demonstrates the success in transfection efficacy of the glioma cell model. In conclusion, this preliminary work can display the success of the rCD-1696-L57 conjugate on glioma targeting. However, many more studies must be

done to fully examine the worth of the rCD-1696-L57 formulation. For further evaluation, the laboratory groups of Prof. Dr. Ernst Wagner and Prof. Dr. Rongqin Huang are currently working on this topic. In addition to the rCD-1696-L57 conjugates several other peptide ligands Teoman Benli-Hoppe synthesized to have rCD-1696-based screening on a trans-well BBB model.[333] These peptide ligands are following: tf2, scr-tf2, scr-L57, reL57, Angiopep-2, TGN, and cdx (for more details see **6.3, 6.4.2, 3.2.4.1** and **6.4.17**).

5 Summary

The delivery of therapeutic materials, including small molecules, genes, and oligonucleotides, offers great opportunities for the treatment of many diseases like genetic disorders, neurodegenerative diseases, and various cancer types. Especially sequence-defined polycationic oligoaminoamids (OAAs), as a polymeric nanoplatform, are interesting candidates to deliver nucleic acids and other structures with a polyanionic surface like red CDs. OAAs not just enhance the nanoparticle properties of the formulation but also bring the benefit of enabling the integration of targeting domains and other surface modifications. This thesis displays the research of fine-tuned OAAs, optimized for their different cargos (pDNA, siRNA, CDs), modified targeting peptides, attached via a monodisperse polyethylene glycol (PEG) spacer via click chemistry for enabling direct targeting of several tumor cell lines.

In the first part a highly advanced cationizable lipo-oligoaminoamide (lipo-OAA), 1214, was used to compact siRNA. The created polyplex then was postmodified with a retro-enantio peptide (reTfR) for TfR targeting. Improved gene silencing is demonstrated in TfR-expressing KB and DU145 cells. Analogous pDNA polyplexes are successfully used for receptor-mediated gene delivery in TfR-rich K562 cells and Neuro2a cells. Six lipo-OAAs differing in their lipidic domain and redox-sensitive attachment of lipid residues were tested to evaluate the impact of core polyplex stability on receptor-dependent gene transfer. The current study could show that well stabilizing 1214 / reTfR-2 polyplexes were far better suitable for siRNA delivery than for pDNA delivery. The less stabilized NonOcA-OAA 1258 or 1285 / reTfR-2 was suitable for pDNA delivery into erythroleukemic K562 cells, and the ssbb-based bioreducible DecA- or NonOcA-OAAs 1284 or 1285 / reTfR-2 best suited for neuroblastoma cells. Concluding, the retro-enantio peptide reTfR presented clear TfR receptor targeting, displaying an interesting candidate for improved *in vivo* application, due to its additional stability against serum proteases.

In the second part a 4-armed OAA library of 21 carrier structures to coat and entrap red CDs (rCDs) was synthesized and screened to evaluate the best performer 1696, which encapsulated rCDs in a superior way, displayed by particle size, distribution, and zeta. As a next step this perfectionated formulation was postmodified with

several peptide ligands to test its efficacy on U87 cells. rCD-1696-L57 conjugates had a superior transfection efficacy compared to non-targeted rCD-1696 conjugates, addressing the targeting efficacy of the L57 peptide to the LRP1 receptor, creating a CD-based model for potential BBB targeting, with the far sight of finding therapeutic agents able to treat CNS related neurogenerative diseases or brain cancer like glioma.

6 Appendix

6.1 Abbreviations

ACN	Acetonitrile
AMT	Adsorptive-mediated transcytosis
BBB	Blood-brain barrier
BCECs	Brain capillary endothelial cells
Boc	tert-butyloxycarbonyl
BPEI	Branched polyethylenimine
CD(s)	Carbon dot(s) or Nanodot(s)
CDTA	1,2-diaminocyclohexane-N,N,N’,N’-tetraacetic acid
CMT	Carrier-mediated transport
CNS	Central nervous systems
CNT	Carbon nanotubes
COF	Covalent organic frameworks
CPD(s)	Carbonized polymer dot(s)
CQD(s)	Carbon quantum dot(s)
CS	Chitosan
Da	Dalton
DBCO	Dibenzocyclooctyne group
DBU	1,8-Diazabicyclo[5.4.0]undec-7-ene
DCM	Dichloromethane
Dde	4,4-Dimethyl-2,6-dioxocyclohexylidene)ethyl protecting group

DecA	Decanoic acid
DFG	Deutsche Forschungsgemeinschaft
DHB	2,3-Dihydroxybenzoic acid
DIC	Diisopropylcarbodiimid
DIPEA	N,N-Diisopropylethylamine
DLS	Dynamic light scattering
DMEM	Dulbecco’s Modified Eagle Medium
DMF	N,N-Dimethylformamide
DMSO	Dimethyl sulfoxide
DNA	Deoxyribonucleic acid
DTT	Dithiothreitol
DU-145	Prostate carcinoma cell line
EDT	1,2-ethanedithiol
EDTA	Ethylendiaminetetraacetic acid
EGF	Epidermal growth factor receptor
eGFP	Enhanced green fluorescent protein
EPR	Enhanced permeability and retention
equiv	Equivalents
EtBr	Ethidium bromide
FBS	Fetal bovine serum
Fmoc	Fluorenylmethoxycarbonyl
GFP	Green fluorescent protein
GQD(s)	Graphene quantum dot(s)

GSH	Glutathione
HA	Hyaluronic acid
HBG	Hepes-buffered glucose
HBTU	2-(1H-benzotriazole-1-yl)-1,1,3,3-tetramethyluronium hexafluorophosphate
HEPES	N-(2-hydroxethyl) piperazine-N‘-(2-ethansulfonic acid)
HES	Hydroxyethyl starch
HMW	High molecular weight
HOBt	1-Hydroxybenzotriazole
HPLC	High-performance liquid chromatography
ivDde	4,4-Dimethyl-2,6-dioxocyclohex-1-ylidene-3-methylbutyl-N-epsilon-(9-fluorenylmethyloxycarbonyl
K-562	Human erythroleukemic suspension cell line
KCN	Potassium cyanide
kDa	Kilodalton
LDLR	Low-density lipoprotein receptor
LNP(s)	Lipid nanoparticle(s)
LPEI	Linear polyethylenimine
LRP1	Receptor low-density lipoprotein receptor-related peptide
LRP-1	Low Density Lipoprotein Receptor-Related Protein 1
Luc	Luciferin
MALDI	Matrix-assisted laser desorption/ionization
MDR	Multi-drug resistance
mM	Millimolar

MRI	Magnetic resonance imaging
mRNA	Messenger RNA
MS	Mass spectrometry
MTBE	Methyl tert-butyl ether
MTT	3-(4,5-dimethylthiazol-2-yl)-2,5-diphenyltetrazolium bromide
mV	Millivolt
N/P	Nitrogen to phosphates ratio
N2a	Murine adherent neuroblastoma cell line
Neuro-2a	Murine adherent neuroblastoma cell line
NHS	N-Hydroxysuccinimide
NIR	Near-Infrared
NIS	Sodium iodide symporter
nm	Nanometer
NMP	N-Methyl-2-pyrrolidone
NMR	Nuclear magnetic resonance
NonOcA	8-nonanamidooctanoic acid
NP(s)	Nanoparticle(s)
OAA(s)	Oligoaminoamid(s)
OleA	Oleic acid
OtBu	tert-butyl
PAA	Polyacrylic acid
Pbf	2,2,4,6,7-pentamethyIdlhydrobenzofuran-5-sulfonyl group
PCL	Poly-ε-caprolactone

pCMVLuc	Luciferase under control of cytomegalovirus promotor and enhancer
PDI	Polydispersity index
pDNA	Plasmid DNA
PEG	Polyethylene glycol
PEI	Polyethylenimine
PGA	Polyglycolic acid
P-gp	P-glycoprotein
pHPMA	N-(2-hydroxypropyl) methacrylamide
pKa	-log10 Ka (acid dissociation constant)
PL	Photoluminescence
PLA	Polylactic acid
PLGA	Poly(lactide-co-glycolide)
PLL	Poly(L-Lysine)
PNVCL	Poly(N-vinylcaprolactam)
PPO	Poly(propylene oxide)
PyBOP	Benzotriazol-1-yloxy-tripyrrolidinophosphonium hexafluorophosphate
QY	High quantum yield
rCD(s)	Red Carbon dot(s)
RES	Reticulo-endothelial system
re	retro-enantio
RLU	Relative light unit
RMT	Receptor-mediated transcytosis
RP-HPLC	Reversed-phase high-performance liquid chromatography

rpm	Rounds per minute
RT	Room temperature
RTP	Room temperature phosphorescence
scr	scramble
SEC	Size-exclusion chromatography
siGFP	Green fluorescent protein specified small interfering RNA
siRNA	Small interfering RNA
siRNA	Small interfering RNA
SN	Substantia nigra
SPAAC	Strain-promoted azide-alkyne cycloaddition
SPDP	Succinimidyl 3-(2-pyridyldithio)propionate
Sph	Succinoyl-pentaethylene hexamine
SPION	Superparamagnetic iron oxide nanoparticles
SPPS	Solid phase peptide synthesis
SPSS	Solid-phase supported synthesis
ssbb	Succinoylcystamine
STOTDA	N-Fmoc-N″-succinyl-4,7,10-trioxa-1,13-tridecandiamin
Stp	Succinoyl tetraethylene pentamine
TADF	Thermally activated delayed fluorescence
TBE	Tris-boric acid-EDTA buffer
tBu	tert-butyl
TCEP	Tris(2-carboxyethyl)phosphine
TEM	Transmission electron microscopy

TEPA	Tetraethylene pentamine
Tf	Transferrin Protein
TFA	Trifluoroacetic acid
TFP	Tetrafluorophenyl esters
TfR	Transferrin Receptor
THF	Tetrahydrofuran
TIS	Triisopropylsilane
TME	Tumor microenvironment
Trt	Trityl
U87	Human brain glioblastoma cell line
ZS	Zetasizer
TOF	Time of flight

6.2 Summary of SPSS derived OAAs

Summary of SPSS derived OAAs

OAA ID	Topology	Sequence (N → C)	Chapter
1284	Lipo-OAA	H_2N-K(N_3)-Y_3-(H-Stp)$_2$-H-K(G-ssbb-K(DecA)$_2$)-H-(Stp-H)$_2$-Y_3-COOH	3.1
1276	Lipo-OAA	H_2N-K(N_3)-C-Y_3-(H-Stp)$_2$-H-K(K(DecA)$_2$)-H-(Stp-H)$_2$-Y_3-C-COOH	3.1
1285	Lipo-OAA	H_2N-K(N_3)-Y_3-(H-Stp)$_2$-H-K(G-ssbb-K(NonOcA)$_2$)-H-(Stp-H)$_2$-Y_3-COOH	3.1
1258	Lipo-OAA	H_2N-K(N_3)-C-Y_3-(H-Stp)$_2$-H-K(K(NonOcA)$_2$)-H-(Stp-H)$_2$-Y_3-C-COOH	3.1
1218	Lipo-OAA	H_2N-K(N_3)-Y_3-(H-Stp)$_2$-H-K(G-ssbb-K(OleA)$_2$)-H-(Stp-H)$_2$-Y_3-COOH	3.1
1214	Lipo-OAA	H_2N-K(N_3)-C-Y_3-(H-Stp)$_2$-H-K(K(OleA)$_2$)-H-(Stp-H)$_2$-Y_3-C-COOH	3.1
1463	4-armed OAA	A-K-(H-K-(H-Stp-H-Stp-H-Stp-H-C-KN3)2)2	3.2
1479	4-armed OAA	A-K-(H-K-(H-Stp-H-Stp-H-Stp-H-YYY-C-KN3)2)2	-
1481	4-armed OAA	A-K-(H-K-(H-Stp-H-K-Stp-H-K-Stp-H-K-C-KN3)2)2	-
1482	4-armed OAA	A-K-(H-K-(H-Stp-H-Stp-H-Stp-H-WWW-C-KN3)2)2	-
1493	4-armed OAA	A-K-(H-K-(H-Stp-H-W-Stp-H-W-Stp-H-W-C-KN3)2)2	-
1494	4-armed OAA	A-K-(H-K-(H-Stp-H-R-Stp-H-R-Stp-H-R-C-KN3)2)2	-
1495	4-armed OAA	A-K-(H-K-(H-Stp-H-Stp-H-Stp-H-RRR-C-KN3)2)2	-
1496	4-armed OAA	A-K-(H-K-(H-Stp-H-Stp-H-Stp-H-C-L)2)2	-
1513	4-armed	A-K-(H-K-(H-Sph-H-Sph-H-Sph-H-C-KN3)2)2	-

	OAA		
1514	4-armed OAA	A-K-(H-K-(H-Sph-H-Sph-H-Sph-H-YYYC-KN3)2)2	-
1515	4-armed OAA	A-K-(H-K-(H-Sph-H-Sph-H-Sph-H-WWWC-KN3)2)2	-
1516	4-armed OAA	A-K-(H-K-(H-Sph-H-Sph-H-Sph-H-RRRC-KN3)2)2	-
1517	4-armed OAA	A-K-(H-K-(H-Sph-H-K-Sph-H-K-Sph-H-K-C-KN3)2)2	-
1518	4-armed OAA	A-K-(H-K-(H-Sph-H-W-Sph-H-W-Sph-H-W-C-KN3)2)2	-
1519	4-armed OAA	A-K-(H-K-(H-Sph-H-R-Sph-H-R-Sph-H-R-C-KN3)2)2	-
1655	4-armed OAA	(*N-α-Fmoc*): A-K-(H-K-(K6-C-KN3)2)2	3.2
1656	4-armed OAA	(*N-α-Fmoc*): A-K-(H-K-(K12-C-KN3)2)2	3.2
1657	4-armed OAA	(*N-α-Fmoc*): A-K-(H-K-(K3-L-K3-L-K-L-C-KN3)2)2	3.2
1658	4-armed OAA	(*N-α-Fmoc*): A-K-(H-K-(K3-L3-K3-L3-K-L3-C-KN3)2)2	3.2
1660	4-armed OAA	(*N-α-Fmoc*): A-K-(H-K-(K3-L2-K3-L2-K3-L2-C-KN3)2)2	3.2
1661	4-armed OAA	(*N-α-Fmoc*): A-K-(H-K-(K-L-K-L-K-L-K-L-K-L-K-L-C-KN3)2)2	3.2
1662	4-armed OAA	(*N-α-Fmoc*): A-K-(H-K-(K4-L4-K4-C-KN3)2)2	3.2
1663	4-armed OAA	(*N-α-Fmoc*): A-K-(H-K-(K3-Y-K3-Y-K3-Y-C-KN3)2)2	3.2
1664	4-armed	(*N-α-Fmoc*): A-K-(H-K-(K3-Y3-K3-Y3-K3-Y3-C-KN3)2)2	3.2

	OAA		
1665	4-armed OAA	(*N-α-Fmoc*): A-K-(H-K-(K3-Y2-K3-Y2-K3-Y2-C-KN3)2)2	3.2
1666	4-armed OAA	(*N-α-Fmoc*): A-K-(H-K-(K-Y-K-Y-K-Y-K-Y-K-Y-K-Y-C-KN3)2)2	3.2
1667	4-armed OAA	(*N-α-Fmoc*): A-K-(H-K-(K4-Y4-K4-C-KN3)2)2	3.2
1694	4-armed OAA	(*N-ε-Fmoc*): A-K-(H-K-(K12-C-KN3)2)2	3.2
1695	4-armed OAA	(*N-ε-Fmoc*): A-K-(H-K-(K3-Y-K3-Y-K3-Y-C-KN3)2)2	3.2
1696	4-armed OAA	(*N-ε-Fmoc*): A-K-(H-K-(K3-Y3-K3-Y3-K3-Y3-C-KN3)2)2	3.2
1697	4-armed OAA	(*N-ε-Fmoc*): A-K-(H-K-(K3-Y2-K3-Y2-K3-Y2-C-KN3)2)2	3.2
1698	4-armed OAA	(*N-ε-Fmoc*): A-K-(H-K-(K-Y-K-Y-K-Y-K-Y-K-Y-K-Y-C-KN3)2)2	3.2
1699	4-armed OAA	(*N-ε-Fmoc*): A-K-(H-K-(K4-Y4-K4-C-KN3)2)2	3.2
1767	4-armed OAA	(*N-ε-Fmoc*): A-K-(H-K-(K6-C-KN3)2)2	3.2
1768	4-armed OAA	(*N-α-Fmoc*): A-K-(H-K-(K9-C-KN3)2)2	3.2
1769	4-armed OAA	(*N-ε-Fmoc*): A-K-(H-K-(K9-C-KN3)2)2	3.2

6.3 Summary of SPSS derived shielding and targeting agents

Summary of SPSS derived shielding and targeting agents

Name	**Sequence (N→C)**	**Transporter**
PEG1	H_2N-**PEG_{24}**-COOH	No targeting
PEG2	$(DBCO\text{-}PEG_4)_2$-K-**PEG_{24}**-COOH	No targeting
R-PEG1	DBCO-PEG24-**R**-COOH	No targeting
R-PEG2	$(DBCO\text{-}PEG_4)_2$-K-PEG_{24}-**R**-COOH	No targeting
reTfR1	DBCO-PEG_{24}-**pwvpswmpprht**-$CONH_2$	TfR
reTfR2	$(DBCO\text{-}PEG_4)_2$-K-PEG_{24}-**pwvpswmpprht**-$CONH_2$	TfR
scr-TfR1	DBCO-PEG_{24}-**vprhptsppmww**-$CONH_2$	TfR
scr-TfR2	$(DBCO\text{-}PEG_4)_2$-K-PEG_{24}-**vprhptsppmww**-$CONH_2$	TfR
hTF4	DBCO-PEG_4-**Human Transferrin**	TfR
hTF12	DBCO-PEG_{12}-**Human Transferrin**	TfR
HSA12	DBCO-PEG_{12}-**Human serum albumin**	
Tf2	DBCO-$CPEG_{24}$-GGG-**HKYLRW**-COOH	Tf-binding, for TfR
Tf2-fluorescein	Fluorescein-CGGG-**HKYLRW**-COOH	Tf-binding, for TfR
scr-Tf2	DBCO-$CPEG_{24}$-GGG-**WRKHLY**-COOH	Tf-binding, for TfR
L57	DBCO-$CPEG_{24}$-**TWPKHFDKHTFYSILKLGKH**-COOH	LRP1
scr-L57	DBCO-$CPEG_{24}$-**KPFKHGTDLLKHFWYSHTKI**-COOH	LRP1
reL57	DBCO-$CPEG_{24}$-**hkGlklisyfthkdfhkpwt**-COOH	LRP1
Angiopep-2	DBCO-$CPEG_{24}$-**TFFYGGSRGKRNNFKTEEY**-COOH	LRP1
cRGD-	DBCO-PEG_{24}-c(**RGDfK**)	integrin

DBCO		
TGN	DBCO-CPEG$_{24}$-**TGNYKALHPHNG**-COOH	unknown
cdx	DBCO-CPEG$_{24}$-**GreirtGraerwsekf**-COOH	nAChRs
reTfR-KN3	N_3K-PEG$_{24}$-**pwvpswmpprht**-CONH$_2$	TfR
cRGD-KN3	c(**RGDfK**)-KN3	integrin
PEG4-KN3	N_3K-PEG$_4$-COOH	No targeting

6.4 Analytical Data

6.4.1 ^{1}H NMR Spectra of OAAs

1463

Sequence (C → N): A-K-(H-K-(H-Stp-H-Stp-H-Stp-H-C-KN3)2)2

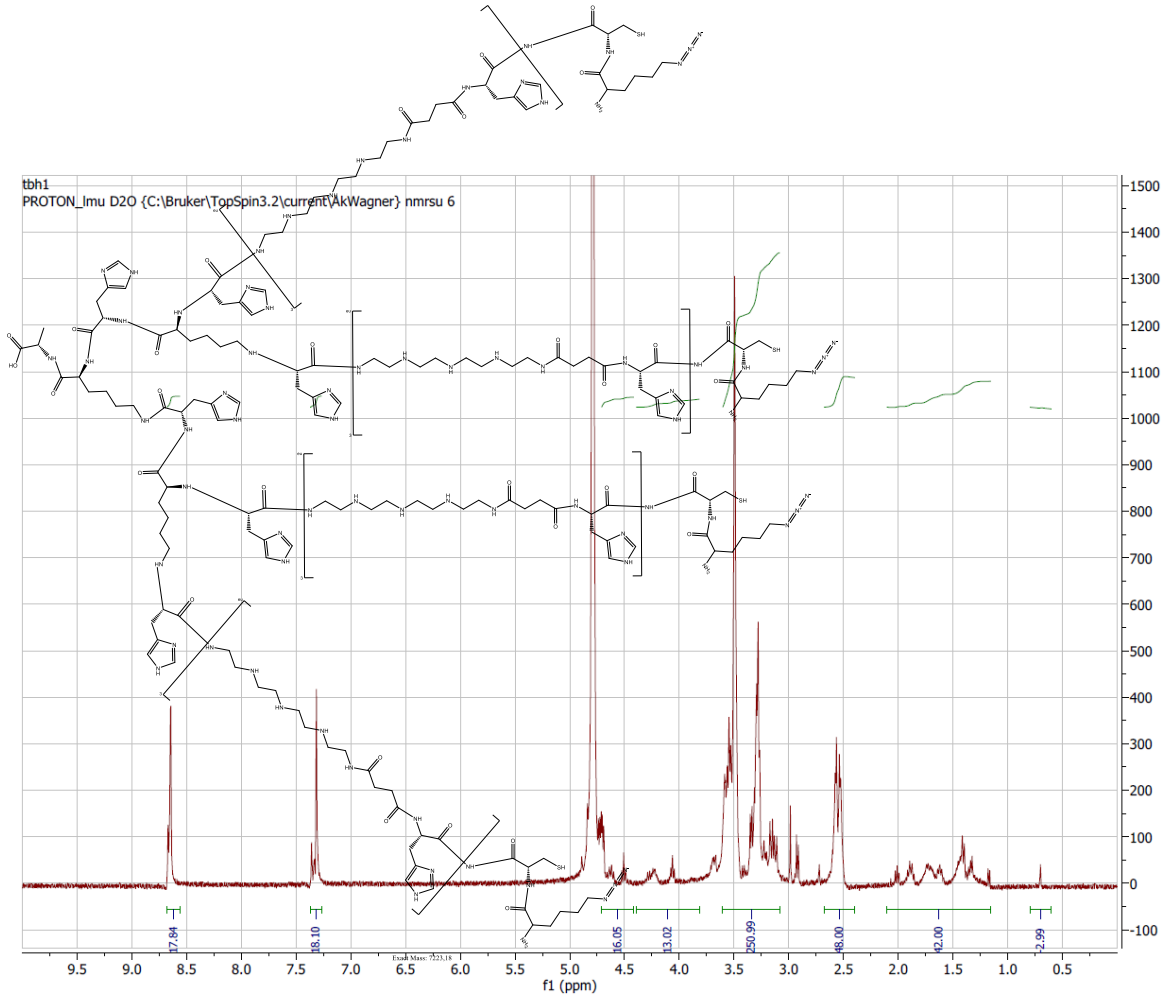

^{1}H-NMR spectrum of 1463 four-arm structure, recorded in D_2O. δ (ppm) = 0.5-1.0 (m, 3 H, βH alanine); 1.0-2.3 (m, 42 H, βγδH lysine); 2.3-2.6 (m, 48 H, -CO-CH_2-CH_2-CO-succinic acid); 2.8-3.6 (m, 250 H, -CH_2- TEPA, βH cysteine, βH histidine, εH lysine); 4.0-4.3 (m, 14 H, αH alanine, αH cysteine, αH lysine); 4.4-4.7 (m, 18 H, αH histidine); 7.0-7.5 (m, 18 H, imidazole); 8.4-8.7 (d, 18 H, imidazole)

1493

Sequence (C → N): A-K-(H-K-(H-Stp-H-W-Stp-H-W-Stp-H-W-C-KN3)2)2

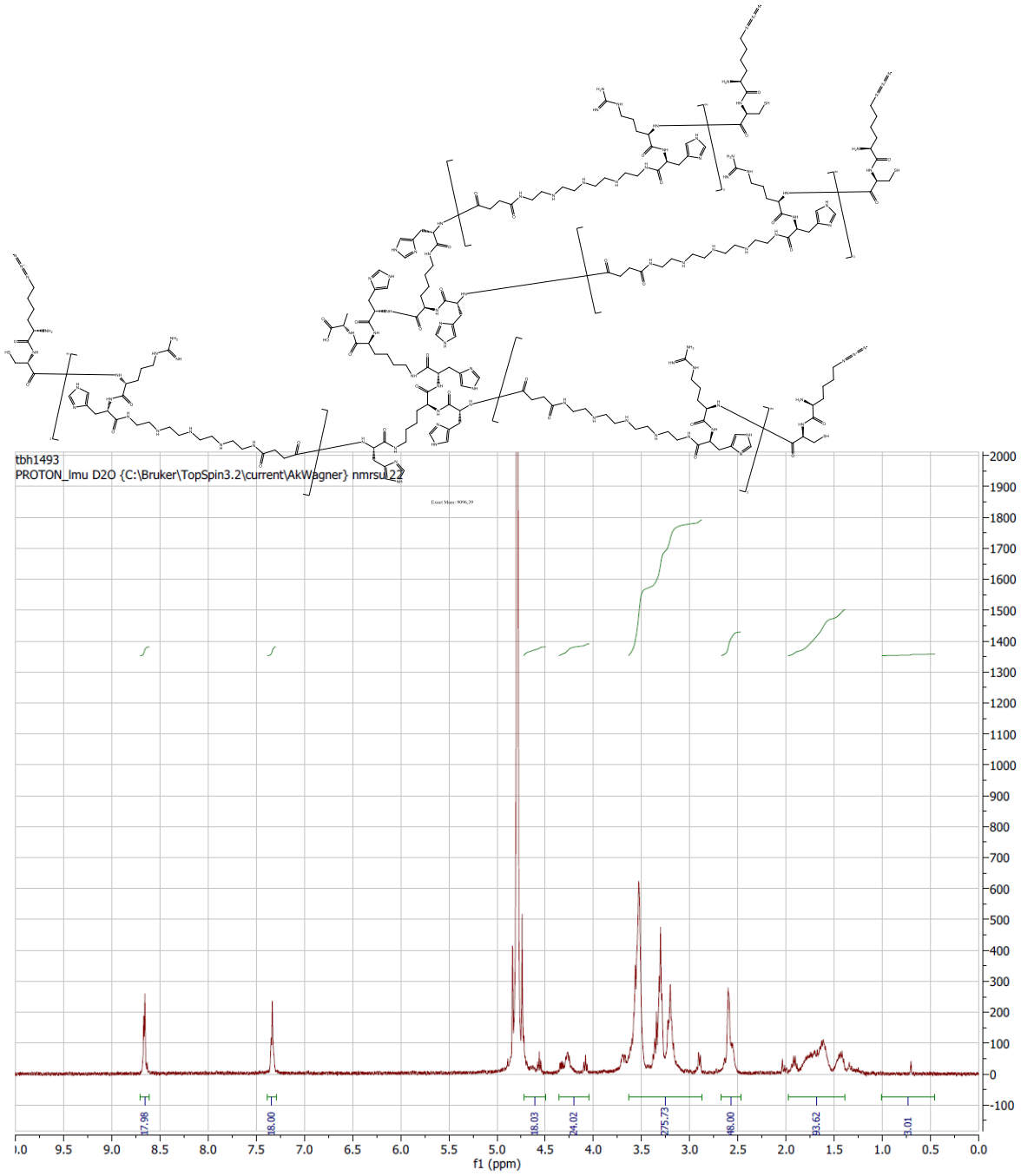

^{1}H-NMR spectrum of 1493 four-arm structure, recorded in D_2O. δ (ppm) = 0.45-1.01(m, 3 H, βH alanine); 1.39-1.98 (m, 90 H, βγδH lysine, βγH arginine); 2.47-2.67 (m, 48 H, -CO-CH_2-CH_2-CO- succinic acid); 2.87-3.64 (m, 274 H, -CH_2- TEPA, βH cysteine, βH histidine, εH lysine, δH arginine); 4.04-4.36 (m, 24 H, αH alanine, αH cysteine, αH lysine, αH arginine); 4.49-4.72 (m, 18 H, αH histidine); 7.29-7.39 (m, 18 H, imidazole); 8.61-8.71 (d, 18 H, imidazole)

1494

Sequence (C → N): A-K-(H-K-(H-Stp-H-R-Stp-H-R-Stp-H-R-C-KN3)2)2

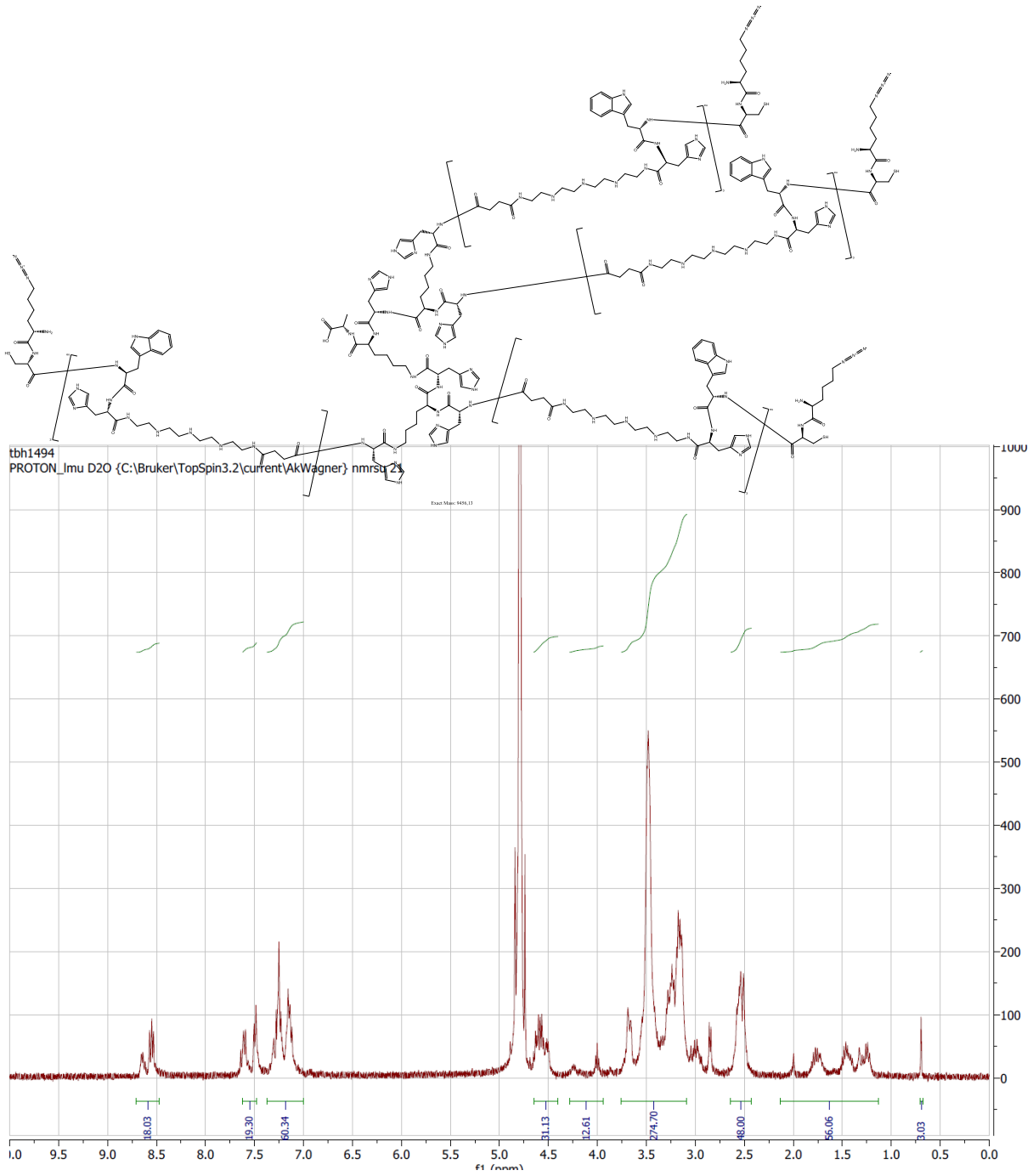

^{1}H-NMR spectrum of 1494 four-arm structure, recorded in D_2O. δ (ppm) = 0.68-0.71 (m, 3 H, βH alanine); 1.13-2.13 (m, 42 H, βγδH lysine); 2.43-2.64 (m, 48 H, -CO-CH_2-CH_2-CO- succinic acid); 3.09-3.76 (m, 274 H, -CH_2- TEPA, βH cysteine, βH histidine, εH lysine, βH tryptophan); 3.94-4.28 (m, 12 H, αH alanine, αH cysteine, αH lysine); 4.4-4.65 (m, 30 H, αH histidine, αH tryptophan); 7.0-7.37 (m, 18 H, imidazole); 7.44-7.52 (m, 12 H, indolaromat); 8.47-8.71 (d, 18 H, imidazole)

1495

Sequence (C → N): A-K-(H-K-(H-Stp-H-Stp-H-Stp-H-RRR-C-KN3)2)2

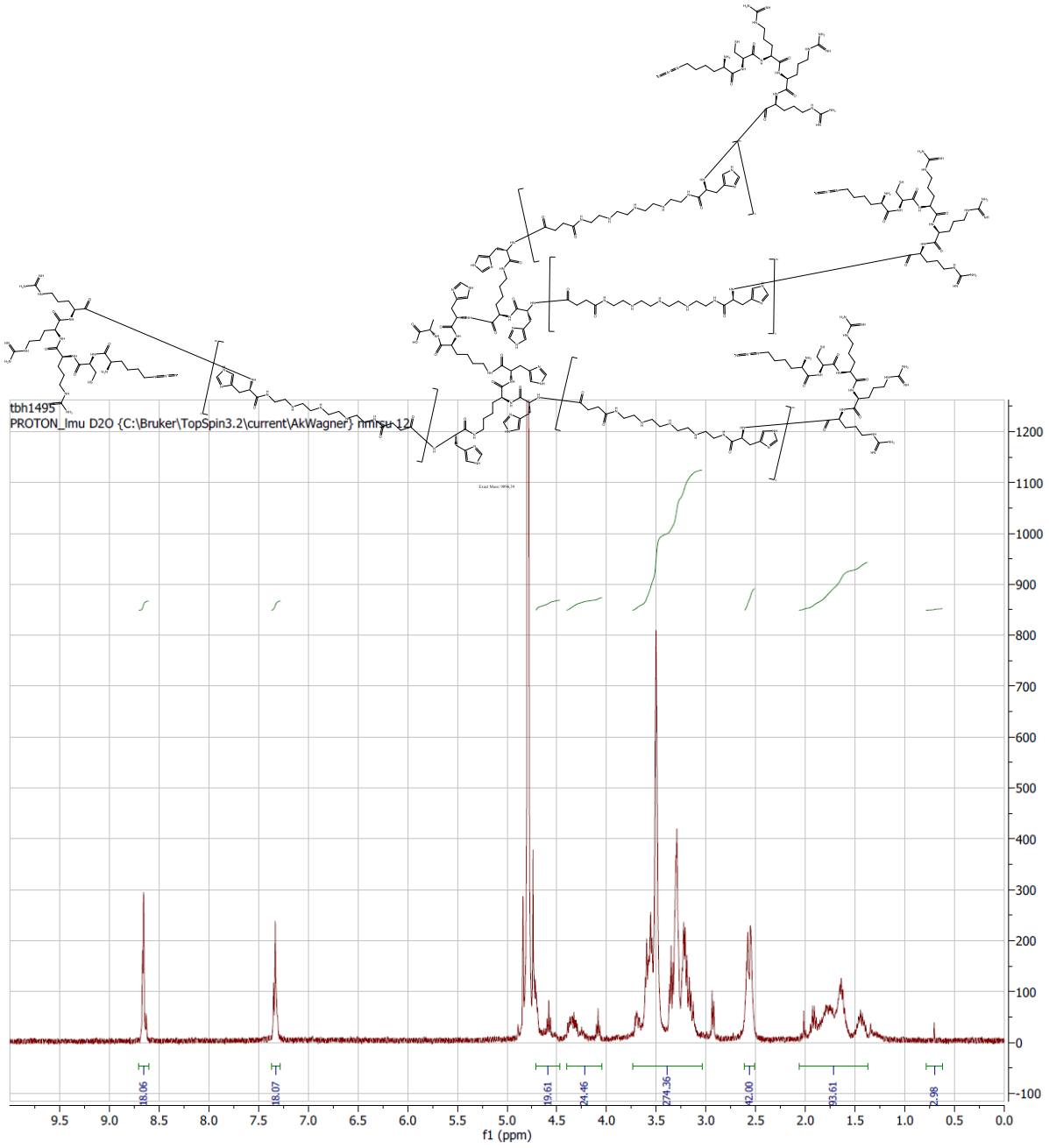

^{1}H-NMR spectrum of 1495 four-arm structure, recorded in D_2O. δ (ppm) = 0.62-0.79 (m, 3 H, βH alanine); 1.38-2.06 (m, 90 H, βγδH lysine, βγH arginine); 2.51-2.61 (m, 48 H, -CO-CH_2-CH_2-CO- succinic acid); 3.04-3.74 (m, 274 H, -CH_2- TEPA, βH cysteine, βH histidine, εH lysine, δH arginine); 4.05-4.40 (m, 24 H, αH alanine, αH cysteine, αH lysine, αH arginine); 4.47-4.71 (m, 18 H, αH histidine); 7.28-7.37 (m, 18 H, imidazole); 8.61-8.70 (d, 18 H, imidazole)

1496

Sequence (C → N): A-K-(H-K-(H-Stp-H-Stp-H-Stp-H-C-L)2)2

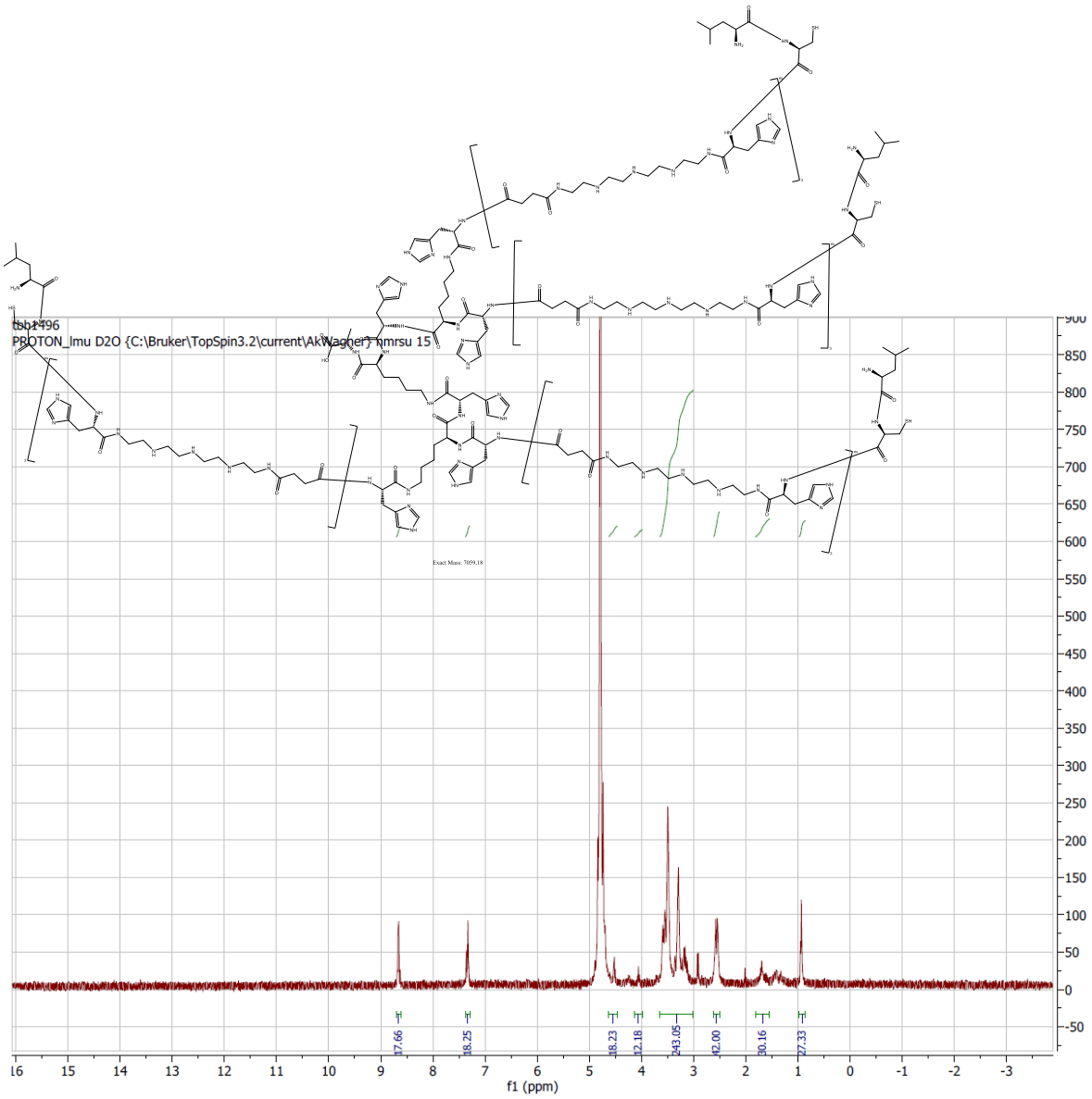

^{1}H-NMR spectrum of 1496 four-arm structure, recorded in D_2O. δ (ppm) = 0.78-0.86 (m, 27 H, βH alanine, δH leucin); 1.55-1.82 (m, 30 H, βγH leucine, βγδH lysine); 2.51-2.62 (m, 48 H, -CO-CH_2-CH_2-CO- succinic acid); 3.01-3.65 (m, 242 H, -CH_2-TEPA, βH cysteine, βH histidine, εH lysine); 3.98-4.14 (m, 12 H, αH alanine, αH cysteine, αH lysine, αH leucine); 4.47-4.63 (m, 18 H, αH histidine); 7.29-7.38 (m, 18 H, imidazole); 8.61-8.71 (d, 18 H, imidazole)

1513

Sequence (C → N): A-K-(H-K-(H-Sph-H-Sph-H-Sph-H-C-KN3)2)2

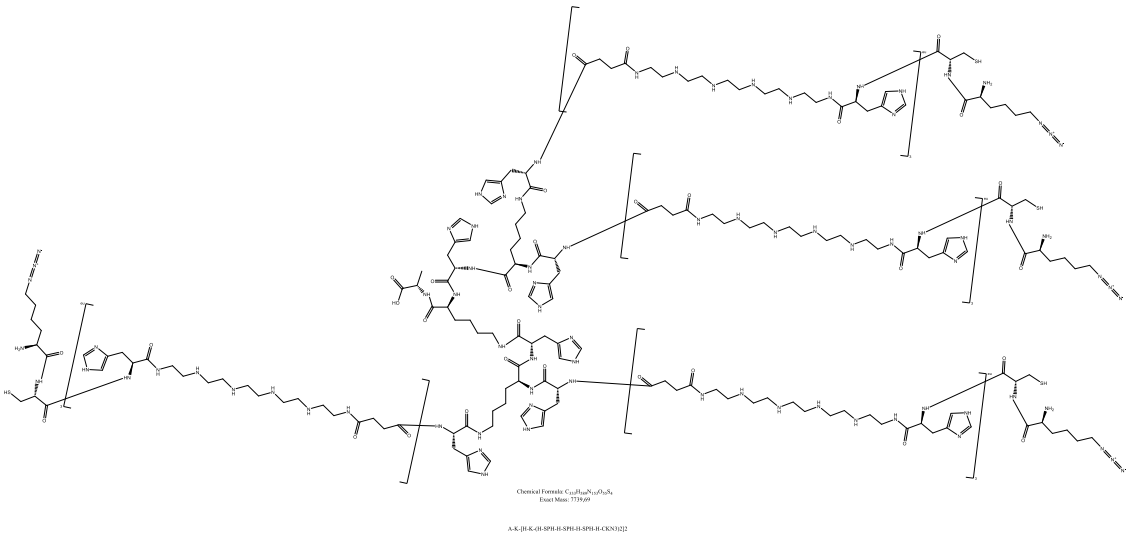

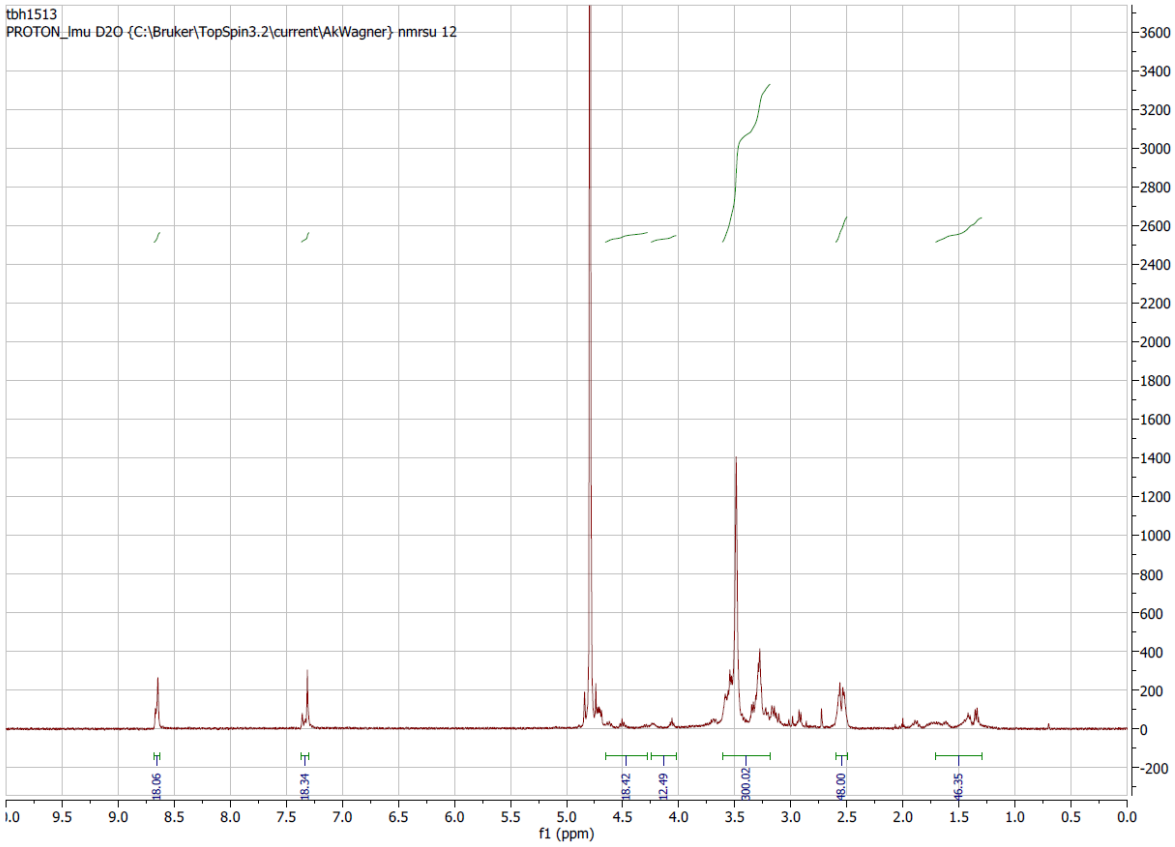

^{1}H-NMR spectrum of 1513 four-arm structure, recorded in D_2O. δ (ppm) = 0.67-0.79 (m, 3 H, βH alanine); 1.30-1.71 (m, 42 H, βγδH lysine); 2.50-2.60 (m, 48 H, -CO-CH_2-CH_2-CO- succinic acid); 3.19-3.61 (m, 298 H, -CH_2- PEHA, βH cysteine, βH histidine, εH lysine); 4.02-4.25 (m, 12 H, αH alanine, αH cysteine, αH lysine); 4.28-4.65 (m, 18 H, αH histidine); 7.30-7.37 (m, 18 H, imidazole), 8.63-8.68 (d, 18 H, imidazole)

1514

Sequence (C → N): A-K-(H-K-(H-Sph-H-Sph-H-Sph-H-YYYC-KN3)2)2

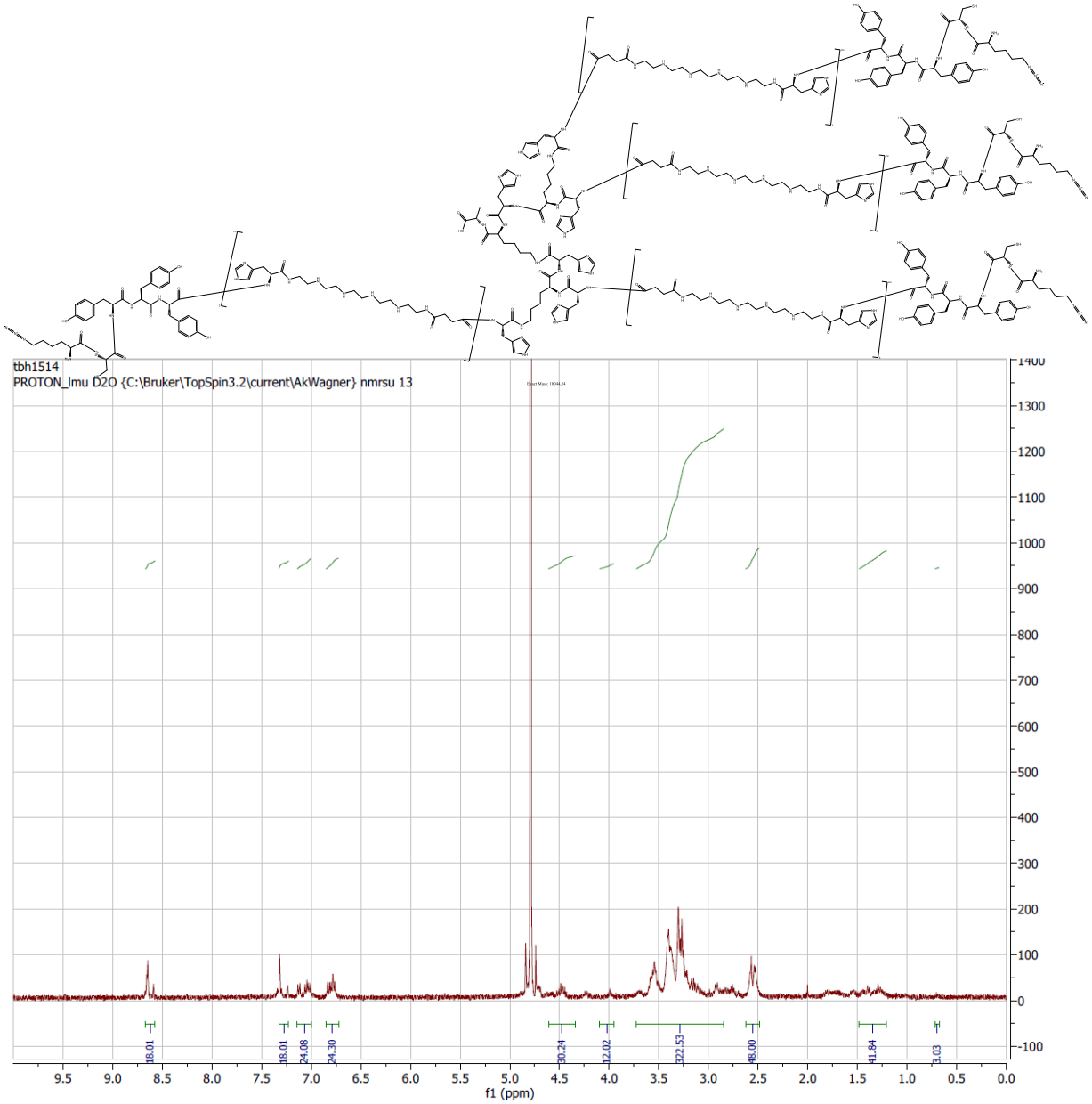

^{1}H-NMR spectrum of 1514 four-arm structure, recorded in D_2O. δ (ppm) = 0.68-0.72 (m, 3 H, βH alanine); 1.21-1.48 (m, 42 H, βγδH lysine); 2.49-2.63 (m, 48 H, -CO-CH_2-CH_2-CO- succinic acid); 2.85-3.73 (m, 322 H, -CH_2- PEHA, βH cysteine, βH histidine, εH lysine, βH tyrosine); 3.95-4.10 (m, 12 H, αH alanine, αH cysteine, αH lysine); 4.34-4.61 (m, 18 H, αH histidine); 6.72-6.85 (m, 48 H, phenole); 7.0-7.14 (m, 12 H, αH tyrosine); 7.23-7.33 (m, 18 H, imidazole); 8.57-8.67 (d, 18H, imidazole)

1515

Sequence (C → N): A-K-(H-K-(H-Sph-H-Sph-H-Sph-H-WWWC-KN3)2)2

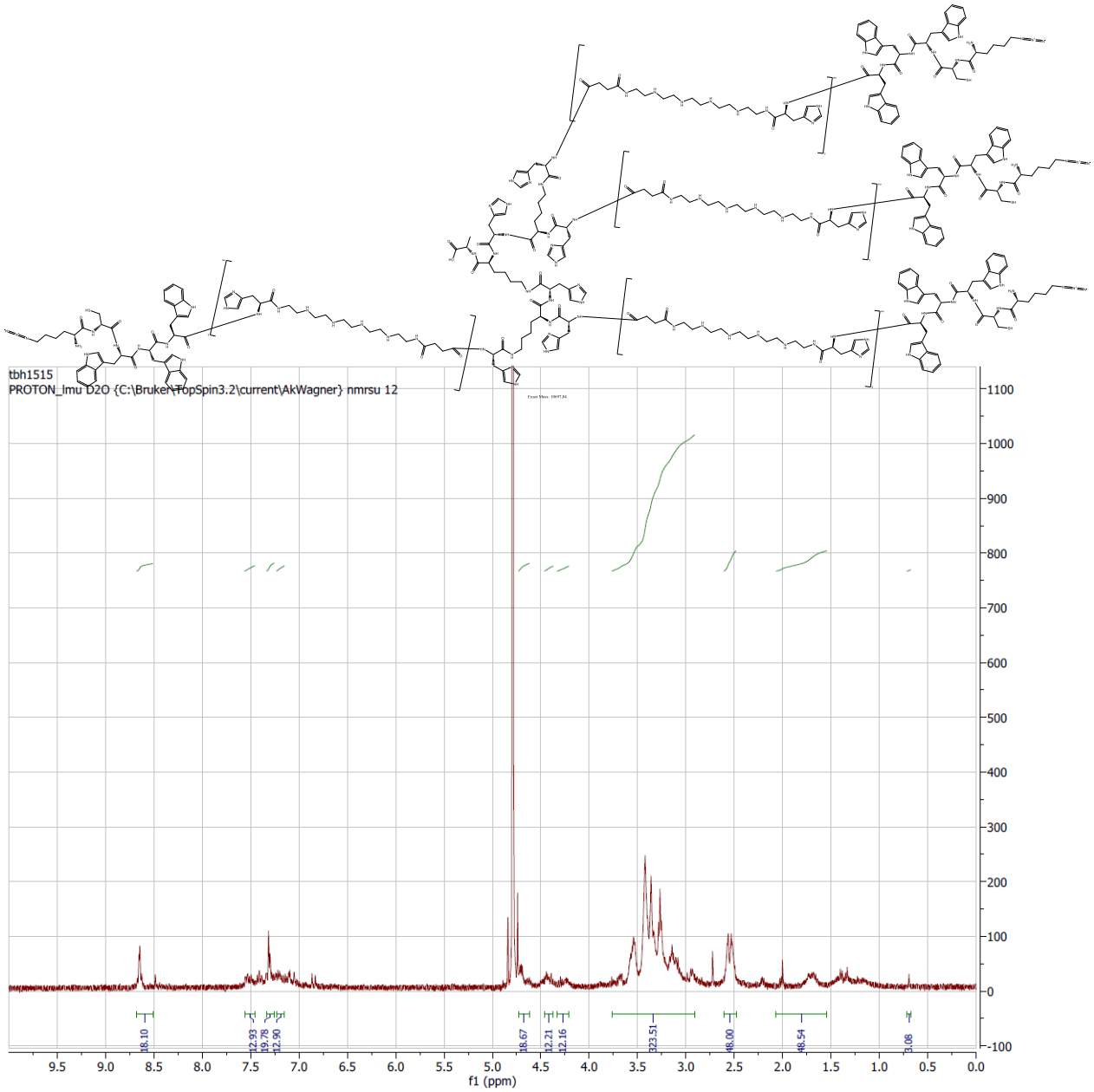

^{1}H-NMR spectrum of 1515 four-arm structure, recorded in D_2O. δ (ppm) = 0.67-0.72 (m, 3 H, βH alanine); 1.54-2.07 (m, 42 H, βγδH lysine); 2.48-2.61 (m, 48 H, -CO-CH_2-CH_2-CO- succinic acid); 2.91-3.77 (m, 322 H, -CH_2- PEHA, βH cysteine, βH histidine, εH lysine, βH tryptophane); 4.21-4.33 (m, 12 H, αH alanine, αH cysteine, αH lysine); 4.37-4.46 (m, 12 H, αH tryptophan); 4.62-4.73 (m, 18 H, αH histidine); 7.15-7.23 (m, 12 H, indolaromat); 7.26-7.34 (m, 18H, imidazole); 7.46-7.56 (m, 12 H, indolaromat); 8.51-8.68 (d, 18H, imidazole)

1516

Sequence (C → N): A-K-(H-K-(H-Sph-H-Sph-H-Sph-H-RRRC-KN3)2)2

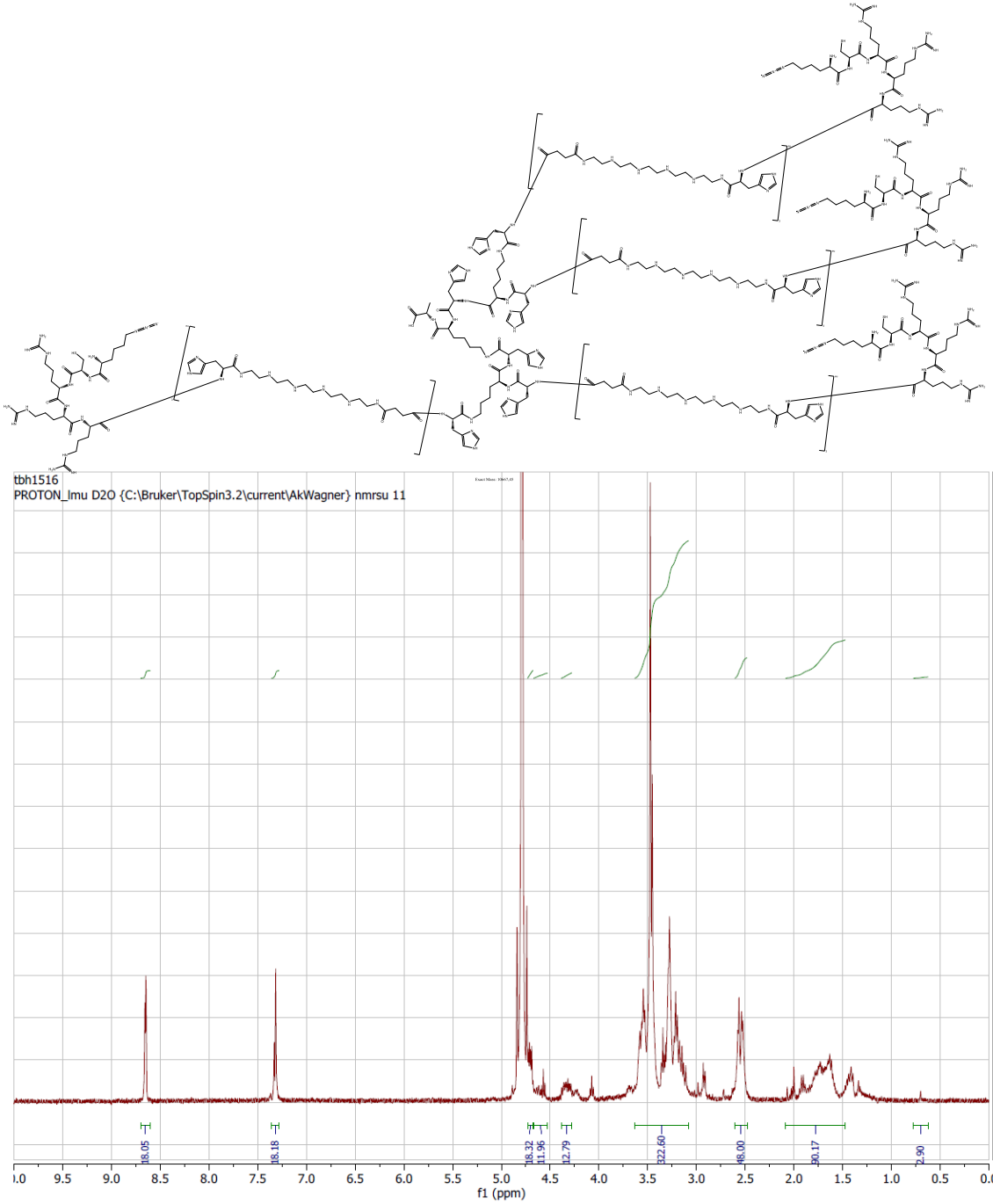

^{1}H-NMR spectrum of 1516 four-arm structure, recorded in D_2O. δ (ppm) = 0.62-0.77 (m, 3 H, βH alanine); 1.47-2.08 (m, 90 H, βγδH lysine, βγH arginine); 2.48-2.61 (m, 48 H, -CO-CH_2-CH_2-CO- succinic acid); 3.8-3.63 (m, 322 H, -CH_2- PEHA, βH cysteine, βH histidine, εH lysine, δH arginine); 4.28-4.39 (m, 12 H, αH alanine, αH cysteine, αH lysine);4.53-4.67 (m, 12 H, αH arginine);4.67-4.73 (m, 18H, αH histidine); 7.28-7.36 (m, 18H, imidazole); 8.60-8.70 (d, 18H, imidazole)

1517

Sequence (C → N): A-K-(H-K-(H-Sph-H-K-Sph-H-K-Sph-H-K-C-KN3)2)2

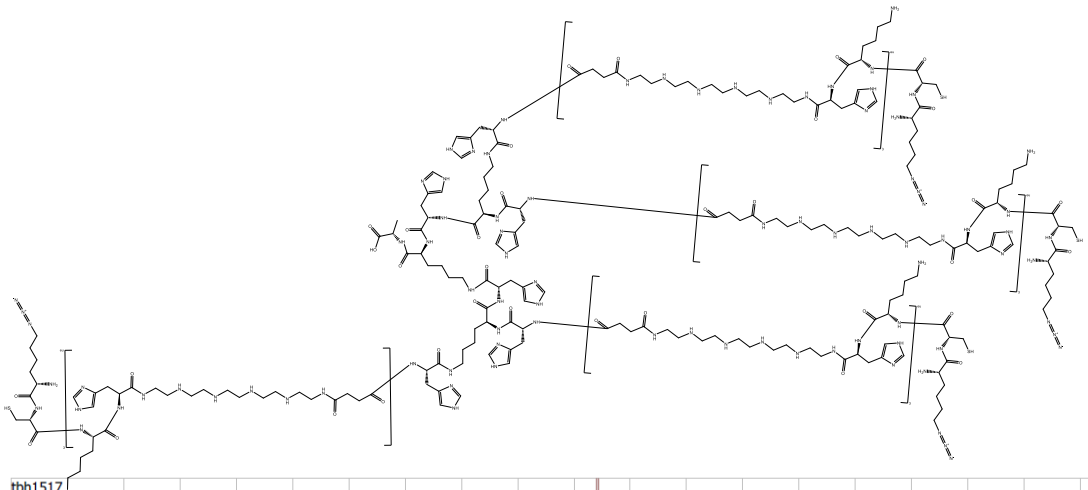

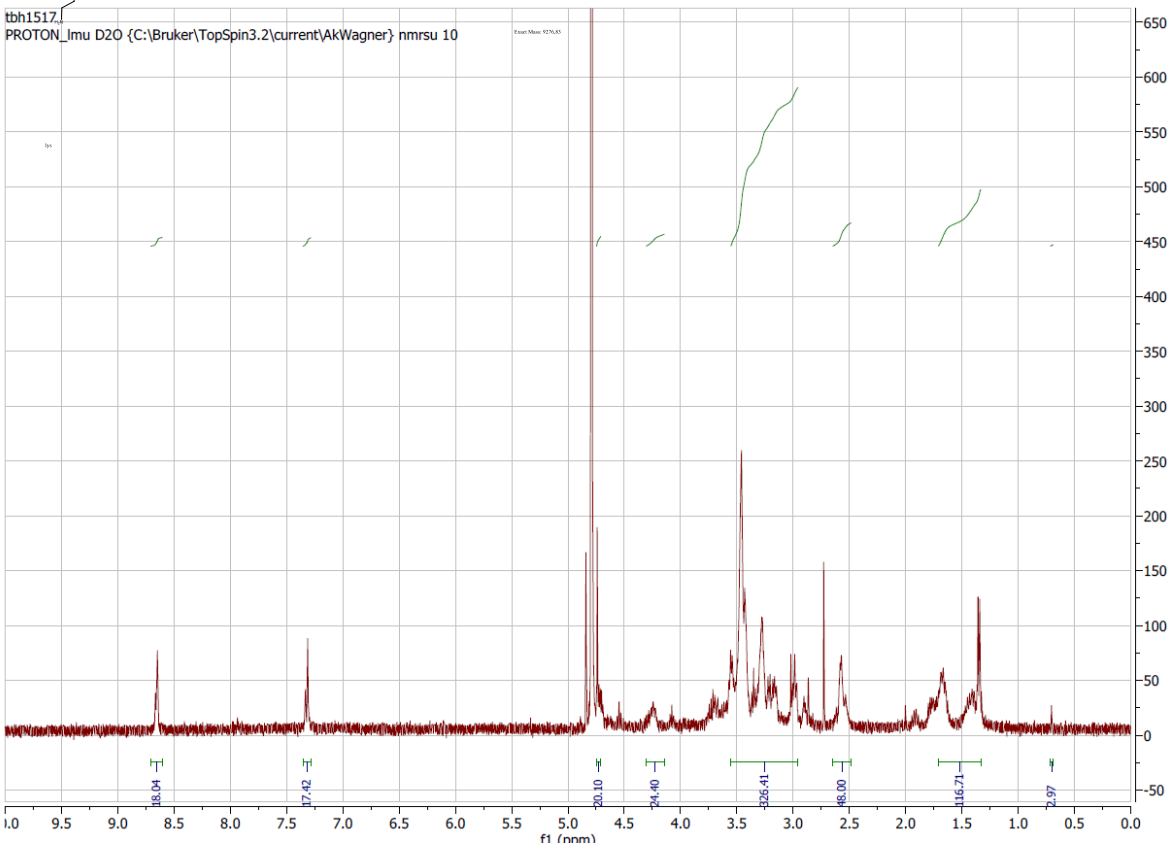

^{1}H-NMR spectrum of 1517 four-arm structure, recorded in D_2O. δ (ppm) = 0.69-0.71 (m, 3 H, βH alanine); 1.33-1.71 (m, 114 H, βγδH lysine); 2.48-2.65 (m, 48 H, -CO-CH_2-CH_2-CO- succinic acid); 2.96-3.55 (m, 322 H, -CH_2- PEHA, βH cysteine, βH histidine, εH lysine); 4.14-4.31 (m, 24 H, αH alanine, αH cysteine, αH lysine); 4.71-4.75 (m, 18H, αH histidine); 7.28-7.36 (m, 18H, imidazole); 8.60-8.71 (d, 18H, imidazole)

1518

Sequence (C → N): A-K-(H-K-(H-Sph-H-W-Sph-H-W-Sph-H-W-C-KN3)2)2

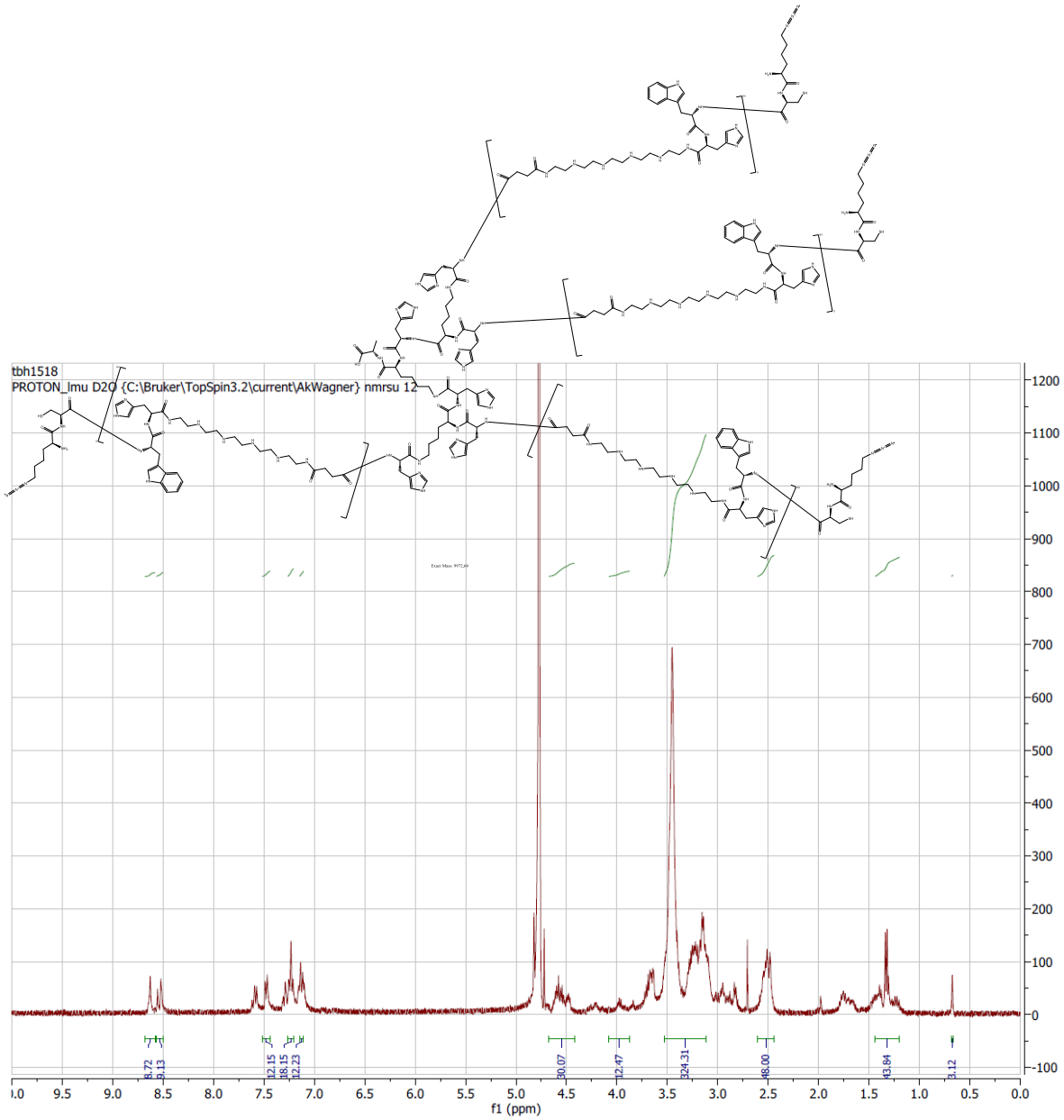

^{1}H-NMR spectrum of 1518 four-arm structure, recorded in D_2O. δ (ppm) = 0.67-0.68 (m, 3 H, βH alanine); 1.20-1.44 (m, 42 H, βH βγδH lysine); 2.44-2.60 (m, 48 H, -CO-CH_2-CH_2-CO- succinic acid); 3.11-3.53 (m, 322 H, -CH_2- PEHA, βH cysteine, βH histidine, εH lysine, βH tryptophane); 3.87-4.08 (m, 12 H, αH alanine, αH cysteine, αH lysine); 4.42-4.67 (m, 30 H, αH histidine); 7.11-7.15 (m, 12 H, indolaromat); 7.21-7.26 (m, 18 H, imidazole); 7.44-7.52 (m, 12 H, indolaromat); 8.58-8.68 (d, 18H, imidazole)

1519

Sequence (C → N): A-K-(H-K-(H-Sph-H-R-Sph-H-R-Sph-H-R-C-KN3)2)2

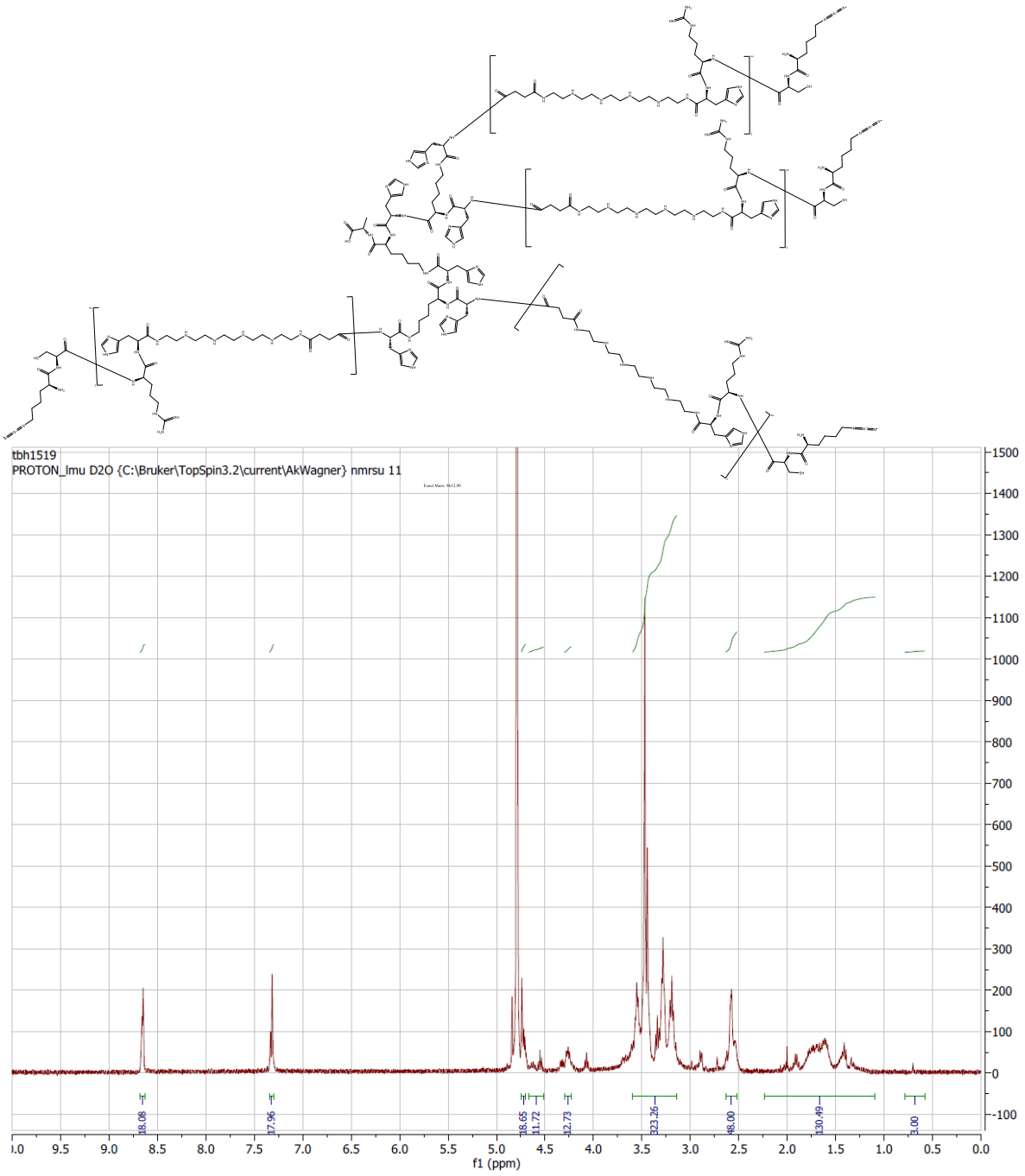

^{1}H-NMR spectrum of 1519 four-arm structure, recorded in D_2O. δ (ppm) = 0.58-0.78 (m, 3 H, βH alanine); 1.09-2.24 (m, 90 H, βγδH lysine, βγH arginine); 2.52-2.63 (m, 48 H, -CO-CH_2-CH_2-CO- succinic acid); 3.14-3.60 (m, 322 H, -CH_2- PEHA, βH cysteine, βH histidine, εH lysine, δH arginine); 4.23-4.30 (m, 12 H, αH alanine, αH cysteine, αH lysine); 4.51-4.67 (m, 18H, αH histidine); 4.70-4.74 (m, 12 H, αH arginine); 4.78 (s, HDO); 7.30-7.35 (m, 18H, imidazole); 8.63-8.68 (d, 18H, imidazole)

1658

Sequence (C → N): (*N-α-Fmoc*): A-K-(H-K-(K3-L3-K3-L3-K-L3-C-KN3)2)2

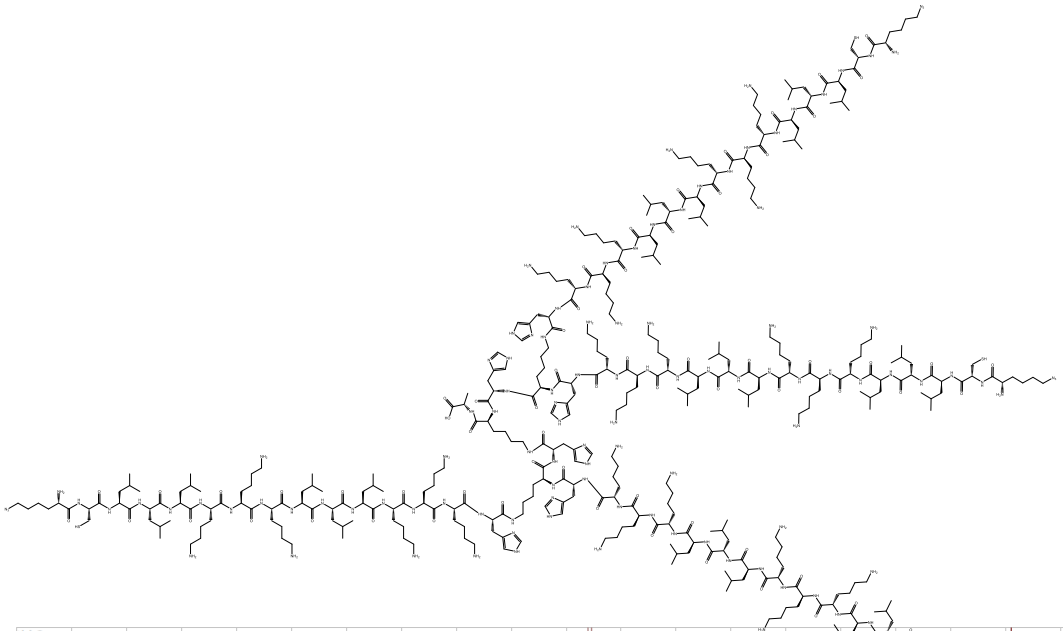

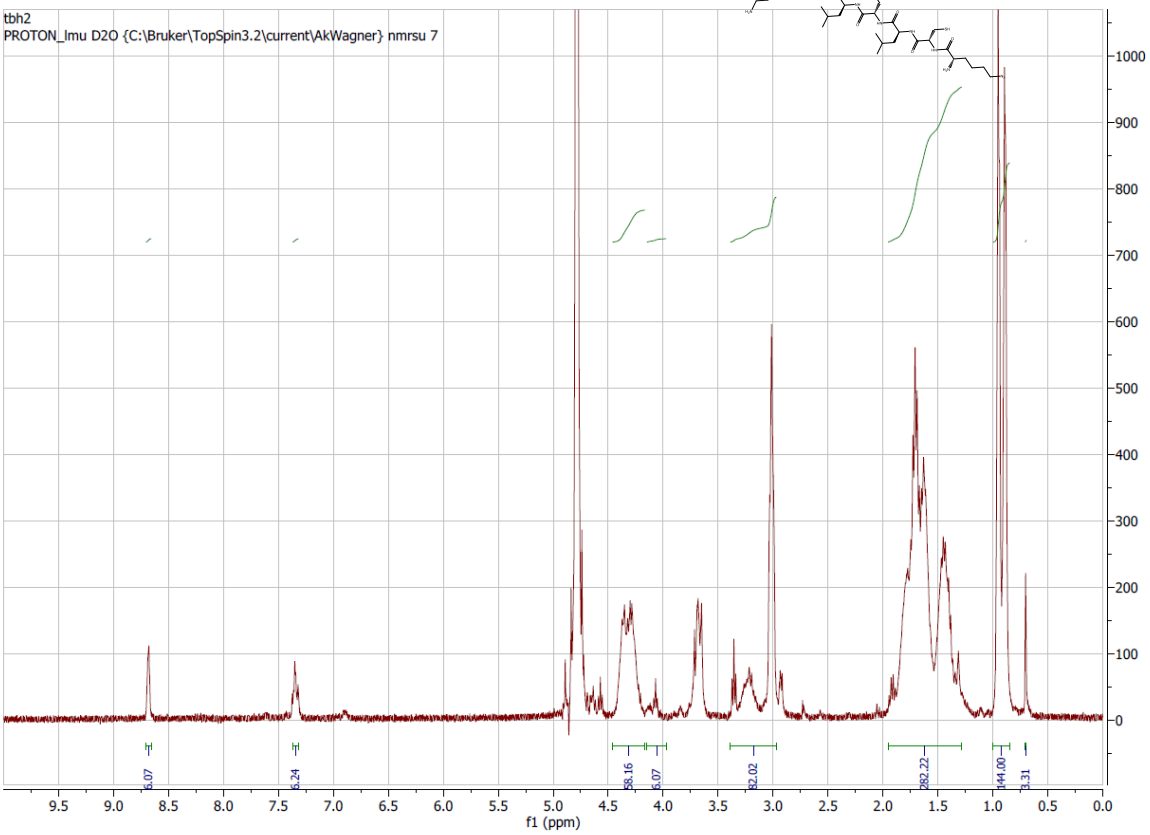

^{1}H-NMR spectrum of 1658 four-arm structure, recorded in D_2O. δ (ppm) = 0.5-0.7 (m, 3 H, βH alanine); 0.8-1.0 (m, 144 H, δH leucine); 1.3-1.9 (m, 282 H, βγδH lysine, βγ H leucine); 2.8-3.7 (m, 82 H, βH cysteine, βH histidine, εH lysine); 3.8-4.1 (m, 6 H, αH histidine); 4.2-4.4 (m, 60 H, αH alanine, αH cysteine, αH lysine, αH leucine); 7.6-7.7 (m, 6 H, imidazole); 8.4-8.5 (d, 6 H, imidazole)

1664

Sequence (C → N): (*N-α-Fmoc*): A-K-(H-K-(K3-Y3-K3-Y3-K3-Y3-C-KN3)2)2

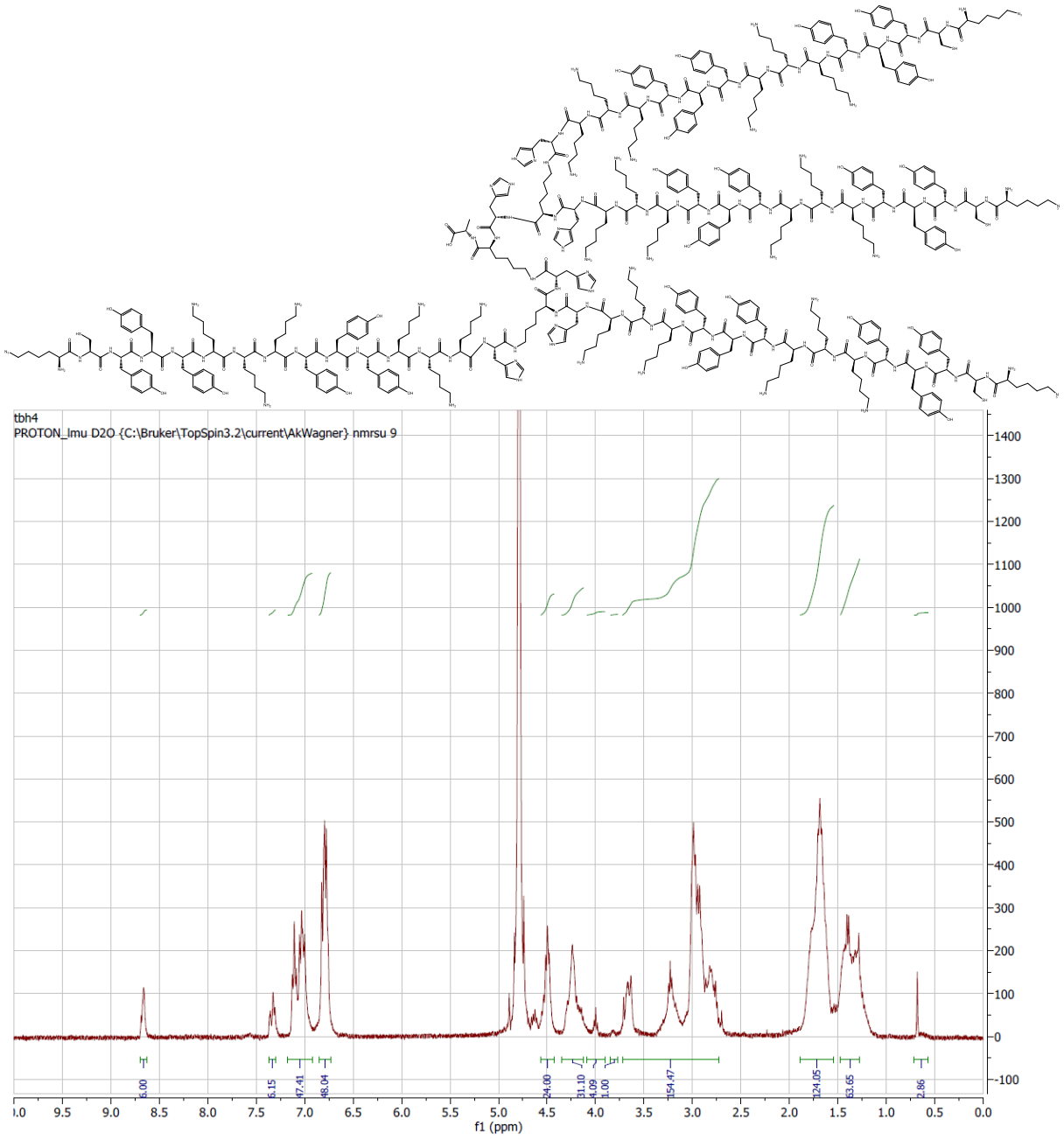

^{1}H-NMR spectrum of 1664 four-arm structure, recorded in D_2O. δ (ppm) = 0.6-0.7 (m, 3 H, βH alanine); 1.25-1.45 (m, 62 H, γH lysine); 1.55-1.8 (m, 124 H, βδH lysine); 2.6-3.65 (m, 154 H, βH cysteine, βH histidine, εH lysine, αβH tyrosine); 3.75-4.1 (m, 5 H, αH cysteine, αH alanine); 4.1-4.4 (m, 31 H, αH lysine); 4.45-4.55 (m, 24 H, αH tyrosine); 6.7-6.8 (m, 48 H, phenol); 6.9-7.2 (d, 48 H, phenol); 7.3-7.4 (m, 6 H, imidazole); 8.6-8.7 (d, 6 H, imidazole)

1696

Sequence (C → N): (*N-ε-Fmoc*): A-K-(H-K-(K3-Y3-K3-Y3-K3-Y3-C-KN3)2)2

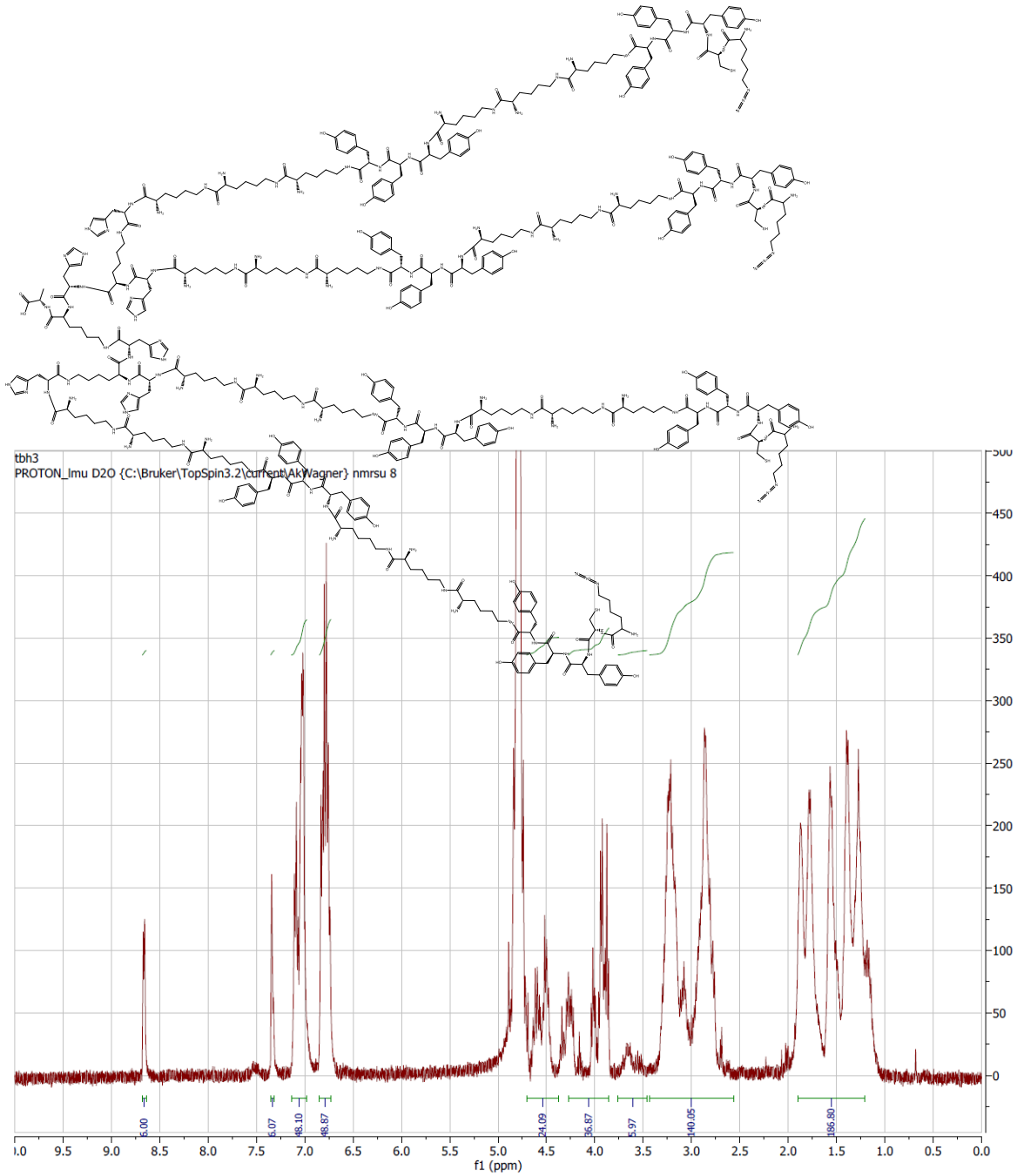

^{1}H-NMR spectrum of 1696 four-arm structure, recorded in D_2O. δ (ppm) = 0.6-0.7 (m, 3 H, βH alanine); 1.2-1.85 (m, 186 H, γβδH lysine); 2.55-3.45 (m, 154 H, βH cysteine, βH histidine, εH lysine, αβH tyrosine); 3.5-3.6 (m, 5 H, αH cysteine, αH alanine); 3.8-4.3 (m, 31 H, αH lysine); 4.4-4.6 (m, 24 H, αH tyrosine); 6.75-6.8 (m, 48 H, phenol); 6.9-7.2 (d, 48 H, phenol); 7.3-7.4 (m, 6 H, imidazole); 8.6-8.7 (d, 6 H, imidazole)

1767

Sequence (C → N): (*N-ε-Fmoc*): A-K-(H-K-(K6-C-KN3)2)2

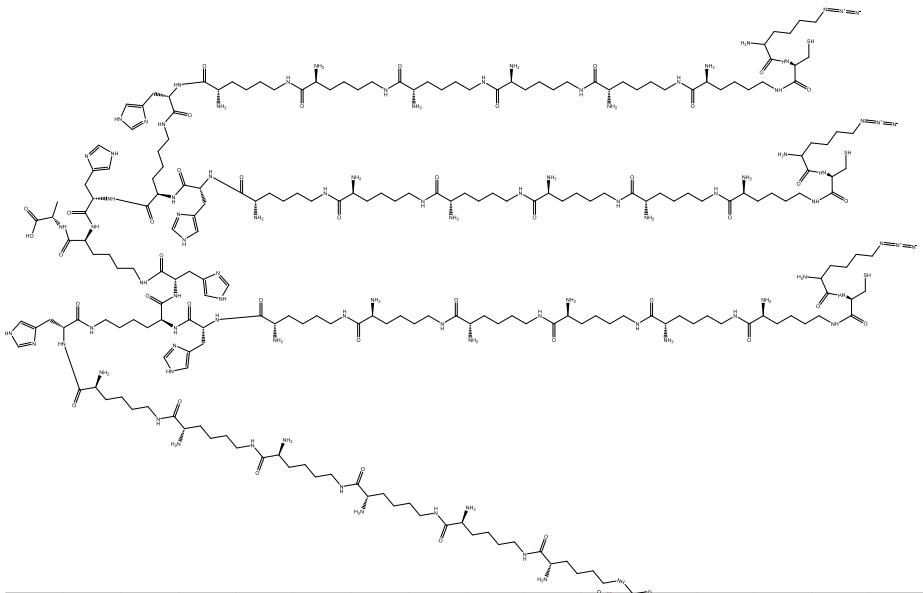

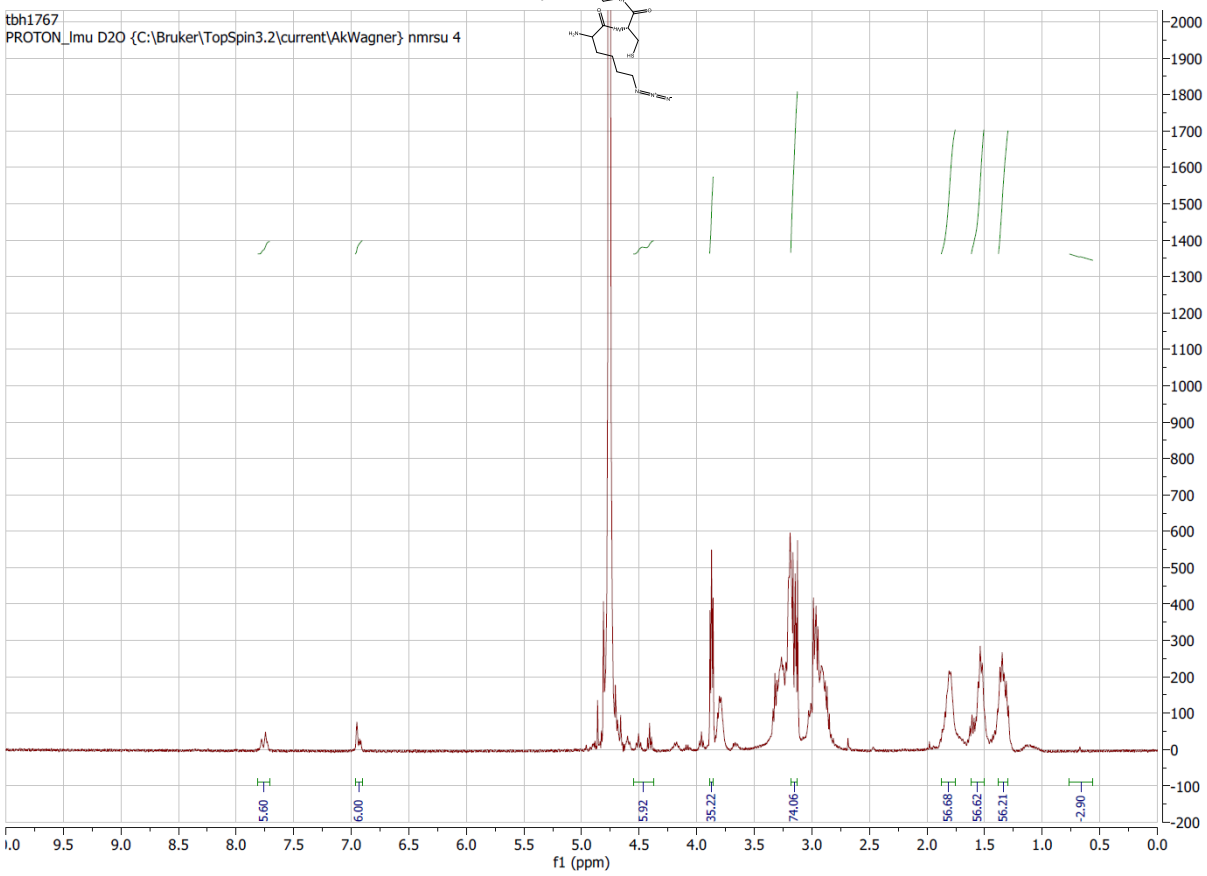

^{1}H-NMR spectrum of 1767 four-arm structure, recorded in D_2O. δ (ppm) = 0.6-0.75 (m, 3 H, βH alanine); 1.25-1.4 (m, 56 H, γH lysine); 1.5-1.6 (m, 56 H, δH lysine); 1.75-1.85 (m, 56 H, βH lysine); 3.15-3.2 (m, 76 H, βH cysteine, βH histidine, εH lysine); 3.8-3.85 (m, 33 H, αH cysteine, αH alanine, αH lysine); 4.4-4.5 (m, 6 H, αH histidine); 6.85-6.95 (m, 6 H, imidazole); 7.7-7.8 (d, 6 H, imidazole)

1768

Sequence (C → N): (*N-α-Fmoc*): A-K-(H-K-(K9-C-KN3)2)2

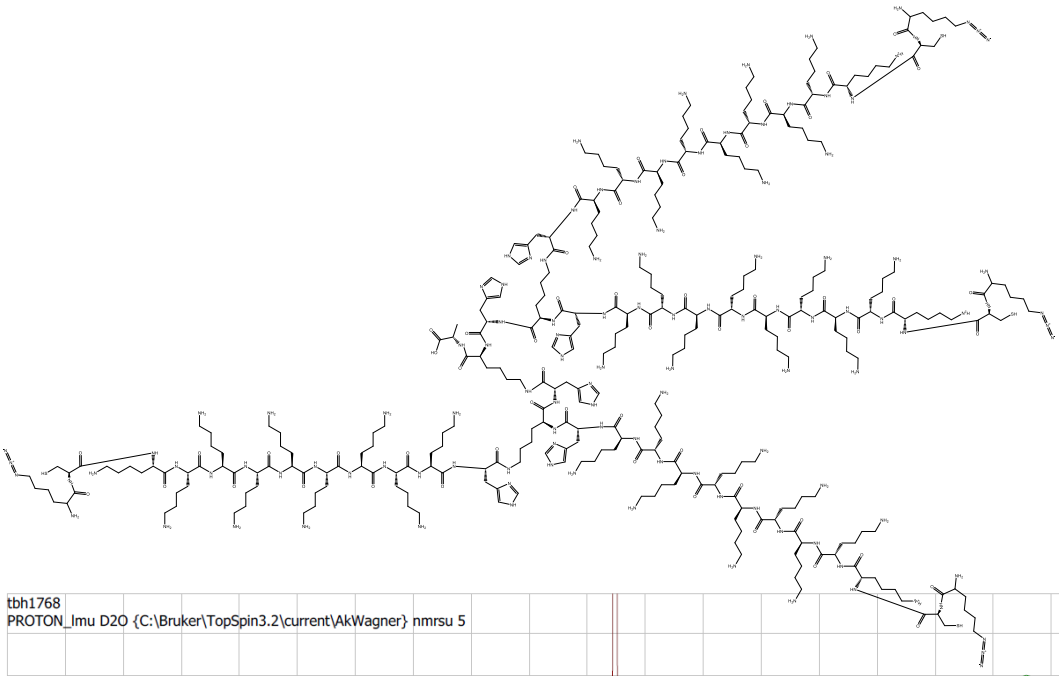

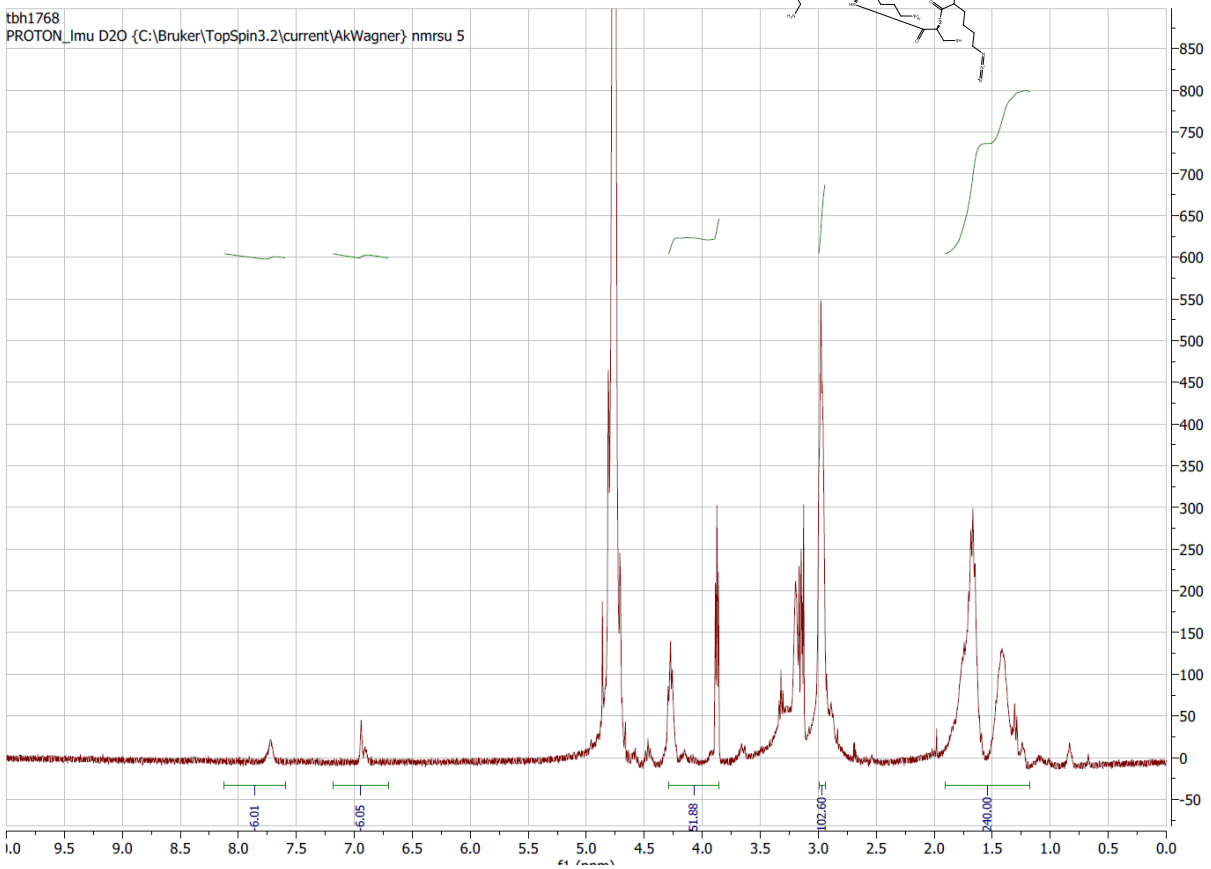

^{1}H-NMR spectrum of 1768 four-arm structure, recorded in D_2O. δ (ppm) = 0.6-0.75 (m, 3 H, βH alanine); 1.2-1.8 (m, 240 H, γδβH lysine); 2.9-3.0 (m, 100 H, βH cysteine, βH histidine, εH lysine); 3.8-4.45 (m, 51 H, αH cysteine, αH alanine, αH lysine, αH histidine); 6.7-7.2 (m, 6 H, imidazole); 7.6-8.1 (d, 6 H, imidazole)

1769

Sequence (C → N): (*N-ε-Fmoc*): A-K-(H-K-(K9-C-KN3)2)2

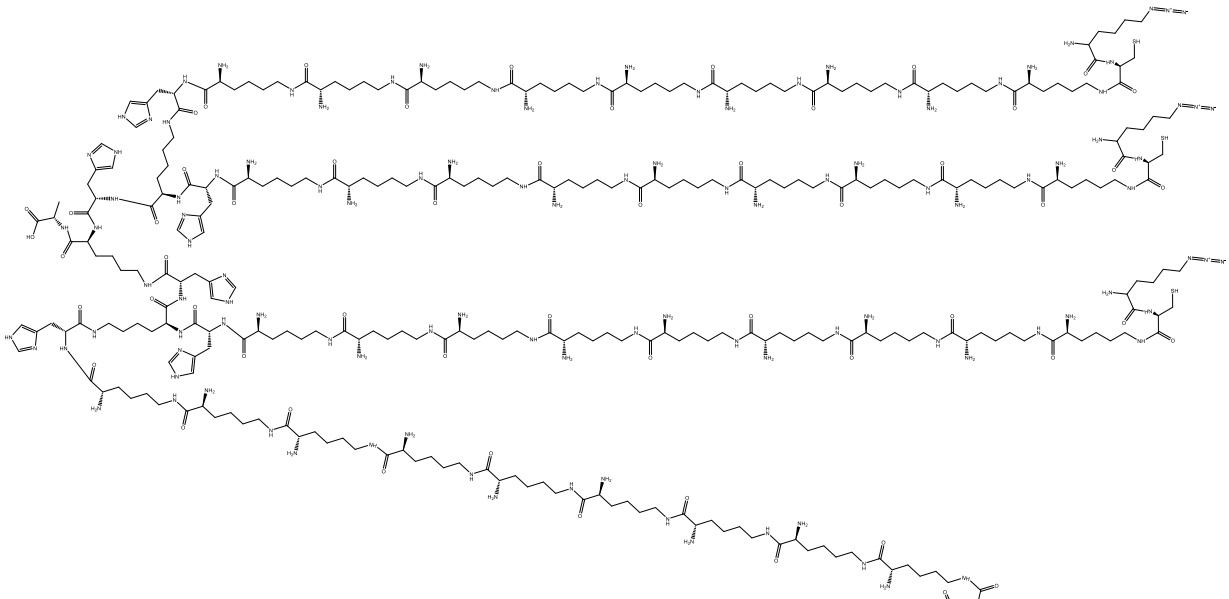

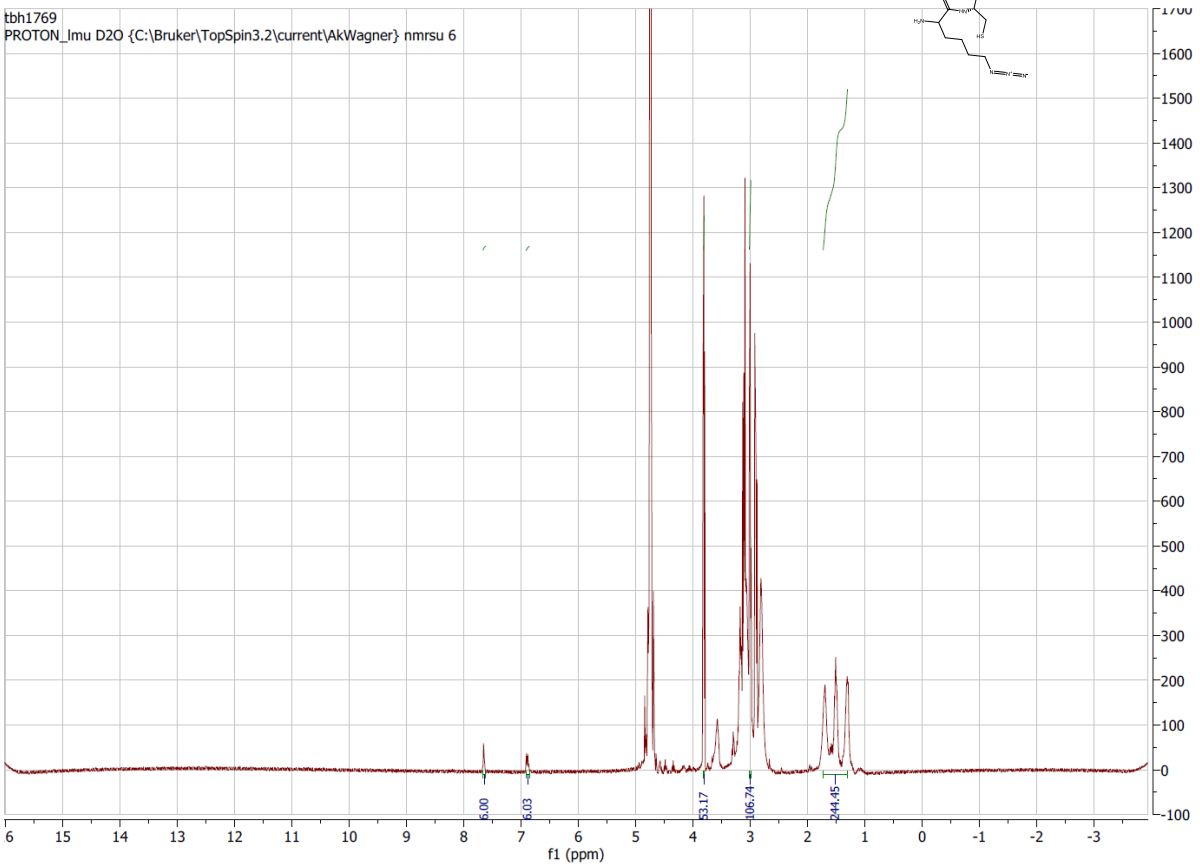

^{1}H-NMR spectrum of 1769 four-arm structure, recorded in D_2O. δ (ppm) = 0.6-0.75 (m, 3 H, βH alanine); 1.2-1.7 (m, 240 H, γδβH lysine); 2.95-3.0 (m, 100 H, βH cysteine, βH histidine, εH lysine); 3.75-3.8 (m, 51 H, αH cysteine, αH alanine, αH lysine, αH histidine); 6.8-6.85 (m, 6 H, imidazole); 7.6-7.65 (d, 6 H, imidazole)

6.4.2 Mass spectra of shielding and targeting agents

Summary of SPSS derived shielding and targeting agents. Calculated and found masses by MALDI-TOF $[M+X]^+$ in Dalton [Da].

Abbreviation	Chemical Formula	Calculated mass in [Da]	Found mass via MALDI-TOF [Da]
PEG1	$C_{72}H_{120}N_2O_{28}$	1460.8	1459.1
PEG2	$C_{128}H_{203}N_9O_{41}$	2522.41	2524.7
reTfR1	$C_{141}H_{213}N_{21}O_{42}S$	2904.49	2901.6
reTfR2	$C_{194}H_{290}N_{28}O_{55}S$	3924.05	3919.0
R-PEG1	$C_{76}H_{128}N_6O_{29}$	1588.87	1587.3
R-PEG2	$C_{129}H_{205}N_{13}O_{42}$	2608.43	2608.8
scr-reTfR1	$C_{141}H_{213}N_{21}O_{42}S$	2904.49	2900.9
scr-reTfR2	$C_{194}H_{290}N_{28}O_{55}S$	3924.05	3917.5
Tf2	$C_{129}H_{199}N_{21}O_{41}S$	2730	2769
Tf2-fluorescein	$C_{79}H_{92}N_{18}O_{20}S$	1644	1643
scr-Tf2	$C_{129}H_{199}N_{21}O_{41}S$	2730	2767
L57	$C_{199}H_{302}N_{36}O_{57}S$	4140	4133
scr-L57	$C_{199}H_{302}N_{36}O_{57}S$	4140	4134
reL57	$C_{199}H_{302}N_{36}O_{57}S$	4140	4134
Angiopep-2	$C_{183}H_{276}N_{34}O_{61}S$	3958	3982
cRGD-DBCO	$C_{98}H_{157}N_{11}O_{34}$	2032	2030
TGN	$C_{130}H_{204}N_{22}O_{45}S$	2826	2847
cdx	$C_{158}H_{255}N_{33}O_{53}S$	3495	3494
reTfR-KN3	$C_{128}H_{211}N_{25}O_{40}S$	2770	2766
cRGD-KN3	$C_{27}H_{39}N_{11}O_7$	629	628
PEG4-KN3	$C_{20}H_{38}N_6O_7$	474	474

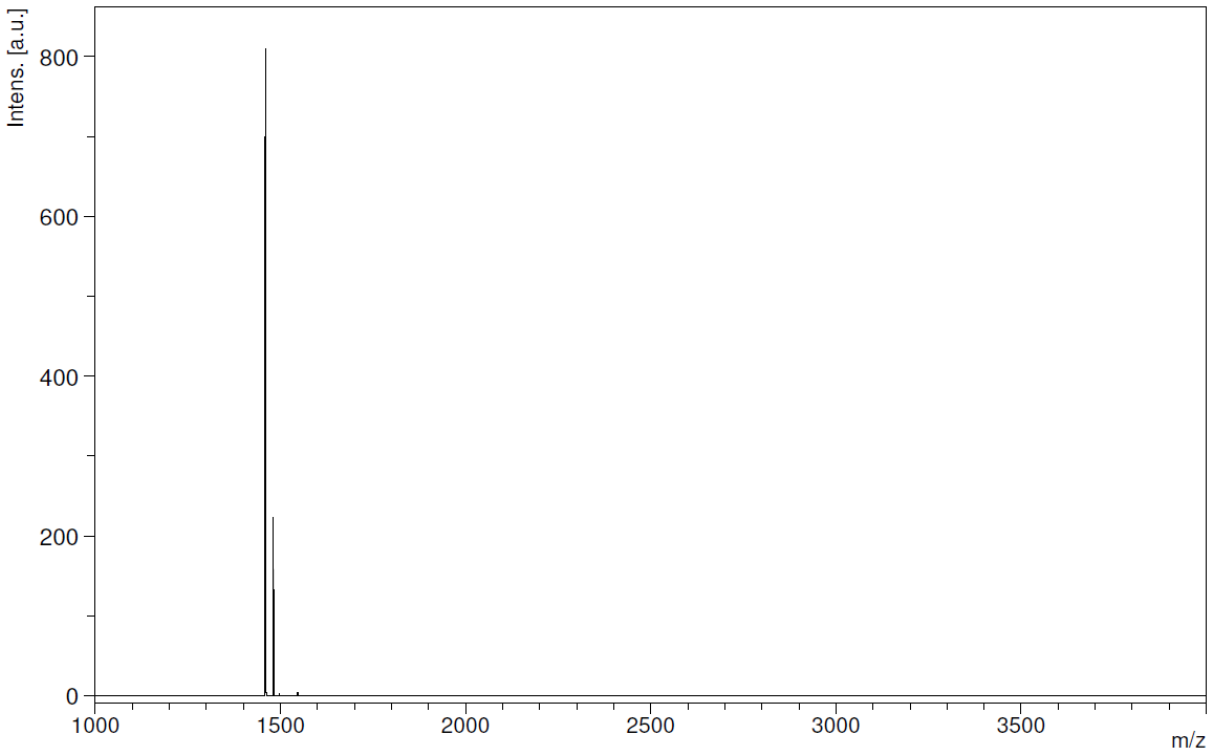

MALDI-TOF-MS spectra of **PEG1**. $[M+H]^+$ calculated 1460.8. $[M+H]^+$ found 1459,1 and $[M+Na]^+$ 1481.1.

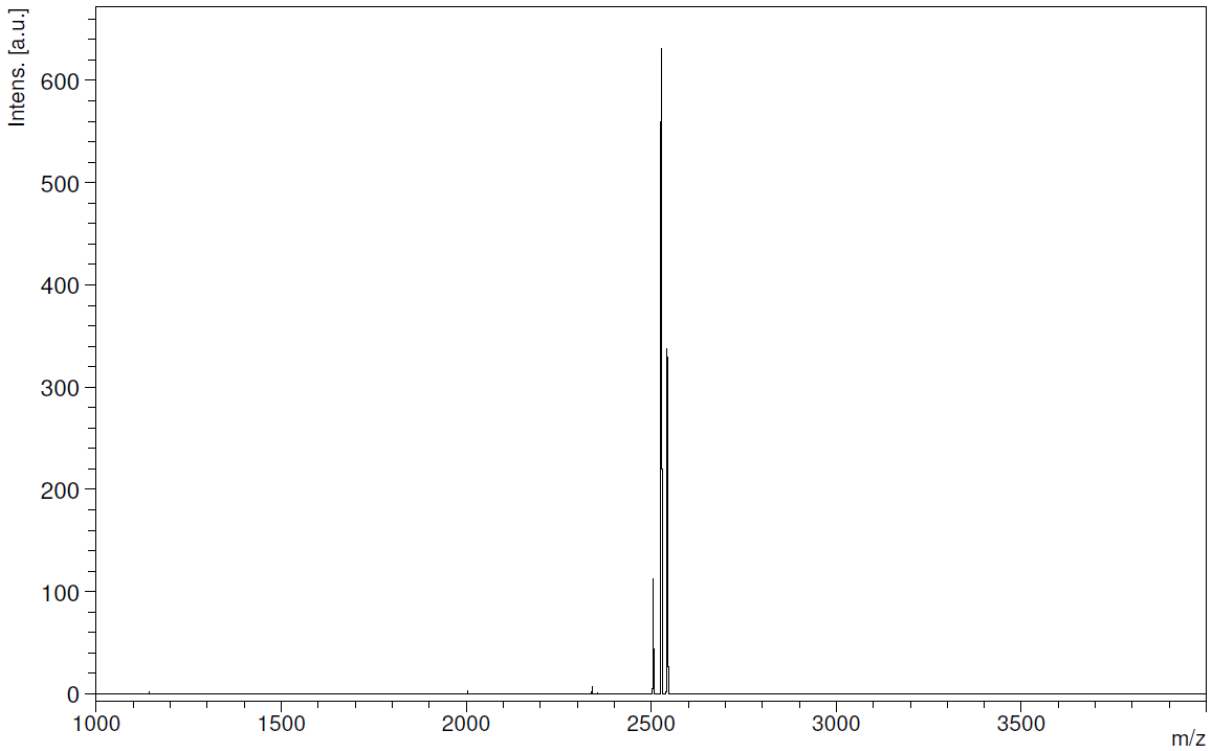

MALDI-TOF-MS spectra of **PEG2**. $[M+H]^+$ calculated 2522.41. $[M+H]^+$ found 2524.7 and $[M+Na]^+$ 2544.1.

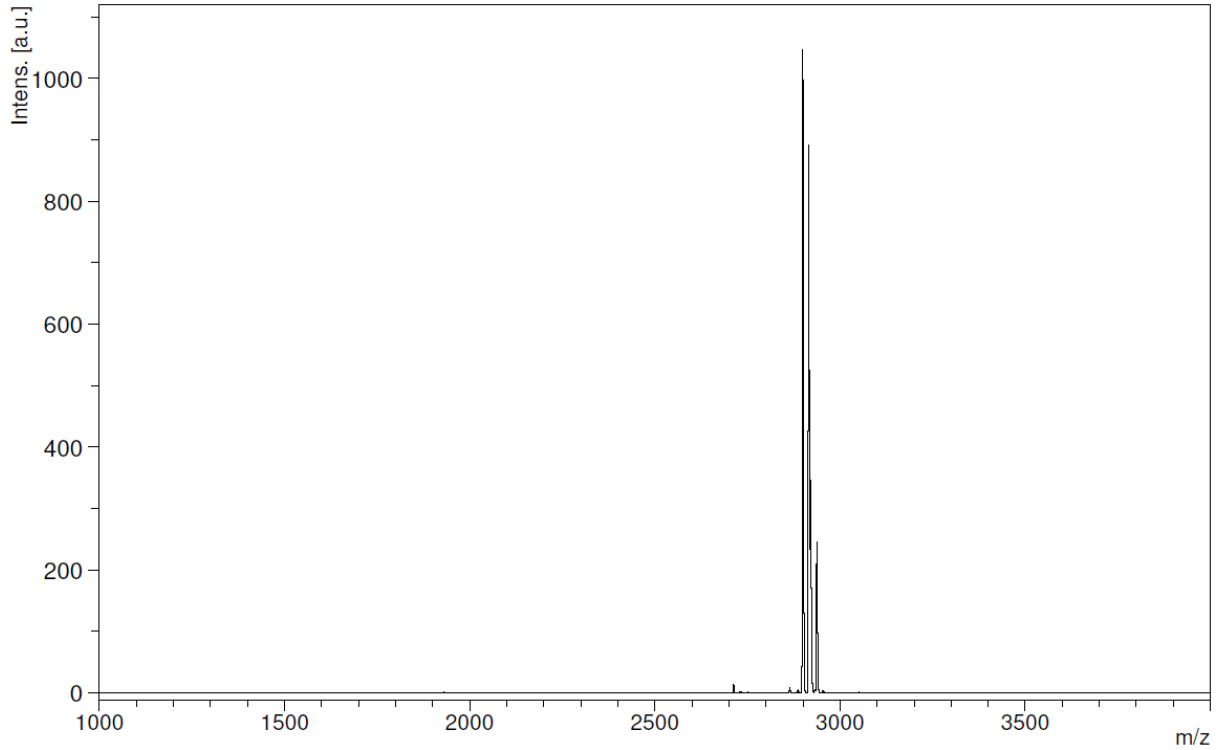

MALDI-TOF-MS spectra of **reTfR1**. $[M+H]^+$ calculated 2904.49. $[M+H]^+$ found 2901.6 and $[M+H_2O]^+$ 2917,4 and $[M+K]^+$ 2937.4.

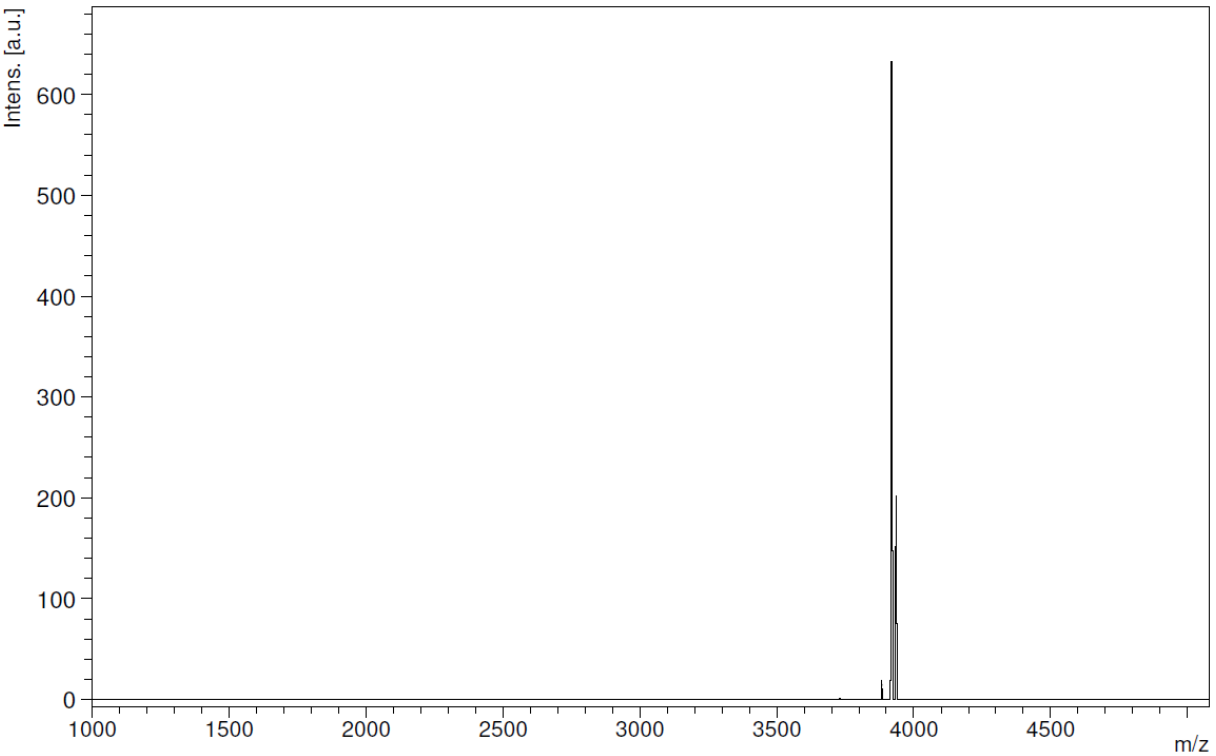

MALDI-TOF-MS spectra of **reTfR2**. $[M+H]^+$ calculated 3924.05. $[M+H]^+$ found 3919.0.

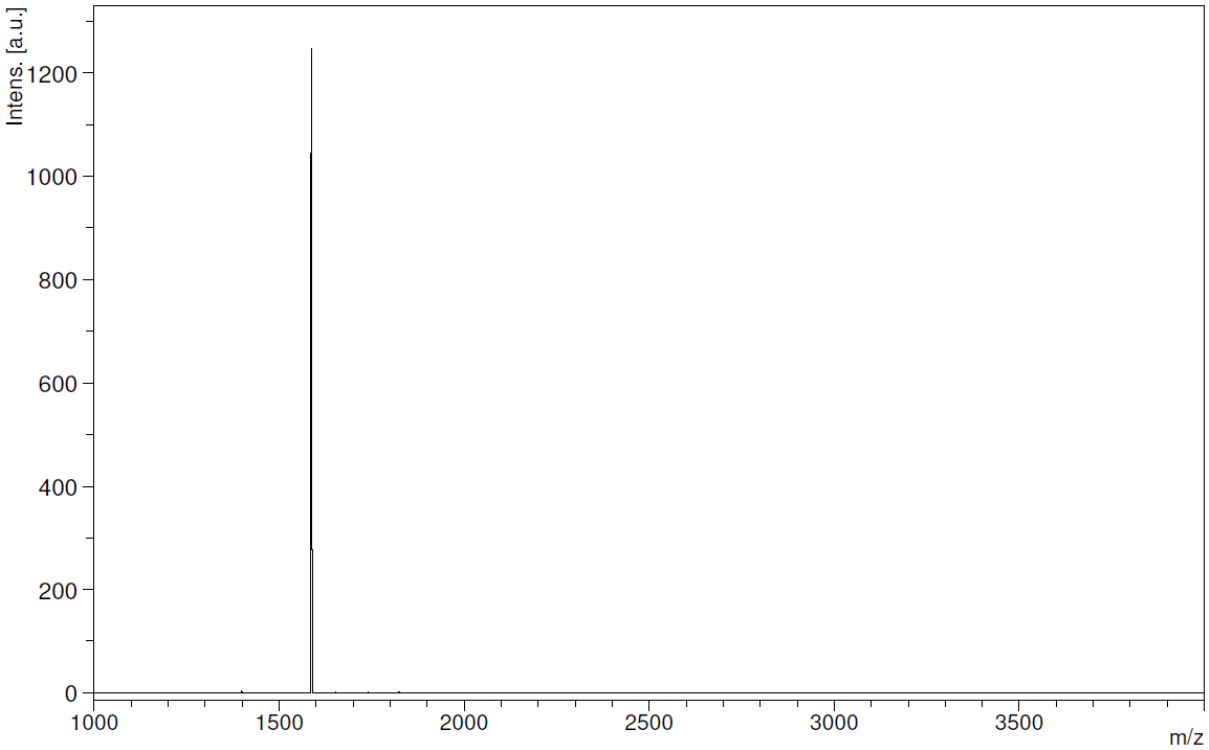

MALDI-TOF-MS spectra of **R-PEG1**. $[M+H]^+$ calculated 1588.87. $[M+H]^+$ found 1587.3.

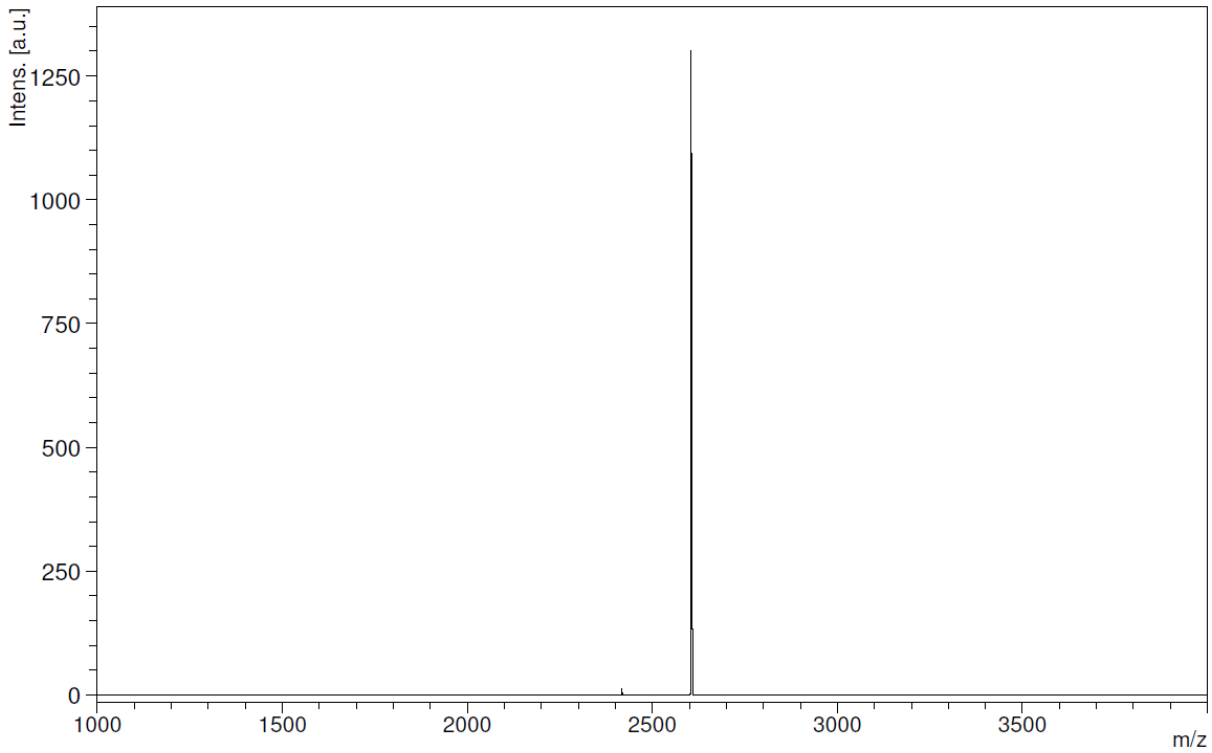

MALDI-TOF-MS spectra of **R-PEG2**. $[M+H]^+$ calculated 2608.43. $[M+H]^+$ found 2608.8.

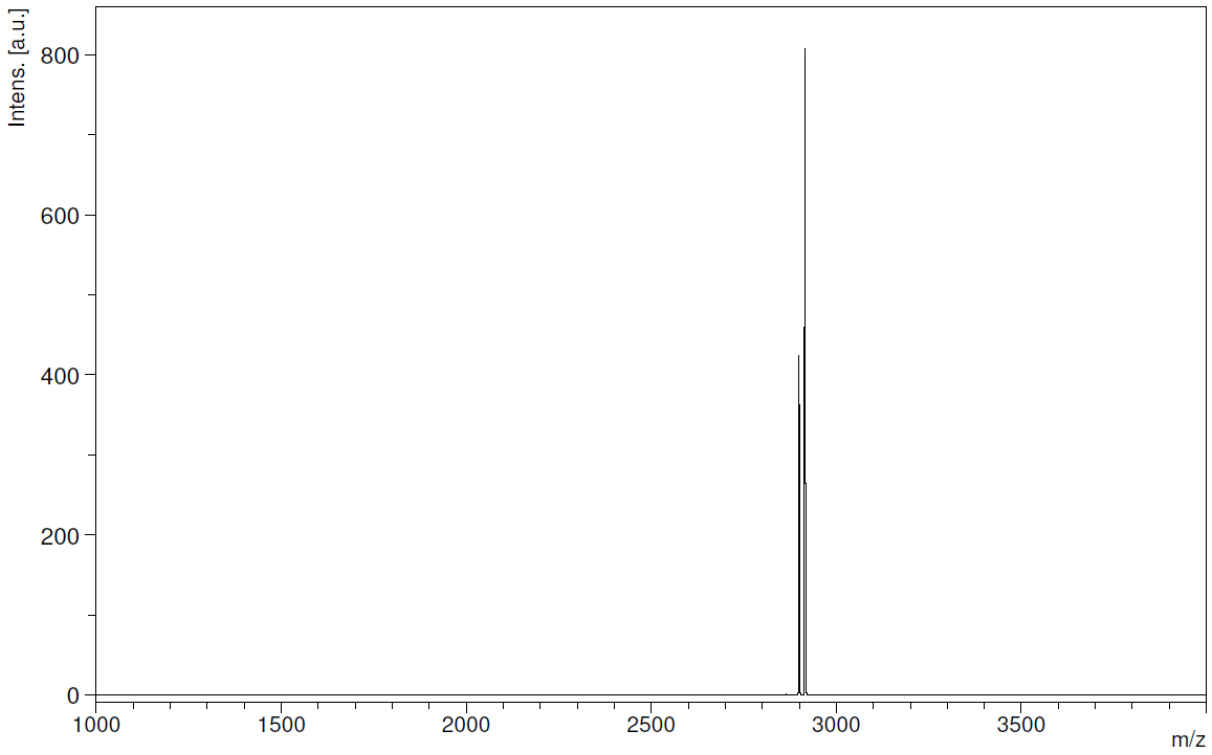

MALDI-TOF-MS spectra of **scr-reTfR1**. $[M+H]^+$ calculated 2904.49. $[M+H]^+$ found 2900.9 and $[M+H_2O]^+$ 2916.4.

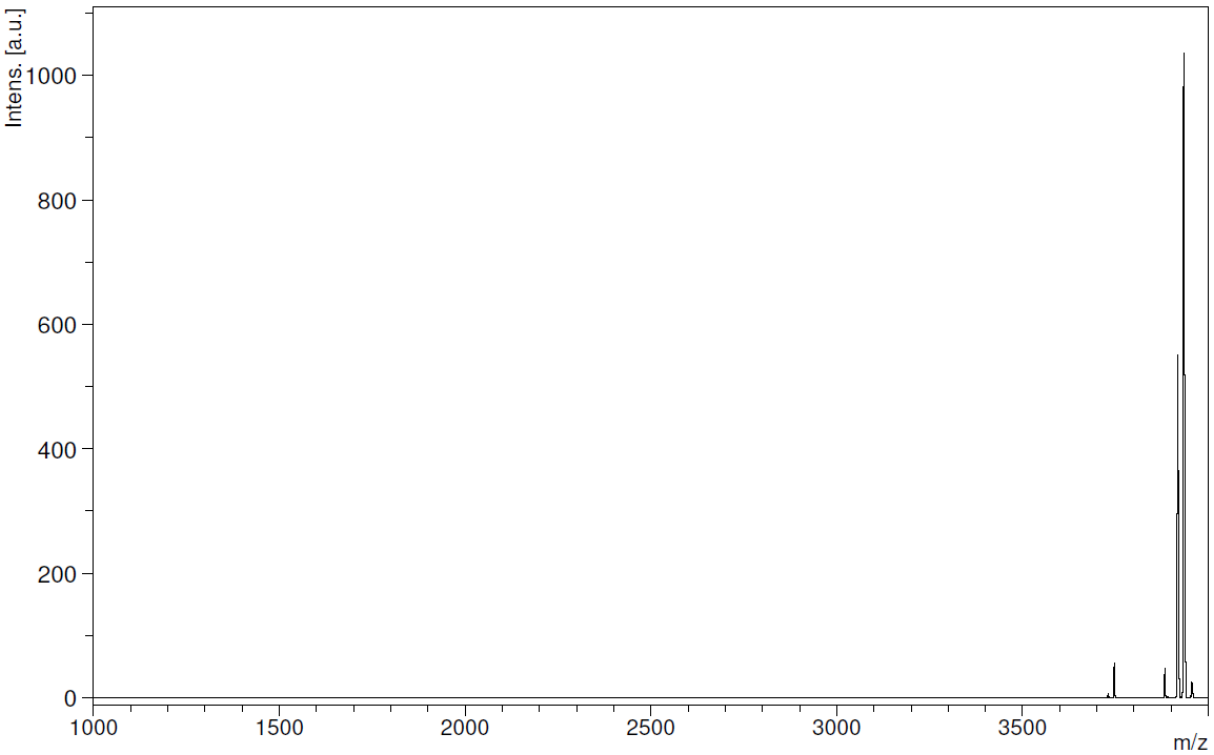

MALDI-TOF-MS spectra of **scr-reTfR2**. $[M+H]^+$ calculated 3924.05. $[M+H]^+$ found 3917.5 and $[M+H_2O]^+$ 3933.6.

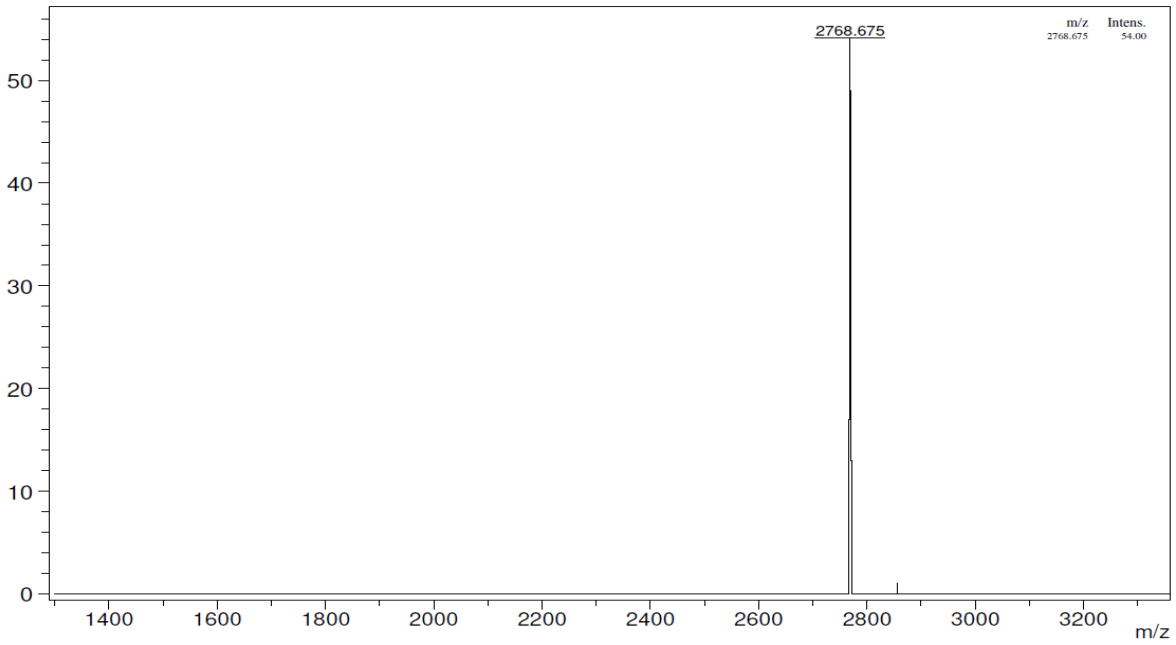

MALDI-TOF-MS spectra of **Tf2 (T10)**. $[M+H]^+$ calculated 2730. $[M+K]^+$ found 2769.

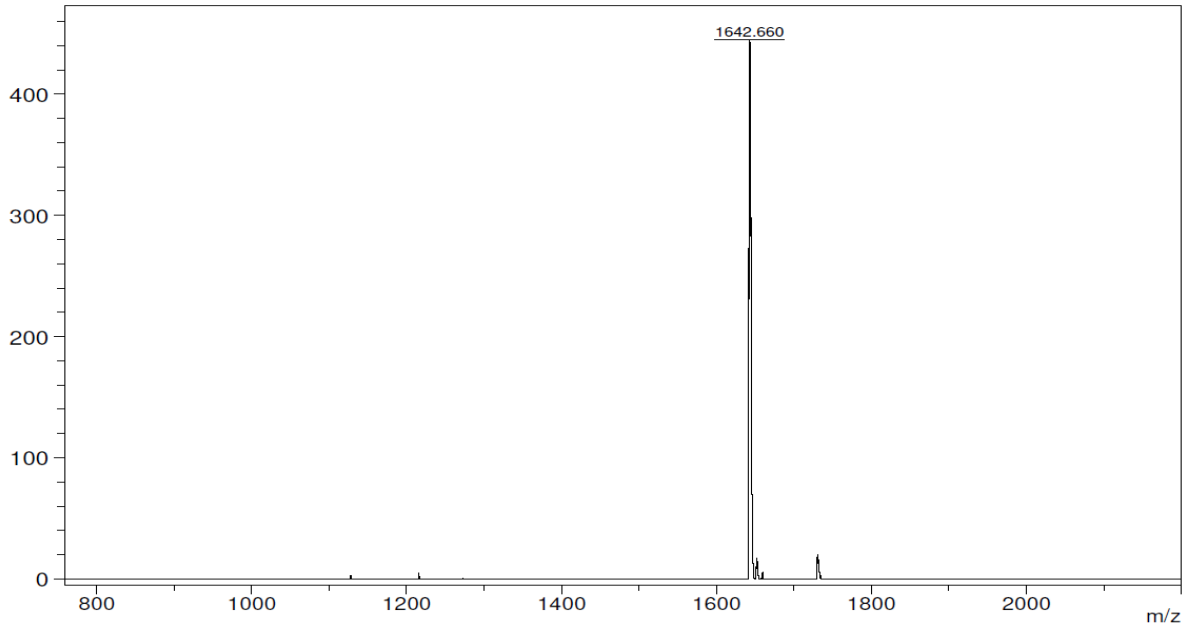

MALDI-TOF-MS spectra of **Tf2-Fluorescein.** $[M+H]^+$ calculated 1644. $[M+K]^+$ found 1643.

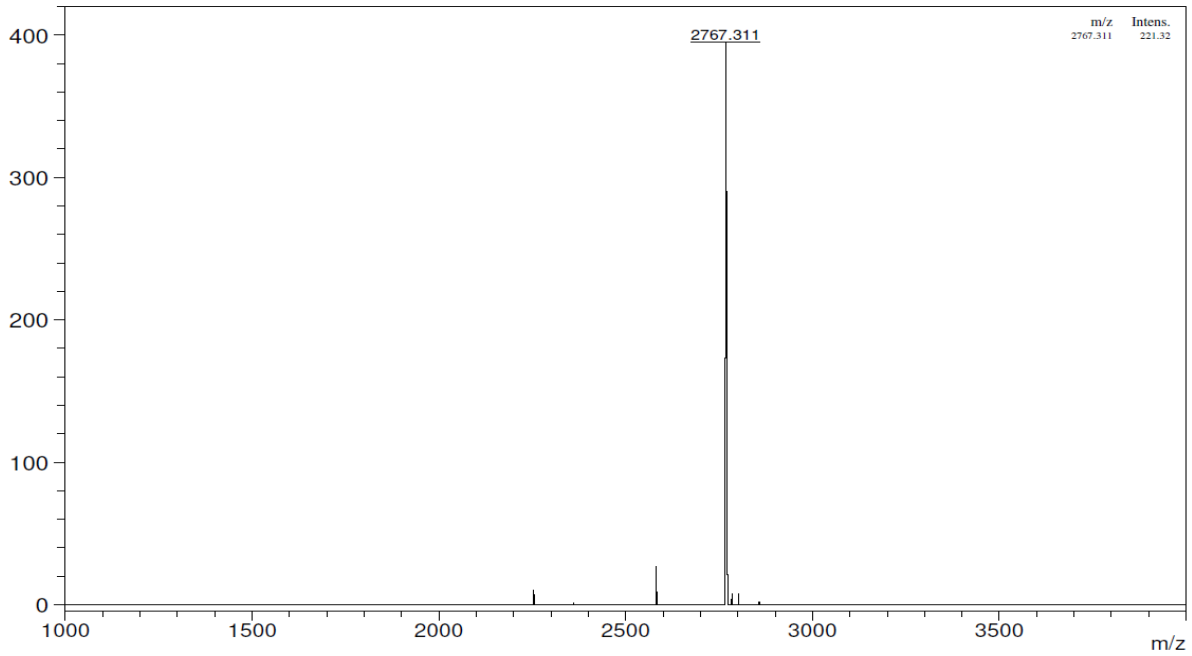

MALDI-TOF-MS spectra of **scr-Tf2 (T10)**. $[M+H]^+$ calculated 2730. $[M+K]^+$ found 2767.

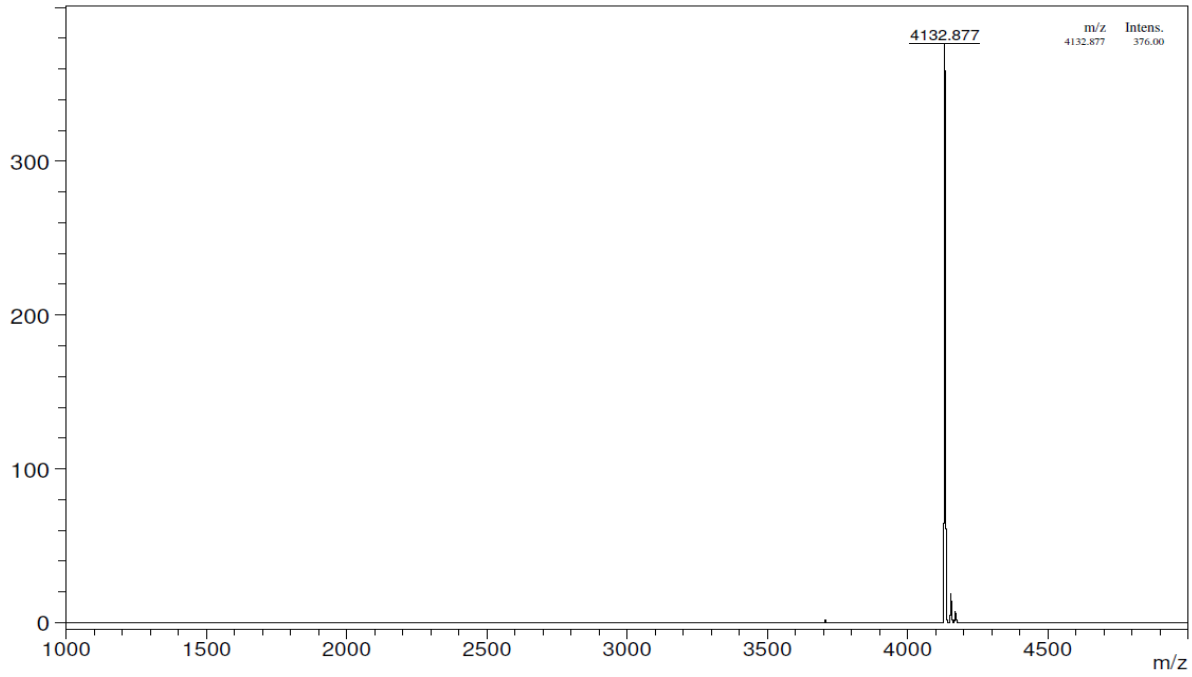

MALDI-TOF-MS spectra of **L57**. $[M+H]^+$ calculated 4140. $[M+H]^+$ found 4133.

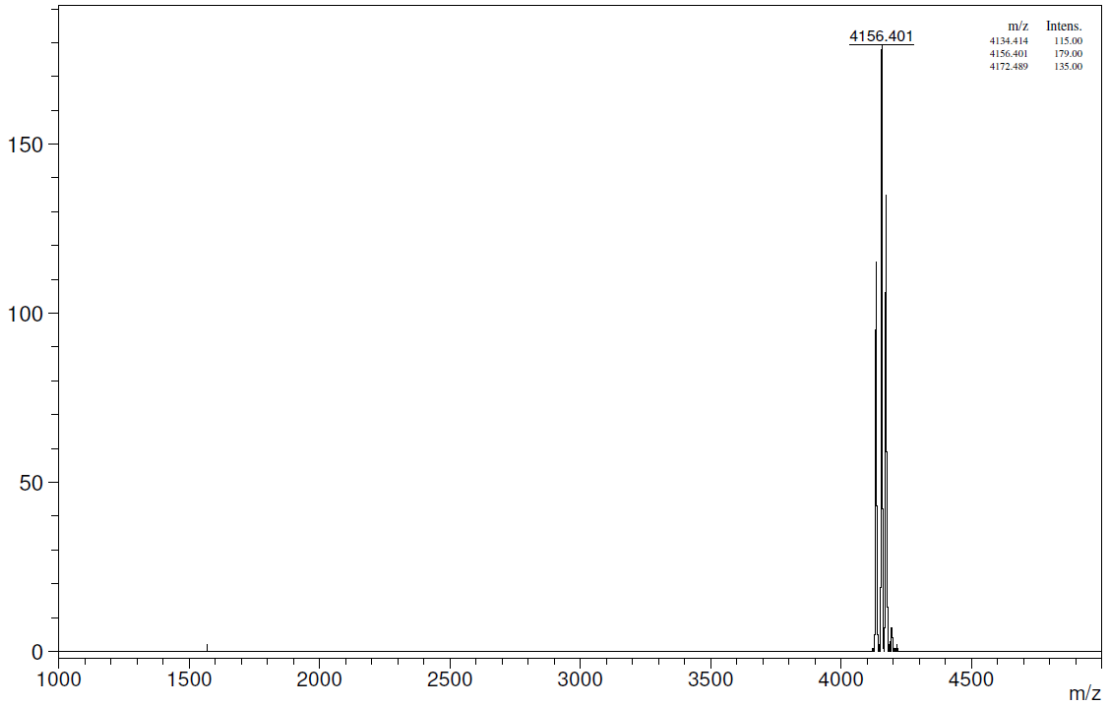

MALDI-TOF-MS spectra of **scr-L57**. $[M+H]^+$ calculated 4140. $[M+H]^+$ found 4134, $[M+Na]^+$ 4156 and $[M+K]^+$ 4172.

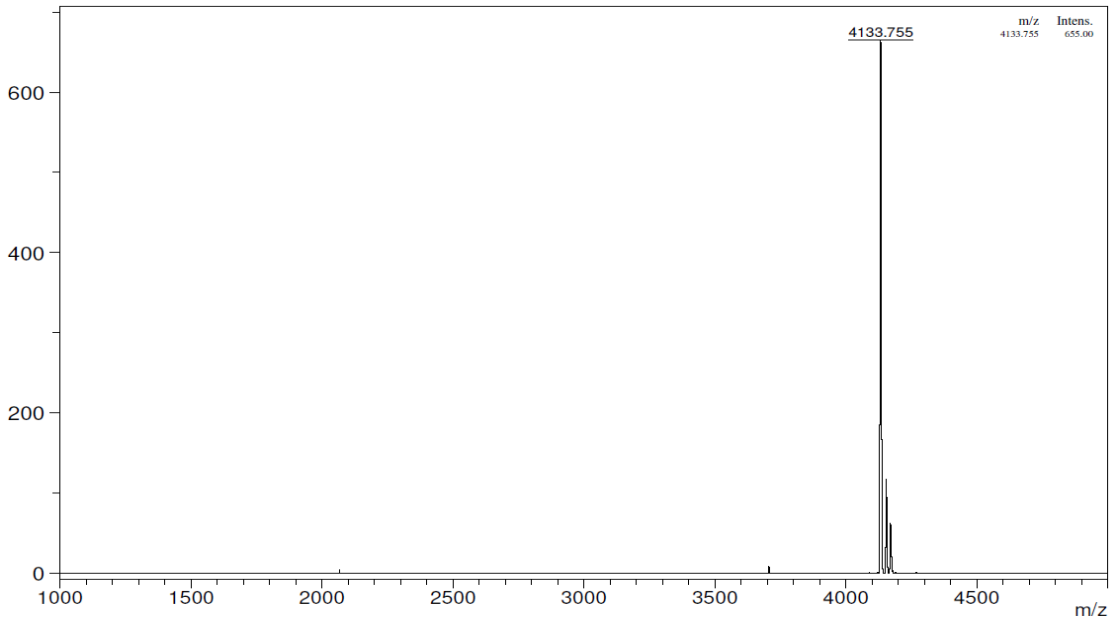

MALDI-TOF-MS spectra of **reL57**. $[M+H]^+$ calculated 4140. $[M+H]^+$ found 4134.

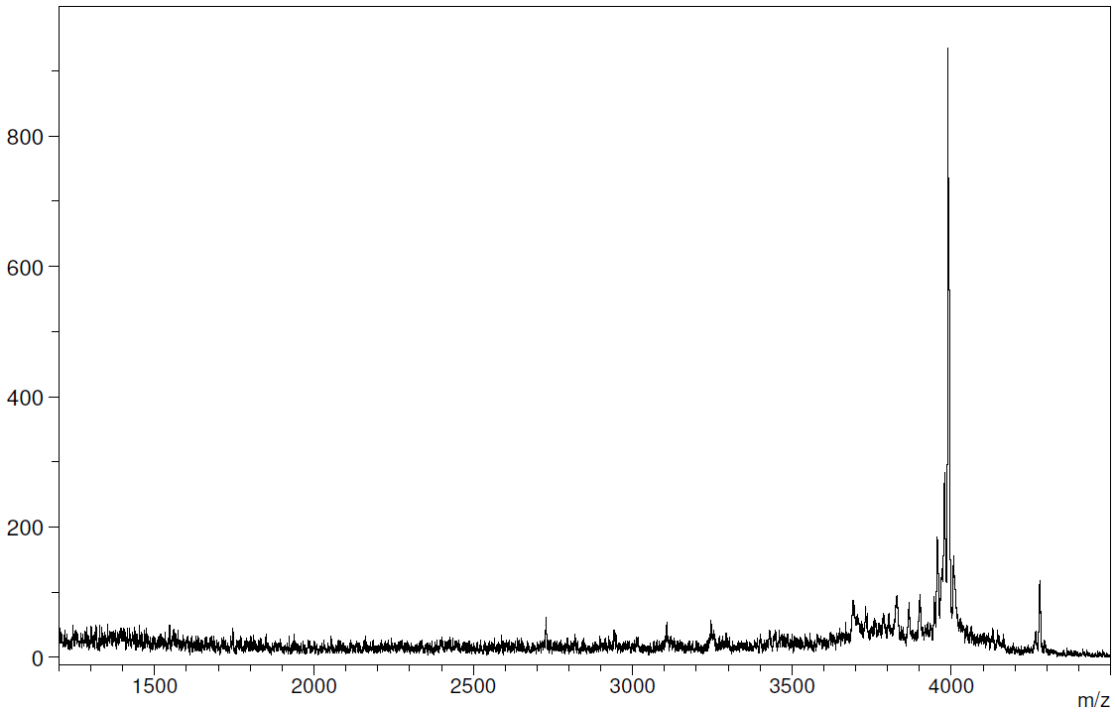

MALDI-TOF-MS spectra of **Angiopep-2**. $[M+H]^+$ calculated 3958. $[M+Na]^+$ found 3982.

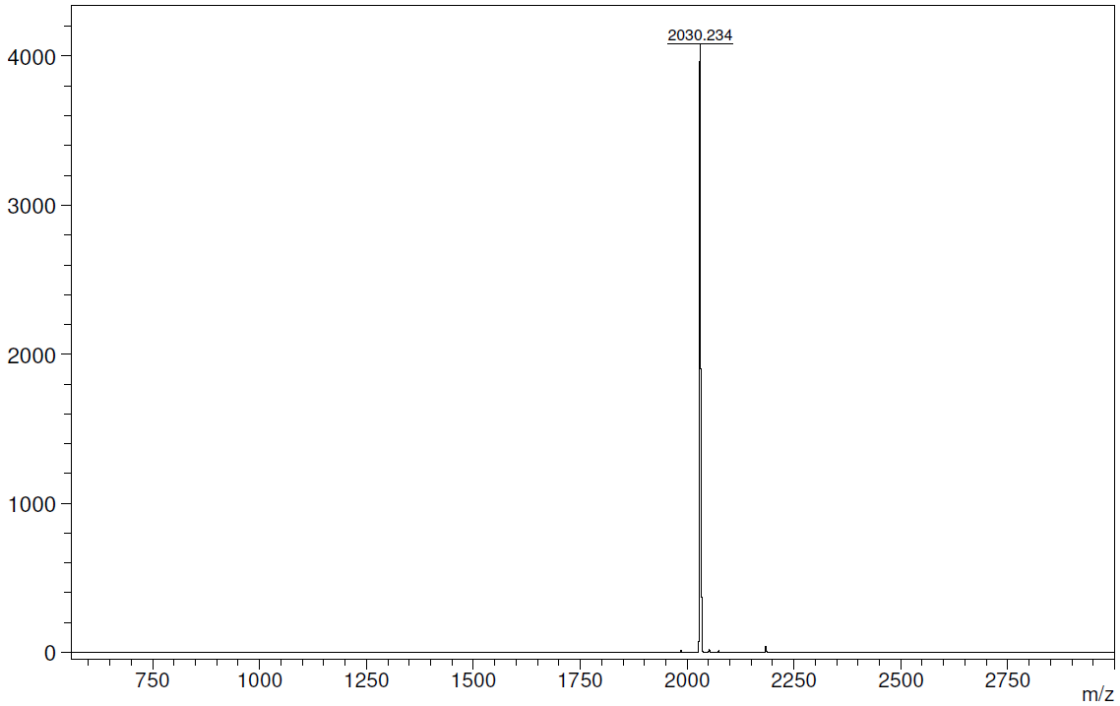

MALDI-TOF-MS spectra of **cRGD-DBCO**. $[M+H]^+$ calculated 2032. $[M+H]^+$ found 2030.

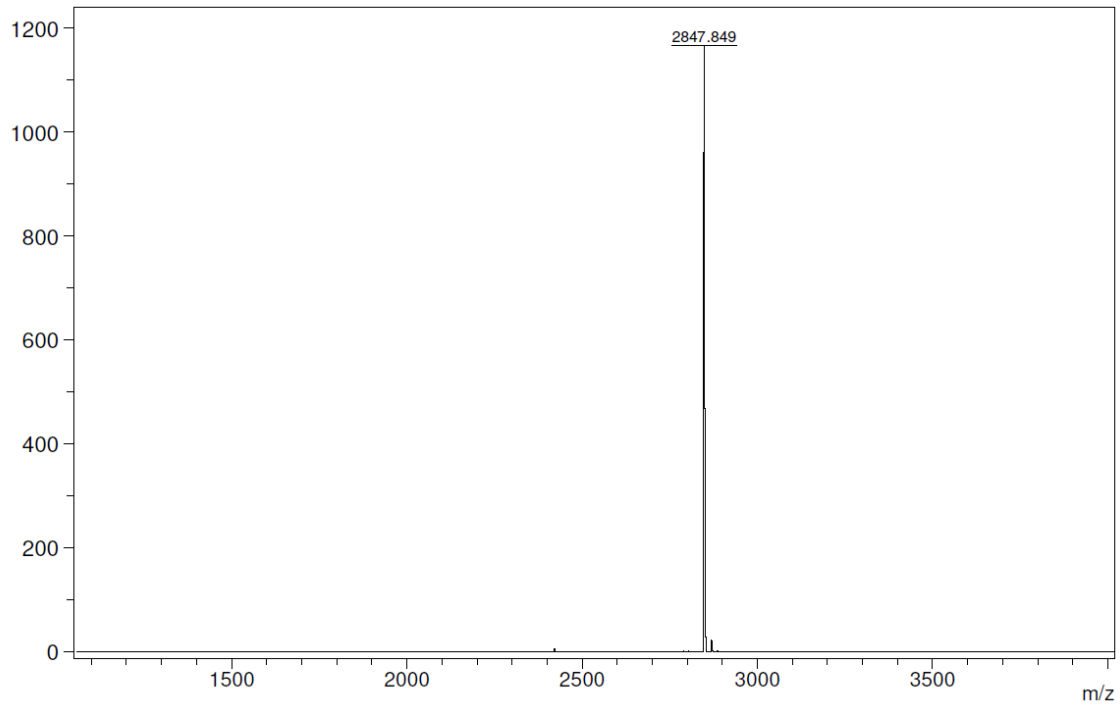

MALDI-TOF-MS spectra of **TGN**. $[M+H]^+$ calculated 2826. $[M+Na]^+$ found 2847.

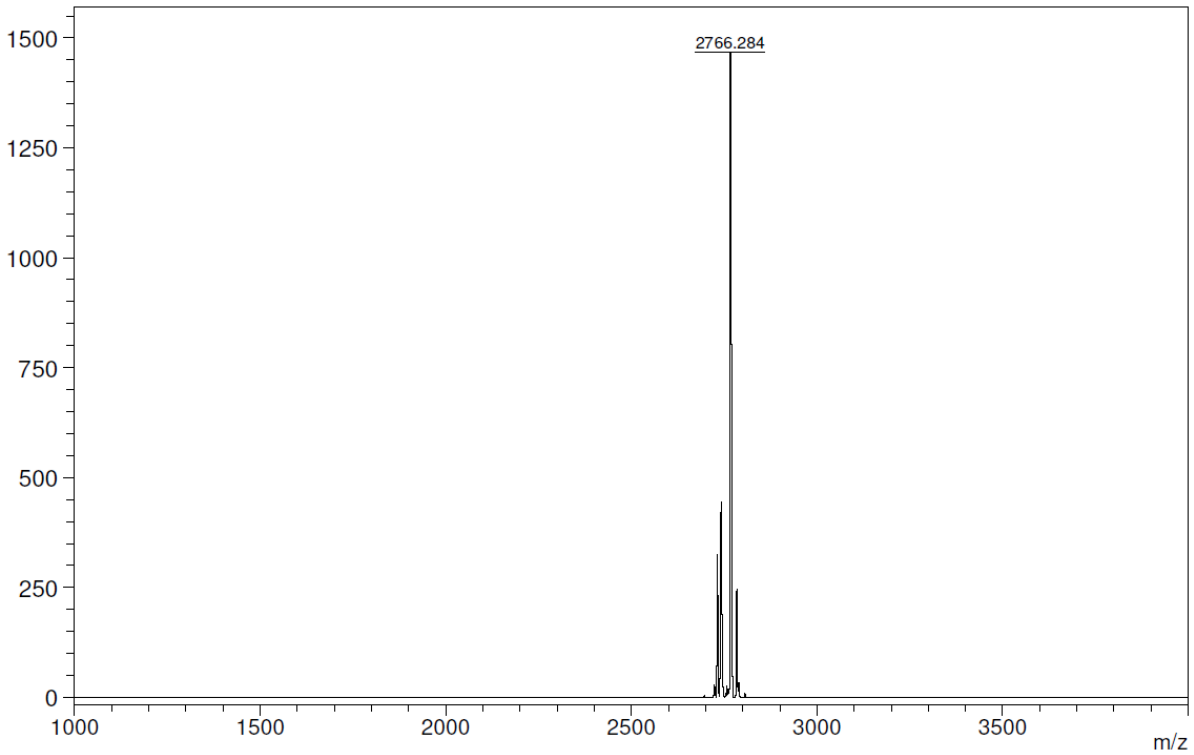

MALDI-TOF-MS spectra of **reTfR1-KN3**. $[M+H]^+$ calculated 2770. $[M+Na]^+$ found 2766.

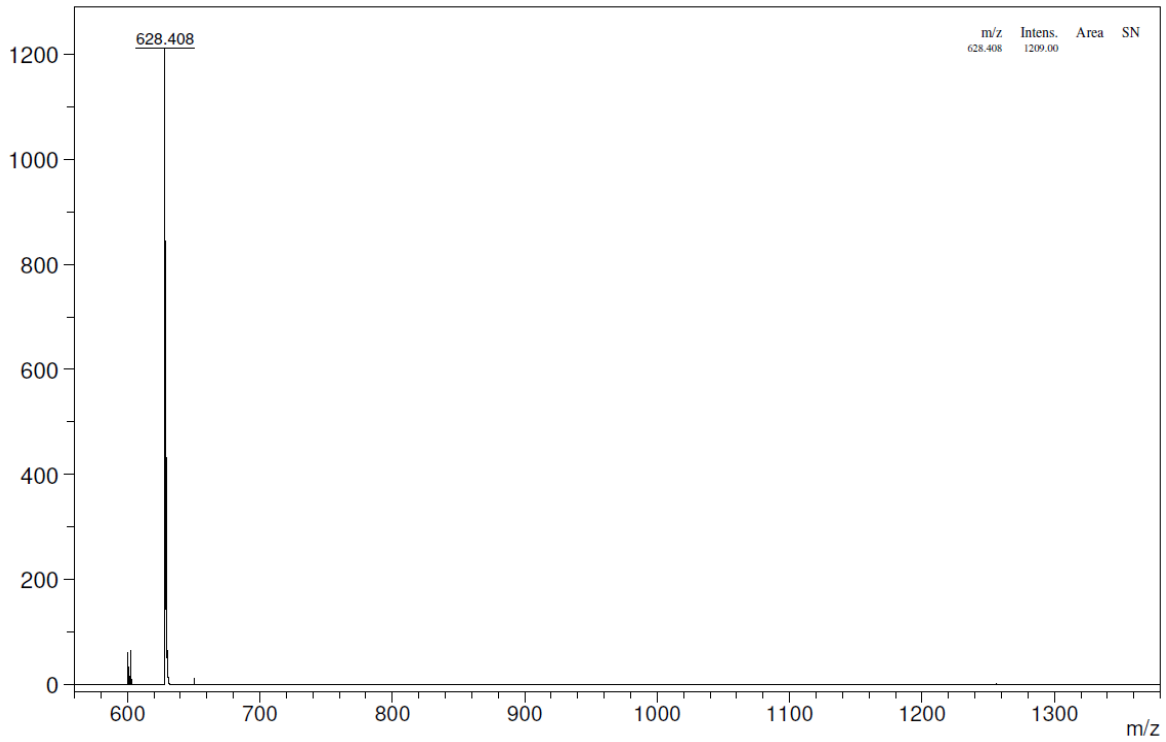

MALDI-TOF-MS spectra of **rRGD-KN3**. $[M+H]^+$ calculated 629. $[M+Na]^+$ found 628.

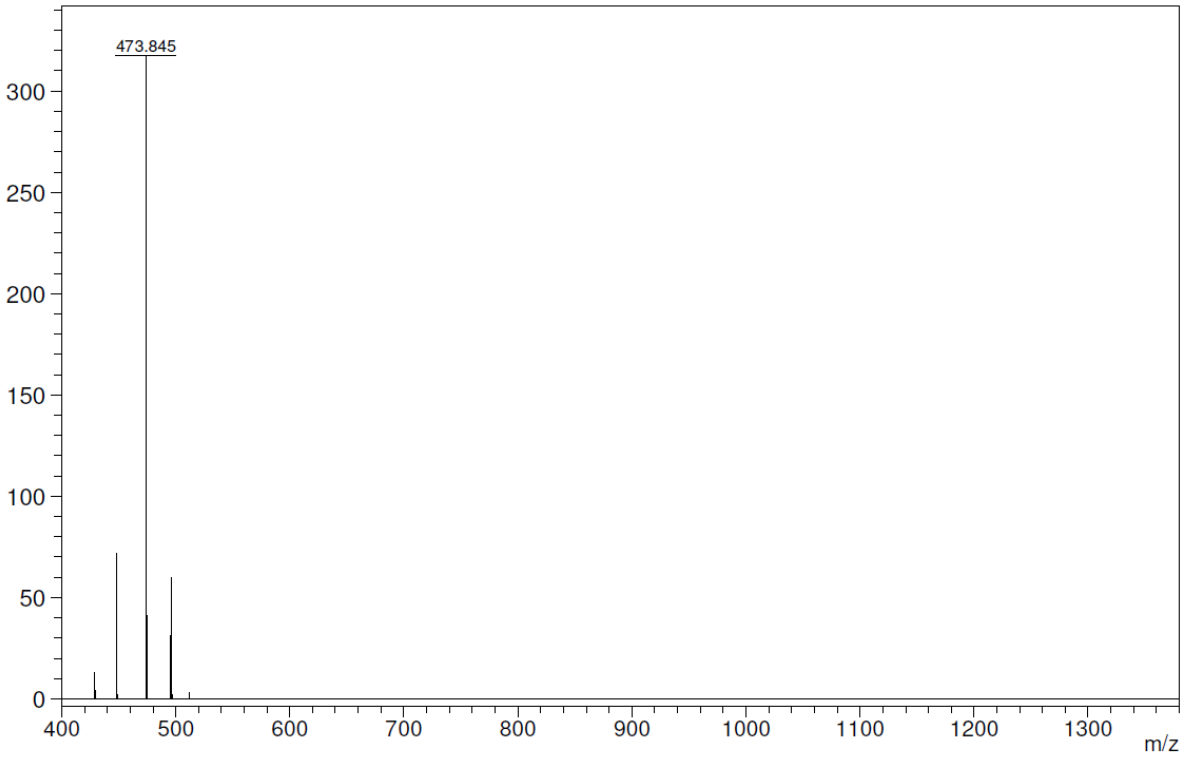

MALDI-TOF-MS spectra of **PEG4-KN3**. $[M+H]^+$ calculated 474. $[M+Na]^+$ found 474.

6.4.3 Evaluation of the SPAAC reaction by HPLC and MALDI MS

HPLC analysis of SPAAC reaction of 1284 with R-PEG-1. 1284 (A), R-PEG-1 (B), mixture of R-PEG-1 + 1284 at time point 0 (after mixing) (C) and at time point 4h (D). Elution times of main peaks: 11.9 min (1284), 13.5 min (R-PEG-1), 12.1 min (broad, conjugate)

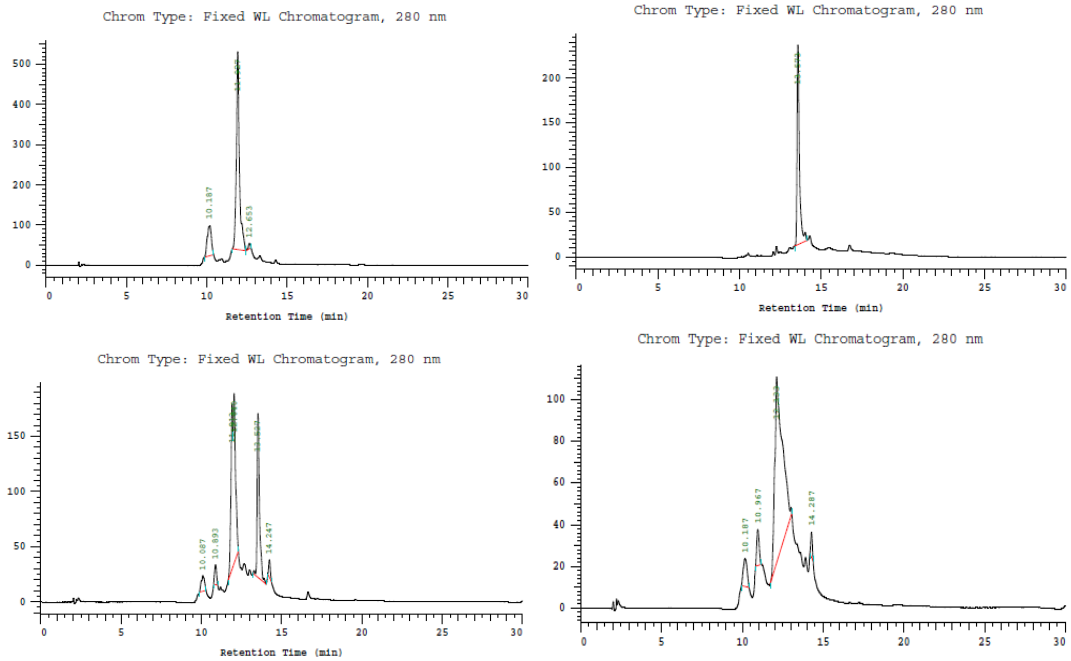

A left up; B right up; C left down; D right down

MALDI-TOF-MS spectra (positive mode) of R-PEG-1 + 1284 after 4 h incubation. [M+H]+ calculated for 1284: 3915. [M+H]+ found 3904.28 ; [M+H]+ calculated for the R-PEG-1 + 1284 conjugate: 5506. [M+H]+ found 5502.6.

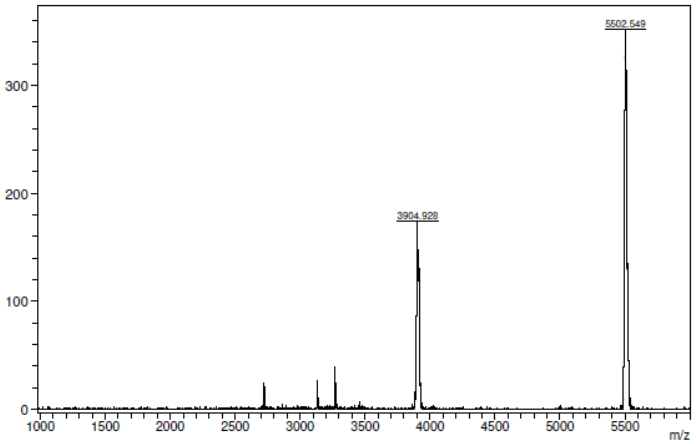

6.4.4 HPLC chromatograms of DBCO agents

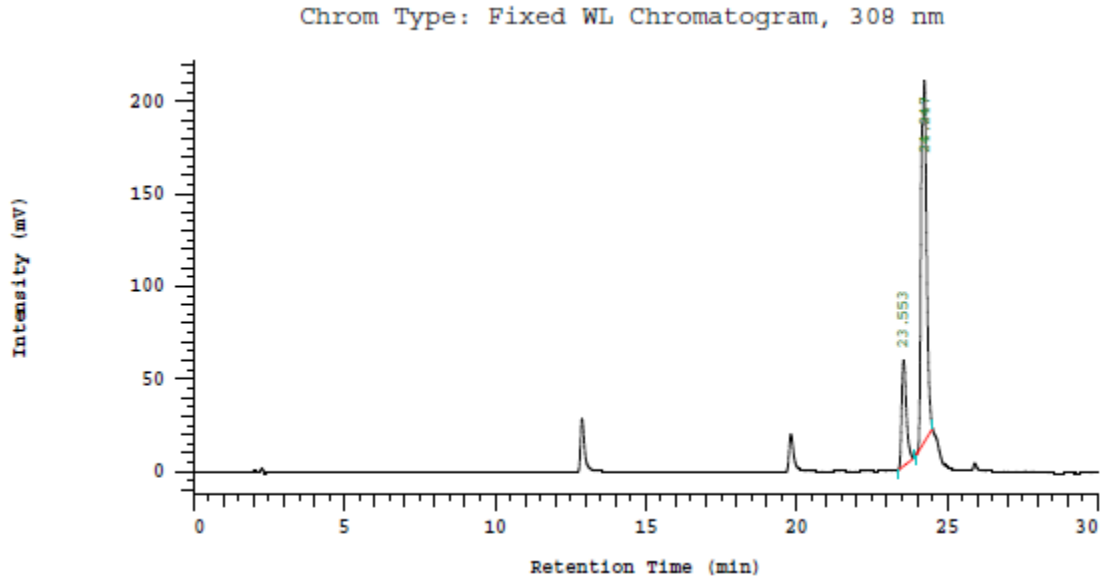

HPLC chromatogram of **reTfR-1**. Detection wavelength: 308nm.

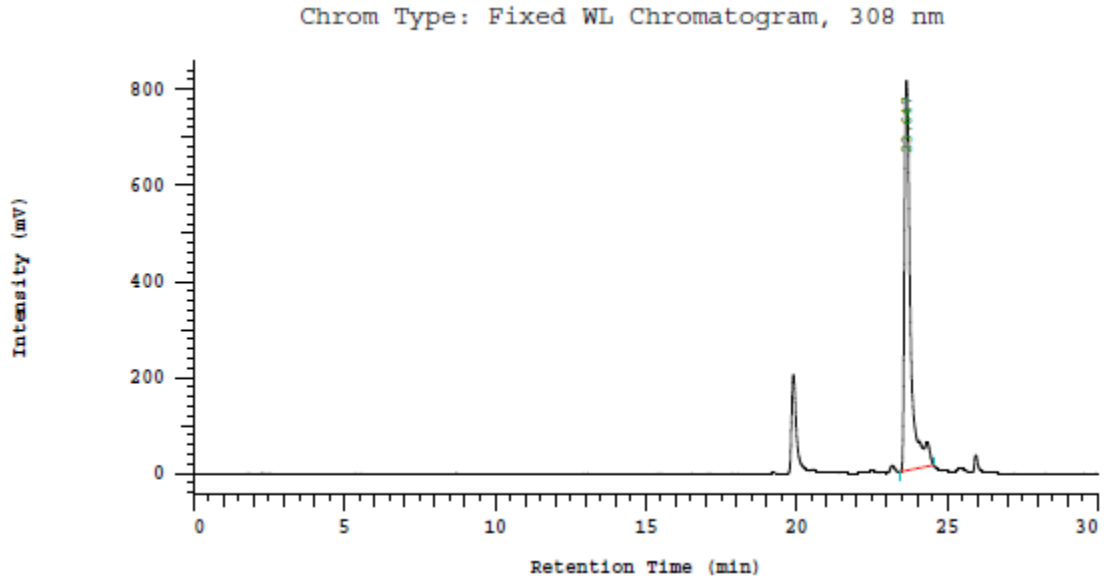

HPLC chromatogram of **reTfR-2**. Detection wavelength: 308nm.

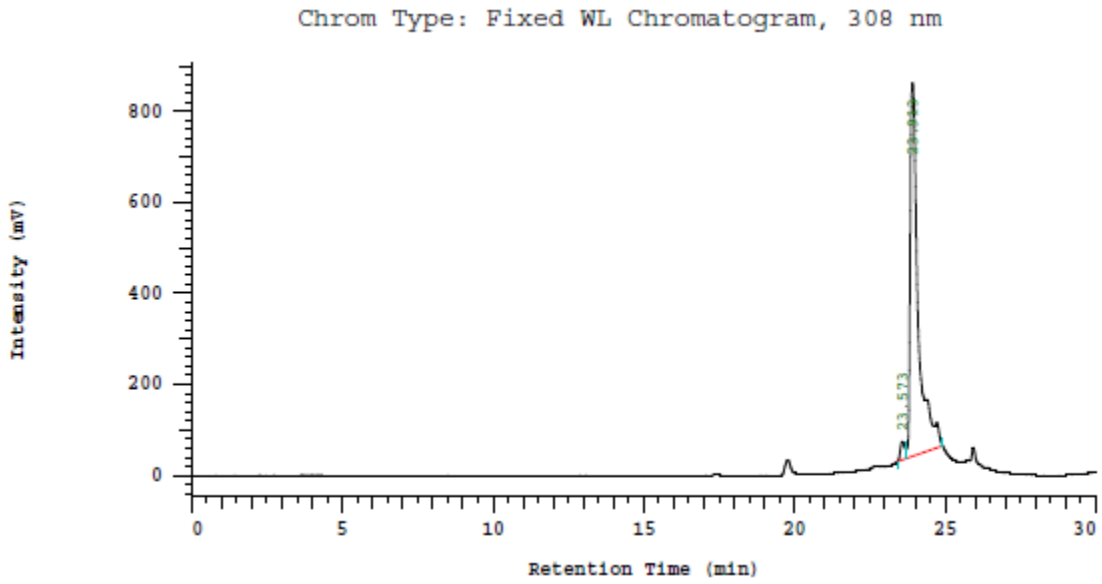

HPLC chromatogram of **scr-reTfR-1**. Detection wavelength: 308nm.

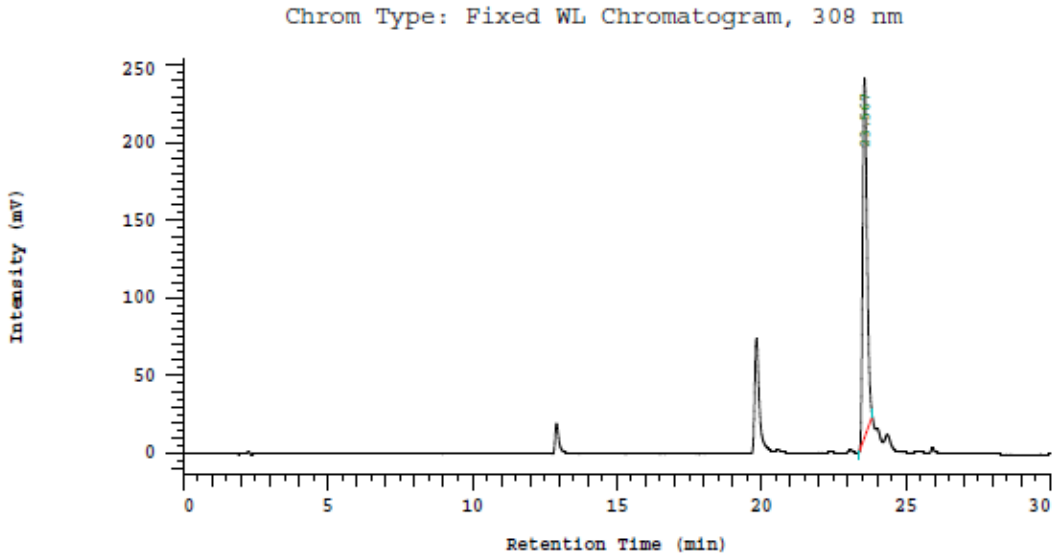

HPLC chromatogram of **scr-reTfR-2**. Detection wavelength: 308nm.

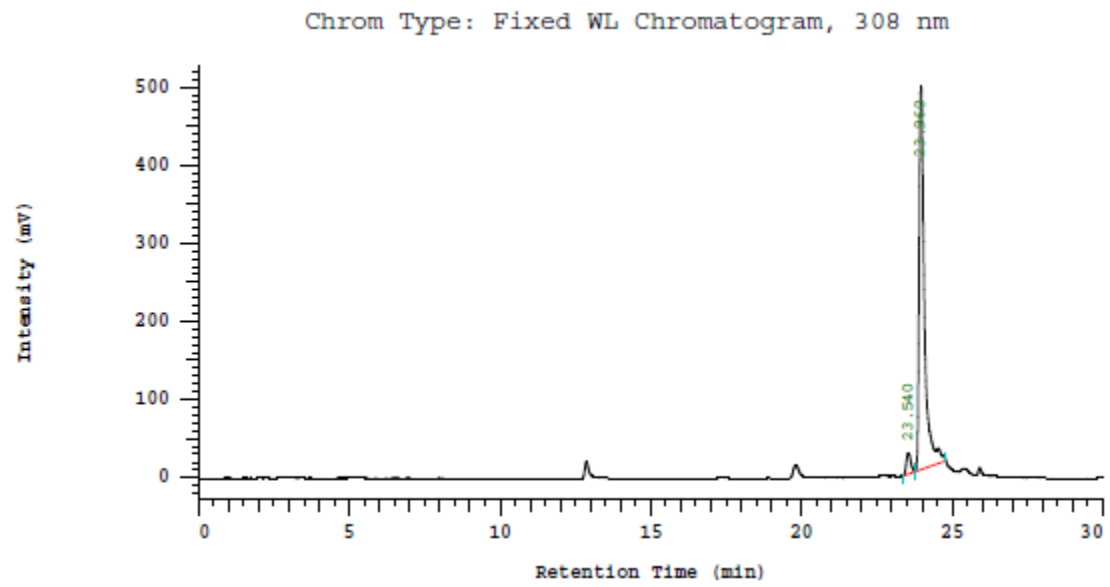

HPLC chromatogram of **R-PEG-1**. Detection wavelength: 308nm.

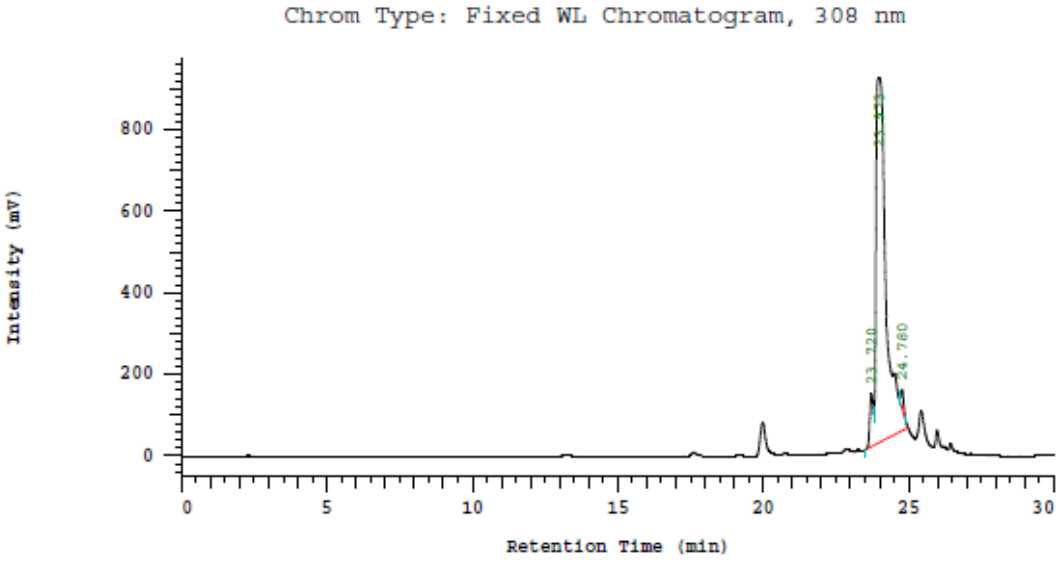

HPLC chromatogram of **R-PEG-2**. Detection wavelength: 308nm.

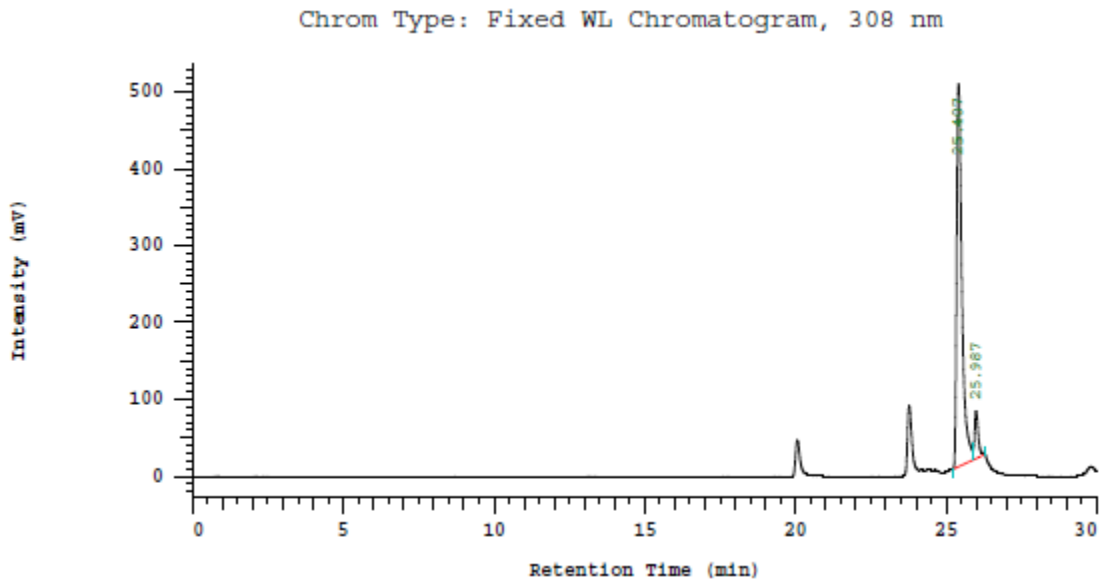

HPLC chromatogram of **PEG-1**. Detection wavelength: 308nm.

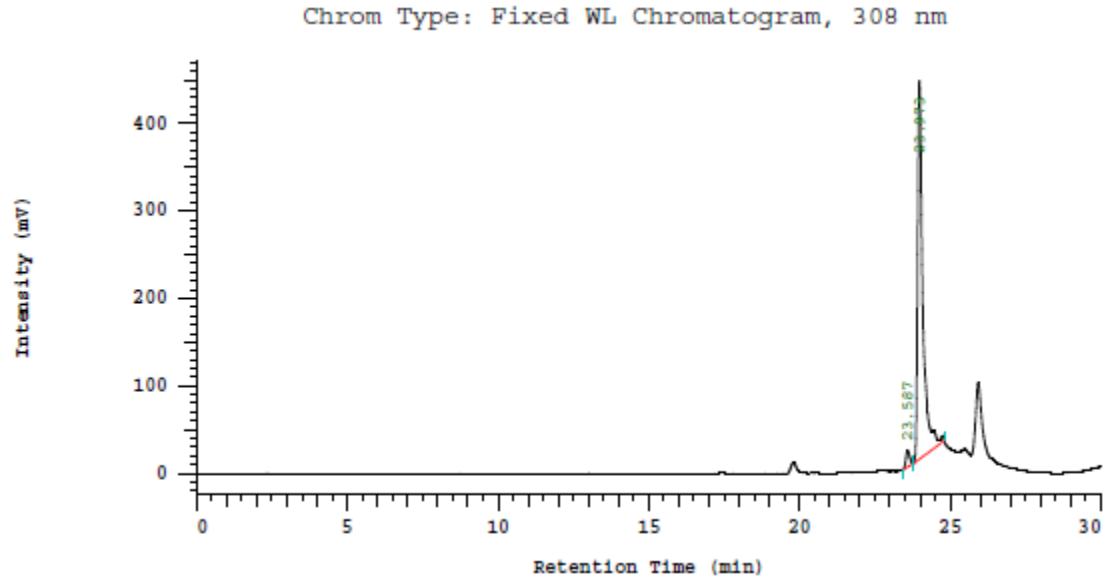

HPLC chromatogram of **PEG-2**. Detection wavelength: 308nm.

6.4.5 Particle size (Z-average), polydispersity index (PDI), and zeta potential of siRNA polyplexes.

1214 siRNA polyplexes	Equiv	Z-average (nm)	PDI	Zeta potential (mV)
non	-	146.4 ± 1.3	0.18 ± 0.02	33.2 ± 2.4
reTfR-1	0.25	153.3 ± 2.7	0.19 ± 0.01	27.1 ± 2.0
	0.5	150.9 ± 2.1	0.19 ± 0.02	26.9 ± 2.2
	0.75	153.5 ± 1.0	0.17 ± 0.02	25.9 ± 0.1
	1	162.1 ± 3.4	0.19 ± 0.03	27.2 ± 1.1
reTfR-2	0.25	153.0 ± 1.6	0.16 ± 0.04	23.5 ± 1.6
	0.5	156.3 ± 0.9	0.19 ± 0.04	21.8 ± 1.4
	0.75	156.6 ± 2.0	0.18 ± 0.02	20.8 ± 0.7
	1	180.6 ± 3.2	0.22 ± 0.01	22.5 ± 1.4
PEG-1	0.25	147.7 ± 0.2	0.18 ± 0.02	13.5 ± 0.8
	0.5	148.9 ± 1.1	0.19 ± 0.03	12.3 ± 0.6
	0.75	150.9 ± 1.4	0.19 ± 0.001	9.6 ± 1.0
	1	153.0 ± 1.7	0.18 ± 0.03	7.7 ± 1.0
PEG-2	0.25	159.2 ± 0.5	0.18 ± 0.02	11.2 ± 0.7
	0.5	162.2 ± 3.0	0.15 ± 0.01	7.6 ± 0.1
	0.75	164.7 ± 2.8	0.18 ± 0.01	5.9 ± 0.3
	1	169.5 ± 0.4	0.18 ± 0.01	2.9 ± 0.7

Polyplexes were formed with siCtrl at N/P 12 and then either left non-modified or modified with different equiv of shielding and targeting agents. DLS & ELS measurements using a Zetasizer Nano ZS (mean ± sd; n = 3). Done by done by Mina Yazdi, Pharmaceutical Biology, LMU.

6.4.6 Particle size (Z-average), polydispersity index (PDI), and zeta potential of pDNA polyplexes.

ID	non		reTfR-1		reTfR-2		PEG-1		PEG-2	
	Z-av (nm)	Zeta (mV)	Z-av (nm)	Zeta (mV)	Z-av (nm)	Zeta (mV)	Z-av (nm)	Zeta (mV)	Z-av (nm)	Zeta (mV)
1284	90.6 ± 0.1	13.7 ± 0.4	93.3 ± 1.9	15.1 ± 0.2	85.8 ± 1.8	16.7 ± 1.5	97.8 ± 2.6	7.3 ± 0.4	102.4 ± 1.0	3.6 ± 0.2
1276	89.6 ± 0.7	32.2 ± 0.9	82.6 ± 0.4	20.1 ± 0.8	76.7 ± 0.5	17.9 ± 1.5	77.7 ± 0.7	13.5 ± 1.1	76.7 ± 1.0	10.4 ± 0.5

1285	87.8 ± 0.8	16.0 ± 0.3	89.0 ± 1.6	19.4 ± 1.0	86.4 ± 1.3	17.8 ± 0.7	4173 ± 110	-0.5 ± 0.8	4811 ± 657	2.3 ± 0.2
1258	70.0 ± 0.8	21.8 ± 1.8	81.5± 1.1	18.9 ± 1.2	75.0 ± 0.5	20.0 ± 0.9	78.5 ± 0.3	17.9 ± 1.5	72.9 ± 0.3	8.0 ± 0.2
1218	119.8 ± 1.7	18.1 ± 0.9	87.5 ± 0.2	19.1 ± 1.4	89.0 ± 1.4	18.4 ± 1.6	80.8 ± 0.8	19.0 ± 1.0	87.5 ± 0.3	8.0 ± 0.8
1214	104.4 ± 1.3	21.2 ± 0.9	91.2 ± 0.6	12.2 ± 1.5	83.3 ± 1.0	17.6 ± 1.0	82.7 ± 0.3	12.0 ± 1.5	85.6 ± 0.5	2.9 ± 0.3

ID	**scr-re-TfR-1**		**scr-re-TfR-2**		**R-PEG-1**		**R-PEG-2**	
	Z- av (nm)	Zeta (mV)	Z- av (nm)	Zeta (mV)	Z- av (nm)	Zeta (mV)	Z- av (nm)	Zeta (mV)
1284	181.4 ± 3.6	10.7 ± 1.1	117.7 ± 1.3	14.0 ± 0.8	103.3 ± 1.7	8.9 ± 1.1	98.7 ± 0.3	6.6 ± 0.9
1276	154.0 ± 0.8	11.3 ± 1.2	104.3 ± 0.4	13.0 ± 0.6	88.3 ± 1.4	9.4 ± 1.2	89.0 ± 0.8	5.9 ± 1.4
1285	4807 ± 492	11.3 ± 0.5	921.4 ± 65	12.5 ± 0.7	6012 ± 1406	2.2 ± 0.2	766.3 ± 23	5.0 ± 0.4
1258	265.6 ± 4.1	10.1 ± 0.4	128.1 ± 0.6	11.2 ± 1.0	131.2 ± 0.8	9.1 ± 0.5	90.3 ± 0.6	6.3 ± 1.1
1218	108.1 ± 0.6	16.1 ± 2.1	128.8 ± 1.8	12.7 ± 2.0	97.0 ± 0.5	13.2 ± 1.1	96.7 ± 0.4	7.9 ± 1.3
1214	95.0 ± 0.4	14.1 ± 0.8	98.6 ± 0.0	12.6 ± 1.2	93.6 ± 0.4	12.1 ± 0.4	92.3 ± 0.6	7.8 ± 0.1

Particle size (Z-average) and zeta potential of pDNA polyplexes pCMVLuc polyplexes (formed at N/P 12), non-modified or modified with 0.5 equiv of shielding and targeting agents, were measured by DLS & ELS (mean ± sd; n = 3). Done by Şurhan Göl, Pharmaceutical Biology, LMU.

	non	reTfR-1	reTfR-2	PEG-1	PEG-2
1284	0.14 ± 0.01	0.16 ± 0.04	0.14 ± 0.02	0.18 ± 0.01	0.12 ± 0.01
1276	0.14 ± 0.01	0.15 ± 0.03	0.13 ± 0.01	0.17 ± 0.03	0.19 ± 0.01
1285	0.14 ± 0.01	0.11 ± 0.00	0.13 ± 0.01	0.34 ± 0.12	0.37 ± 0.04
1258	0.12 ± 0.02	0.13 ± 0.01	0.13 ± 0.02	0.21 ± 0.01	0.16 ± 0.01
1218	0.19 ± 0.02	0.11 ± 0.02	0.10 ± 0.02	0.21 ± 0.00	0.16 ± 0.02
1214	0.15 ± 0.03	0.13 ± 0.03	0.12 ± 0.02	0.12 ± 0.03	0.12 ± 0.04

	scr-reTfR-1	scr-reTfR-2	R-PEG-1	R-PEG-2
1284	0.19 ± 0.01	0.14 ± 0.02	0.16 ± 0.03	0.16 ± 0.03
1276	0.13 ± 0.01	0.13 ± 0.01	0.13 ± 0.01	0.11 ± 0.01
1285	0.20 ± 0.08	0.59 ± 0.06	0.35 ± 0.18	0.59 ± 0.03
1258	0.24 ± 0.02	0.17 ± 0.01	0.14 ± 0.03	0.15 ± 0.02
1218	0.11 ± 0.03	0.25 ± 0.00	0.09 ± 0.03	0.09 ± 0.00
1214	0.10 ± 0.01	0.14 ± 0.02	0.09 ± 0.01	0.11 ± 0.03

pCMVLuc polyplexes (formed at N/P 12), non-modified or modified with 0.5 equiv of shielding and targeting agents, were measured by DLS (mean ± sd; n = 3). Done by Şurhan Göl, Pharmaceutical Biology, LMU.

6.4.7 Agarose gel shift of siRNA polyplexes

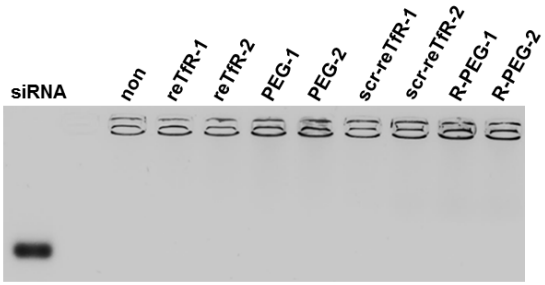

Standard agarose (2.5%, TBE buffer) gel shift of ***1214/***siCtrl polyplexes formed at N/P 12 in HBG. Non-modified polyplexes or polyplexes modified with 0.5 equiv of

shielding and targeting agents were analyzed. Done by done by Mina Yazdi, Pharmaceutical Biology, LMU.

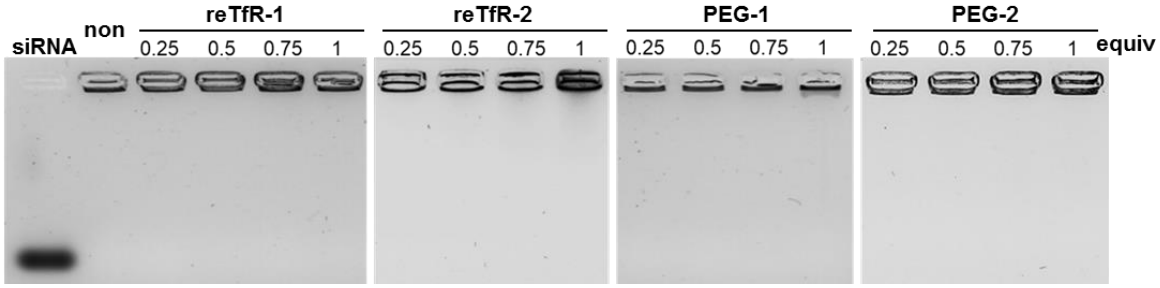

Standard agarose (2.5%, TBE buffer) gel shift of 1214/siCtrl polyplexes formed at N/P 12 in HBG. Non-modified polyplexes or polyplexes modified with different equiv of shielding and targeting agents were analyzed). Done by done by Mina Yazdi, Pharmaceutical Biology, LMU.

6.4.8 Agarose gel shift of pDNA polyplexes

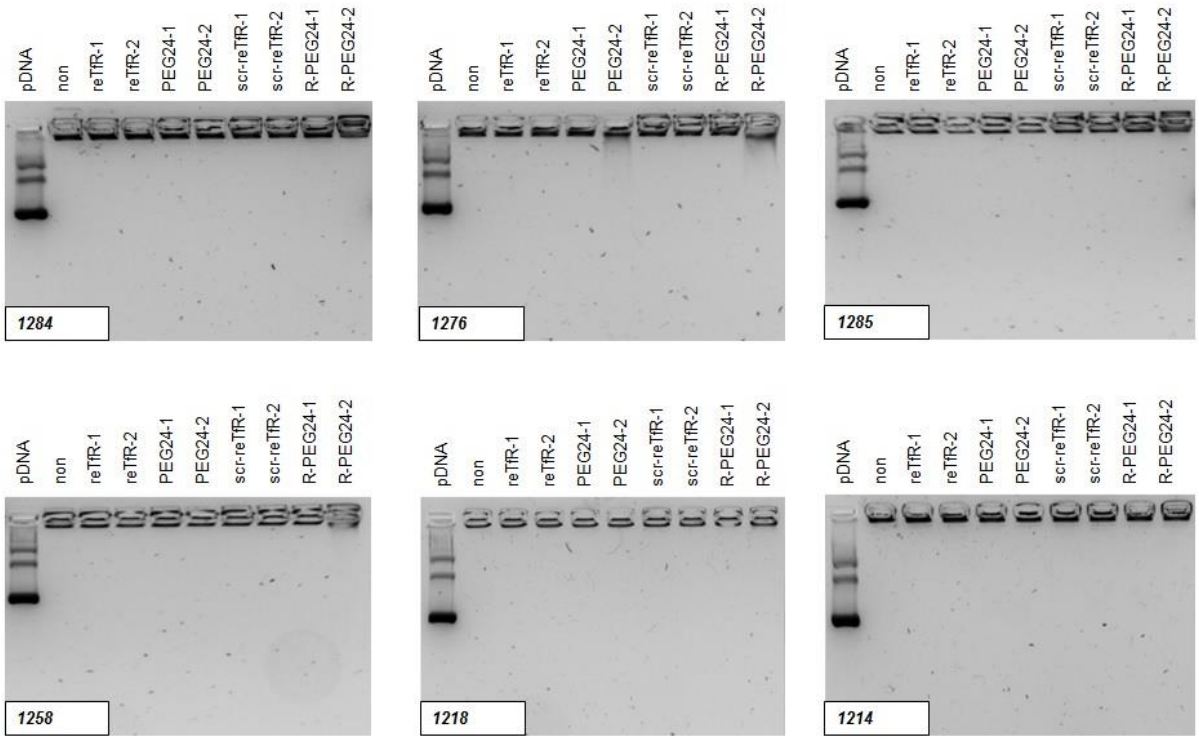

Standard agarose (1%, TBE buffer) gel shift of pDNA polyplexes formed at N/P 12 in HBG. Non-modified polyplexes or polyplexes modified with 0.5 equiv of shielding and targeting agents were analyzed. Done by Şurhan Göl, Pharmaceutical Biology, LMU.

6.4.9 eGFPLuc gene silencing activity of siRNA polyplexes

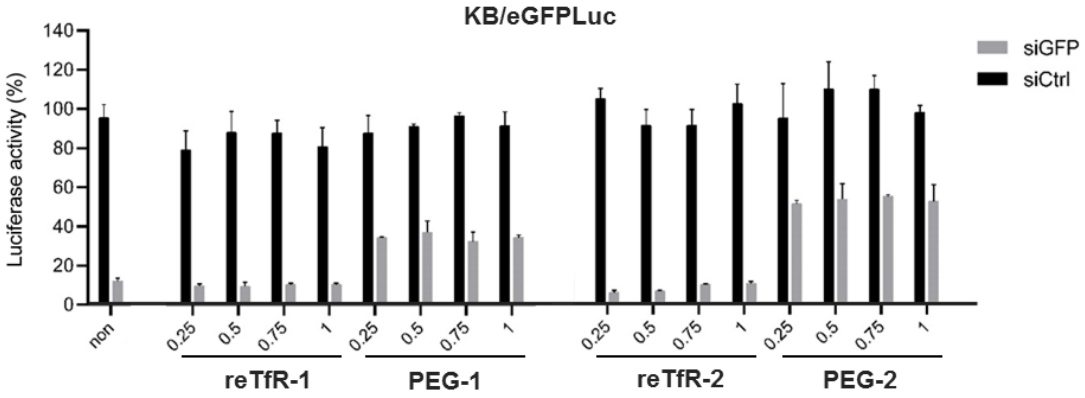

The eGFPLuc gene silencing activity of 1214/siRNA polyplexes evaluated by luciferase assay in KB/eGFPLuc reporter cell line after 4 h incubation followed by medium replacement and further incubation for 44 h at 37°C. The polyplexes were formed at N/P 12 and then either left non-modified or modified with different equiv of shielding and targeting agents (mean ± sd; n = 3). Done by done by Mina Yazdi, Pharmaceutical Biology, LMU.

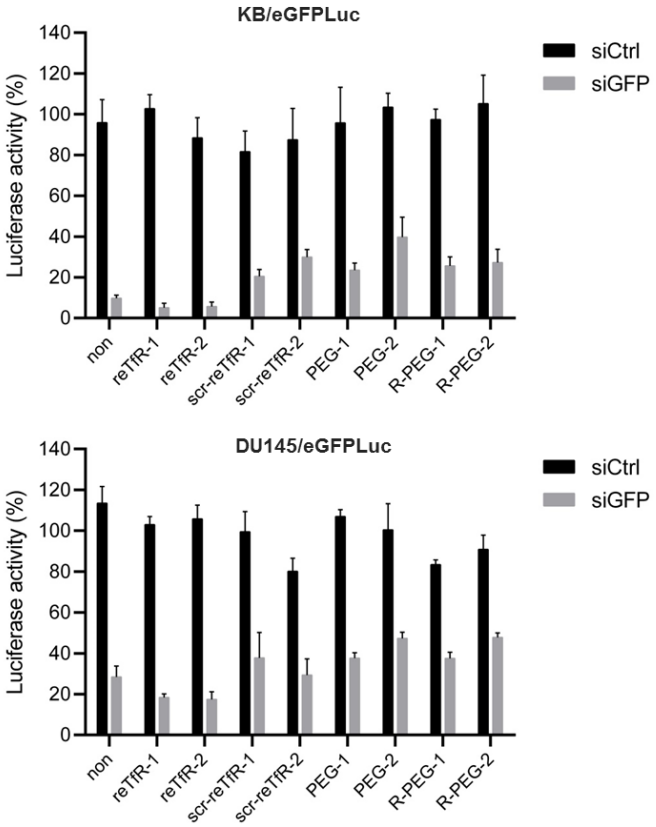

The eGFPLuc gene silencing activity of ***1214***/siRNA polyplexes evaluated by luciferase assay in KB/eGFPLuc and DU145/eGFPLuc reporter cell lines after 4 h incubation followed by medium replacement and further incubation for 44 h at 37°C. The polyplexes were formed at N/P 12 and then either left non-modified or modified with 0.5 equiv of shielding and targeting agents (mean ± sd; n = 3). Done by done by Mina Yazdi, Pharmaceutical Biology, LMU.

6.4.10 Ethidium bromide (EtBr) exclusion assay of pDNA polyplexes

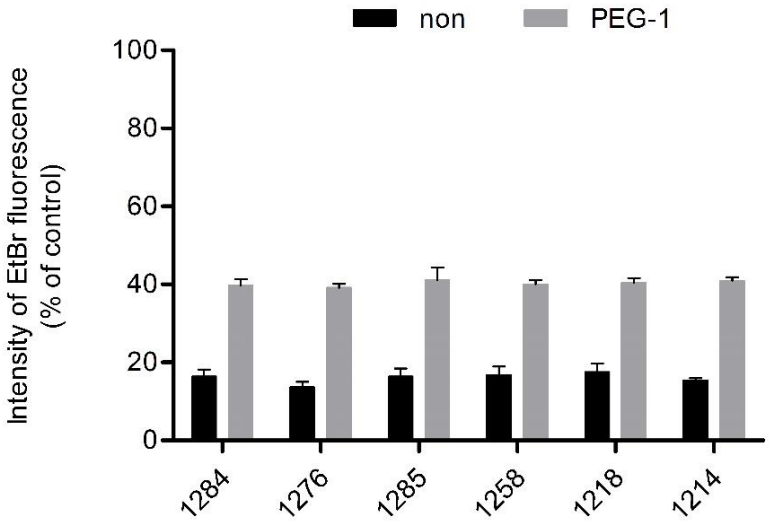

Ethidium bromide (EtBr) exclusion assay of pDNA polyplexes (N/P 12, HBG), nonmodified or modified with 0.5 equiv of PEG-1 (mean ± sd; n = 3). Intensity of EtBr fluorescence is presented as percentage relative to free noncompacted pDNA. Done by Şurhan Göl, Pharmaceutical Biology, LMU.

6.4.11 TEM data of pDNA polyplexes

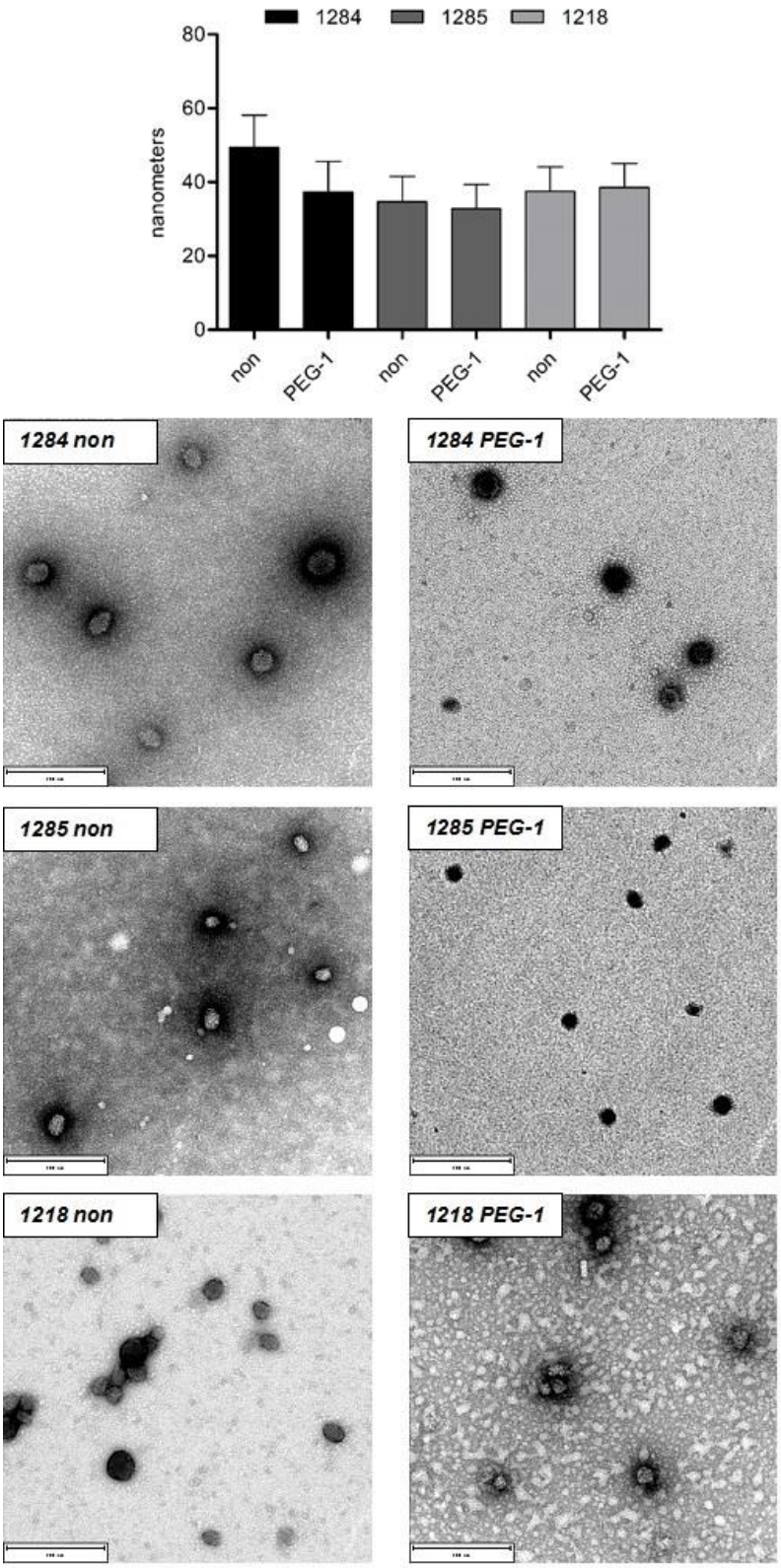

Top: TEM size data (diameter, nm) of pDNA lipo-polyplexes (N/P 12, H_2O) formed with selected carriers 1284, 1285 and 1218 without (non) or with 0.5 equiv of monovalent DBCO agent PEG-1. Below: Corresponding representative TEM images

of the pDNA lipo-polyplexes (N/P 12, H_2O) formed with selected carriers 1284, 1285 and 1218 without (non) or with 0.5 equiv of monovalent DBCO agent PEG-1. (Scale bars = 200 nm). The experiment was managed and analyzed by Özgür Öztürk, Pharmaceutical Biology, LMU.

6.4.12 MTT assay of pDNA polyplexes

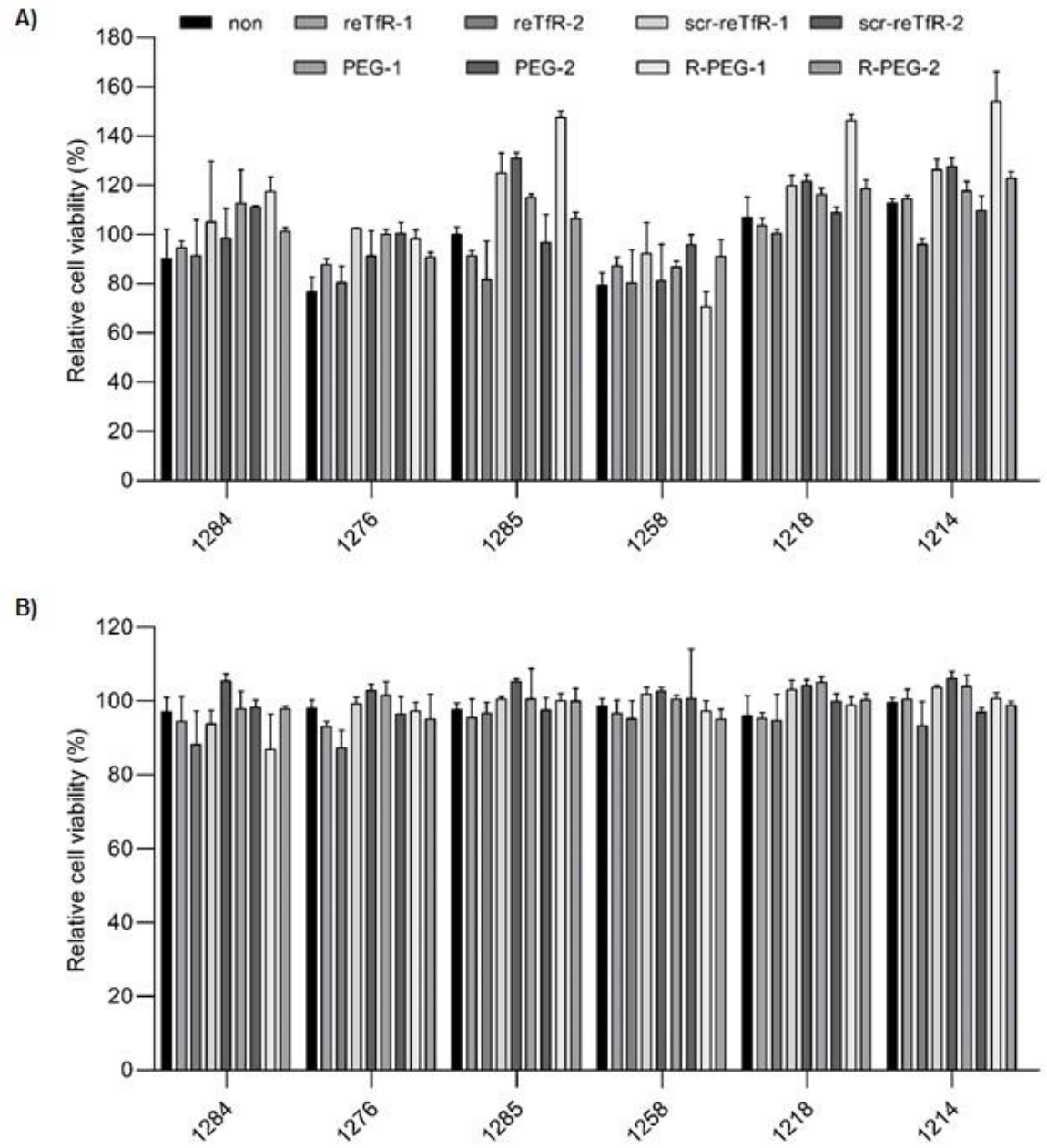

Metabolic activity of pDNA transfection in K562 (A) and N2a (B) cells. Metabolic activity of the cells determined by the CellTiter-Glo® assay after incubation with pDNA polyplexes for 24 h. Metabolic activities are presented as percentage relative

to HBG buffer-treated control cells (mean ± sd; n = 3). Done by Şurhan Göl, Pharmaceutical Biology, LMU.

6.4.13 Cellular association of pDNA polyplexes

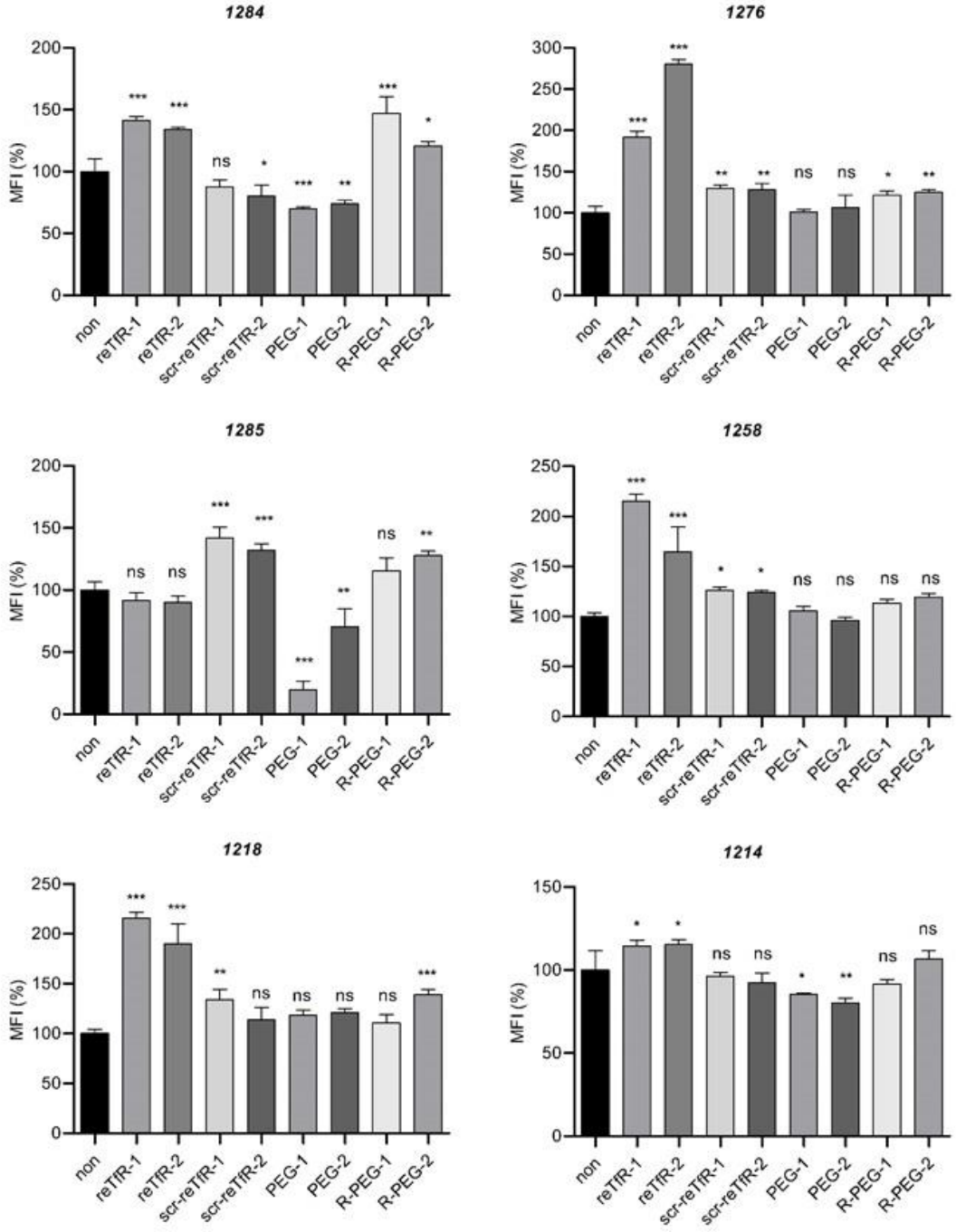

Cellular association of pDNA polyplexes with K562 cells. Cells were incubated with 200 ng/well 20% Cy5 labeled pDNA polyplexes (N/P12, HBG; 0.5 equiv of DBCO agent) for 45 min at 37°C. Mean fluorescent intensity (MFI, % of non-modified polyplexes)

was measured by flow cytometry (mean ± sd; n = 3). The statistical significance was determined by one-way ANOVA; ns, not significant; *p ≤ 0.05, **p ≤ 0.01, ***p ≤ 0.001. Done by Şurhan Göl, Pharmaceutical Biology, LMU.

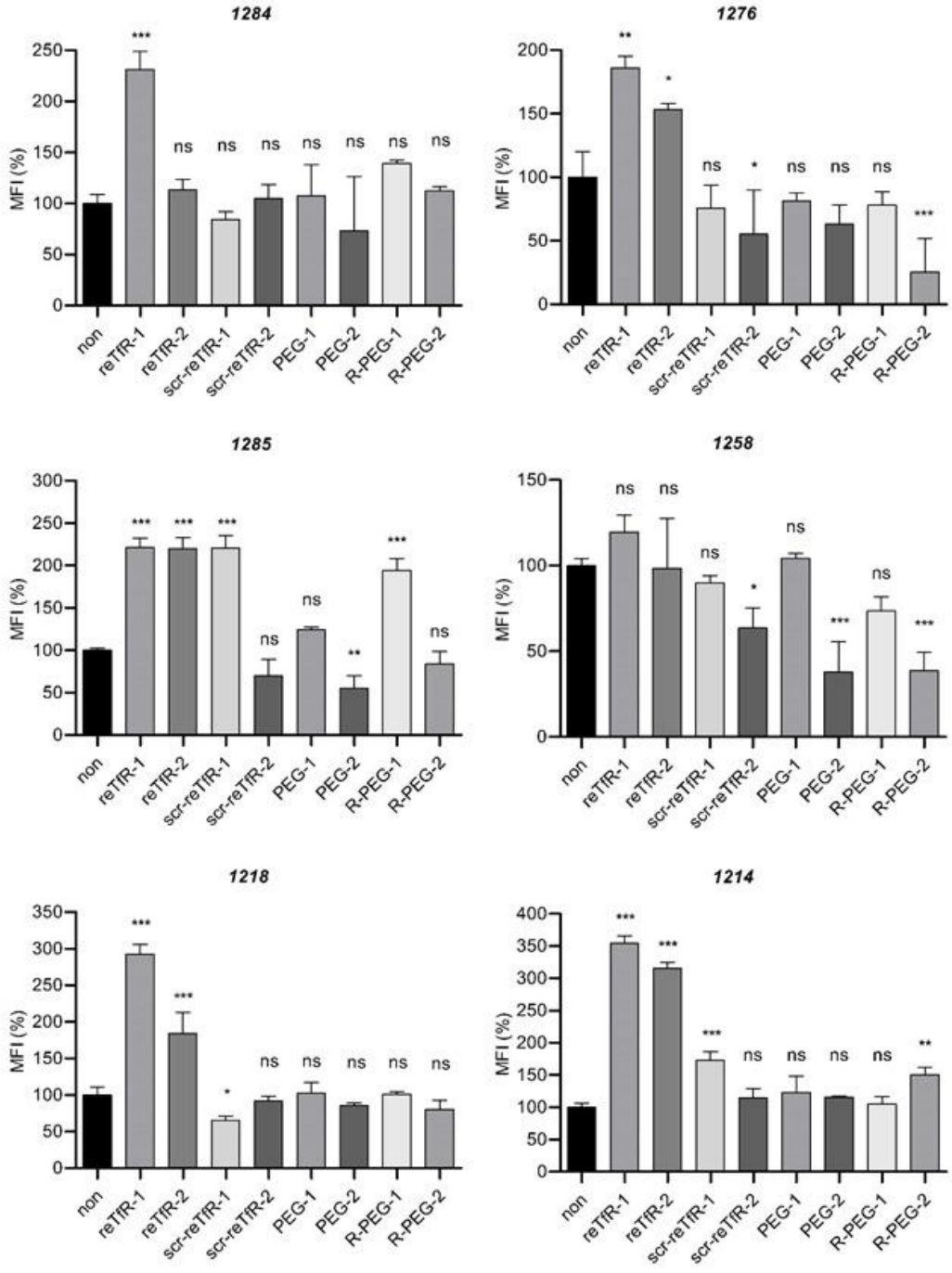

Cellular association of pDNA polyplexes with N2a cells. Cells were incubated with 200 ng/well 20% Cy5 labeled pDNA polyplexes (N/P 12, HBG; 0.5 equiv of DBCO agent) for 45 min at 37°C. Mean fluorescent intensity (MFI, % of non-modified polyplexes) was measured by flow cytometry (mean ± sd; n = 3). The statistical significance was

determined by one-way ANOVA; ns, not significant; *p ≤ 0.05, **p ≤ 0.01, ***p ≤ 0.001. Done by Şurhan Göl, Pharmaceutical Biology, LMU.

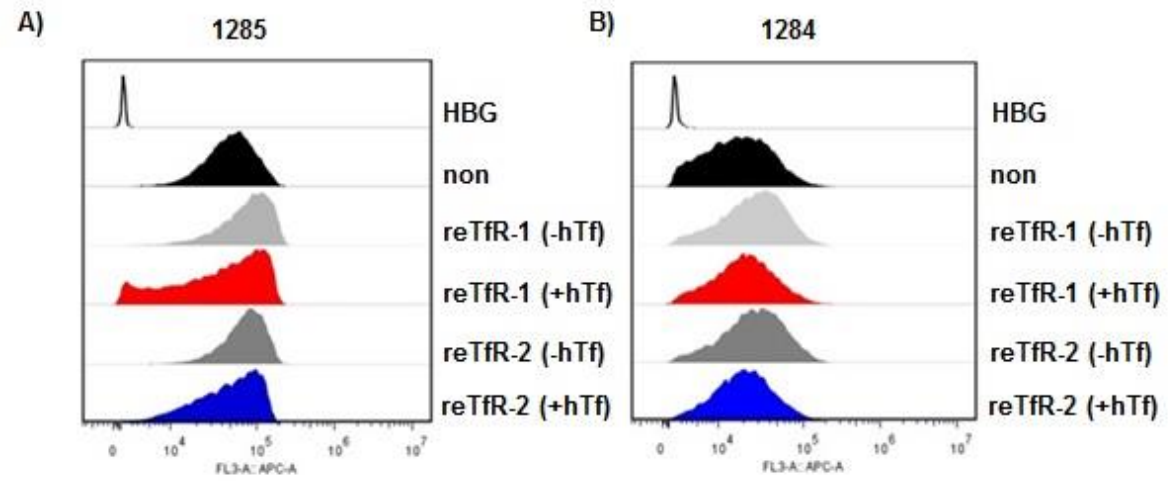

Cellular association of pDNA polyplexes. K562 cells (A) or N2a cells (B) were incubated with 200 ng/well 20% Cy5 labeled pDNA polyplexes for 45 min at 37°C and measured by flow cytometry. TfR blockade performed with (+) or without (-) 5 mg/ml free iron saturated human transferrin (hTf) for 30 min at 4°C prior to addition of polyplexes to cells. Data are presented as histograms of cells (x-axis, increasing Cy5 fluorescence intensity; y-axis, the number of cells). Done by Şurhan Göl, Pharmaceutical Biology, LMU.

6.4.14 Summary of SPSS derived 4-armed OAAs for rCD coating and entrapment and rCD

Sequences of the newly synthesized 4-armed OAA library, tailor cut for negatively charged rCDs. KN_3: azido-lysine; C: cysteine; Y: tyrosine; K: ε-amino linked lysine. The specifically names of the structures are originated by the respective composition of the arms. Shown as table and figure. For the detailed protocol of rCD-OAA see **2.2.7**.

ID	Abbreviation	Length of arms in pm	PDI	z-average/ number in nm	Zeta potential in mV
1655	(*N-α-Fmoc*): “K6 - CKN3”	2088	0,581	196/28	22
1767	(*N-ε-Fmoc*): “K6 - CKN3”	3950	0,496	252/109	17
1768	(*N-α-Fmoc*): “K9 - CKN3”	2757	0,651	232/76	24
1769	(*N-ε-Fmoc*): “K9 - CKN3”	5550	0,421	253/95	24
1656	(*N-α-Fmoc*): “K12 - CKN3”	3426	0,423	158/26	25
1694	(*N-ε-Fmoc*): “K12 - CKN3”	7150	0,433	290/99	23
1657	(*N-α-Fmoc*): “K3LK3LK3L - CKN3”	3426	0,524	308/19	21
1658	(*N-α-Fmoc*): “K3L3K3L3 - CKN3”	3426	0,728	219/42	25
1660	(*N-α-Fmoc*): “K3L2K3L2K3L2 - CKN3”	4095	0,314	174/25	26
1661	(*N-α-Fmoc*): “KLKLKLKLKLKL - CKN3”	3426	0,455	236/28	21
1662	(*N-α-Fmoc*): “K4L4K4 - CKN3”	3426	0,381	156/33	19
1663	(*N-α-Fmoc*): “K3YK3YK3Y - CKN3	3426	0,453	167/14	21
1695	(*N-ε-Fmoc*): “K3YK3YK3Y - CKN3	6238	0,309	238/94	22
1664	(*N-α-Fmoc*): “K3Y3K3Y3 - CKN3”	3426	0,310	264/38	20
1696	(*N-ε-Fmoc*): “K3Y3K3Y3 - CKN3”	5326	0,188	128/74	19
1665	(*N-α-Fmoc*): “K3Y2K3Y2K3Y2 - CKN3”	4095	0,358	232/21	19
1697	(*N-ε-Fmoc*): “K3Y2K3Y2K3Y2 - CKN3”	6907	0,280	138/78	23

1666	(*N-α-Fmoc*): “KYKYKYKYKYKY - CKN3”	3426	0,451	154/21	22
1698	(*N-ε-Fmoc*): “KYKYKYKYKYKY - CKN3”	5326	0,393	184/130	20
1667	(*N-α-Fmoc*): “K4Y4K4 - CKN3”	3426	0,612	238/24	20
1699	(*N-ε-Fmoc*): “K4Y4K4 - CKN3”	5934	0,321	144/110	21
rCD	Untreated	-	0,66	589/68	-17
rCD	Centrifuged	-	0,406	235/79	-22
1463	Starting OAA for study	5286	0,600	116/74	17

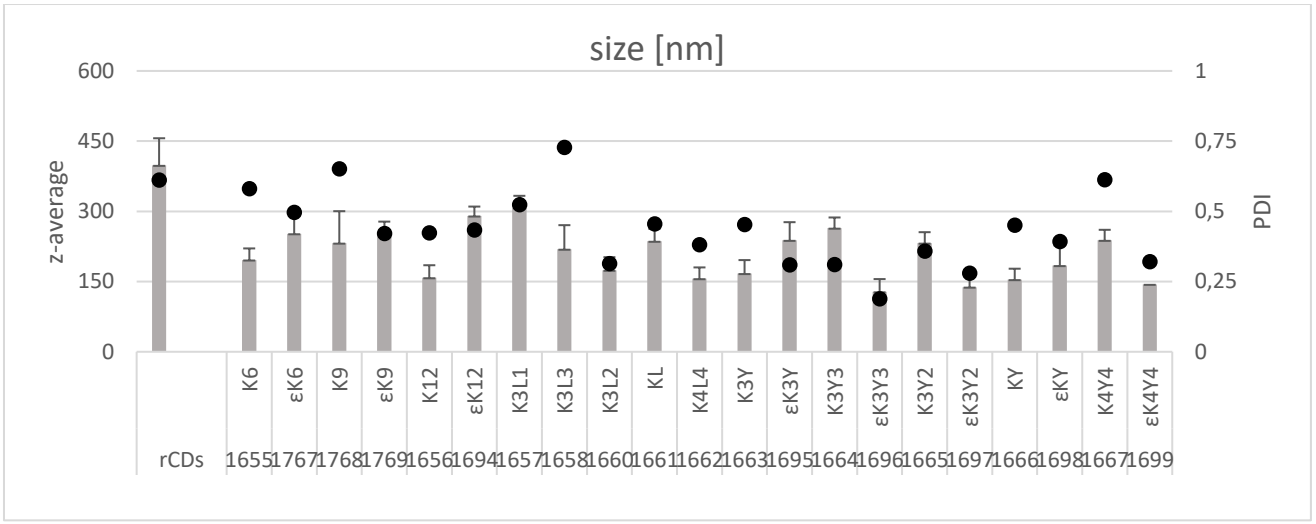

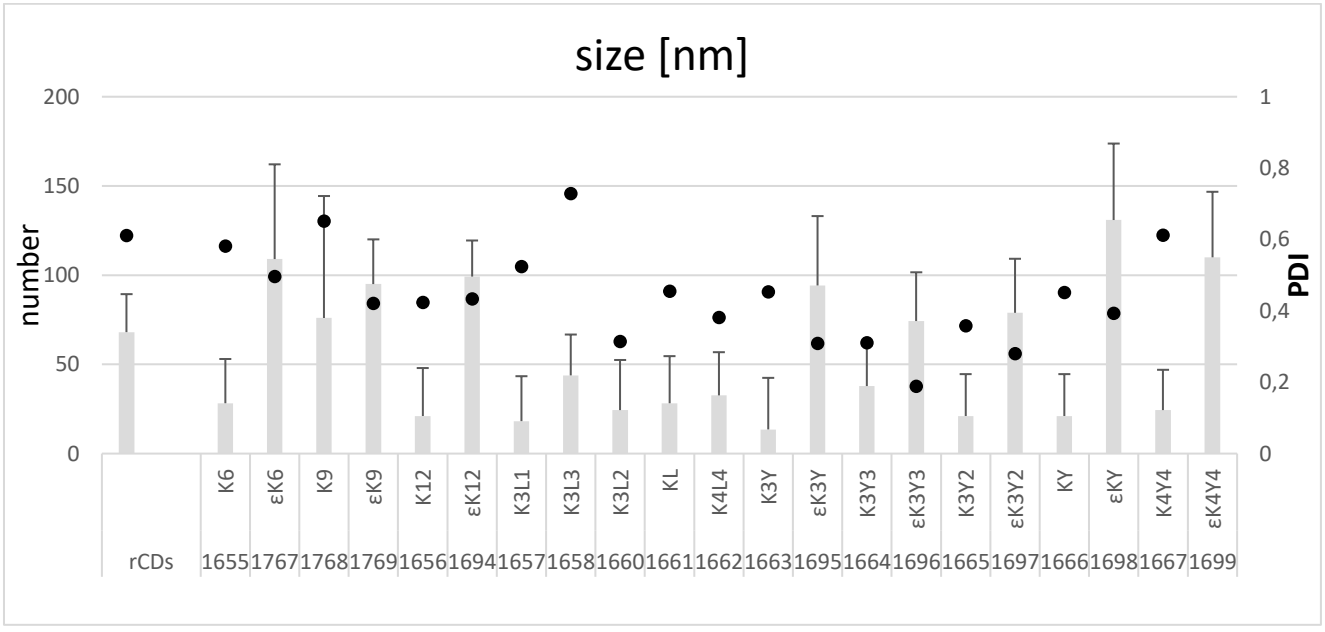

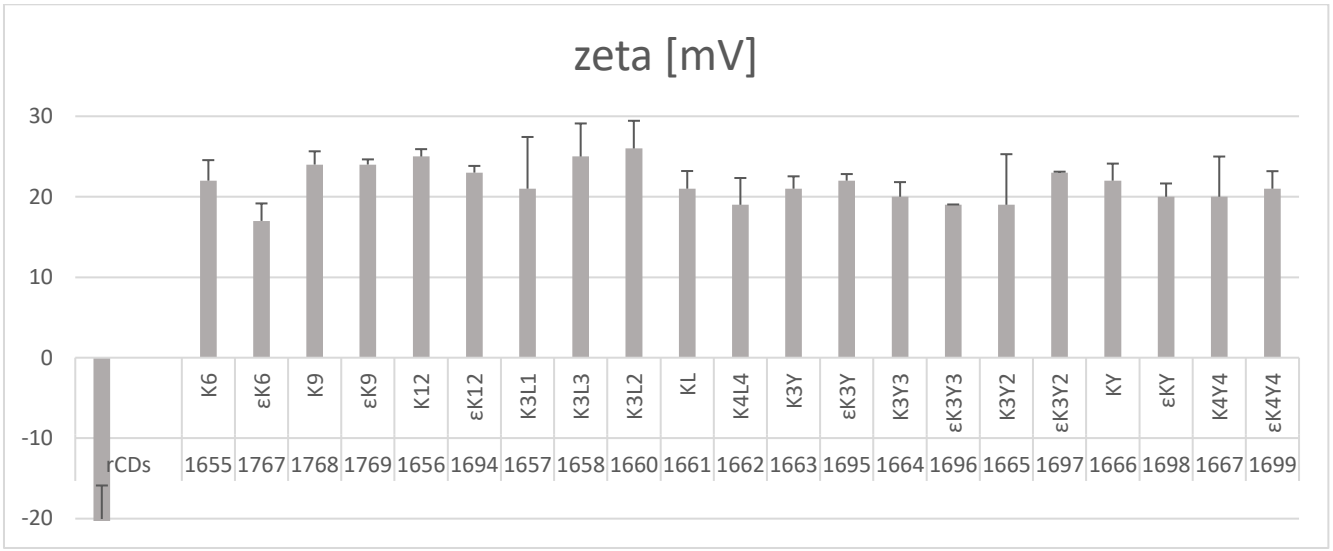

6.4.15 rCD-1696 (w/w) titration

No benefit in size & PDI post 2,7 w_{1696}/w_{rCD}
No significant higher zeta post 5,4 w_{1696}/w_{rCD}
Turning point in zeta at 0,9 w_{1696}/w_{rCD}

→ w_{1696}/w_{rCD} ratio of 2,7 used as most beneficial ratio
(lowest PDI, smallest particle, no big zeta changes to higher ratios of w_{1696}/w_{rCD}

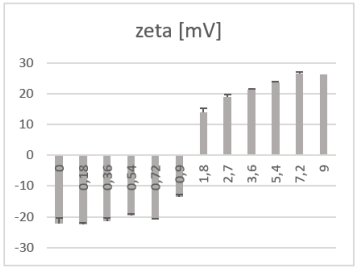

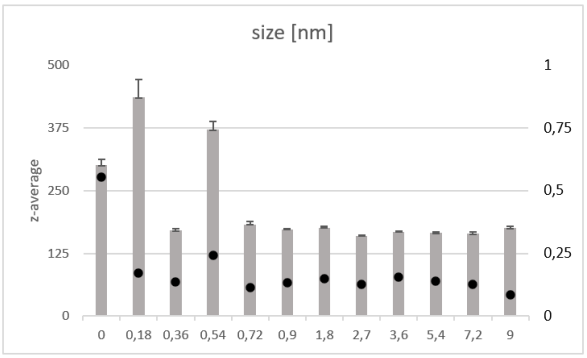

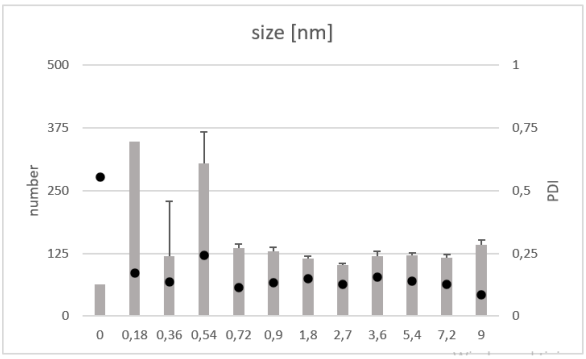

rCD-1696 (w/w) titration: dependency of the right ratio between rCD and OAA exemplary for rCD-1696, with 1000 ng of rCD to a range of different amounts (w/w) of 1696 ranging from 180 ng to 9000 ng in dependency to particle diameter (z-average & number) and polydispersity index (PDI), as well as its zeta potential in mV. DLS measurements using a Zetasizer Nano ZS (mean ± sd; n = 3). For the detailed protocol see **2.2.7**.

6.4.16 Time dependency of incubation for the formulation of rCD-OAA conjugation

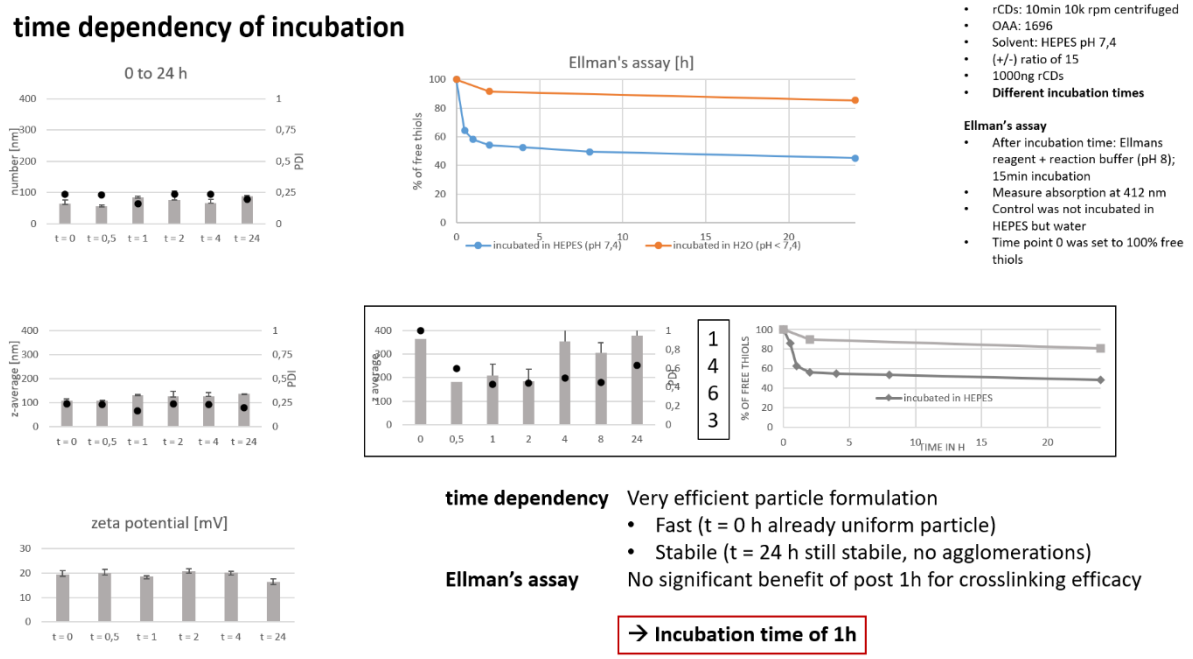

Time dependency of incubation for the formulation of rCD-OAA conjugation shown in the change of particle diameter (z-average & normal) in nm, zeta potential in mV, and polydispersity index (PDI), as well as with Ellman's assay for rCD-1696 and rCD-1463. Particle were formed of a w/w ratio of 2,7 (rCD 1: OAA 2,7). DLS measurements using a Zetasizer Nano ZS (mean ± sd; n = 3). For all particle formulation data see Figure top right and for the detailed protocol see **2.2.7**.

6.4.17 Cellular uptake of rCD-1696-Ligands in U87 cell line

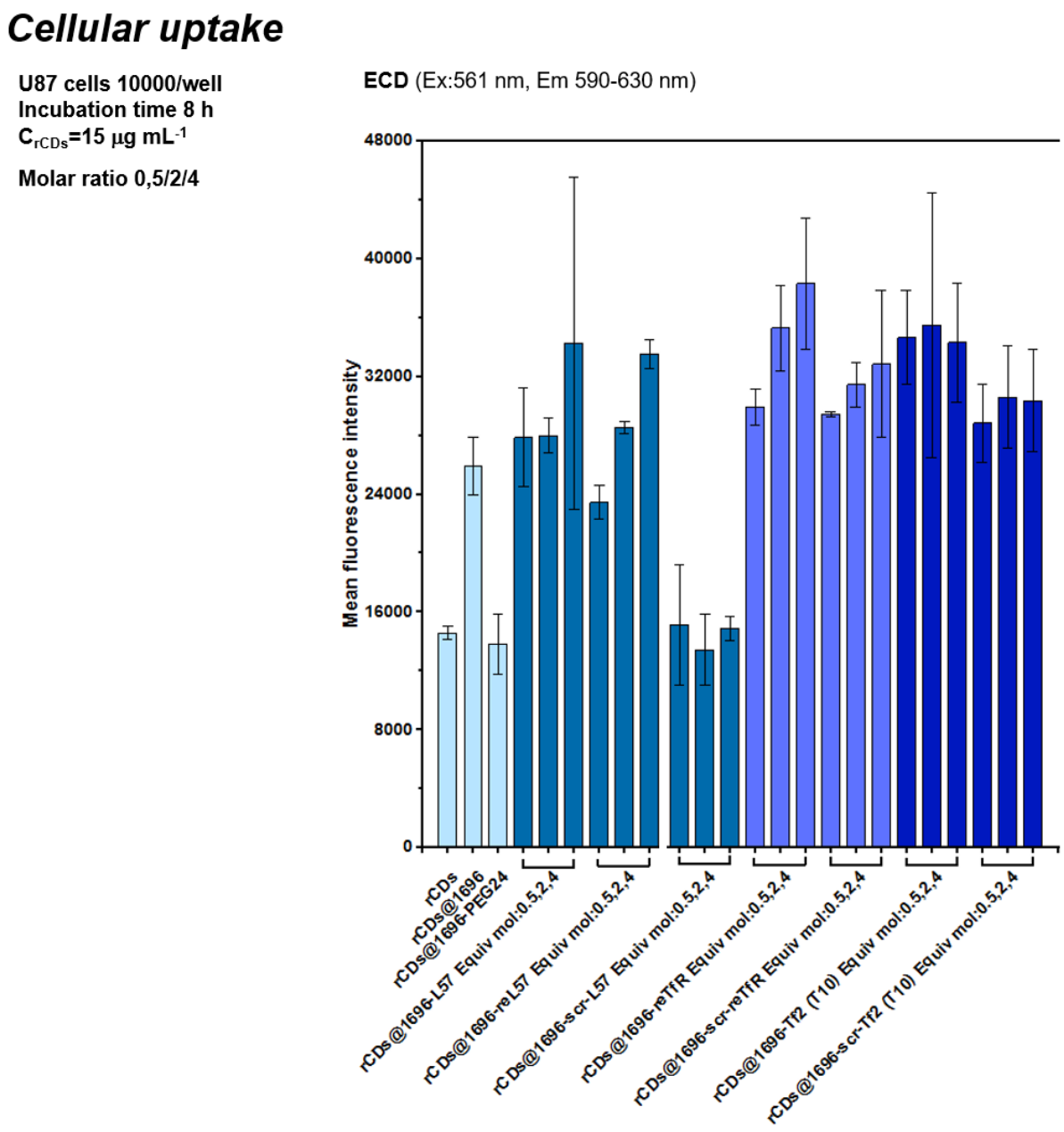

Cellular uptake of rCD-1696 conjugates, surface modified with targeting and shielding agents done by Fengrong Zhang, Pharmaceutical Biology, LMU. The cellular uptake was done with U87 cells with 10000/well, an incubation time of 8 h and a concentration C_{rCDs}=15 µg mL^{-1} (mean ± sd; n = 3). As channels for the mean fluorescence intensity PE (Ex:561 nm, Em 542-626 nm was chosen, since it performed the best, as addressed in **Figure 3.2.4.1**. Different equivalents of 0,5/2/4 were chosen for the ligands mol OAA/ mol shielding & targeting agent).

7 References

[1] J. Fang, H. Nakamura, H. Maeda, *Adv Drug Deliv Rev* **2011**, *63*, 136.
[2] S. K. Golombek, J. N. May, B. Theek, L. Appold, N. Drude, F. Kiessling, T. Lammers, *Adv Drug Deliv Rev* **2018**, *130*, 17.
[3] E. Wagner, *Expert.Opin.Biol Ther* **2007**, *7*, 587.
[4] J. Wu, J. Chen, Y. Feng, H. Tian, X. Chen, *J Gene Med* **2019**, e3088.
[5] B. Haley, E. Frenkel, *Urol Oncol* **2008**, *26*, 57.
[6] N. Kamaly, Z. Xiao, P. M. Valencia, A. F. Radovic-Moreno, O. C. Farokhzad, *Chem Soc Rev* **2012**, *41*, 2971.
[7] C. He, Y. Hu, L. Yin, C. Tang, C. Yin, *Biomaterials* **2010**, *31*, 3657.
[8] F. Zhao, Y. Zhao, Y. Liu, X. Chang, C. Chen, Y. Zhao, *Small* **2011**, *7*, 1322.
[9] J. Hu, Y. Sheng, J. Shi, B. Yu, Z. Yu, G. Liao, *Curr Drug Metab* **2018**, *19*, 723.
[10] R. Duncan, *Nat.Rev.Drug Discov.* **2003**, *2*, 347.
[11] J. Li, F. Yu, Y. Chen, D. Oupicky, *Journal of controlled release : official journal of the Controlled Release Society* **2015**, *219*, 369.
[12] I. Ekladious, Y. L. Colson, M. W. Grinstaff, *Nat Rev Drug Discov* **2019**, *18*, 273.
[13] P. L. Felgner, Y. Barenholz, J. P. Behr, S. H. Cheng, P. Cullis, L. Huang, J. A. Jessee, L. Seymour, F. Szoka, A. R. Thierry, E. Wagner, G. Wu, *Hum Gene Ther* **1997**, *8*, 511.
[14] R. H. Prabhu, V. B. Patravale, M. D. Joshi, *Int J Nanomedicine* **2015**, *10*, 1001.
[15] S. Palazzolo, S. Bayda, M. Hadla, I. Caligiuri, G. Corona, G. Toffoli, F. Rizzolio, *Curr Med Chem* **2018**, *25*, 4224.
[16] A. O. Elzoghby, W. M. Samy, N. A. Elgindy, *Journal of controlled release : official journal of the Controlled Release Society* **2012**, *157*, 168.
[17] K. Y. Choi, H. Chung, K. H. Min, H. Y. Yoon, K. Kim, J. H. Park, I. C. Kwon, S. Y. Jeong, *Biomaterials* **2010**, *31*, 106.
[18] S. A. Agnihotri, N. N. Mallikarjuna, T. M. Aminabhavi, *Journal of controlled release : official journal of the Controlled Release Society* **2004**, *100*, 5.
[19] J. Panyam, V. Labhasetwar, *Adv Drug Deliv Rev* **2003**, *55*, 329.
[20] M. Ogris, S. Brunner, S. Schuller, R. Kircheis, E. Wagner, *Gene Ther* **1999**, *6*, 595.
[21] M. Meyer, C. Dohmen, A. Philipp, D. Kiener, G. Maiwald, C. Scheu, M. Ogris, E. Wagner, *Mol Pharm* **2009**, *6*, 752.
[22] A. Dirisala, K. Osada, Q. Chen, T. A. Tockary, K. Machitani, S. Osawa, X. Liu, T. Ishii, K. Miyata, M. Oba, S. Uchida, K. Itaka, K. Kataoka, *Biomaterials* **2014**, *35*, 5359.
[23] R. N. Johnson, D. S. Chu, J. Shi, J. G. Schellinger, P. M. Carlson, S. H. Pun, *Journal of controlled release : official journal of the Controlled Release Society* **2011**, *155*, 303.
[24] R. Laga, R. Carlisle, M. Tangney, K. Ulbrich, L. W. Seymour, *Journal of controlled release : official journal of the Controlled Release Society* **2012**, *161*, 537.
[25] M. Noga, D. Edinger, W. Rodl, E. Wagner, G. Winter, A. Besheer, *Journal of controlled release : official journal of the Controlled Release Society* **2012**, *159*, 92.
[26] M. Guter, M. Breunig, *European journal of pharmaceutics and biopharmaceutics : official journal of Arbeitsgemeinschaft fur Pharmazeutische Verfahrenstechnik e.V* **2017**, *113*, 34.

[27] F. Manzenrieder, R. Luxenhofer, M. Retzlaff, R. Jordan, M. G. Finn, *Angewandte Chemie (International ed. in English)* **2011**, *50*, 2601.
[28] P. M. Klein, K. Klinker, W. Zhang, S. Kern, E. Kessel, E. Wagner, M. Barz, *Polymers* **2018**, *10*, 689.
[29] P. Chollet, M. C. Favrot, A. Hurbin, J. L. Coll, *J Gene Med* **2002**, *4*, 84.
[30] F. Alexis, E. Pridgen, L. K. Molnar, O. C. Farokhzad, *Mol Pharm* **2008**, *5*, 505.
[31] U. Lächelt, E. Wagner, *Chem Rev* **2015**, *115*, 11043.
[32] W. B. Liechty, D. R. Kryscio, B. V. Slaughter, N. A. Peppas, *Annu Rev Chem Biomol Eng* **2010**, *1*, 149.
[33] L. Zhu, V. P. Torchilin, *Integrative Biology* **2012**, *5*, 96.
[34] K. Muller, P. M. Klein, P. Heissig, A. Roidl, E. Wagner, *Nanotechnology* **2016**, *27*, 464001.
[35] P. M. Klein, S. Kern, D. J. Lee, J. Schmaus, M. Hohn, J. Gorges, U. Kazmaier, E. Wagner, *Biomaterials* **2018**, *178*, 630.
[36] W. Zhang, K. Muller, E. Kessel, S. Reinhard, D. He, P. M. Klein, M. Hohn, W. Rodl, S. Kempter, E. Wagner, *Adv Healthc Mater* **2016**, *5*, 1493.
[37] R. Sinha, G. J. Kim, S. Nie, D. M. Shin, *Mol Cancer Ther* **2006**, *5*, 1909.
[38] J. M. Chan, P. M. Valencia, L. Zhang, R. Langer, O. C. Farokhzad, *Methods Mol Biol* **2010**, *624*, 163.
[39] M. E. Davis, Z. Chen, D. M. Shin, *Nature Reviews Drug Discovery* **2008**, *7*, 771.
[40] L. Brannon-Peppas, J. O. Blanchette, *Adv Drug Deliv Rev* **2004**, *56*, 1649.
[41] C. Vauthier, K. Bouchemal, *Pharm Res* **2009**, *26*, 1025.
[42] R. A. Jain, *Biomaterials* **2000**, *21*, 2475.
[43] A. Drogoz, L. David, C. Rochas, A. Domard, T. Delair, *Langmuir* **2007**, *23*, 10950.
[44] A. Fernandez-Fernandez, R. Manchanda, A. J. McGoron, *Appl Biochem Biotechnol* **2011**, *165*, 1628.
[45] S. Wilhelm, A. J. Tavares, Q. Dai, S. Ohta, J. Audet, H. F. Dvorak, W. C. W. Chan, *Nature Reviews Materials* **2016**, *1*, 16014.
[46] P. Zhang, E. Wagner, *Top Curr Chem (Cham)* **2017**, *375*, 26.
[47] C. Plank, K. Mechtler, F. C. Szoka, Jr., E. Wagner, *Hum Gene Ther* **1996**, *7*, 1437.
[48] S. Xiaoli, Z. Na, *Mini-Reviews in Medicinal Chemistry* **2010**, *10*, 108.
[49] L. Jin, X. Zeng, M. Liu, Y. Deng, N. He, *Theranostics* **2014**, *4*, 240.
[50] T. Nomoto, Y. Matsumoto, K. Miyata, M. Oba, S. Fukushima, N. Nishiyama, T. Yamasoba, K. Kataoka, *Journal of Controlled Release* **2011**, *151*, 104.
[51] S. D. Li, L. Huang, *Gene Therapy* **2006**, *13*, 1313.
[52] T. Blessing, M. Kursa, R. Holzhauser, R. Kircheis, E. Wagner, *Bioconjug Chem* **2001**, *12*, 529.
[53] M. Ogris, G. Walker, T. Blessing, R. Kircheis, M. Wolschek, E. Wagner, *Journal of controlled release : official journal of the Controlled Release Society* **2003**, *91*, 173.
[54] I. Keiji, K. Kazunori, *Current Gene Therapy* **2011**, *11*, 457.
[55] X. Nie, Z. Zhang, C.-H. Wang, Y.-S. Fan, Q.-Y. Meng, Y.-Z. You, *Bioconjugate Chemistry* **2019**, *30*, 284.
[56] V. A. Bloomfield, *Biopolymers* **1991**, *31*, 1471.
[57] E. Wagner, M. Cotten, R. Foisner, M. L. Birnstiel, *Proc Natl Acad Sci U S A* **1991**, *88*, 4255.
[58] S. Reinhard, E. Wagner, *Macromol Biosci* **2017**, *17*.
[59] S. Brunner, T. Sauer, S. Carotta, M. Cotten, M. Saltik, E. Wagner, *Gene Ther* **2000**, *7*, 401.

[60] A. K. Levacic, S. Morys, S. Kempter, U. Lachelt, E. Wagner, *Hum Gene Ther* **2017**, *28*, 862.
[61] S. Boeckle, J. Fahrmeir, W. Roedl, M. Ogris, E. Wagner, *Journal of controlled release : official journal of the Controlled Release Society* **2006**, *112*, 240.
[62] J. Kloeckner, S. Boeckle, D. Persson, W. Roedl, M. Ogris, K. Berg, E. Wagner, *Journal of controlled release : official journal of the Controlled Release Society* **2006**, *116*, 115.
[63] G. F. Walker, C. Fella, J. Pelisek, J. Fahrmeir, S. Boeckle, M. Ogris, E. Wagner, *Mol Ther* **2005**, *11*, 418.
[64] J.-P. Behr, *CHIMIA International Journal for Chemistry* **1997**, *51*, 34.
[65] U. Lachelt, P. Kos, F. M. Mickler, A. Herrmann, E. E. Salcher, W. Rodl, N. Badgujar, C. Brauchle, E. Wagner, *Nanomedicine* **2014**, *10*, 35.
[66] R. J. Christie, K. Kataoka, N. Nishiyama, *Endocrinology* **2010**, *151*, 466.
[67] A. Dirisala, K. Osada, Q. Chen, T. A. Tockary, K. Machitani, S. Osawa, X. Liu, T. Ishii, K. Miyata, M. Oba, S. Uchida, K. Itaka, K. Kataoka, *Biomaterials* **2014**, *35*, 5359.
[68] T. A. Tockary, K. Osada, Q. Chen, K. Machitani, A. Dirisala, S. Uchida, T. Nomoto, K. Toh, Y. Matsumoto, K. Itaka, K. Nitta, K. Nagayama, K. Kataoka, *Macromolecules* **2013**, *46*, 6585.
[69] Q. Chen, K. Osada, M. Pennisi, S. Uchida, T. A. Tockary, A. Dirisala, Y. Li, K. M. Takeda, S. Oniyanagi, K. Itaka, K. Kataoka, *Soft Matter* **2015**, *11*, 2718.
[70] K. Osada, T. Shiotani, T. A. Tockary, D. Kobayashi, H. Oshima, S. Ikeda, R. J. Christie, K. Itaka, K. Kataoka, *Biomaterials* **2012**, *33*, 325.
[71] M. A. Mintzer, E. E. Simanek, *Chemical Reviews* **2009**, *109*, 259.
[72] J. Nicolas, S. Mura, D. Brambilla, N. Mackiewicz, P. Couvreur, *Chemical Society Reviews* **2013**, *42*, 1147.
[73] D. D. Dunlap, A. Maggi, M. R. Soria, L. Monaco, *Nucleic Acids Res* **1997**, *25*, 3095.
[74] M. X. Tang, F. C. Szoka, *Gene Ther* **1997**, *4*, 823.
[75] G. Liu, M. Molas, G. A. Grossmann, M. Pasumarthy, J. C. Perales, M. J. Cooper, R. W. Hanson, *J Biol Chem* **2001**, *276*, 34379.
[76] W. T. Godbey, K. K. Wu, A. G. Mikos, *Proc Natl Acad Sci U S A* **1999**, *96*, 5177.
[77] E. Wagner, C. Plank, K. Zatloukal, M. Cotten, M. L. Birnstiel, *Proc.Natl.Acad.Sci.U.S.A* **1992**, *89*, 7934.
[78] M. Cotten, M. Saltik, M. Kursa, E. Wagner, G. Maass, M. L. Birnstiel, *Virology* **1994**, *205*, 254.
[79] E. Wagner, *Journal of controlled release : official journal of the Controlled Release Society* **1998**, *53*, 155.
[80] M. Meyer, A. Philipp, R. Oskuee, C. Schmidt, E. Wagner, *J Am Chem Soc* **2008**, *130*, 3272.
[81] A. Hall, U. Lachelt, J. Bartek, E. Wagner, S. M. Moghimi, *Mol Ther* **2017**, *25*, 1476.
[82] J. Kloeckner, S. Bruzzano, M. Ogris, E. Wagner, *Bioconjug Chem* **2006**, *17*, 1339.
[83] V. Knorr, V. Russ, L. Allmendinger, M. Ogris, E. Wagner, *Bioconjug Chem* **2008**, *19*, 1625.
[84] V. Russ, H. Elfberg, C. Thoma, J. Kloeckner, M. Ogris, E. Wagner, *Gene Ther* **2008**, *15*, 18.
[85] G. Abourbeh, A. Shir, E. Mishani, M. Ogris, W. Rodl, E. Wagner, A. Levitzki, *IUBMB Life* **2012**, *64*, 324.

[86] Y. Nie, D. Schaffert, W. Rodl, M. Ogris, E. Wagner, M. Gunther, *Journal of controlled release : official journal of the Controlled Release Society* **2011**, *152*, 127.
[87] J. Wang, Y. Lei, C. Xie, W. Lu, E. Wagner, Z. Xie, J. Gao, X. Zhang, Z. Yan, M. Liu, *Bioconjug Chem* **2014**, *25*, 414.
[88] A. F. Jorge, R. Roder, P. Kos, R. S. Dias, E. Wagner, A. A. Pais, *Biochim Biophys Acta* **2015**, *1850*, 1325.
[89] M. Noga, D. Edinger, E. Wagner, G. Winter, A. Besheer, *J Biomater Sci Polym Ed* **2014**, *25*, 855.
[90] W. Rodl, A. Taschauer, D. Schaffert, E. Wagner, M. Ogris, *Methods Mol Biol* **2019**, *1943*, 83.
[91] R. Haase, T. Magnusson, B. Su, F. Kopp, E. Wagner, H. Lipps, A. Baiker, M. Ogris, *BMC Biotechnol* **2013**, *13*, 49.
[92] M. Ogris, E. Wagner, *Cold Spring Harb Protoc* **2012**, *2012*, 246.
[93] O. M. Merkel, R. Urbanics, P. Bedocs, Z. Rozsnyay, L. Rosivall, M. Toth, T. Kissel, J. Szebeni, *Biomaterials* **2011**, *32*, 4936.
[94] D. He, E. Wagner, *Macromolecular Bioscience* **2015**, *15*, 600.
[95] T. Lehto, E. Wagner, *Nanomedicine* **2014**, *9*, 2843.
[96] L. Hartmann, E. Krause, M. Antonietti, H. G. Borner, *Biomacromolecules.* **2006**, *7*, 1239.
[97] I. Martin, C. Dohmen, C. Mas-Moruno, C. Troiber, P. Kos, D. Schaffert, U. Lachelt, M. Teixido, M. Gunther, H. Kessler, E. Giralt, E. Wagner, *Org Biomol Chem* **2012**, *10*, 3258.
[98] T. Frohlich, D. Edinger, R. Klager, C. Troiber, E. Salcher, N. Badgujar, I. Martin, D. Schaffert, A. Cengizeroglu, P. Hadwiger, H. P. Vornlocher, E. Wagner, *J Control Release* **2012**, *160*, 532.
[99] C. Dohmen, D. Edinger, T. Frohlich, L. Schreiner, U. Lachelt, C. Troiber, J. Radler, P. Hadwiger, H. P. Vornlocher, E. Wagner, *ACS Nano* **2012**, *6*, 5198.
[100] D. Schaffert, C. Troiber, E. E. Salcher, T. Fröhlich, I. Martin, N. Badgujar, C. Dohmen, D. Edinger, R. Kläger, G. Maiwald, K. Farkasova, S. Seeber, K. Jahn-Hofmann, P. Hadwiger, E. Wagner, *Angewandte Chemie International Edition* **2011**, *50*, 8986.
[101] E. E. Salcher, P. Kos, T. Fröhlich, N. Badgujar, M. Scheible, E. Wagner, *Journal of Controlled Release* **2012**, *164*, 380.
[102] D. Schaffert, N. Badgujar, E. Wagner, *Organic letters* **2011**, *13*, 1586.
[103] B. Oller-Salvia, M. Sánchez-Navarro, E. Giralt, M. Teixidó, *Chemical Society Reviews* **2016**, *45*, 4690.
[104] N. J. Abbott, *J Inherit Metab Dis* **2013**, *36*, 437.
[105] W. M. Pardridge, *Drug Discov Today* **2007**, *12*, 54.
[106] Y. Omidi, J. Barar, *Bioimpacts* **2012**, *2*, 5.
[107] E. Belykh, K. V. Shaffer, C. Lin, V. A. Byvaltsev, M. C. Preul, L. Chen, *Front Oncol* **2020**, *10*, 739.
[108] O. L. Chinot, W. Wick, W. Mason, R. Henriksson, F. Saran, R. Nishikawa, A. F. Carpentier, K. Hoang-Xuan, P. Kavan, D. Cernea, A. A. Brandes, M. Hilton, L. Abrey, T. Cloughesy, *N Engl J Med* **2014**, *370*, 709.
[109] M. Demeule, J.-C. Currie, Y. Bertrand, C. Ché, T. Nguyen, A. Régina, R. Gabathuler, J.-P. Castaigne, R. Béliveau, *Journal of Neurochemistry* **2008**, *106*, 1534.
[110] A. P. Lillis, L. B. Van Duyn, J. E. Murphy-Ullrich, D. K. Strickland, *Physiol Rev* **2008**, *88*, 887.

[111] W. Ke, K. Shao, R. Huang, L. Han, Y. Liu, J. Li, Y. Kuang, L. Ye, J. Lou, C. Jiang, *Biomaterials* **2009**, *30*, 6976.
[112] J. Drappatz, A. Brenner, E. T. Wong, A. Eichler, D. Schiff, M. D. Groves, T. Mikkelsen, S. Rosenfeld, J. Sarantopoulos, C. A. Meyers, R. M. Fielding, K. Elian, X. Wang, B. Lawrence, M. Shing, S. Kelsey, J. P. Castaigne, P. Y. Wen, *Clin Cancer Res* **2013**, *19*, 1567.
[113] C. Ché, G. Yang, C. Thiot, M.-C. Lacoste, J.-C. Currie, M. Demeule, A. Régina, R. Béliveau, J.-P. Castaigne, *Journal of Medicinal Chemistry* **2010**, *53*, 2814.
[114] Y. Zhu, E. Nadia, Y. Yao, Z. Shi, G. Ren, *Journal of Bioscience and Bioengineering* **2018**, *126*, 1.
[115] H. Xin, X. Sha, X. Jiang, W. Zhang, L. Chen, X. Fang, *Biomaterials* **2012**, *33*, 8167.
[116] A. Régina, M. Demeule, C. Ché, I. Lavallée, J. Poirier, R. Gabathuler, R. Béliveau, J.-P. Castaigne, *British Journal of Pharmacology* **2008**, *155*, 185.
[117] M. Demeule, N. Beaudet, A. Régina, É. Besserer-Offroy, A. Murza, P. Tétreault, K. Belleville, C. Ché, A. Larocque, C. Thiot, R. Béliveau, J. M. Longpré, É. Marsault, R. Leduc, J. E. Lachowicz, S. L. Gonias, J. P. Castaigne, P. Sarret, *J Clin Invest* **2014**, *124*, 1199.
[118] Y. Zou, X. Sun, Y. Wang, C. Yan, Y. Liu, J. Li, D. Zhang, M. Zheng, R. S. Chung, B. Shi, *Advanced Materials* **2020**, *32*, 2000416.
[119] Z.-Z. Yang, J.-Q. Li, Z.-Z. Wang, D.-W. Dong, X.-R. Qi, *Biomaterials* **2014**, *35*, 5226.
[120] X. Sun, Z. Pang, H. Ye, B. Qiu, L. Guo, J. Li, J. Ren, Y. Qian, Q. Zhang, J. Chen, X. Jiang, *Biomaterials* **2012**, *33*, 916.
[121] D. W. Hwang, S. Son, J. Jang, H. Youn, S. Lee, D. Lee, Y.-S. Lee, J. M. Jeong, W. J. Kim, D. S. Lee, *Biomaterials* **2011**, *32*, 4968.
[122] S. Huang, J. Li, L. Han, S. Liu, H. Ma, R. Huang, C. Jiang, *Biomaterials* **2011**, *32*, 6832.
[123] S. An, D. He, E. Wagner, C. Jiang, *Small* **2015**, *11*, 5142.
[124] A. Srimanee, M. Arvanitidou, K. Kim, M. Hällbrink, Ü. Langel, *Peptides* **2018**, *104*, 62.
[125] K. Sakamoto, T. Shinohara, Y. Adachi, T. Asami, T. Ohtaki, *Biochemistry and Biophysics Reports* **2017**, *12*, 135.
[126] J. P. Rodrigues, N. Prajapati, M. A. DeCoster, S. Poh, T. A. Murray, *Journal of Pharmaceutical Sciences* **2021**, *110*, 824.
[127] A. K. Iyer, G. Khaled, J. Fang, H. Maeda, *Drug Discov Today* **2006**, *11*, 812.
[128] F. Danhier, *Journal of controlled release : official journal of the Controlled Release Society* **2016**, *244*, 108.
[129] Y. Matsumura, H. Maeda, *Cancer Res* **1986**, *46*, 6387.
[130] S. Hua, M. B. C. de Matos, J. M. Metselaar, G. Storm, *Front Pharmacol* **2018**, *9*, 790.
[131] Y. H. Bae, K. Park, *Journal of controlled release : official journal of the Controlled Release Society* **2011**, *153*, 198.
[132] J. E. Schnitzer, *American Journal of Physiology-Heart and Circulatory Physiology* **1992**, *262*, H246.
[133] C. Pichon, L. Billiet, P. Midoux, *Current Opinion in Biotechnology* **2010**, *21*, 640.
[134] K. von Gersdorff, N. N. Sanders, R. Vandenbroucke, S. C. De Smedt, E. Wagner, M. Ogris, *Molecular Therapy* **2006**, *14*, 745.
[135] H. Maeda, T. Sawa, T. Konno, *Journal of Controlled Release* **2001**, *74*, 47.
[136] J. Yoo, C. Park, G. Yi, D. Lee, H. Koo, *Cancers (Basel)* **2019**, *11*.

[137] X. Liu, P. Lin, I. Perrett, J. Lin, Y.-P. Liao, C. H. Chang, J. Jiang, N. Wu, T. Donahue, Z. Wainberg, A. E. Nel, H. Meng, *The Journal of Clinical Investigation* **2017**, *127*, 2007.
[138] V. C. Vetter, E. Wagner, *Journal of controlled release : official journal of the Controlled Release Society* **2022**, *346*, 110.
[139] R. Sutherland, D. Delia, C. Schneider, R. Newman, J. Kemshead, M. Greaves, *Proc Natl Acad Sci U S A* **1981**, *78*, 4515.
[140] J. E. Shindelman, A. E. Ortmeyer, H. H. Sussman, *Int J Cancer* **1981**, *27*, 329.
[141] A. N. Luck, A. B. Mason, *Curr Top Membr* **2012**, *69*, 3.
[142] T. R. Daniels, E. Bernabeu, J. A. Rodriguez, S. Patel, M. Kozman, D. A. Chiappetta, E. Holler, J. Y. Ljubimova, G. Helguera, M. L. Penichet, *Biochim Biophys Acta* **2012**, *1820*, 291.
[143] E. Wagner, M. Zenke, M. Cotten, H. Beug, M. L. Birnstiel, *Proc Natl Acad Sci U S A* **1990**, *87*, 3410.
[144] R. Kircheis, L. Wightman, A. Schreiber, B. Robitza, V. Rossler, M. Kursa, E. Wagner, *Gene Ther* **2001**, *8*, 28.
[145] M. Kursa, G. F. Walker, V. Roessler, M. Ogris, W. Roedl, R. Kircheis, E. Wagner, *Bioconjug Chem* **2003**, *14*, 222.
[146] S. Hu-Lieskovan, J. D. Heidel, D. W. Bartlett, M. E. Davis, T. J. Triche, *Cancer Res* **2005**, *65*, 8984.
[147] R. Q. Huang, Y. H. Qu, W. L. Ke, J. H. Zhu, Y. Y. Pei, C. Jiang, *Faseb j* **2007**, *21*, 1117.
[148] J. D. Heidel, Z. Yu, J. Y. Liu, S. M. Rele, Y. Liang, R. K. Zeidan, D. J. Kornbrust, M. E. Davis, *Proc Natl Acad Sci U S A* **2007**, *104*, 5715.
[149] N. Tietze, J. Pelisek, A. Philipp, W. Roedl, T. Merdan, P. Tarcha, M. Ogris, E. Wagner, *Oligonucleotides* **2008**, *18*, 161.
[150] W. Zhang, W. Rödl, D. He, M. Döblinger, U. Lächelt, E. Wagner, *The Journal of Gene Medicine* **2015**, *17*, 161.
[151] L. Xu, W. H. Tang, C. C. Huang, W. Alexander, L. M. Xiang, K. F. Pirollo, A. Rait, E. H. Chang, *Mol Med* **2001**, *7*, 723.
[152] M. Weaver, D. W. Laske, *J Neurooncol* **2003**, *65*, 3.
[153] Y. Miyajima, H. Nakamura, Y. Kuwata, J.-D. Lee, S. Masunaga, K. Ono, K. Maruyama, *Bioconjugate Chemistry* **2006**, *17*, 1314.
[154] N. Sakaguchi, C. Kojima, A. Harada, K. Koiwai, N. Emi, K. Kono, *Bioconjugate Chemistry* **2008**, *19*, 1588.
[155] K. Sasaki, K. Kogure, S. Chaki, Y. Nakamura, R. Moriguchi, H. Hamada, R. Danev, K. Nagayama, S. Futaki, H. Harashima, *Anal Bioanal Chem* **2008**, *391*, 2717.
[156] R. Suzuki, T. Takizawa, Y. Kuwata, M. Mutoh, N. Ishiguro, N. Utoguchi, A. Shinohara, M. Eriguchi, H. Yanagie, K. Maruyama, *Int J Pharm* **2008**, *346*, 143.
[157] J. Tang, Q. Wang, Q. Yu, Y. Qiu, L. Mei, D. Wan, X. Wang, M. Li, Q. He, *Acta Biomater* **2019**, *83*, 379.
[158] G. Stingl, E.-B. Bröcker, R. Mertelsmann, K. Wolff, S. Schreiber, E. Kämpgen, A. Schneeberger, W. Dummer, U. Brennscheid, H. Veelken, M. L. Bimstiel, K. Zatloukal, W. Schmidt, G. Maass, E. Wagner, M. Buschle, M. Giese, E.-R. Kempe, H. A. Weber, T. Voigt, "Phase I Study to the Immunotherapy of Metastatic Malignant Melanoma by a Cancer Vaccine Consisting of Autologous Cancer Cells Transfected with the Human IL-2 Gene. University of Vienna, Austria", Mary Ann Liebert Inc, 1996, p. 7/551.
[159] S. Schreiber, E. Kampgen, E. Wagner, D. Pirkhammer, J. Trcka, H. Korschan, A. Lindemann, R. Dorffner, H. Kittler, F. Kasteliz, Z. Kupcu, A. Sinski, K. Zatloukal, M.

Buschle, W. Schmidt, M. Birnstiel, R. E. Kempe, T. Voigt, H. A. Weber, H. Pehamberger, R. Mertelsmann, E. B. Brocker, K. Wolff, G. Stingl, *Hum Gene Ther* **1999**, *10*, 983.
[160] M. E. Davis, J. E. Zuckerman, C. H. Choi, D. Seligson, A. Tolcher, C. A. Alabi, Y. Yen, J. D. Heidel, A. Ribas, *Nature* **2010**, *464* 1067.
[161] M. E. Davis, *Molecular Pharmaceutics* **2009**, *6*, 659.
[162] J. H. Lee, J. A. Engler, J. F. Collawn, B. A. Moore, *Eur J Biochem* **2001**, *268*, 2004.
[163] R. Prades, B. Oller-Salvia, S. M. Schwarzmaier, J. Selva, M. Moros, M. Balbi, V. Grazu, J. M. de La Fuente, G. Egea, N. Plesnila, M. Teixido, E. Giralt, *Angew Chem Int Ed Engl* **2015**, *54*, 3967.
[164] S. Berger, A. Krhač Levačić, E. Hörterer, U. Wilk, T. Benli-Hoppe, Y. Wang, Ö. Öztürk, J. Luo, E. Wagner, *Biomacromolecules* **2021**, *22*, 1282.
[165] J. Luo, J. Schmaus, M. Cui, E. Hörterer, U. Wilk, M. Höhn, M. Däther, S. Berger, T. Benli-Hoppe, L. Peng, E. Wagner, *Journal of controlled release : official journal of the Controlled Release Society* **2021**, *329*, 919.
[166] M. Santi, G. Maccari, P. Mereghetti, V. Voliani, S. Rocchiccioli, N. Ucciferri, S. Luin, G. Signore, *Bioconjugate Chemistry* **2017**, *28*, 471.
[167] T. Huo, W. Li, D. Liang, R. Huang, *Pharmaceutics* **2022**, *14*.
[168] W. Arap, R. Pasqualini, E. Ruoslahti, *Science* **1998**, *279*, 377.
[169] H. M. Ellerby, W. Arap, L. M. Ellerby, R. Kain, R. Andrusiak, G. D. Rio, S. Krajewski, C. R. Lombardo, R. Rao, E. Ruoslahti, D. E. Bredesen, R. Pasqualini, *Nat Med* **1999**, *5*, 1032.
[170] E. A. Murphy, B. K. Majeti, L. A. Barnes, M. Makale, S. M. Weis, K. Lutu-Fuga, W. Wrasidlo, D. A. Cheresh, *Proc Natl Acad Sci U S A* **2008**, *105*, 9343.
[171] Y. Sakurai, H. Hatakeyama, Y. Sato, M. Hyodo, H. Akita, N. Ohga, K. Hida, H. Harashima, *Journal of controlled release : official journal of the Controlled Release Society* **2014**, *173*, 110.
[172] Y. Sakurai, T. Hada, A. Kato, Y. Hagino, W. Mizumura, H. Harashima, *Mol Ther Oncolytics* **2018**, *11*, 102.
[173] E. Khabazian, F. Vakhshiteh, P. Norouzi, Y. Fatahi, R. Dinarvand, F. Atyabi, *J Drug Target* **2022**, *30*, 522.
[174] M. Oba, S. Fukushima, N. Kanayama, K. Aoyagi, N. Nishiyama, H. Koyama, K. Kataoka, *Bioconjugate Chemistry* **2007**, *18*, 1415.
[175] M. Oba, K. Aoyagi, K. Miyata, Y. Matsumoto, K. Itaka, N. Nishiyama, Y. Yamasaki, H. Koyama, K. Kataoka, *Molecular Pharmaceutics* **2008**, *5*, 1080.
[176] T. Lammers, F. Kiessling, M. Ashford, W. Hennink, D. Crommelin, G. Storm, *Nat Rev Mater* **2016**, *1*.
[177] F. Yuan, M. Dellian, D. Fukumura, M. Leunig, D. A. Berk, V. P. Torchilin, R. K. Jain, *Cancer Res* **1995**, *55*, 3752.
[178] T. Ojha, V. Pathak, Y. Shi, W. E. Hennink, C. T. W. Moonen, G. Storm, F. Kiessling, T. Lammers, *Adv Drug Deliv Rev* **2017**, *119*, 44.
[179] B. C. Ahn, *Theranostics* **2012**, *2*, 392.
[180] K. Klutz, D. Schaffert, M. J. Willhauck, G. K. Grünwald, R. Haase, N. Wunderlich, C. Zach, F. J. Gildehaus, R. Senekowitsch-Schmidtke, B. Göke, E. Wagner, M. Ogris, C. Spitzweg, *Molecular Therapy* **2011**, *19*, 676.
[181] S. Urnauer, S. Morys, A. Krhac Levacic, A. M. Muller, C. Schug, K. A. Schmohl, N. Schwenk, C. Zach, J. Carlsen, P. Bartenstein, E. Wagner, C. Spitzweg, *Mol Ther* **2016**, *24*, 1395.

[182] K. A. Schmohl, A. Gupta, G. K. Grunwald, M. Trajkovic-Arsic, K. Klutz, R. Braren, M. Schwaiger, P. J. Nelson, M. Ogris, E. Wagner, J. T. Siveke, C. Spitzweg, *Oncotarget* **2017**, *8*, 33393.
[183] S. Urnauer, K. Klutz, G. K. Grunwald, S. Morys, N. Schwenk, C. Zach, F. J. Gildehaus, W. Rodl, M. Ogris, E. Wagner, C. Spitzweg, *J Gene Med* **2017**, *19*.
[184] P. Mi, F. Wang, N. Nishiyama, H. Cabral, *Macromol Biosci* **2017**, *17*.
[185] A. G. Arranja, V. Pathak, T. Lammers, Y. Shi, *Pharmacol Res* **2017**, *115*, 87.
[186] J. R. Upponi, K. Jerajani, D. K. Nagesha, P. Kulkarni, S. Sridhar, C. Ferris, V. P. Torchilin, *Biomaterials* **2018**, *170*, 26.
[187] K. Li, H. Nejadnik, H. E. Daldrup-Link, *Drug Discov Today* **2017**, *22*, 1421.
[188] J. Chen, S. Ratnayaka, A. Alford, V. Kozlovskaya, F. Liu, B. Xue, K. Hoyt, E. Kharlampieva, *ACS Nano* **2017**, *11*, 3135.
[189] X. Yue, Q. Zhang, Z. Dai, *Adv Drug Deliv Rev* **2017**, *115*, 155.
[190] A. Zintchenko, A. S. Susha, M. Concia, J. Feldmann, E. Wagner, A. L. Rogach, M. Ogris, *Mol Ther* **2009**, *17*, 1849.
[191] S. Wang, C. Li, M. Qian, H. Jiang, W. Shi, J. Chen, U. Lächelt, E. Wagner, W. Lu, Y. Wang, R. Huang, *Biomaterials* **2017**, *141*, 29.
[192] Y. Wang, K. Wang, R. Zhang, X. Liu, X. Yan, J. Wang, E. Wagner, R. Huang, *ACS Nano* **2014**, *8*, 7870.
[193] Y. Yan, J. Gong, J. Chen, Z. Zeng, W. Huang, K. Pu, J. Liu, P. Chen, *Advanced Materials* **2019**, *31*, 1808283.
[194] J. Liu, Y. Geng, D. Li, H. Yao, Z. Huo, Y. Li, K. Zhang, S. Zhu, H. Wei, W. Xu, J. Jiang, B. Yang, *Advanced Materials* **2020**, *32*, 1906641.
[195] K. Jiang, Y. Wang, X. Gao, C. Cai, H. Lin, *Angewandte Chemie International Edition* **2018**, *57*, 6216.
[196] C. Hu, M. Li, J. Qiu, Y.-P. Sun, *Chemical Society Reviews* **2019**, *48*, 2315.
[197] M. L. Liu, B. B. Chen, C. M. Li, C. Z. Huang, *Green Chemistry* **2019**, *21*, 449.
[198] S. Zhu, Y. Song, X. Zhao, J. Shao, J. Zhang, B. Yang, *Nano Research* **2015**, *8*, 355.
[199] V. C. Hoang, K. Dave, V. G. Gomes, *Nano Energy* **2019**, *66*, 104093.
[200] Z. Zhang, G. Yi, P. Li, X. Zhang, H. Fan, Y. Zhang, X. Wang, C. Zhang, *Nanoscale* **2020**, *12*, 13899.
[201] F. Yuan, Y.-K. Wang, G. Sharma, Y. Dong, X. Zheng, P. Li, A. Johnston, G. Bappi, J. Z. Fan, H. Kung, B. Chen, M. I. Saidaminov, K. Singh, O. Voznyy, O. M. Bakr, Z.-H. Lu, E. H. Sargent, *Nature Photonics* **2020**, *14*, 171.
[202] X. Xu, R. Ray, Y. Gu, H. J. Ploehn, L. Gearheart, K. Raker, W. A. Scrivens, *Journal of the American Chemical Society* **2004**, *126*, 12736.
[203] S. Tao, S. Lu, Y. Geng, S. Zhu, S. A. T. Redfern, Y. Song, T. Feng, W. Xu, B. Yang, *Angewandte Chemie International Edition* **2018**, *57*, 2393.
[204] W. Li, W. Zhou, Z. Zhou, H. Zhang, X. Zhang, J. Zhuang, Y. Liu, B. Lei, C. Hu, *Angewandte Chemie International Edition* **2019**, *58*, 7278.
[205] M. Park, H. S. Kim, H. Yoon, J. Kim, S. Lee, S. Yoo, S. Jeon, *Advanced Materials* **2020**, *32*, 2000936.
[206] S. Lu, L. Sui, J. Liu, S. Zhu, A. Chen, M. Jin, B. Yang, *Advanced Materials* **2017**, *29*, 1603443.
[207] D. Li, P. Jing, L. Sun, Y. An, X. Shan, X. Lu, D. Zhou, D. Han, D. Shen, Y. Zhai, S. Qu, R. Zbořil, A. L. Rogach, *Advanced Materials* **2018**, *30*, 1705913.
[208] H. Ding, S.-B. Yu, J.-S. Wei, H.-M. Xiong, *ACS Nano* **2016**, *10*, 484.
[209] X. Miao, D. Qu, D. Yang, B. Nie, Y. Zhao, H. Fan, Z. Sun, *Advanced Materials* **2018**, *30*, 1704740.

[210] J. Liu, R. Li, B. Yang, *ACS Central Science* **2020**, *6*, 2179.
[211] S. Zhu, Q. Meng, L. Wang, J. Zhang, Y. Song, H. Jin, K. Zhang, H. Sun, H. Wang, B. Yang, *Angewandte Chemie International Edition* **2013**, *52*, 3953.
[212] S. Sun, L. Zhang, K. Jiang, A. Wu, H. Lin, *Chemistry of Materials* **2016**, *28*, 8659.
[213] J. Liu, S. Lu, Q. Tang, K. Zhang, W. Yu, H. Sun, B. Yang, *Nanoscale* **2017**, *9*, 7135.
[214] D. Bouzas-Ramos, J. Cigales Canga, J. C. Mayo, R. M. Sainz, J. Ruiz Encinar, J. M. Costa-Fernandez, *Advanced Functional Materials* **2019**, *29*, 1903884.
[215] Y. Liu, J. Liu, J. Zhang, X. Li, F. Lin, N. Zhou, B. Yang, L. Lu, *Biomaterials Science* **2019**, *7*, 1574.
[216] J. Liu, D. Li, K. Zhang, M. Yang, H. Sun, B. Yang, *Small* **2018**, *14*, 1703919.
[217] X. Zhao, Q. Tang, S. Zhu, W. Bu, M. Yang, X. Liu, Y. Meng, W. Yu, H. Sun, B. Yang, *Nanoscale* **2019**, *11*, 9526.
[218] Y. Song, H. Li, F. Lu, H. Wang, M. Zhang, J. Yang, J. Huang, H. Huang, Y. Liu, Z. Kang, *Journal of Materials Chemistry B* **2017**, *5*, 6008.
[219] F. Lu, Y. Song, H. Huang, Y. Liu, Y. Fu, J. Huang, H. Li, H. Qu, Z. Kang, *Carbon* **2017**, *120*, 95.
[220] F. Lin, C. Li, L. Dong, D. Fu, Z. Chen, *Nanoscale* **2017**, *9*, 9056.
[221] J. Yang, G. Gao, X. Zhang, Y.-H. Ma, X. Chen, F.-G. Wu, *Carbon* **2019**, *146*, 827.
[222] H. Li, J. Huang, Y. Song, M. Zhang, H. Wang, F. Lu, H. Huang, Y. Liu, X. Dai, Z. Gu, Z. Yang, R. Zhou, Z. Kang, *ACS Applied Materials & Interfaces* **2018**, *10*, 26936.
[223] S. Wang, Y. Zhang, P. Zhuo, Q. Hu, Z. Chen, L. Zhou, *Journal of Materials Chemistry B* **2020**, *8*, 5877.
[224] W. Li, H. Zhang, Y. Zheng, S. Chen, Y. Liu, J. Zhuang, W.-R. Liu, B. Lei, *Nanoscale* **2017**, *9*, 12976.
[225] Z. Ji, D. M. Arvapalli, W. Zhang, Z. Yin, J. Wei, *Journal of Materials Science* **2020**, *55*, 6093.
[226] X. Geng, Y. Sun, Z. Li, R. Yang, Y. Zhao, Y. Guo, J. Xu, F. Li, Y. Wang, S. Lu, L. Qu, *Small* **2019**, *15*, 1901517.
[227] Y. Liu, J. Liu, J. Zhang, X. Li, F. Lin, N. Zhou, B. Yang, L. Lu, *ACS Omega* **2018**, *3*, 7888.
[228] L. Wang, B. Wu, W. Li, Z. Li, J. Zhan, B. Geng, S. Wang, D. Pan, M. Wu, *Journal of Materials Chemistry B* **2017**, *5*, 5355.
[229] R. S. Li, P. F. Gao, H. Z. Zhang, L. L. Zheng, C. M. Li, J. Wang, Y. F. Li, F. Liu, N. Li, C. Z. Huang, *Chemical Science* **2017**, *8*, 6829.
[230] X.-W. Hua, Y.-W. Bao, F.-G. Wu, *ACS Applied Materials & Interfaces* **2018**, *10*, 10664.
[231] H. Liu, J. Yang, Z. Li, L. Xiao, A. A. Aryee, Y. Sun, R. Yang, H. Meng, L. Qu, Y. Lin, X. Zhang, *Analytical Chemistry* **2019**, *91*, 9259.
[232] D.-W. Zheng, B. Li, C.-X. Li, J.-X. Fan, Q. Lei, C. Li, Z. Xu, X.-Z. Zhang, *ACS Nano* **2016**, *10*, 8715.
[233] J. Li, S. Yang, Y. Deng, P. Chai, Y. Yang, X. He, X. Xie, Z. Kang, G. Ding, H. Zhou, X. Fan, *Advanced Functional Materials* **2018**, *28*, 1800881.
[234] S.-Y. Sung, Y.-L. Su, W. Cheng, P.-F. Hu, C.-S. Chiang, W.-T. Chen, S.-H. Hu, *Nano Letters* **2019**, *19*, 69.

[235] S. Li, W. Su, H. Wu, T. Yuan, C. Yuan, J. Liu, G. Deng, X. Gao, Z. Chen, Y. Bao, F. Yuan, S. Zhou, H. Tan, Y. Li, X. Li, L. Fan, J. Zhu, A. T. Chen, F. Liu, Y. Zhou, M. Li, X. Zhai, J. Zhou, *Nature Biomedical Engineering* **2020**, *4*, 704.
[236] P. Gao, S. Liu, Y. Su, M. Zheng, Z. Xie, *Bioconjugate Chemistry* **2020**, *31*, 646.
[237] C. Scialabba, A. Sciortino, F. Messina, G. Buscarino, M. Cannas, G. Roscigno, G. Condorelli, G. Cavallaro, G. Giammona, N. Mauro, *ACS Applied Materials & Interfaces* **2019**, *11*, 19854.
[238] S. Ghosh, K. Ghosal, S. A. Mohammad, K. Sarkar, *Chemical Engineering Journal* **2019**, *373*, 468.
[239] J. Han, K. Na, *Journal of Industrial and Engineering Chemistry* **2019**, *80*, 722.
[240] C. E. Dunbar, K. A. High, J. K. Joung, D. B. Kohn, K. Ozawa, M. Sadelain, *Science* **2018**, *359*, eaan4672.
[241] T. Huo, Y. Yang, M. Qian, H. Jiang, Y. Du, X. Zhang, Y. Xie, R. Huang, *Biomaterials* **2020**, *260*, 120305.
[242] C. Plank, K. Zatloukal, M. Cotten, K. Mechtler, E. Wagner, *Bioconjug Chem* **1992**, *3*, 533.
[243] D. Schaffert, M. Kiss, W. Rödl, A. Shir, A. Levitzki, M. Ogris, E. Wagner, *Pharmaceutical Research* **2011**, *28*, 731.
[244] W. Rodl, D. Schaffert, E. Wagner, M. Ogris, *Methods Mol Biol* **2013**, *948*, 105.
[245] M. Qian, Y. Du, S. Wang, C. Li, H. Jiang, W. Shi, J. Chen, Y. Wang, E. Wagner, R. Huang, *ACS Appl Mater Interfaces* **2018**, *10*, 4031.
[246] U. Lächelt, P. Kos, F. M. Mickler, A. Herrmann, E. E. Salcher, W. Rödl, N. Badgujar, C. Bräuchle, E. Wagner, *Nanomedicine: Nanotechnology, Biology and Medicine* **2014**, *10*, 35.
[247] D. Schaffert, N. Badgujar, E. Wagner, *Organic Letters* **2011**, *13*, 1586.
[248] P. M. Klein, S. Reinhard, D.-J. Lee, K. Müller, D. Ponader, L. Hartmann, E. Wagner, *Nanoscale* **2016**, *8*, 18098.
[249] I. Truebenbach, W. Zhang, Y. Wang, S. Kern, M. Höhn, S. Reinhard, J. Gorges, U. Kazmaier, E. Wagner, *Int J Pharm* **2019**, *569*, 118570.
[250] Y. Wang, J. Luo, I. Truebenbach, S. Reinhard, P. M. Klein, M. Höhn, S. Kern, S. Morys, D. M. Loy, E. Wagner, W. Zhang, *ACS Biomaterials Science & Engineering* **2020**, *6*, 1074.
[251] I. Truebenbach, W. Zhang, Y. Wang, S. Kern, M. Höhn, S. Reinhard, J. Gorges, U. Kazmaier, E. Wagner, *Int J Pharm* **2019**, *569*, 118570.
[252] E. Kaiser, R. L. Colescott, C. D. Bossinger, P. I. Cook, *Anal Biochem* **1970**, *34*, 595.
[253] S. Reinhard, W. Zhang, E. Wagner, *ChemMedChem* **2017**, *12*, 1464.
[254] P. K. Wan, A. J. Ryan, L. W. Seymour, *Molecular therapy : the journal of the American Society of Gene Therapy* **2021**, *29*, 1668.
[255] U. T. Hacker, M. Bentler, D. Kaniowska, M. Morgan, H. Büning, *Cancers (Basel)* **2020**, *12*.
[256] Z. Zhou, X. Liu, D. Zhu, Y. Wang, Z. Zhang, X. Zhou, N. Qiu, X. Chen, Y. Shen, *Advanced drug delivery reviews* **2017**, *115*, 115.
[257] W. Ji, B. Sun, C. Su, *Genes (Basel)* **2017**, *8*.
[258] X. Song, C. Liu, N. Wang, H. Huang, S. He, C. Gong, Y. Wei, *Advanced drug delivery reviews* **2021**, *168*, 158.
[259] S. L. Ginn, A. K. Amaya, I. E. Alexander, M. Edelstein, M. R. Abedi, *The journal of gene medicine* **2018**, e3015.
[260] T. M. Allen, C. Hansen, *Biochimica et biophysica acta* **1991**, *1068*, 133.

[261] A. Gabizon, D. Papahadjopoulos, *Proceedings of the National Academy of Sciences of the United States of America* **1988**, *85*, 6949.
[262] I. Alberg, S. Kramer, M. Schinnerer, Q. Hu, C. Seidl, C. Leps, N. Drude, D. Möckel, C. Rijcken, T. Lammers, M. Diken, M. Maskos, S. Morsbach, K. Landfester, S. Tenzer, M. Barz, R. Zentel, *Small* **2020**, *16*, e1907574.
[263] H. Maeda, G. Y. Bharate, J. Daruwalla, *Eur. J. Pharm. Biopharm.* **2009**, *71*, 409.
[264] A. A. Gabizon, Y. Patil, N. M. La-Beck, *Drug Resist Updat* **2016**, *29*, 90.
[265] S. Tran, P. J. DeGiovanni, B. Piel, P. Rai, *Clin Transl Med* **2017**, *6*, 44.
[266] D. Schaffert, E. Wagner, *Gene Ther* **2008**, *15*, 1131.
[267] M. A. Mintzer, E. E. Simanek, *Chem Rev* **2009**, *109*, 259.
[268] C. Pichon, L. Billiet, P. Midoux, *Curr Opin Biotechnol* **2010**, *21*, 640.
[269] D. W. Pack, A. S. Hoffman, S. Pun, P. S. Stayton, *Nat.Rev.Drug Discov.* **2005**, *4*, 581.
[270] Y. Wang, L. Miao, A. Satterlee, L. Huang, *Advanced drug delivery reviews* **2015**, *87*, 68.
[271] P. R. Cullis, M. J. Hope, *Molecular therapy : the journal of the American Society of Gene Therapy* **2017**, *25*, 1467.
[272] J. Luo, E. Wagner, Y. Wang, *J Mater Chem B* **2020**, *8*, 2020.
[273] R. Kumar, C. F. Santa Chalarca, M. R. Bockman, C. V. Bruggen, C. J. Grimme, R. J. Dalal, M. G. Hanson, J. K. Hexum, T. M. Reineke, *Chemical reviews* **2021**.
[274] A. I. S. van den Berg, C. O. Yun, R. M. Schiffelers, W. E. Hennink, *J Control Release* **2021**, *331*, 121.
[275] E. Wagner, D. Curiel, M. Cotten, *Adv Drug Del Rev* **1994**, *14*, 113.
[276] R. Kircheis, E. Ostermann, M. F. Wolschek, C. Lichtenberger, C. Magin-Lachmann, L. Wightman, M. Kursa, E. Wagner, *Cancer Gene Ther* **2002**, *9*, 673.
[277] N. C. Bellocq, S. H. Pun, G. S. Jensen, M. E. Davis, *Bioconjug.Chem.* **2003**, *14*, 1122.
[278] S. Hu-Lieskovan, J. D. Heidel, D. W. Bartlett, M. E. Davis, T. J. Triche, *Cancer Res.* **2005**, *65*, 8984.
[279] J. D. Heidel, Z. Yu, J. Y. Liu, S. M. Rele, Y. Liang, R. K. Zeidan, D. J. Kornbrust, M. E. Davis, *Proc.Natl.Acad.Sci U.S.A* **2007**, *104*, 5715.
[280] W. Zhang, W. Rodl, D. He, M. Doblinger, U. Lachelt, E. Wagner, *J Gene Med* **2015**, *17*, 161.
[281] Y. Miyajima, H. Nakamura, Y. Kuwata, J. D. Lee, S. Masunaga, K. Ono, K. Maruyama, *Bioconjug Chem* **2006**, *17*, 1314.
[282] N. Sakaguchi, C. Kojima, A. Harada, K. Koiwai, N. Emi, K. Kono, *Bioconjug Chem* **2008**, *19*, 1588.
[283] K. Sasaki, K. Kogure, S. Chaki, Y. Nakamura, R. Moriguchi, H. Hamada, R. Danev, K. Nagayama, S. Futaki, H. Harashima, *Anal.Bioanal.Chem* **2008**, *391*, 2717.
[284] Y. Kuang, S. An, Y. Guo, S. Huang, K. Shao, Y. Liu, J. Li, H. Ma, C. Jiang, *Int J Pharm* **2013**, *454*, 11.
[285] G. Stingl, E. B. Brocker, R. Mertelsmann, K. Wolff, S. Schreiber, E. Kampgen, A. Schneeberger, W. Dummer, U. Brennscheid, H. Veelken, M. L. Birnstiel, K. Zatloukal, W. Schmidt, G. Maass, E. Wagner, M. Baschle, M. Giese, E. R. Kempe, H. A. Weber, T. Voigt, *Human gene therapy* **1996**, *7*, 551.
[286] M. E. Davis, *Mol Pharm* **2009**, *6*, 659.
[287] M. E. Davis, J. E. Zuckerman, C. H. Choi, D. Seligson, A. Tolcher, C. A. Alabi, Y. Yen, J. D. Heidel, A. Ribas, *Nature* **2010**, *464*, 1067.

[288] R. Prades, B. Oller-Salvia, S. M. Schwarzmaier, J. Selva, M. Moros, M. Balbi, V. Grazú, J. M. de La Fuente, G. Egea, N. Plesnila, M. Teixidó, E. Giralt, *Angewandte Chemie International Edition* **2015**, *54*, 3967.
[289] J. Luo, J. Schmaus, M. Cui, E. Hörterer, U. Wilk, M. Höhn, M. Däther, S. Berger, T. Benli-Hoppe, L. Peng, *Journal of Controlled Release* **2021**, *329*, 919.
[290] J. C. Jewett, C. R. Bertozzi, *Chemical Society Reviews* **2010**, *39*, 1272.
[291] Y. Tao, D. Qu, C. Tian, Y. Huang, L. Xue, C. Ju, M. Hao, C. Zhang, *International Journal of Pharmaceutics* **2021**, *605*, 120798.
[292] M. F. Debets, S. S. van Berkel, S. Schoffelen, F. P. J. T. Rutjes, J. C. M. van Hest, F. L. van Delft, *Chemical Communications* **2010**, *46*, 97.
[293] C. Scholz, E. Wagner, *J Control Release* **2012**, *161*, 554.
[294] F. Freitag, E. Wagner, *Advanced drug delivery reviews* **2021**, *168*, 30.
[295] Y. Wang, E. Wagner, *Pharmaceutics* **2020**, *12*.
[296] L. Hartmann, *Macromolecular Chemistry and Physics* **2011**, *212*, 8.
[297] S. A. Hill, C. Gerke, L. Hartmann, *Chemistry, an Asian journal* **2018**, *13*, 3611.
[298] D. Schaffert, C. Troiber, E. E. Salcher, T. Frohlich, I. Martin, N. Badgujar, C. Dohmen, D. Edinger, R. Klager, G. Maiwald, K. Farkasova, S. Seeber, K. Jahn-Hofmann, P. Hadwiger, E. Wagner, *Angew Chem Int Ed Engl* **2011**, *50*, 8986.
[299] P. Kos, U. Lachelt, A. Herrmann, F. M. Mickler, M. Doblinger, D. He, A. Krhac Levacic, S. Morys, C. Brauchle, E. Wagner, *Nanoscale* **2015**, *7*, 5350.
[300] S. Morys, A. Krhac Levacic, S. Urnauer, S. Kempter, S. Kern, J. O. Radler, C. Spitzweg, U. Lachelt, E. Wagner, *Polymers* **2017**, *9*.
[301] C. Troiber, D. Edinger, P. Kos, L. Schreiner, R. Klager, A. Herrmann, E. Wagner, *Biomaterials* **2013**, *34*, 1624.
[302] Y. Wang, J. Luo, I. Truebenbach, S. Reinhard, P. M. Klein, M. Hohn, S. Kern, S. Morys, D. M. Loy, E. Wagner, W. Zhang, *ACS Biomater Sci Eng* **2020**, *6*, 1074.
[303] P. M. Klein, E. Wagner, *Methods Mol Biol* **2019**, *2036*, 141.
[304] J. F. Patrick Erickson, Michael Kay, *ChemRxiv* **2020**.
[305] J. C. Sunshine, D. Y. Peng, J. J. Green, *Molecular Pharmaceutics* **2012**, *9*, 3375.
[306] J. C. Sunshine, M. I. Akanda, D. Li, K. L. Kozielski, J. J. Green, *Biomacromolecules* **2011**, *12*, 3592.
[307] I. Muljajew, S. Huschke, A. Ramoji, Z. Cseresnyés, S. Hoeppener, I. Nischang, W. Foo, J. Popp, M. T. Figge, C. Weber, M. Bauer, U. S. Schubert, A. T. Press, *ACS Nano* **2021**, *15*, 12298.
[308] L. Bekale, D. Agudelo, H. A. Tajmir-Riahi, *Colloids and Surfaces B: Biointerfaces* **2015**, *130*, 141.
[309] J. Luo, M. Höhn, S. Reinhard, D. M. Loy, P. M. Klein, E. Wagner, *Advanced Functional Materials* **2019**, *29*, 1900697.
[310] E. Wagner, *Accounts of chemical research* **2012**, *45*, 1005.
[311] J. D. Heidel, J. Y. Liu, Y. Yen, B. Zhou, B. S. Heale, J. J. Rossi, D. W. Bartlett, M. E. Davis, *Clin Cancer Res* **2007**, *13*, 2207.
[312] Y. Hattori, K. Tamaki, S. Sakasai, K. I. Ozaki, H. Onishi, *Molecular Medicine Reports* **2020**, *22*, 4183.
[313] V. Kumar, J. Qin, Y. Jiang, R. G. Duncan, B. Brigham, S. Fishman, J. K. Nair, A. Akinc, S. A. Barros, P. V. Kasperkovitz, *Molecular Therapy-Nucleic Acids* **2014**, *3*, e210.
[314] S. Morys, S. Urnauer, C. Spitzweg, E. Wagner, *Macromol Biosci* **2018**, *18*.
[315] M. Zheng, S. Ruan, S. Liu, T. Sun, D. Qu, H. Zhao, Z. Xie, H. Gao, X. Jing, Z. Sun, *ACS Nano* **2015**, *9*, 11455.

[316] T. Tian, J. Li, C. Xie, Y. Sun, H. Lei, X. Liu, J. Xia, J. Shi, L. Wang, W. Lu, C. Fan, *ACS Appl Mater Interfaces* **2018**, *10*, 3414.
[317] Y. Bertrand, J. C. Currie, J. Poirier, M. Demeule, A. Abulrob, D. Fatehi, D. Stanimirovic, H. Sartelet, J. P. Castaigne, R. Béliveau, *Br J Cancer* **2011**, *105*, 1697.
[318] M. M. Wilhelmus, J. G. Bol, E. S. Van Haastert, A. J. Rozemuller, G. Bu, B. Drukarch, J. J. Hoozemans, *Am J Pathol* **2011**, *179*, 2152.
[319] R. Huang, W. Ke, L. Han, Y. Liu, K. Shao, L. Ye, J. Lou, C. Jiang, Y. Pei, *Journal of Cerebral Blood Flow & Metabolism* **2009**, *29*, 1914.
[320] H. Kafa, J. T. Wang, N. Rubio, R. Klippstein, P. M. Costa, H. A. Hassan, J. K. Sosabowski, S. S. Bansal, J. E. Preston, N. J. Abbott, K. T. Al-Jamal, *Journal of controlled release : official journal of the Controlled Release Society* **2016**, *225*, 217.
[321] R. Röder, J. Helma, T. Preiß, J. O. Rädler, H. Leonhardt, E. Wagner, *Pharm Res* **2017**, *34*, 161.
[322] Y. Lei, J. Wang, C. Xie, E. Wagner, W. Lu, Y. Li, X. Wei, J. Dong, M. Liu, *J Gene Med* **2013**, *15*, 291.
[323] X. Wei, C. Zhan, X. Chen, J. Hou, C. Xie, W. Lu, *Molecular Pharmaceutics* **2014**, *11*, 3261.
[324] L. Marinelli, A. Lavecchia, K.-E. Gottschalk, E. Novellino, H. Kessler, *Journal of Medicinal Chemistry* **2003**, *46*, 4393.
[325] D. Heckmann, H. Kessler, "Design and Chemical Synthesis of Integrin Ligands", in *Methods in Enzymology*, Academic Press, 2007, p. 463.
[326] M. Pfaff, K. Tangemann, B. Müller, M. Gurrath, G. Müller, H. Kessler, R. Timpl, J. Engel, *J Biol Chem* **1994**, *269*, 20233.
[327] M. Ferrari, *Nature Reviews Cancer* **2005**, *5*, 161.
[328] T. Sun, Y. S. Zhang, B. Pang, D. C. Hyun, M. Yang, Y. Xia, *Angewandte Chemie (International ed. in English)* **2014**, *53*, 12320.
[329] Y. Du, M. Qian, C. Li, H. Jiang, Y. Yang, R. Huang, *International Journal of Pharmaceutics* **2018**, *552*, 84.
[330] Y. Wang, T. Huo, H. Jiang, Y. Xie, X. Zhang, H. Nie, Y. Yang, M. Qian, W. Li, T. Hao, W. Guo, Y. Qin, J. Shi, W. Shi, R. Huang, *Nano Today* **2021**, *38*, 101200.
[331] W. Zhang, G. Sigdel, K. J. Mintz, E. S. Seven, Y. Zhou, C. Wang, R. M. Leblanc, *Int J Nanomedicine* **2021**, *16*, 5003.
[332] D. Kim, J. M. Yoo, H. Hwang, J. Lee, S. H. Lee, S. P. Yun, M. J. Park, M. Lee, S. Choi, S. H. Kwon, S. Lee, S. H. Kwon, S. Kim, Y. J. Park, M. Kinoshita, Y. H. Lee, S. Shin, S. R. Paik, S. J. Lee, S. Lee, B. H. Hong, H. S. Ko, *Nat Nanotechnol* **2018**, *13*, 812.
[333] S. Wang, S. Reinhard, C. Li, M. Qian, H. Jiang, Y. Du, U. Lachelt, W. Lu, E. Wagner, R. Huang, *Mol Ther* **2017**, *25*, 1556.

8 Publications

Original articles

Benli-Hoppe, T., Göl, S., Öztürk, Ö., Berger, S., Wagner, E., Yazdi, M. (2022) Transferrin Receptor Targeted Polyplexes Completely Comprised of Sequence-Defined Components. Macromol. Rapid Commun. 2022, 43, e2100602.

Berger, S., Krhač Levačić, A., Hörterer, E., Wilk, U., **Benli-Hoppe, T.**, Wang, Y., Öztürk, Ö., Luo, J., Wagner, E. (2021) Optimizing pDNA lipo-polyplexes: A balancing act between stability and cargo release. Biomacromolecules. 2021 Mar 8;22(3):1282-1296

Luo, J., Schmaus, J., Cui, M., Hörterer, E., Wilk, U., Höhn, M., Däther, M., Berger, S., **Benli-Hoppe, T**., Peng, L., Wagner, E. (2021) Hyaluronate siRNA nanoparticles with positive charge display rapid attachment to tumor endothelium and penetration into tumors, J Control Release 2021 Jan 10;329:919-933

Spellerberg, R., **Benli-Hoppe, T**., Kitzberger, C., Berger, S., Schmohl, KA., Schwenk, N., Yen, HY., Zach, C., Weber, WA., Kälin, RE., Glass, R., Nelson, PJ., Wagner, E., Spitzweg, C. (2021) Selective sodium iodide symporter (NIS) genetherapy of glioblastoma mediated by EGFR-targeted lipopolyplexes, Mol Ther Oncolytics. 2021 Oct; 30;23:432-446

Spellerberg, R., **Benli-Hoppe, T**., Kitzberger, C., Hageneier, M., Schwenk, N., Öztürk, Ö., Steiger, K., Multhoff, G., Eiber, M., Schilling, F., Weber, WA., Kälin, RE., Glass, R., Nelson, PJ., Wagner, E., Spitzweg, C. (2022) Dual EGFR- and TfR-targeted gene transfer for sodium iodide symporter gene therapy of glioblastoma, Mol Ther Oncolytics. 2022 Dec; 15;27:272-287

Reviews and book chapters

Benli-Hoppe, T., Wagner E. (2020) Polymer-Based Tumor-targeted Nanosystems. In: Huang R., Wang Y. (eds) New Nanomaterials and Techniques for Tumor-targeted Systems. Springer, Singapore.

9 Acknowledgements

The Ph.D. is not a sprint but a marathon. It was a long journey, interspersed with ups and downs.

But even a marathon comes to an end, just as Pheidippides once ran from Athens to Sparta, so I am now coming to the end of this phase of my life. In my case, the background of the marathon is luckily not because of the war. I moved from Kiel to Munich. I started a new life here, met new people and, came into the pleasures of getting to know and being able to work in a highly sophisticated scientifical environment.

In this sense, I would like to thank my doctoral supervisor Prof. Dr. Ernst Wagner and Prof. Dr. Christine Spitzweg, made my doctorate possible in the first place. I would also like to thank all the lovely people who have accompanied and supported me on this journey. I would especially like to thank my parents, my brother, and my partner who have always been there for me.

Pheidippides collapsed on the ground at the end of his journey and said goodbye with the words "νενικήκαμεν". I agree with that and close this section of my life with them as well.